

# Nutrient dynamics in temporary waters of Mediterranean catchments

Von der Fakultät für Bauingenieurwesen und Geodäsie

der

Gottfried Wilhelm Leibniz Universität Hannover

zur Erlangung des Grades eines

DOKTOR – INGENIEUR

Dr.-Ing.

genehmigte Dissertation

von

Dipl.-Ing. Matthias Obermann

geboren am 22. Juni 1977

in Hannover

Hannover, Januar 2007

Referent

Prof. Dr.-Ing. Karl-Heinz Rosenwinkel

Institut für Siedlungswasserwirtschaft und Abfalltechnik

Gottfried Wilhelm Leibniz Universität Hannover

Welfengarten 1, 30167 Hannover

Korreferent

Prof. Mike Kirkby

School of Geography

University of Leeds

Leeds LS2 9JT, United Kingdom

Tag der Promotion

09. März 2007

---

## Acknowledgements

My thanks belong to the many people who contributed to this work:

- Prof. Dr.-Ing. K.-H. Rosenwinkel (Leibniz Universität Hannover) and Prof. Mike Kirkby (University of Leeds), who not only reviewed and evaluated the thesis, but also helped me with their guidance and advice,
  - Dr. Jochen Froebrich (Leibniz Universität Hannover) who gave me the possibility to do this work within the tempQsim project and for the fruitful discussions,
  - Dr. Marie-George Tournoud (Université Montpellier II), Dr. Jean-Louis Perrin (IRD) for their encouragement and the willingness to share all their knowledge and data with me,
  - Dr. Victor Castillo (CSIC-CEBAS, Murcia), Paolo Botti (EAF) and Dr. Ludovica Diliberto (Hydrocontrol, Capoterra) for the collection and preparation of their data,
  - Prof. Ramiro Neves, Frank Braunschweig, Ana Rosa Trancoso and Pedro Chambel Leitão (Universidade de Lisboa) for the continuous and extraordinary help on the MOHID Water Modelling System,
  - Dr. David M. Cooper (CEH Wallingford) and Prof. Nikolaos Nikolaidis (Technical University of Crete) for their help with CASCADE and HSPF,
  - my colleagues, especially Dr. Melanie Bauer for her intensive administrative work and her good tips, Oliver Olsson, Lutz Brödel, Nadine Stelle, Christian Reder and Wassim Abu Abed,
  - the DAAD which allowed me an important final stay at the Vène catchment and the European Commission for funding the project tempQsim,
  - Annette Rutz and Dr. Nanée Chahinian for detailed reading and their good ideas,
  - my parents Karin and Manfred and my sister Sabine for their faith in me.
-





---

## Zusammenfassung

*Schlagnörter: temporäre Flüsse, Spülstoß, semi-aride Flusseinzugsgebiete, Massenretention, Wasserqualitätsdynamik, Wasserqualitätsmodellierung*

Temporäre Flüsse sind einzigartige Ökosysteme. Sie erfordern spezielle Kenntnisse, die nicht zwangsläufig aus dem bisherigen Wissen über beständige Fließgewässer abgeleitet werden können. Bedingt durch zukünftige oder bereits erfolgte globale klimatische Veränderungen wird der Anteil temporärer Flüsse im Mittelmeerraum zunehmen. Bereits vorhandene temporäre Gewässer werden längere Trockenzeiten und eine größere Variabilität erfahren – mit dramatischen Auswirkungen für diese sensiblen Systeme.

Im Hinblick auf die Forderung der Europäischen Wasserrahmenrichtlinie nach einer guten Wasserqualität für Oberflächengewässer bis 2015 besteht der Bedarf, auch für temporäre Gewässer Qualitätsmerkmale zu definieren, sowie Untersuchungsmethoden und –modelle bereitzustellen.

Die Intention der vorliegenden Arbeit ist es, wesentliche Merkmale temporärer Flusssysteme in Bezug auf deren Nährstofftransportvariabilität mit Hilfe neuer Methoden zu untersuchen, zu bewerten und in einem Wasserqualitätsmodell nachzubilden.

Dies folgt dem Zweck, zukünftig Möglichkeiten der Steuerung und Vorhersage der komplexen Interaktionsprozesse zwischen Fließgewässern und den nachgeordneten Wasserkörpern (Lagunen, Talsperren etc.) dieser Ökosysteme zu erlauben.

Hierzu werden am Beispiel von drei mediterranen Flusseinzugsgebieten Regen-, Abfluss- und Wasserqualitätsdaten bezüglich der zeitlichen und räumlichen Verteilung der Nährstofffrachten analysiert. Das Hauptaugenmerk liegt in der Untersuchung zweier unterschiedlicher Skalen: der jahreszeitlichen Schwankungen sowie der Schwankungen innerhalb eines Abflussereignisses.

Gestützt auf diesen Erkenntnissen wurde ein Wasserqualitätsmodell entwickelt und weiter modifiziert. Das tempQsim – STREAM Modell ist in der Lage, wichtige Komponenten temporärer Flüsse richtig nachzubilden. Erhöhte Transmissionsverluste durch Verdunstung und Versickerung, starke Schwankungen in der Abflussmenge bis hin zum vollständigen Trockenfallen des gesamten Flusses oder großer Teile davon, und die damit einhergehende Retention von eingebrachten Nähr- und Schadstoffen hat große Einflüsse auf die Transportvariabilität und lässt viele herkömmliche Modellansätze an ihre Grenzen stoßen.

Bedingt durch eine massentreue Finite Volumen Diskretisierung des Flussgebietes können insbesondere die komplizierte Interaktion zwischen Sediment und Wasserphase sowie stark erhöhte Frachten partikulärer organischer Stoffe im Übergang zwischen Trocken- und Regenperiode am Ende des Sommers korrekt abgebildet werden.

Die Berücksichtigung dieser wichtigen Prozesse ermöglichen Vorhersage und Steuerungsoptionen und sind daher ein bedeutender Baustein für eine zukünftige Umsetzung Europäischen Wasserrahmenrichtlinie in semi-ariden Regionen.

---

---

## Abstract

*Keywords: temporary rivers, dry rivers, first flush, semi-arid river basins, mass retention, water quality dynamics, water quality modelling*

Temporary rivers are unique ecosystems. They require special knowledge, which cannot necessarily be derived from the experiences which were already gained in perennial rivers. In consequence of future and already happening global climatic changes the number of temporary rivers will increase in the Mediterranean. Present temporary waters will encounter longer dry periods and a higher variability – including dramatic effects for these sensitive systems.

With regard to the requirements of the European Water Framework Directive for a good water quality in surface waters until 2015, there is a need to define quality characteristics for temporary waters and to provide suitable methods and models for the investigation.

The intention of this work is to analyse and to evaluate essential features of temporary river systems in terms of the variability in nutrient transport using newly developed methods and to reproduce these in a water quality model.

This will enable to predict and manage the complex processes of interaction between flowing water courses and receiving water bodies in the future.

On the example of three Mediterranean river basins, rainfall, discharge and water quality data is analysed in terms of the temporal and spatial fluctuation of nutrient loads. The main attention is given to the investigation of two different scales: the annual fluctuation and the fluctuation within a flood event.

Based on these findings, a water quality model was developed and further modified. The tempQsim – STREAM model is able to correctly simulate important components of temporary rivers. Increased transmission losses are often caused by evaporation and infiltration and can lead up to the complete discontinuation of the river. High fluctuations in the instream water flow are associated with the retention of nutrients and pollutants. This has great influences on the transport variability and limits the application of many common model approaches.

Due to a mass conserving finite volume discretisation of the river network, especially the complex interactions between sediment and water phase and the highly increased loads of particulate organic matter during the transition period from dry to rainy season at the end of the summer can be simulated correctly.

The consideration of these important processes allows a prediction and management and is therefore an important milestone for a future implementation of the European Water Framework Directive in semi-arid regions.

---

---

# TABLE OF CONTENTS

---

<b>1</b>	<b>INTRODUCTION</b>	<b>12</b>
<b>2</b>	<b>METHODS TO DESCRIBE THE PARTICULARITY OF MEDITERRANEAN CATCHMENTS</b>	<b>16</b>
2.1	GENERAL DEFINITIONS AND FUNCTIONING OF TEMPORARY WATERS.....	16
2.1.1	<i>Definition of aridity</i> .....	16
2.1.2	<i>Correlation coefficients</i> .....	16
2.1.2.1	Regression and correlation.....	17
2.1.2.2	Pearson Product-Moment Correlation Coefficient.....	17
2.1.2.3	Nash-Sutcliffe efficiency.....	17
2.1.3	<i>Definition of temporary waters and dryland rivers</i> .....	17
2.1.4	<i>Importance of transmission and evaporation losses</i> .....	20
2.1.5	<i>Interruption of flow and interaction of events</i> .....	20
2.1.6	<i>Definition of a reach chain</i> .....	21
2.1.7	<i>Definition of flow threshold</i> .....	21
2.1.8	<i>Sources of accumulation</i> .....	22
2.1.9	<i>Mode of accumulation and resuspension</i> .....	22
2.2	THE FIRST-FLUSH PHENOMENON .....	23
2.2.1	<i>Driving forces influencing a first flush</i> .....	25
2.2.2	<i>Influence of sampling points</i> .....	25
2.2.3	<i>Definition and quantification of first-flush</i> .....	27
2.2.4	<i>Calculation of normalize cumulative load plots</i> .....	28
2.2.5	<i>Calculation of relative mass fluxes</i> .....	32
2.2.6	<i>Indexes as classification methods for first flushes</i> .....	33
<b>3</b>	<b>MODELLING TOOLS FOR TEMPORARY STREAMS</b>	<b>37</b>
3.1	CLASSIFICATION OF MODELS.....	37
3.2	FLOW ROUTING .....	39
3.2.1	<i>Dynamic Wave</i> .....	39
3.2.2	<i>Non-inertia wave</i> .....	40
3.2.3	<i>Kinematic Wave</i> .....	40
3.2.4	<i>Example of a numerical solution of the kinematic wave equation</i> .....	41
3.3	ROUTING OF PROPERTIES USING THE KINEMATIC WAVE EQUATION .....	43
3.3.1	<i>Soluble properties</i> .....	43
3.3.2	<i>Particulate properties</i> .....	44
3.3.2.1	Transport of individual particles.....	44
3.3.2.2	Transport of a continuum of particles.....	45
3.3.2.3	Actual shear stress .....	46
3.3.2.4	Critical shear stress .....	49
3.3.2.5	Common approaches for sediment transport.....	50
3.4	REACTION KINETICS .....	51
3.4.1	<i>Zero-order reactions</i> .....	51
3.4.2	<i>First-order reaction</i> .....	52
3.4.3	<i>Second-order reactions</i> .....	52
3.4.4	<i>Michaelis-Menten kinetic</i> .....	52
3.5	HSPF.....	53

---

3.5.1	<i>General</i> .....	53
3.5.2	<i>Framework of the model</i> .....	53
3.5.3	<i>Programming philosophy</i> .....	54
3.5.4	<i>Input and Output</i> .....	54
3.5.5	<i>Flow routing</i> .....	54
3.5.6	<i>Temporal scale</i> .....	55
3.5.7	<i>Water quality</i> .....	55
3.5.8	<i>Particulate transport and benthic processes</i> .....	55
3.6	CASCADE.....	57
3.6.1	<i>General</i> .....	57
3.6.2	<i>Framework of the model</i> .....	57
3.6.3	<i>Programming philosophy</i> .....	57
3.6.4	<i>Input and output</i> .....	57
3.6.5	<i>Flow routing</i> .....	58
3.6.6	<i>Temporal scale</i> .....	59
3.6.7	<i>Water quality</i> .....	59
3.6.8	<i>Particulate transport and benthic processes</i> .....	60
3.7	MOHID WATER MODELLING SYSTEM AND THE TEMPQSIM – STREAM MODEL.....	60
3.7.1	<i>General</i> .....	60
3.7.2	<i>Framework of the model</i> .....	60
3.7.3	<i>Programming philosophy</i> .....	61
3.7.4	<i>Input and output</i> .....	61
3.7.5	<i>Flow routing</i> .....	62
3.7.6	<i>Temporal scale</i> .....	62
3.7.7	<i>Water quality</i> .....	62
3.7.8	<i>Particulate transport and benthic processes</i> .....	63
3.8	CONCLUSIONS OF THE MODEL SURVEY AND EXTENSION OF THE TEMPQSIM – STREAM MODEL.....	64
3.8.1	<i>Output of loads</i> .....	64
3.8.2	<i>Modification of post processor “timeseries editor”</i> .....	64
3.8.3	<i>Bacterial growth in pools</i> .....	64
3.8.4	<i>Fractioned sediment transport</i> .....	67
3.8.5	<i>Calculation of TSS and VSS</i> .....	67
3.8.6	<i>New calculation of available erosion capacity for each fraction</i> .....	68
<b>4</b>	<b>WATER QUALITY DYNAMICS OF MEDITERRANEAN RIVERS, DATA AND RESULTS</b>	<b>70</b>
4.1	THE BASIN OF LA VÈNE, FRANCE.....	70
4.1.1	<i>River characteristics</i> .....	70
4.1.2	<i>Relevancy of the dataset</i> .....	73
4.1.3	<i>Annual cycle of transport – magnitude of months to years</i> .....	73
4.1.3.1	<i>Distribution of precipitation</i> .....	75
4.1.3.2	<i>Relevancy of antecedent dry weather period</i> .....	77
4.1.3.3	<i>Comparison of monthly rainfall</i> .....	77
4.1.3.4	<i>Monthly discharges and loads for the year 2002/2003</i> .....	78
4.1.3.5	<i>Monthly discharges and loads for the year 2003/2004</i> .....	81
4.1.3.6	<i>Correlation between flow, rain and the constituents</i> .....	83
4.1.3.7	<i>NCL-curves of the hydrologic years 2002/2003 and 2003/2004</i> .....	84
4.1.3.8	<i>Relative mass fluxes</i> .....	86
4.1.3.9	<i>Conclusions</i> .....	92
4.1.4	<i>Examples for floods and flushes – magnitude of days to hours</i> .....	92

4.1.4.1	Mass balance and weighting of events for the sites K, S and V .....	96
4.1.4.2	Pollutographs of the event starting at 2003-09-22 .....	96
4.1.4.3	Pollutographs of the event starting at 2004-09-13 .....	99
4.1.4.4	NCL-plots of the event 2003-09-22 .....	103
4.1.4.5	NCL-plots of the event 2004-09-13 .....	104
4.1.4.6	Measurements of conductivity .....	106
4.1.4.7	Application of rating methods for first flushes of each parameter .....	109
4.1.4.8	Conclusions .....	110
4.1.5	<i>Regression of measured flow and water quality properties</i> .....	110
4.1.5.1	Comparison of flow and concentration .....	111
4.1.5.2	Comparison of flow and load .....	113
4.2	SELECTED EXAMPLES IN OTHER CATCHMENTS .....	115
4.2.1	<i>The Mulargia River, Sardinia, Italy</i> .....	115
4.2.1.1	River characteristics .....	115
4.2.1.2	Relevancy of the dataset .....	118
4.2.1.3	Annual cycle of transport – magnitude of months to years .....	118
4.2.1.4	Examples for floods and flushes – magnitude of days to hours – site B .....	119
4.2.1.5	Examples for floods and flushes– magnitude of days to hours – site D .....	127
4.2.1.6	NCL-plots .....	129
4.2.1.7	Conclusions .....	133
4.2.2	<i>El Albuñón River, Murcia, Spain</i> .....	133
4.2.2.1	River characteristics .....	133
4.2.2.2	Relevancy of the dataset .....	135
4.2.2.3	Examples of a first flush – magnitude of days to hours .....	135
4.2.2.4	Conclusions .....	140
4.3	GENERAL CONCLUSIONS OF THE DATA ANALYSIS .....	140
<b>5</b>	<b>APPLICATION OF THE TEMPQSIM – STREAM MODEL TO THE VÈNE</b> .....	<b>142</b>
5.1	SPATIAL DISCRETISATION .....	142
5.2	CALIBRATION OF THE SYSTEM .....	143
5.3	SCENARIOS FOR THE MODELLING .....	144
5.4	ANNUAL SIMULATION AND RESULTS .....	145
5.4.1	<i>Pollutographs for 2002-2004</i> .....	145
5.4.2	<i>Accumulation of organic matter in the river bed and importance of events during the dry phase</i> .....	148
5.4.3	<i>Monthly VSS loads for 2002/2003</i> .....	149
5.4.4	<i>Monthly VSS loads for 2003/2004</i> .....	152
5.5	EVENT SCALE ANALYSIS AND RESULTS .....	153
5.5.1	<i>Pollutographs for the event at 2003-09-22</i> .....	153
5.5.2	<i>Pollutographs for the event at 2004-09-13</i> .....	155
5.5.3	<i>Sensitivity of the processes in the flushing months September 2003 and 2004</i> .....	157
5.5.4	<i>NCL-plots for the scenarios</i> .....	159
5.6	REGRESSION OF SIMULATIONS AND MEASUREMENTS .....	161
5.7	CONCLUSIONS OF THE MODELLING .....	164
<b>6</b>	<b>SUMMARY AND CONCLUSIONS</b> .....	<b>165</b>
<b>7</b>	<b>ANNEX</b> .....	<b>171</b>
7.1	ADDITIONAL FORMULAS CONCERNING TRANSPORT OF PARTICULATE MATERIALS .....	171
7.1.1	<i>Fall velocity of single, spherical particles</i> .....	171
7.1.2	<i>Drag coefficient <math>C_d</math></i> .....	171
7.1.3	<i>Fall velocity of a cloud of particles</i> .....	172

---

7.1.4	<i>Occurrence of suspended load transport</i> .....	173
7.2	RUNOFF COEFFICIENTS IN THE VÈNE.....	174
7.3	CALIBRATION AND SENSITIVITY ANALYSIS.....	175
7.3.1	<i>Sensitivity of the Manning Coefficient</i> .....	175
7.3.2	<i>Sensitivity of the transmission losses</i> .....	175
7.3.3	<i>Water quality properties</i> .....	177
7.4	NCL-PLOTS FOR ALL SCENARIOS.....	178
7.5	SENSITIVITY OF NCL-PLOTS.....	182
7.6	INFLUENCES OF LOW-FLOW VARIABILITY OF CONCENTRATION ON REGRESSION OF DATASETS.....	183
7.7	TESTING AND EXTENSION OF THE CASCADE MODEL.....	184
7.7.1	<i>Time step</i> .....	184
7.7.2	<i>In-stream sediment formula</i> .....	184
7.7.3	<i>Transmission losses</i> .....	184
7.7.4	<i>Mass retention and first flush</i> .....	186
7.7.5	<i>Lack of mass conservation due to leading edge dip phenomena, test examples with the modified model</i> .....	187
7.7.6	<i>Conclusions if the testing</i> .....	195
7.8	MASS BALANCE FOR POOL ACCUMULATION IN FINITE DIFFERENCE MUSKINGUM-CUNGE ROUTING METHOD.....	197
7.9	IMPORTANT FORMULAS FOR THE BENTHOS MODULE IN THE TEMPQSIM –STREAM MODEL.....	199
7.10	ADDED AND MODIFIED CODE IN THE TEMPQSIM – STREAM MODEL.....	202
7.10.1	<i>ModuleBenthos</i> .....	202
7.10.1.1	Subroutine for the benthic bacteria computation.....	202
7.10.1.2	Parameters for bacteria computation in benthos.....	204
7.10.2	<i>ModuleDrainageNetwork</i> .....	205
7.10.2.1	Calculate loads.....	206
7.10.2.2	Calculate TSS.....	206
7.10.2.3	Calculate VSS.....	207
7.10.3	<i>ModuleGlobalData</i> .....	207
7.10.3.1	Function to define VSS.....	208
7.10.4	<i>ModuleWaterQuality</i> .....	208
7.10.4.1	Get NC-Ratios.....	208
7.11	FURTHER ENHANCEMENTS OF THE DELIVERY PART IN THE VÈNE.....	209
7.11.1	<i>Delivery Model</i> .....	209
7.11.2	<i>Simulations with measured flow at S</i> .....	211
7.11.3	<i>Simulations with production function and variable delivery concentrations</i> .....	212
7.12	PICTURES OF THE VÈNE AT DIFFERENT STAGES OF THE YEAR.....	218
<b>8</b>	<b>REFERENCES</b>	<b>220</b>

---

---

## LIST OF FIGURES

---

Figure 2-1: Examples for different flow conditions .....	18
Figure 2-2: Classification of stream in terms of aridity (Uys and O’Keeffe, 1997).....	19
Figure 2-3: Explanation of the reach chain (flow path).....	21
Figure 2-4: Possible event classification .....	22
Figure 2-5: Channel chain - process of accumulation and resuspension.....	23
Figure 2-6: Forms of first-flushes from different origin (based on Krebs et al. (1999), modified) .....	24
Figure 2-7: Influence of sampling points on the occurrence of flushes .....	26
Figure 2-8: Time lag of suspended sediment concentrations in tidal flow van Rijn (1993), modified.....	26
Figure 2-9: Example of a NCL-plot .....	29
Figure 2-10: Resulting NCL-curves from scenarios a to c .....	31
Figure 2-11: Resulting NCL-curves from scenarios d to f .....	32
Figure 2-12: Resulting NCL-curves and the Geiger (1984) criteria as difference of normalized cumulative load from the bisector .....	34
Figure 2-13: Comparison of "one-value" classifications for first flushes for the scenarios of Figure 2-11.....	35
Figure 3-1: Concept of hydrodynamic-numerical models.....	38
Figure 3-2: Common notation in solutions for the kinematic wave.....	42
Figure 3-3: Classification of single particle movement, Bollich (1989), modified.....	45
Figure 3-4: Classification of sediment transport .....	46
Figure 3-5: Shear stress on a control volume of the length dx.....	47
Figure 3-6: Shear stress, particle and bed form related.....	48
Figure 3-7: Shields (1936) diagram .....	49
Figure 3-8: Approximation of the Shields diagram by van Rijn (1993) .....	50
Figure 3-9 BOD release in HSPF .....	56
Figure 3-10: Leading edge dip phenomenon in Muskingum-Cunge flood routing.....	59
Figure 3-11: Internal structure of the MOHID framework.....	61
Figure 3-12: Scheme for processes of heterotrophic bacteria introduced in the tempQsim – STREAM model.....	66
Figure 4-1: DEM and main field measurement sites of the Vène catchment.....	70
Figure 4-2: Land uses of the Vène catchment .....	72
Figure 4-3: Effluent of the WWTP at Montbazin for selected constituents.....	72
Figure 4-4: Distribution of measurements over flow condition at the Vène.....	73
Figure 4-5: Hydrograph of stations K, S and V at the Vène.....	74
Figure 4-6: Mean Monthly values for precipitation in Hannover and Montpellier.....	76
Figure 4-7: Normalized cumulative rainfall and antecedent dry period for three weather stations in the Vène catchment.....	76
Figure 4-8: Rain at the station Montbazin for the hydrological years 2002/2003 and 2003/2004.....	78
Figure 4-9: Monthly flow at the outlet of the Vène for the year 2002/2003.....	78
Figure 4-10: Monthly loads of total suspended solids (TSS) and volatile suspended solids (VSS) for 2002/2003.....	79
Figure 4-11: Monthly loads of soluble reactive phosphorus (ortho-phosphate or SRP) and particulate phosphorus (PP) for 2002/2003.....	79
Figure 4-12: Monthly loads total nitrogen (TN), nitrate (NO <sub>3</sub> -N), ammonium (NH <sub>4</sub> -N) and organic nitrogen (orgN) for 2002/2003.....	80
Figure 4-13: Monthly flow at the outlet of the Vène for the year 2003/2004.....	81
Figure 4-14: Monthly load of total suspended solids (TSS) and volatile suspended solids (VSS) for 2003/2004.....	81
Figure 4-15: Monthly load of soluble reactive phosphorus and particulate phosphorus for 2003/2004.....	82

---

---

Figure 4-16: Monthly loads total nitrogen (TN), nitrate (NO <sub>3</sub> -N), ammonium (NH <sub>4</sub> -N) and organic nitrogen (orgN) for 2003/2004.....	83
Figure 4-17: Normalized cumulative loadings in comparison to normalized cumulative discharge for the hydrologic year 2002/2003 in S and V starting in October.....	84
Figure 4-18: Normalized cumulative loadings in comparison to normalized cumulative discharge for the hydrologic year 2003/2004 in S and V starting in October.....	85
Figure 4-19: Relative mass fluxes for the measured parameters from October 2002 until September 2004 at site V.....	87
Figure 4-20: Rainfall for September, October and December of 2003.....	90
Figure 4-21: Distribution of phosphorus loads for the years 2002/2003-2003/2004, particulate phosphorus and soluble reactive phosphorus.....	91
Figure 4-22: Distribution of forms of nitrogen loads over the years 2002/2003-2003/2004.....	91
Figure 4-23: Rainfall at the weather station Mas Plagnol and flow at station S during two significant events in the Vène catchment.....	93
Figure 4-24: Normalized cumulative flow and rainfall for the two events.....	95
Figure 4-25: Weighting of the three sites K, S and V for the main parameters for the event 2003-09-22.....	96
Figure 4-26: Concentrations and loads of particulate parameters of Sanglier (S) and Poussan (V) for 2003-09-22.....	97
Figure 4-27: Concentration and loads of nitrogen parameters of Sanglier (S) and Poussan (V) for 2003-09-22.....	98
Figure 4-28: Concentrations and loads of phosphorus parameters of Sanglier (S) and Poussan (V) for 2003-09-22.....	99
Figure 4-29: Concentrations and loads of particulate parameters of Sanglier (S) and Poussan (V) for 2004-09-13.....	100
Figure 4-30: Concentrations and loads of nitrogen parameters of Sanglier (S) and Poussan (V) for 2004-09-13.....	101
Figure 4-31: Concentrations and loads of phosphorus parameters of Sanglier (S) and Poussan (V) for 2004-09-13.....	102
Figure 4-32: Comparison of concentrations of particulate phosphorus and volatile suspended solids for the flood of 2004-09-13.....	102
Figure 4-33: NCL-plot of 2003-09-22 for points S and V - normalized cumulative loads against normalized cumulative discharge.....	103
Figure 4-34: NCL-plot of 2004-09-13 for points S and V - normalized cumulative loads against normalized cumulative discharge.....	105
Figure 4-35: Conductivity against flow at four different sites of the catchment.....	107
Figure 4-36: Conductivity for both floods at S and V.....	108
Figure 4-37: Rating of flushes for the site S on September 2003 and 2004 events.....	109
Figure 4-38: Relationship between flow and concentration of TSS at station S.....	111
Figure 4-39: Relationship between flow and concentration of VSS at station S.....	112
Figure 4-40: Relationship between flow and concentration of TP at station S.....	112
Figure 4-41: Relationship between flow and concentration of NO <sub>3</sub> -N at station S.....	113
Figure 4-42: Relationship between flow and load of TSS at station S.....	113
Figure 4-43: Relationship between flow and load of VSS at station S.....	114
Figure 4-44: Relationship between flow and load of NO <sub>3</sub> -N at station S.....	115
Figure 4-45: Location of the Mulargia catchment on the Island of Sardinia.....	116
Figure 4-46: Mulargia stream flow statistics of the years 1992-2004.....	116
Figure 4-47: Elevation, point sources and weather stations in the Mulargia catchment.....	117
Figure 4-48: Distribution of measurements over flow intensity in the Mulargia.....	118
Figure 4-49: Mean monthly and normalized cumulative precipitation on basis of data from September 1991 to August 1998 at the Mulargia.....	119

---



Figure 4-50: Pollutographs at site B of the events 2003-10-17 and 2003-10-22 for particulate properties.....	120
Figure 4-51: Pollutographs at site B of the events 2003-10-17 and 2003-10-22 for properties associated with carbon.....	121
Figure 4-52: Pollutographs at site B of the events 2003-10-17 and 2003-10-22 for properties associated with nitrogen.....	122
Figure 4-53: Pollutographs at site B of the events 2003-10-17 and 2003-10-22 for properties associated with phosphorus.....	123
Figure 4-54: Pollutographs at site B of the events 2003-10-17 and 2003-10-22 for properties associated with phosphorus.....	124
Figure 4-55: Pollutographs at site B of the events 2003-11-20 for particulate and phosphorus properties.....	125
Figure 4-56: Pollutographs at site B of the events 2003-11-20 for Nitrogen, temperature, pH and conductivity.....	126
Figure 4-57: Pollutographs at site B of the event 2003-11-27 for particulate and phosphorus properties.....	127
Figure 4-58: Pollutographs at site D of the event 2003-11-27 for particulate and phosphorus properties.....	128
Figure 4-59: Pollutographs at site D of the events 2003-11-27 for Nitrogen, temperature, pH and conductivity.....	129
Figure 4-60: NCL plot for the period from 2003-10-17 06:00 to 2003-10-21 14:00 for site B.....	130
Figure 4-61: NCL plot for the period from 2003-10-21 14:00 to 2003-10-24 00:00 for site B, recession limb approximated.....	130
Figure 4-62: NCL plot for the period from 2003-11-20 19:00 to 2003-11-22 02:00 for site B.....	131
Figure 4-63: NCL plot for the period from 2003-11-27 13:00 to 2003-11-27 21:00 for site B.....	132
Figure 4-64: NCL plot for the period from 2003-12-03 10:00 to 2003-12-06 04:00 for site B.....	132
Figure 4-65: Digital elevation and weather stations at the Albuji3n.....	134
Figure 4-66: Pollutographs of the flood of 2003-10-17.....	136
Figure 4-67: NCL-plot of the flood of 2003-10-17.....	137
Figure 4-68: Pollutographs of the flood of 2003-11-19.....	138
Figure 4-69: NCL-plot of the flood of 2003-11-19.....	138
Figure 4-70: Pollutographs of the event at 2004-04-15.....	139
Figure 4-71: NCL-plot of the flood of 2004-04-16.....	140
Figure 5-1: Spatial discretisation and DEM of the V3ne in MOHID-GIS, grid width 50m.....	142
Figure 5-2: Methodology for calibration and validation of the model.....	143
Figure 5-3: Measured and simulated concentrations (scenario 1, “all”) at site S for the years 2002-2004 for particulates and dissolved inorganic nitrogen.....	146
Figure 5-4: Measured and simulated concentrations (scenario 1, “all”) at site S for the year 2002-2004 for inorganic phosphorus, particulate (organic) phosphorus and (particulate) organic nitrogen.....	147
Figure 5-5: Accumulation of VSS downstream the outlet of a WWTP at site d.....	148
Figure 5-6: Loadings during the event of 2003-08-17 for VSS in sites S and V.....	149
Figure 5-7: Measured and simulated concentrations at Sanglier (S) for 2003-09-22, Scenario “all” for particulates and dissolved inorganic nitrogen.....	153
Figure 5-8: Measured and simulated concentrations at Sanglier (S) for 2003-09-22, Scenario “all” for inorganic phosphorus, particulate (organic) phosphorus and (particulate) organic nitrogen.....	154
Figure 5-9: Measured and simulated concentrations at Sanglier (S) for 2004-09-13, Scenario “all” for particulates and dissolved inorganic nitrogen.....	155
Figure 5-10: Measured and simulated concentrations at Sanglier (S) for 2004-09-13, Scenario “all” for inorganic phosphorus, particulate (organic) phosphorus and (particulate) organic nitrogen.....	156
Figure 5-11: Comparison of normalized cumulative loads of measured TSS and all scenarios at S for 2003-09-22.....	159
Figure 5-12: Comparison of normalized cumulative loads of measured VSS and all scenarios at S for 2003-09-22.....	160

---

Figure 5-13: Comparison of normalized cumulative loads of measured NO <sub>3</sub> -N and all scenarios at S for 2003-09-22 .....	161
Figure 5-14: Data simulated with variant "all" over measured data.....	162
Figure 7-1: Runoff over rainfall for the events from 2002-2004.....	174
Figure 7-2: Variation of the Manning coefficient for the event of 2003-09-22 at site S.....	175
Figure 7-3: Calibration of hydraulic conductivity of the channel bed at site S for the flood of 2003-09-22 .....	176
Figure 7-4: Calibration of hydraulic conductivity of the channel bed at site S in for the flood of 2003-04-19.....	176
Figure 7-5: Absolute monthly loadings of VSS for the 2002-2004 at site S.....	177
Figure 7-6: Absolute monthly loadings of TSS for the 2002-2004 at site S.....	177
Figure 7-7: Absolute monthly loadings of NO <sub>3</sub> -N for the 2002-2004 at site S.....	177
Figure 7-8: NCL- plots for measured TSS and all scenarios at sites K and S for 2003-09-22.....	178
Figure 7-9: NCL- plots for measured VSS and all scenarios at sites K and S for 2003-09-22.....	179
Figure 7-10: NCL- plots for measured NH <sub>4</sub> -N and all scenarios at sites K and S for 2003-09-22 .....	180
Figure 7-11: NCL- plots for measured NO <sub>3</sub> -N and all scenarios at sites K and S for 2003-09-22 .....	181
Figure 7-12: Sensitivity of NCL plots, comparison between two different periods of the of the same dataset at S.....	182
Figure 7-13: Demonstration of the influence of low flow variations on the regression of concentrations .....	183
Figure 7-14: Interaction of pool volume, inflow and outflow .....	185
Figure 7-15: Effluent of the WWTP – situation in a typical model.....	186
Figure 7-16: Flow chart for pool generation.....	187
Figure 7-17: Network structure of the test cases .....	188
Figure 7-18: Characterization of networks and tested flood intensities.....	188
Figure 7-19: Scheme of fluxes at a reach segment .....	189
Figure 7-20: Resulting error in mass stored in an accumulation reach .....	190
Figure 7-21: Situation in the pool at the transition phase from “no-flow” to “flow” condition .....	191
Figure 7-22: Development of concentration (conservative tracer) in a pool after flush of clear water.....	192
Figure 7-23: Parameter in the Variable Parameter Muskingum-Cunge method (VPMC).....	193
Figure 7-24: Development with a linear gradation of concentration as starting conditions .....	194
Figure 7-25: Expected development in an advection scheme without dispersion.....	195
Figure 7-26: PON dynamics in the tempQsim - STREAM model.....	199
Figure 7-27: Bacteria dynamics in the tempQsim - STREAM model.....	200
Figure 7-28: Variation of the runoff coefficient c in the delivery model without retention for 2003-09-22 .....	209
Figure 7-29: Variation of the runoff coefficient c in the delivery model with retention of a 3 linear storage cascade with storage constant = 53 min for 2003-09-22.....	210
Figure 7-30: Variation of the runoff coefficient c in the delivery model with retention of a 3 linear storage cascade with storage constant = 53 min for 2003-04-19.....	211
Figure 7-31: Simulation with input of measured flow from S upstream from d for 2003-09-22.....	212
Figure 7-32: Variable runoff concentrations depending on antecedent dry day period and actual rainfall intensity for September 2003.....	215
Figure 7-33: Variable runoff concentrations depending on antecedent dry day period and actual rainfall intensity for September 2004.....	215
Figure 7-34: Results of the adoption of runoff concentrations for the event at 2003-09-22.....	216
Figure 7-35: Results of the adoption of runoff concentrations for the event at 2004-09-13.....	217
Figure 7-36: Picture of the Vène at site d, directly downstream the WWTP outlet in July 2004 (left) and October 2004 (right) .....	218
Figure 7-37: Picture of the Vène ca. one kilometre downstream site d, directly downstream the WWTP inflow at July 2004 (left) and October 2004 (right) .....	219

---

---

## LIST OF TABLES

---

Table 2-1: Classification of aridity according to (UNEP, 1997).....	16
Table 2-2: Definitions of a first-flush.....	28
Table 2-3: Boundaries of classification approaches for first flushes .....	36
Table 3-1: Considered state variables in HSPF .....	55
Table 3-2: Possible state variables in CASCADE.....	60
Table 3-3: Considered state variables in the tempQsim – STREAM model.....	63
Table 4-1: Pearson correlation between the constituents and flow resp. rain at Montbazin for monthly values for the period 2002-2004.....	83
Table 4-2: Relative mass flux for October 2002 until September 2003 .....	88
Table 4-3: Relative mass flux for October 2003 until September 2004.....	88
Table 4-4: Comparison of transport activity for three autumn months 2003.....	89
Table 4-5: Basic flow data of the two floods .....	94
Table 4-6: Basic rainfall data for the two floods .....	94
Table 4-7: Summary of the floods for the Vène at site S .....	95
Table 4-8: FF <sub>25</sub> for the all events at station B.....	133
Table 4-9: Summary of the floods for El Albujión.....	135
Table 5-1: Scenarios applied to the Vène .....	144
Table 5-2: Absolute monthly loadings of VSS for the year 2002/2003 at site S.....	150
Table 5-3: Monthly percentage of VSS loads in terms of the year 2002/2003 at site S.....	151
Table 5-4: Absolute monthly loadings of VSS for the year 2003/2004 at site S.....	152
Table 5-5: Loads of VSS for September 2003 and 2004 at site S, total values and percentages in terms of scenario 1 .....	157
Table 5-6: Loads of TSS for September 2003 and 2004 at site S, total values and percentages in terms of scenario 1 .....	158
Table 5-7: Loads of NO <sub>3</sub> -N for September 2003 and 2004 at site S, total values and percentages for scenario 1 .....	159
Table 5-8: Correlation simulated and measured concentration at the Vène catchment for the years 2002-2004, point S.....	163
Table 7-1: Mass balance calculation for VAR1 with CASCADE .....	197
Table 7-2: Mass balance calculation for VAR2 with CASCADE .....	198

**LIST OF ACRONYMS**

---

ADD	Antecedent Dry Days
ADWP	Antecedent Dry Weather Period
AI	Aridity Index
ARM	Agricultural Runoff Management
ASCE	American Society of Civil Engineers
ASM3	Activated Sludge Model No. 3
BASINS	Better Assessment Science Integrating Point Sources
COND	Conductivity
DO	Dissolved Oxygen
DOC	Dissolved Organic Carbon
DON	Dissolved Organic Nitrogen
EPA, US EPA	U.S. Environmental Protection Agency
EU	European Union
FDM	Finite Difference Method
FEM	Finite Element Method
FVM	Finite Volume Method
HSPF	Hydrologic Simulation Program – FORTRAN
IRD	Institut de recherche pour le développement
KN	Kjeldahl Nitrogen
L	SI unit of Length
M	SI unit of Mass
MENA	Middle East and North Africa
MSE, MSEM	Maison des Sciences de l'Eau Montpellier
NCF	Normalized Cumulative Flow
NCL	Normalized Cumulative Load
NH <sub>4</sub> -N	Ammonium Nitrogen
NO <sub>2</sub> -N	Nitrite Nitrogen
NO <sub>3</sub> -N	Nitrate Nitrogen
NO <sub>x</sub> -N	Nitrate and Nitrite Nitrogen
NPSM	NonPoint Source Model
orgN	Organic Nitrogen
PDE	Partial Differential Equations
POC	Particulate Organic Carbon
PON	Particulate Organic Nitrogen
POP	Particulate Organic Phosphorus
PP	Particulate Phosphorus
RMF	Relative Mass Flux
RMSE	Root Mean Square Error
SAE	System of Algebraic Equations
SERATRA	Sediment and Radionuclides Transport
SRP	Soluble Reactive Phosphorus
T	SI unit of Time
TDN	Total Dissolved Nitrogen
TMDL	Total Maximum Daily Loads
TN	Total Nitrogen

---

TOC	Total Organic Carbon
TP	Total Phosphorus
TSS	Total Suspended Solids
UNEP	United Nations Environmental Programme
USACE	U.S. Army Corps of Engineers
USGS	U.S. Geological Survey
VSS	Volatile Suspended Solids
WFD	Water Framework Directive
WWTP	Waste Water Treatment Plant

## 1 Introduction

---

Knowledge about the nature of droughts and the functioning of ecosystems which are affected by extended dry periods is still rudimentary (Humphries and Baldwin, 2003). There is a rising awareness, that droughts are important events in many natural systems and that their removal can be even more harmful than their occurrence. However, the majority of rivers in Europe is already heavily altered and far away from their natural state, which is often unknown or difficult to define. In regions where anthropogenic pressures are high, where intensive agriculture, industry and the existence of sewage water inflows exist, there is a need for measures to mitigate the impact in these sensitive ecosystems, especially in the transition period just before or during the early rainy season.

The implementation of the EU Water Framework Directive requests a more adapted understanding of processes in water quality and ecosystem functioning, an adequate monitoring and the specific design of management options. It is well known, that temporary streams form an important part of Mediterranean basins (e.g. Bull and Kirkby, 2002), but the occurrence of first flush effects in such water bodies is still poorly understood. The comparison of effects is hindered, as long as no suitable methods and criteria are available (Obermann et al., 2006).

This work aims at (i) the development of new methods allowing an enhanced analysis of temporary streams and (ii) the improvement of a water quality model, which is able to simulate the important fluctuations of nutrients in these systems. For this purpose, common approaches are reviewed and tested during real applications on Mediterranean basins.

### ***Recent and current awareness in the field of temporary waters and dryland rivers***

There already have been many investigations about the so called first flush effect, especially regarding metal accumulation and loading distribution in urban catchments (Sansalone and Buchberger, 1997), pollutant loadings of various other parameters during first flush events in urban areas (Deletic, 1998; Larsen et al., 1998; Lee and Bang, 2000; Stenstrom and Kayhanian, 2005) and on small paved transportation catchments (Sansalone and Cristina, 2004). Some were focused on the particle size distributions from highway runoff (Li et al., 2005), others investigated in detail the seasonal variations (Lee et al., 2004). A lot of work has been done in separate or combined sewer systems (Bertrand-Krajewski et al., 1998; Gupta and Saul, 1996; Saget et al., 1996).

Apart from these smaller basins, there have been studies for large catchments either with an annual reoccurrence of flushes (Parks and Baker, 1997), more or less regular regimes (Alexandrov et al., 2003) or with unpredictable, long dry spells over periods of years (Bunn et al., 2006). These studies underlined the importance of organic matter build-up and retention as well as the significance of variations of source areas of particulates.

Attempts were made to describe flushes with third polynomial equations (Lee et al., 2003), to define it in terms of water volumes (Epa, 1993), in terms of normalized cumulative loads

---

(Bedient et al., 1978; Geiger, 1984; Geiger, 1987) as well as in the percentage of load transported with the first percentage (often 20%) of runoff (Saget et al., 1996; Vorreiter and Hickey, 1994).

Additionally, the spatial and temporal dynamics of diffuse pollution of surface waters (Donohue et al., 2005) and spatial distributions of nitrogen and phosphorus loads in a Mediterranean river (Tournoud et al., 2005) have been studied before. Nutrient retention in arid watersheds (Welter et al., 2005) and floodplains (van der Lee et al., 2004) as well as the dynamics in riverine biofilms (Baldwin et al., 2006) were shown to be important drivers in these systems. In combination with the complexity of phosphorus precipitation in arid environments (Carreira et al., 2006) and the increased variability in nitrogen releases from sediments before and after droughts (Baldwin et al., 2005), these aspects make clear, that there is no simple relationship of flow (or rain) and flux of nutrients respective pollutants.

Further problems arise from the fact that data collection in catchments in semi-arid or arid regions is always difficult. Only sophisticated measuring concepts, operated over years may provide sufficient data necessary to understand the system and to allow a model calibration for further prognosis. Even where long term studies exist e.g. for small, sparsely vegetated catchments with steep gradients in the Spanish Pyrenees (Belmonte and Beltran, 2001; Gallart et al., 2002) or for the Southern Judean Desert in Israel (Hai Cohen, 2005), they are often restricted to only hydrological or sediment issues and their results are very specific which hinders transferability to other regions.

The help of modern modelling software may be a promising aid in this effort, but modelling of temporary rivers is a complex multi-dimensional task. Different temporal scales have to be considered, ranging from long term accumulation periods in the order of months or years to the finer scale during the onset of the transporting (flow) period whose most important period may not last more than hours or days. Spatial issues play a role especially in fluxes for particulates: hot spots of concentrated matter, built up during the dry period, can be successively transported downstream. While those are passing a measuring site the concentration will change most likely. But if there is no dense network of measuring stations in the river, it cannot be verified, if this is just a local phenomenon. So in terms of the influence on downstream water bodies, there remains a high degree of uncertainty.

Instream concentration of pollutants depends on the complex interaction of dissolved and particulate nutrients and their consumers. During the dry period, turnover rates, mostly directly bound to concentration values, are very sensitive to even minor inflows which disturb the settled, equilibrium system.

Models have been already developed for more humid environments e.g. for processes of nutrient retention of lowland river-lake systems (Kneis et al., 2006; Venohr et al., 2005) or phosphorus retention and spatial variation (Gelbrecht et al., 2005). Further, models were built especially addressed to first flushes on urban zones (Deng et al., 2005) or for suspended solids wash-off loadings from impervious surfaces (Deletic et al., 1997).

Simulations were already applied for the Thau lagoon in France to evaluate long term nutrient balances (Chapelle, 1995; La Jeunesse et al., 2002), also taking into account the simulations of the delivering rivers (Plus et al., 2006).

Based on the framework of the MOHID Water Modelling System, described e.g. in Miranda et al. (2000) or Trancoso et al. (2005), a new model was developed during the European project tempQsim. This tempQsim – STREAM model was applied to reproduce the instream processes in a medium time scale.

### ***Focus of the following work***

The following work aims at the continuation of the prior effort following two main goals: (i) the analysis of the dynamic of nutrient and pollutant transport in medium-sized agricultural, semi-arid catchments and (ii) the modellisation of these systems with the help of a newly developed and adopted state-of-the-art water quality models.

After a small introduction to the topic by giving a synopsis of the prior work, chapter 2 deals with methods, which can be applied to investigate temporal variation in nutrient concentrations and loadings. Some important definitions are given, and the general nature of semi-arid watersheds is explained with special focus on first flush dynamics. The methods of normalized cumulative loadings (NCL) are explained along with some normally used indexes for the characterization of nutrient transport. Based on available approaches, new indexes are proposed and a new method for the identification of periods with high nutrient transport is derived: the method of relative mass fluxes (RMF).

The theory of water quality models is then subject in chapter 3. A short and general introduction of the most important approaches and formulas used in current models is followed by the characterisation of the herein discussed models HSPF, CASCADE and tempQsim – STREAM. Because of extensive data need and the unavailability of the source code of HSPF, only the latter two were considered in the extension and testing. Further, due to limitations in mass balance and pre- and post processing capabilities of CASCADE, the tempQsim – STREAM model was developed in the context of the European project tempQsim (EVK1-CT2002-00112). The work presented comprises in particular in the development of an approach for the accumulation of biomass accumulation caused by heterotrophic bacteria and the transport of fractioned sediments in order to allow the storage of particulates at the top sediment layers during the dry period.

The application of the methods explained in chapter 2 is shown for three catchments in chapter 4. After a brief presentation of the corresponding rivers, the observed data is discussed at two different scales: an annual scale aiming at the annual fluctuation and an event scale during the first significant flood events. While the methods are applied on both of these scales to identify the nutrient transport regime, they are also briefly discussed and valued in terms of their usability. Floods occurring at the beginning of the flow season are compared to later events.

In order to test the modifications and to get deeper insights in the system function of temporary rivers, a detailed application of the tempQsim – STREAM model at the Vène is discussed in

---



chapter 5. A set of 11 scenarios were chosen to analyse important processes under consideration of the proven methods shown in chapter 2. The model was calibrated on data of the year 2002/2003 and later validated on the following year for flow and the main water quality variables. The idea of two differing scales was taken up in the discussion of the simulation results. In order to account for varying concentrations in overland runoff depending on the system wetness, two methods for the enhancement for the rainfall-runoff model parts of water quality models are proposed.

The work closes with a summary, concluding the added value to knowledge in investigation and modellisation in semi-arid regions as well as the remaining unsolved subjects and a possible perspective of future research.

## 2 Methods to describe the particularity of Mediterranean catchments

The following paragraphs are dedicated to the particular characteristics of Mediterranean watersheds as a special case for drylands. The herein used terms will be defined and some important mechanisms in temporary waters will be explained. The second part considers the phenomenon of first flushes and the methods to describe them.

### 2.1 General definitions and functioning of temporary waters

#### 2.1.1 *Definition of aridity*

A variety of schemes have been developed to classify aridity of climate zones, each aiming at other targets as e.g. food production, water-supply or geomorphology. Generally, they are based on the balance of the main drivers precipitation and evapotranspiration and they most often include subdivisions as semi-arid, arid and hyper-arid, based on a scale of increasing aridity.

Arid zones are those where evapotranspiration exceeds precipitation. Unlike in humid environments, amount of rainfall alone is not the most dominating control.

An example of a widely applied classification is the one provided by the United Nations (UNEP, 1997).

Table 2-1: Classification of aridity according to (UNEP, 1997)

AI = N/V	category	global land area
< 0.05	hyper-arid	7.5 %
0.05 – 0.20	arid	12.1 %
0.20 – 0.50	semi-arid	17.7 %
0.50 – 0.65	dry-subhumid	9.9 %
	total	47.2 %

It uses the aridity index AI as the ratio of annual precipitation to potential annual evapotranspiration derived from meteorological data. The classification of the index is shown in Table 2-1.

#### 2.1.2 *Correlation coefficients*

As for perennial rivers, the strength of correlations between flow and concentrations or loads of observed and modelled values can be investigated by many different parameters. Two of the most common will be presented below and used in this work.

### 2.1.2.1 Regression and correlation

Regression searches for the type of the relationship of two or more variables, whereas correlation addresses the degree and direction of the relationship. If there is assumed e.g. a linear relationship between two variables, the regression analysis can be used to find the type of the linear function which approximates the relation best, and the correlation analysis gives information, whether the assumption of the relationship (here linearity) was justified or not.

### 2.1.2.2 Pearson Product-Moment Correlation Coefficient

The Pearson correlation coefficient  $r_{xy}$  can be calculated for two variables by the division of the covariance of the variables by the product of their standard deviations

$$r_{xy} = \frac{\sum_{i=1}^N (y_i - y_m)(x_i - x_m)}{\sqrt{\sum_{i=1}^N (y_i - y_m)^2 \sum_{i=1}^n (x_i - x_m)^2}} \quad \text{EQ. 2-1}$$

where

N:	number of values
$x_m$ :	mean of the observed values
$y_i$ :	simulated value at time i

It is a measure of the degree of linear association between two or more variables and represents the amount of variability that is explained by another variable.

Depending on the strength of the linear relationship, the  $r_{xy}$  can vary from -1 to 1, with 1 indicating a perfect positive linear relation (the bigger x, the bigger y) and -1 indicating a perfect opposing relation (the bigger x, the smaller y) between observed and predicted values.

### 2.1.2.3 Nash-Sutcliffe efficiency

This parameter was presented in (Nash and Sutcliffe, 1970) and was recommended by ASCE (1993) to be used in hydrological studies.

$$E = 1 - \frac{\sum_{i=1}^N (x_i - y_i)^2}{\sum_{i=1}^N (x_i - \bar{x})^2} \quad \text{EQ. 2-2}$$

Values equal to 1 indicate a perfect fit between observed and simulated data, whereas values equal to 0 indicate that the model is predicting no better than using an average distribution. Any positive value above 0 suggests therefore that the model has some utility, with higher values indicating better model performance.

## 2.1.3 Definition of temporary waters and dryland rivers

The hydrological response of catchments in arid or semiarid regions is characterised by features not seen in perennial flow. These features require particular attention during data analysis and especially in the application of hydrological models. Figure 2-1 shows examples for the differences in the flow regimes and some consequences.

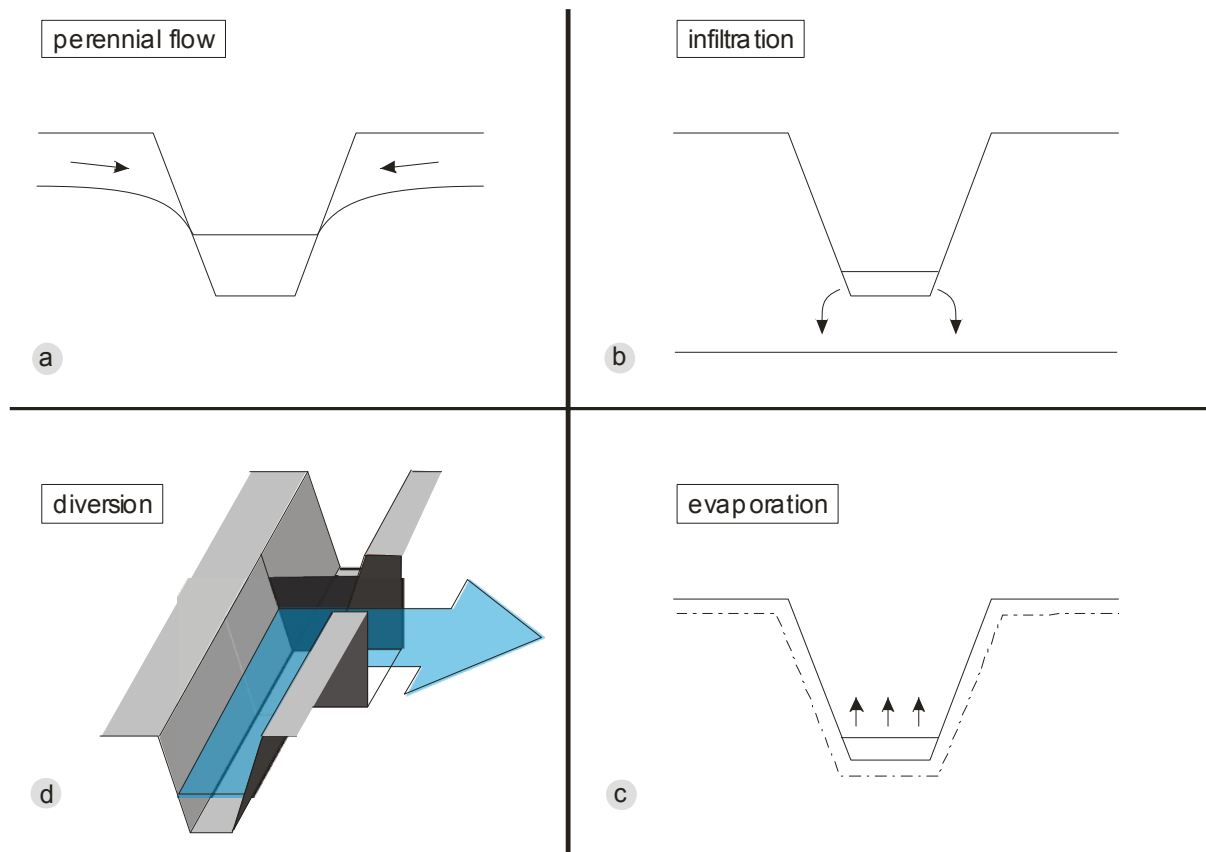


Figure 2-1: Examples for different flow conditions

Perennially flowing rivers in humid areas (a) typically receive water from the surrounding landscape with sufficient regularity. These inflows are normally much smaller semi-arid regions. In many rivers with deeper groundwater, a great quantity of water is lost through the river bed (b). With high temperatures and direct solar radiation the flow may also be depleted significantly by evaporation (c). In some cases, transmission losses may lead to complete drying up of the river. In low flow situation, it may be even diverted, if there are essential elevation differences in the river bed (d). In other situations, the river may be reduced to a sequence of pools, with hydrological contact only through seepage within the river bed. These natural phenomena are normally further altered by anthropogenic influences as e.g. abstractions, point sources, agricultural practices or constructions which modify the stream.

The classification of streams in terms of their aridity is clearly a topic of its own. Even the general terms dryland river (climatic definition) and temporary river (definition concerning the time-dependent dynamics) often lack clear distinction.

There are studies referring to the groundwater connection of a river (see e.g. Neitsch et al., 2002), to the time in which flow is present during the year (Matthews, 1988), to the climatic conditions (Bayly and Williams, 1973; Davies et al., 1994).

Generally, streams can be classified into

- *ephemeral*: flowing briefly and rarely, contain water during and immediately after a storm event, dry the rest of the year, normally only sourced by precipitation,
- *intermittent*: flow occasionally, dry for part of the year, but contain flow when groundwater is high enough or during and after a storm event,
- *perennial*: flow continuously, receive continuous groundwater contributions and flow throughout the year.

There is a continuous progression from perennial streams to ephemeral streams which makes a clear distinction difficult. Even if lower reaches of streams in humid regions rarely or never cease flowing, almost every year many of their upstream parts run dry. A more intensive review of terms as indicated in Figure 2-2 can be found in Uys and O’Keeffe (1997).

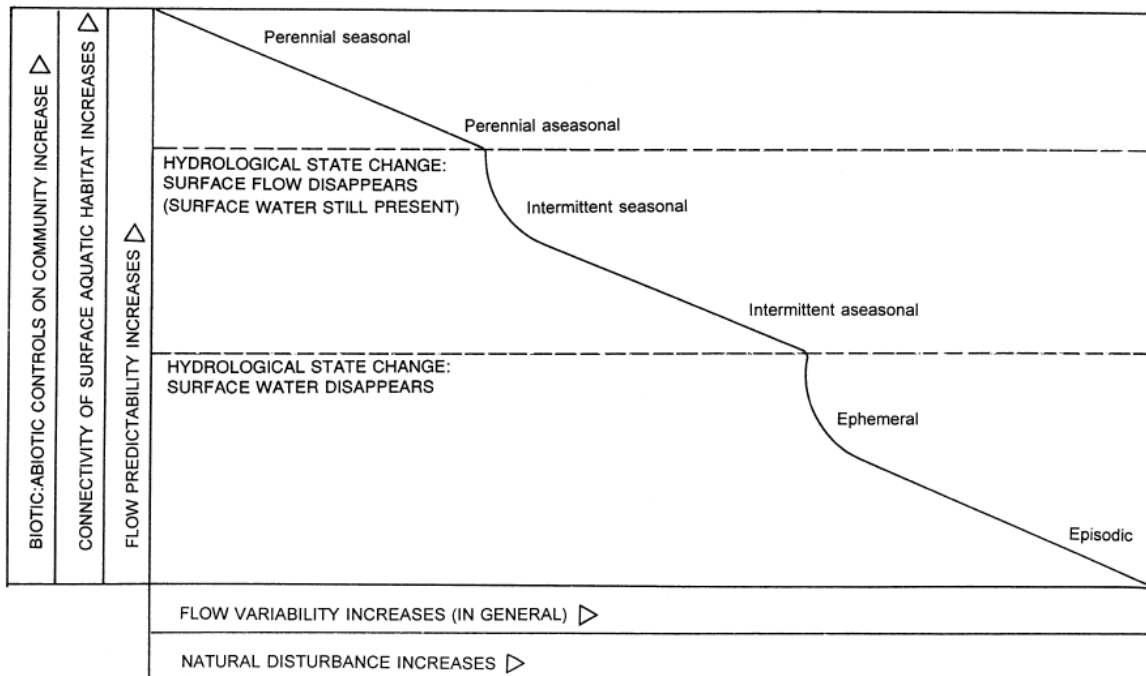


Figure 2-2: Classification of stream in terms of aridity (Uys and O’Keeffe, 1997)

Besides the impact of climatic variations, the flow variability will generally increase, if the channel bed is build up of impermeable bedrock, because in- or exfiltration smoothes rapid changes. Basins in karstic areas usually imply variability, as they often posses streams that are spatially intermittent. Furthermore, they also contain temporally intermittent streams (even if there is no groundwater connection) which only flow when heavy rain raises the water table and reactivates karstic springs.

In general, variations in flood magnitudes are much larger than experienced for perennial rivers, and the discharge of the largest flood is very much larger than the mean flood discharge (McMahon, 1979). In humid regions such as Pennsylvania, USA, the discharge of the 50-year flood can be about 2.5 times the discharge of the mean annual flow (Wall and Englot, 1985),

whereas the one of the Gila River in Arizona is about 280 times the mean annual flow discharge (Graf, 1988).

Most of the conventional modelling tools for watersheds were designed for continuous flow conditions. The often deviating situation in more arid catchments leads to several problems:

- consequences of the drying up process on biota and accumulation processes are not considered,
- spatial and temporal variation of storm events is more important in semiarid regions due to the relatively higher intensity and lower reoccurrence interval of precipitation,
- there are no features in post-processing modules for the analysis of temporary waters,
- accumulation processes have higher impact; accumulation is advantaged in the dry periods and leads to high gradients during floods.

It is clear that dryland hydrology cannot be predicted by extrapolation of humid region hydrology (McMahon, 1979; McMahon et al., 1987) and further, that there are additional demands to models applied to these regions.

#### *2.1.4 Importance of transmission and evaporation losses*

An important feature of dryland rivers is the usually great influence of evaporation and infiltration. Whereas in humid regions discharge tends to increase in downstream direction, flow can decrease in dryland rivers.

Normally, instream evaporation is an order of magnitude lower than infiltration. The more the flow or the volume in the river section decreases, the more important evaporation becomes. Examples for approaches to estimate transmission losses in arid rivers can be found e.g. in Jordan (1977), Lane (1982), Sharma and Murthy (1994) or Walters (1990).

The effects of transmission losses are various: the channel flow is disconnected and aggradation of particulate matter as sediment or organic matter is favoured.

Infiltration reduces not only the water volume stored in a pool or reach, but also reduces total mass of solubles, which are lost from the surface system. Evaporation increases concentration of all constituents, but leaves the total mass in a reach or pool unchanged.

Also linked to transmission losses is the ability of floodplains to retain large quantities of particulate matter until the next strong event removes this depot (e.g. see Pickup, 1991).

#### *2.1.5 Interruption of flow and interaction of events*

As mentioned before, there is not only a temporal variation in flow, but of course also a spatial one. So even during a rain event, the flow may be discontinuous, e.g. when rainfall is highly variable in space. Two cases can be distinguished, see Figure 2-3.

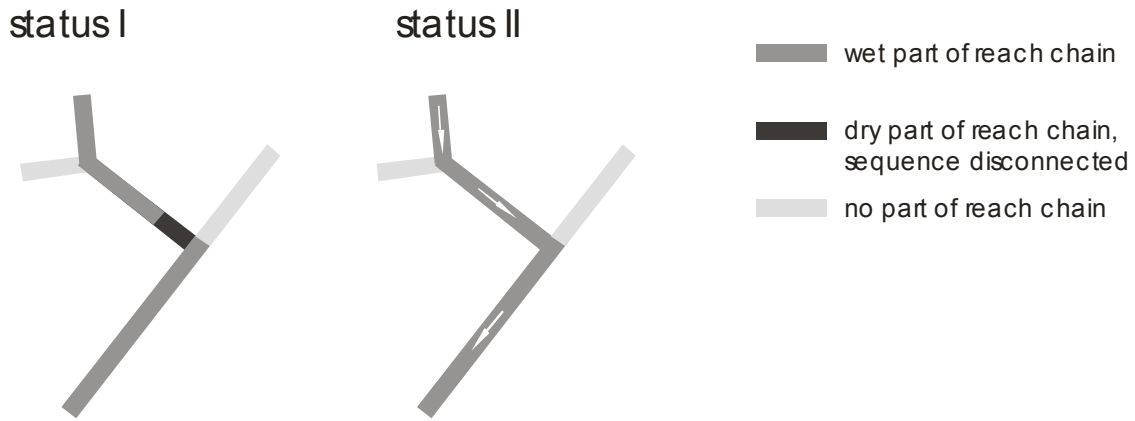


Figure 2-3: Explanation of the reach chain (flow path)

The state of the system is mainly affected by the intensity and duration of an event and the magnitude of the transmission losses (driven by the hydraulic conductivity of the soil, bank storage and potential evaporation).

#### 2.1.6 *Definition of a reach chain*

In order to distinguish between the effects of different events, the term *reach chain* is introduced. A reach chain can be defined as a sequence of channels which are connected to each other in a downstream direction for the duration of one event. Two main states of the system can be identified:

1. *events affecting only parts of the reach chain*: the chain is not closed so that accumulation is likely; during these events, the mass of accumulation spots may be displaced further downstream but remains within the channel network.
2. *events affecting the whole reach chain*: local sediment and nutrient storages can drain and cause a sudden flush.

#### 2.1.7 *Definition of flow threshold*

For the data analysis and interpretation as well as planning of measurement campaigns, it may be useful to assign the effective runoff of events in terms of their rainfall intensity and/or duration (cp. Figure 2-4) to the classes in the definition above.

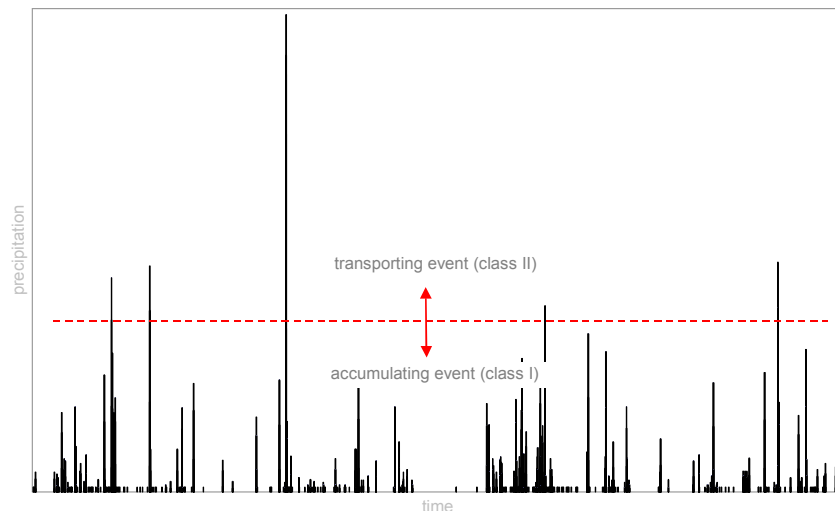


Figure 2-4: Possible event classification

In this definition, vents of class I are not sufficient to produce significant flow at the whole river length and cause the system to be in status I (Figure 2-3), whereas larger events of class II will cause a status II. This could help to estimate reoccurrence intervals of transporting events and gives some information about the possibility to manage the system.

#### 2.1.8 Sources of accumulation

In low flow situation, the flow regime is often dominated by the interaction of discharges from point sources and by transmission losses. A significant accumulation of organic matter during the summer months may occur due to the effluents of wastewater treatment plants (WWTP, see chapter 7.12).

During late spring and summer, the river can progressively dry up until only separated pools remain. If these pools are neither interconnected nor any one is connected to the outlet through surface flow there will be an excessive supply of nutrients and therefore a potential for significant growth of biomass in these sites.

#### 2.1.9 Mode of accumulation and resuspension

Accumulation normally takes place during status I or similar conditions, when precipitation or other sources are insufficient to produce uninterrupted discharge on the whole length of the river. Great quantities of water then infiltrate, evaporate or are temporarily stored and the flow path is disconnected in downstream direction (cp. Figure 2-5).



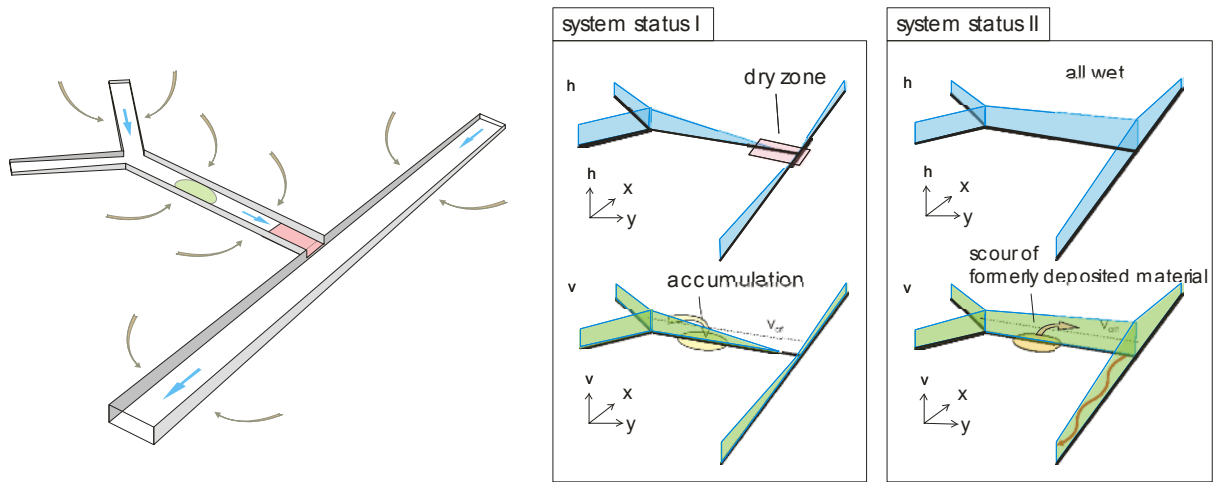


Figure 2-5: Channel chain - process of accumulation and resuspension

At some point between entering the channel and the dry zone, the velocity may fall below a critical value and particulate substances are deposited.

Resuspension will then take place during the next transporting event (class II), which often occurs in early autumn or late summer in Mediterranean climates.

The instantaneous release of formerly retained matter is a special and very important mechanism which only occurs to this extent in temporary rivers and is often called *first flush effect*.

## 2.2 The first-flush phenomenon

The term *first-flush* was in the past mainly used in the context of urban hydrology and referred to a disproportionate increase of particulate materials (in terms of concentration or load) in the rising limb of a flood event. But as shown in Krebs et al. (1999), there are also effects which may cause an initial peak in loads for even dissolved compounds. If a combined sewer, which is not totally dry but contains polluted water, is flooded with rain water of low pollution, an increase of mass flux of dissolved materials can be observed. This “wash-out effect” is caused by a wave of waste water formed downstream of the front of the rapidly entering rain water. This wave travels faster than the water flow and retains its original concentration, but leads to a flow rate increase of dissolved matter, which is proportional to the flow rate increase in the worst case (Krebs et al., 1999). Figure 2-6 shows this in the first variation and explains two general possibilities for shape of the pollutographs in a combined sewer: the transport of dissolved material and the transport of suspended particulate materials.

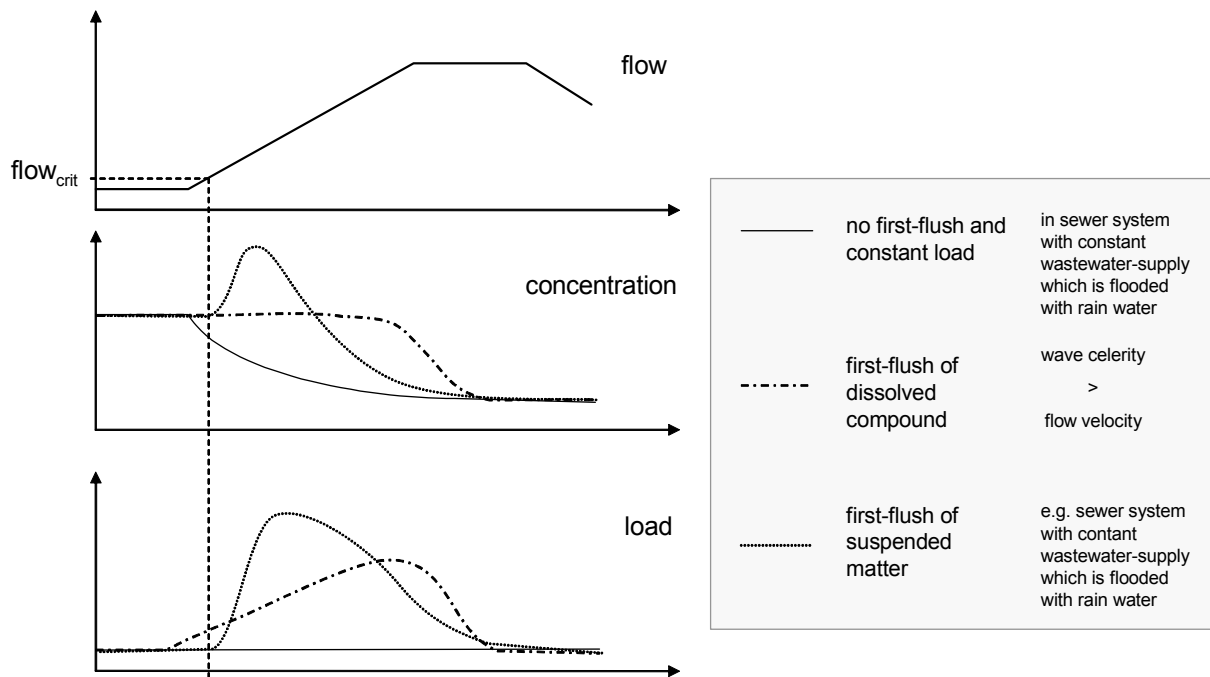


Figure 2-6: Forms of first-flushes from different origin (based on Krebs et al. (1999), modified)

The second plot in Figure 2-6 shows the reaction of the concentration on the flow rate increase, the third plot the reaction of the load. The continuous line represents the normally expected curve including dilution and excluding any celerity effects.

For dissolved compounds (first variation, dash-dotted line), the concentration will stay constant for a certain time before the fresh (rainfall-) discharge starts dilution. Due to the increase in flow rate, the load will also increase. If the storage is exhausted, i.e. the pollutant is washed out from the system; the concentration as well as the load will decrease.

The situation may be slightly different for suspended particulate matter, as shown in the dotted lines. After the flow intensity (which is amongst others related to the flow rate) reaches a critical level, formerly deposited matter can be resuspended from the bed, leading to a distinct peak in concentration and intensifying the peak of loading.

Figure 2-6 makes clear, that a peak due to a flush in concentration, which is often considered to be a major criterion in the definition of a first flush, is only possible

- i) for particulate constituents, which were stored in the bed or
- ii) for dissolved constituents if the flushing rainwater picked up enough of the constituent during its overland passage, so that the concentration is higher than it is in the river.

In the case when the bed is totally dry and it contains resolvable materials, usually no peak in concentration will occur, as every inflow of water would mean a decrease of concentration.

### 2.2.1 *Driving forces influencing a first flush*

Based on Deletic (1998) the main factors influencing the occurrence of a first-flush are

- i) *climate characteristics*: the antecedent dry weather period (ADWP), often given as antecedent dry days (ADD) as the number of days without rainfall before a specific event.
- ii) *rainfall characteristics*: the duration of the rainfall event and the rainfall intensity or the total rainfall volume above a critical threshold which must generally be exceeded to produce significant runoff. The spatial variation of rainfall will also influence the flush, for example with dilution effects when the precipitation is equally distributed over the whole basin.
- iii) *runoff/discharge characteristics*: the flow velocity (respective discharge) governs the capacity for remobilisation and erosion
- iv) *basin characteristics*: main factors are possibilities for early or delayed delivery of mass within the system in combination with point or localised non-point sources and/or partial sinks, such as distributary zones or reservoirs as well as soil characteristics and the type of cultivation.

Although it is obvious that these factors are the main driving forces for the dynamics of water quality in semi-arid watersheds, a successful correlation between them and the occurrence of a first flush has only been possible in the past for a combination of factors, rather than being able to isolate a single dominant influence. This correlation is then generally only valid for the specific site which was studied (e.g. Gupta and Saul, 1996).

### 2.2.2 *Influence of sampling points*

In addition to the independent drivers above, the choice of the sampling points may have great influence on the shape of the pollutographs and with that also on the first flush: if the measurements are taken at a site in a pool, where water remains and pollutant accumulate during low-flow, a flush of these pollutants will be difficult to notice because a strong dilution effect occurs. Additionally, the impulse, which can lead to a downstream flush in sewers as described above, cannot be passed, if the water bodies are not connected. This could be the case in natural rivers during summer due to their often uneven slope (see Figure 2-7).

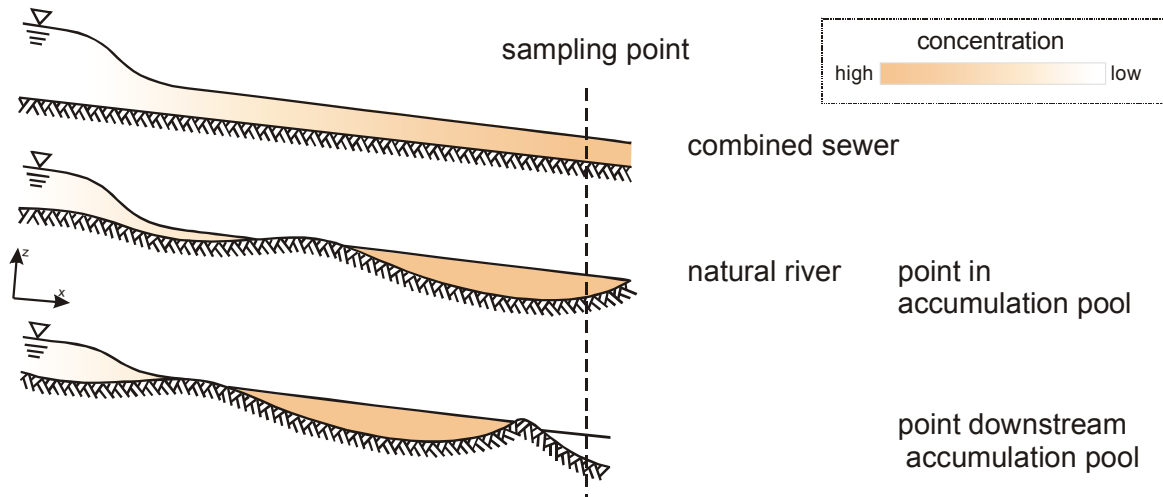


Figure 2-7: Influence of sampling points on the occurrence of flushes

Therefore, it must be taken care in the choice of the measurement points. In order to record impacts of flushes, they should be situated far enough downstream of eventual accumulation sites and especially not in the same pool.

First flush effects are not only clouded by dilution. It is widely known, that the transport rate of suspended matter does not directly follow the transport capacity of the flow (which is the similar to the flow's maximal energy available for transport) but needs some time to adapt to rapidly changing conditions. Particles have to be picked up from the bottom and transported upwards in the current, to access the available transport capacity there and to dispose capacity at the bottom to resuspend additional matter.

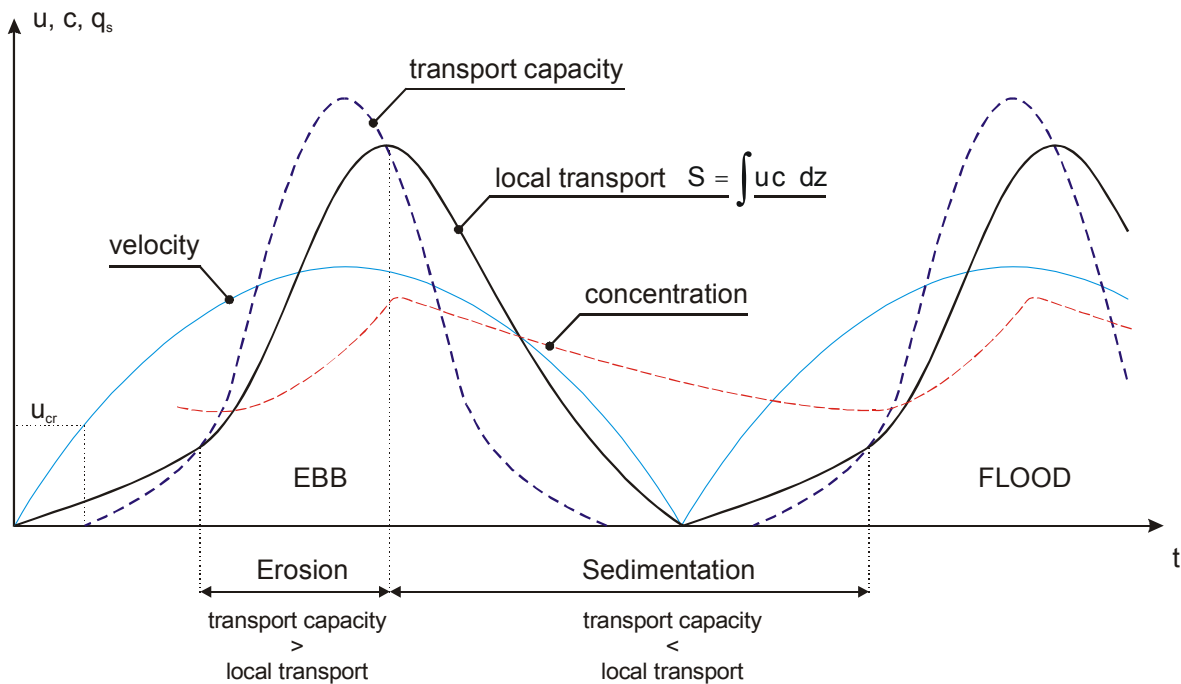


Figure 2-8: Time lag of suspended sediment concentrations in tidal flow van Rijn (1993), modified

Figure 2-8 shows an example given in van Rijn (1993) which shows the time difference between the three variables transport capacity, actual transport and concentration for tidal flows. Due to

the fact, that i) velocity has to reach a certain critical value to create a significant net excess of erosion over deposition, and ii) the deposition process needs some time to establish equilibrium transport (equilibrium condition here means that transport capacity is equal to actual transport as in Figure 2-8), the peak of the concentration could be further delayed in time, making a first flush even more unlikely.

### 2.2.3 *Definition and quantification of first-flush*

As mentioned before, it is well known in urban hydrology, that the constituents are normally more concentrated in the first part of runoff. This phenomenon was first described by Metcalf and Eddy (1916) as *first flush* or *first foul flush*.

There are various definitions of the first flush phenomenon, ranging from just qualitative ones up to strictly quantified normalized loadings, which have to pass a channel point to form a flush, e.g. in Gupta and Saul (1996) or Bertrand-Krajewski et al. (1998).

In general, they can be grouped into

- i) general definitions,
- ii) definitions in terms of water volume (or first centimetres of runoff per contributing area),
- iii) definitions dependent on concentration and,
- iv) definitions dependent on loads.

The term *first flush effect* refers to rapid changes in water quality (concentration or load) within a distinct flood event. They occur frequently after early season rains with an antecedent accumulation of mass. Soil and vegetation particles wash into the channels, sediments and other accumulated organic particles on the river bed are remobilised and dissolved substances from soil and shallow groundwater can be flushed out into the streams.

The term is sometimes also used to address the first flood which occurs after a dry period and which is supposed to contain higher mean concentrations than subsequent ones. In the following this will be referred to as *first significant flood* referring to an absolute comparison of different floods, whereas *first flush flood* describes the first significant flood which carries also a first flush (Obermann et al., 2006).

A first flush can be characterised by evaluation of i) pollutographs against time, ii) normalized pollutographs against normalized water flux (NCL-plots) or iii) aggregated rating parameters.

Because the reference of the first flush is not always clear, Sansalone and Christina (2004) introduced the terms *concentration-based first flush* and *mass-based first flush*.

There are a number of indexes in literature to determine the occurrence or intensity of a first flush (see Table 2-2).

Table 2-2: Definitions of a first-flush

type	criteria	definition	author
ii	$\int_{t_1}^{t_2} Q(t) dt$ $\forall t_1 = t(c \geq c_b)$ $\wedge t_2 = t(c \leq c_b)$	definition of $c_b$ as mean dry weather concentration, calculation of volume to enable dimensioning of treatment facility	Epa (1993)
iv	NCL-bisector $> 0.2$	the difference between the NCL-plot (chapter 2.2.4) and the bisector is greater than 0.2	Geiger (1984)
iv	$\frac{\Delta NCL}{\Delta NCF} > 1$	initial slope of normalized cumulative load/ normalized cumulative runoff –plot $> 45^\circ$	Geiger (1987) Bedient et al. (1978)
iv	FF <sub>30</sub> $> 0.8$	80% of the load is transported by the first 30% of discharge	Saget et al. (1995)
iv	FF <sub>25</sub> $> 0.4 \sim 0.6$	40 – 60 % of the load is transported by the first 25 percent of discharge	Vorreiter and Hickey (1994)
iv	cumulative load curve $>$ cumulative runoff curve	cumulative load against time is greater than cumulative runoff against time	Sansalone and Buchberger (1997)

These can be based on e.g. the basis of differences between normalized loadings and normalized flow (Geiger, 1984), fitted exponential parameters of NCL-plots (Bertrand-Krajewski et al., 1998; Saget et al., 1996), initial slopes of NCL-curves (Bedient et al., 1978) and approximations of the percentage of mass transported at a specific percentage of flow (Saget et al., 1996; Vorreiter and Hickey, 1994).

#### 2.2.4 Calculation of normalized cumulative load plots

Finding the best management of stream systems is often an optimisation between two main boundary conditions: (i) the amount of water which has to be stored or diverted should be minimised and (ii) the amount of nutrients or pollutants which can be prevented from entering downstream water bodies should be maximised. Hence it is often important to know, when the transport of pollutants is most intense in comparison to the water flow, so that most of the constituents can be stored with the least effort.

One common method to identify phases of increased nutrient fluxes are diagrams of normalized cumulative loads over normalized cumulative flow. The normalized cumulative flow (NCF) and the normalized cumulative load (NCL) of a parameter X can be calculated from

$$NCF = \frac{\int_{t_0}^t Q(t) dt}{\int_{t_0}^{t_e} Q(t) dt} \quad \wedge \quad NCL = \frac{\int_{t_0}^t X(t) \cdot Q(t) dt}{\int_{t_0}^{t_e} X(t) \cdot Q(t) dt} \quad \text{EQ. 2-3}$$

(a)                      (b)

where

- X(t):     parameter at a time t, water quality characteristic such as concentration [ML<sup>-3</sup>],  
conductivity or temperature  
Q(t):     flow rate of water [L<sup>3</sup>T<sup>-1</sup>]  
t<sub>0</sub>, t<sub>e</sub>:   defined beginning respective end of the discharge event or the regarded period  
(hydrological year) [T]

When the NCL is plotted against NCF, information of the temporal distribution of loadings over the event duration can be derived more easily.

These types of curves derived from the NCL enable a dimensionless classification of the pollutograph in terms of the temporal distribution of loadings over the event duration (cp. Figure 2-9).

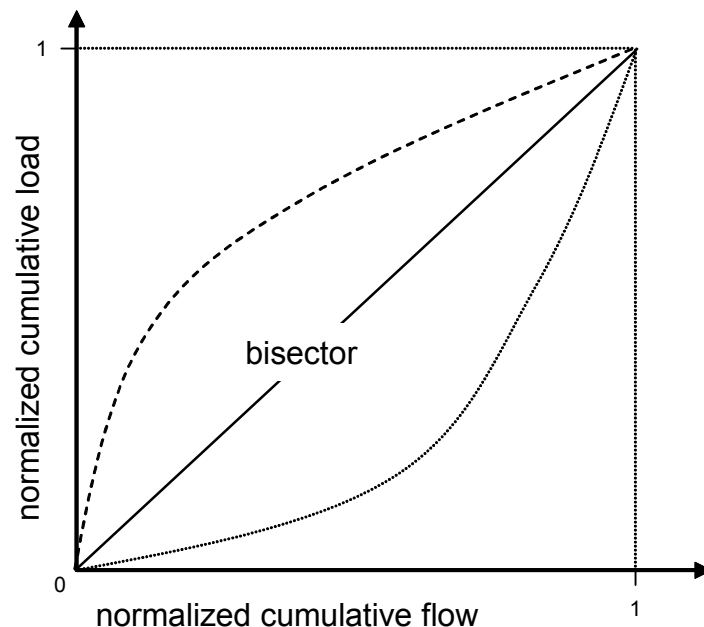


Figure 2-9: Example of a NCL-plot

If the increase of the load is proportional to the increase of the flow, which happens if concentration remains constant during the event, then the NCL vs. NCF curve will follow the 1:1 bisector line.

In case the water quality characteristic is subject to an over-proportional increase at the beginning of the period, the curve will look like the dashed line in Figure 2-9. If the transport is more intense at the end of the regarded period, the plot will match the dotted line instead.

Sometimes the NCL is also referred to as  $M(V)$  curve, i.e. mass as a function of flow-volume, as in Saget et al. (1996) or Bertrand-Krajewski et al. (1998), which limits the meaning to masses derived from volumes and concentrations whereas the approach of the NCL also implies e.g. temperature or conductivity.

### ***Definition of beginning and end of the period***

The period which is used to construct an NCL-plot is not fixed and has to be chosen on the basis of the regarded event. Before the analysis, the beginning and end of the discharge event has to be defined. In case of significant flow in the river before the start of the rainfall, the discharge event could be defined as a distraction from the base flow.

Especially in basins of temporary rivers with distinct flash floods, the recession can take much longer than the rising limb of a flood. So the definition of the end of a flood (e.g. in the Vène with its long lasting karstic flows) is not always obvious. For the analysis of first flush floods, the period included in the analysis should cover the main changes in flow rate and concentrations, but generally not the whole recession limb, where all these are more or less constant. The duration should not be chosen much longer than 2-3 days, as the flush effects may then not be visible any more.

Additionally, it is often difficult to calibrate automatic samplers and to catch water quality data from the direct beginning of the flood. The first samples are normally taken in a shorter timescale, but because the space in automatic samplers is limited, they have to be reduced in the later stages. This means that there might be a uncertainty in terms of the reliability of the course of the load interpolation ( see chapter 7.5 for an example).

### ***Artificial scenarios for NCL-curves***

In order to demonstrate the general behaviour of NCL-plots and the influences of the choice of the regarded period, Figure 2-10 and Figure 2-11 show some simplified scenarios. All scenarios have been calculated with the same discharge, rising linearly from 0.5 to 1.5 and falling again to 0.5 after a short time.



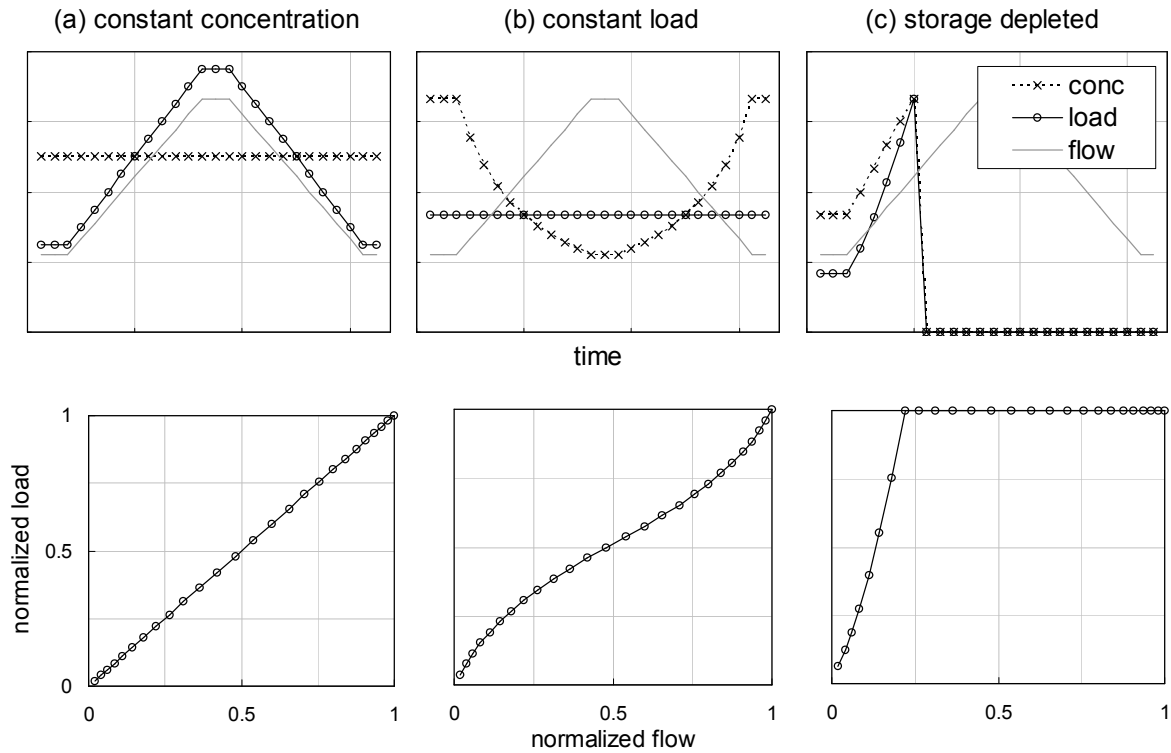


Figure 2-10: Resulting NCL-curves from scenarios a to c

- (a) *constant concentration*: the concentration is set constant in this example, but due to the flow rate increase the load also increases; the NCL-plot is equal to the bisector.
- (b) *constant load*: the load is set constant during this event, a strong dilution effect for the concentration can be observed; the NCL-plot is close to the bisector.
- (c) *storage depleted*: if the concentration increases with the flow, but the storage of the parameter is exhausted before the end of the regarded event; the NCL is very steep and all of the total mass is transported before the end of the event, so there is a strong flush effect; this is an example of a case with a limited storage.

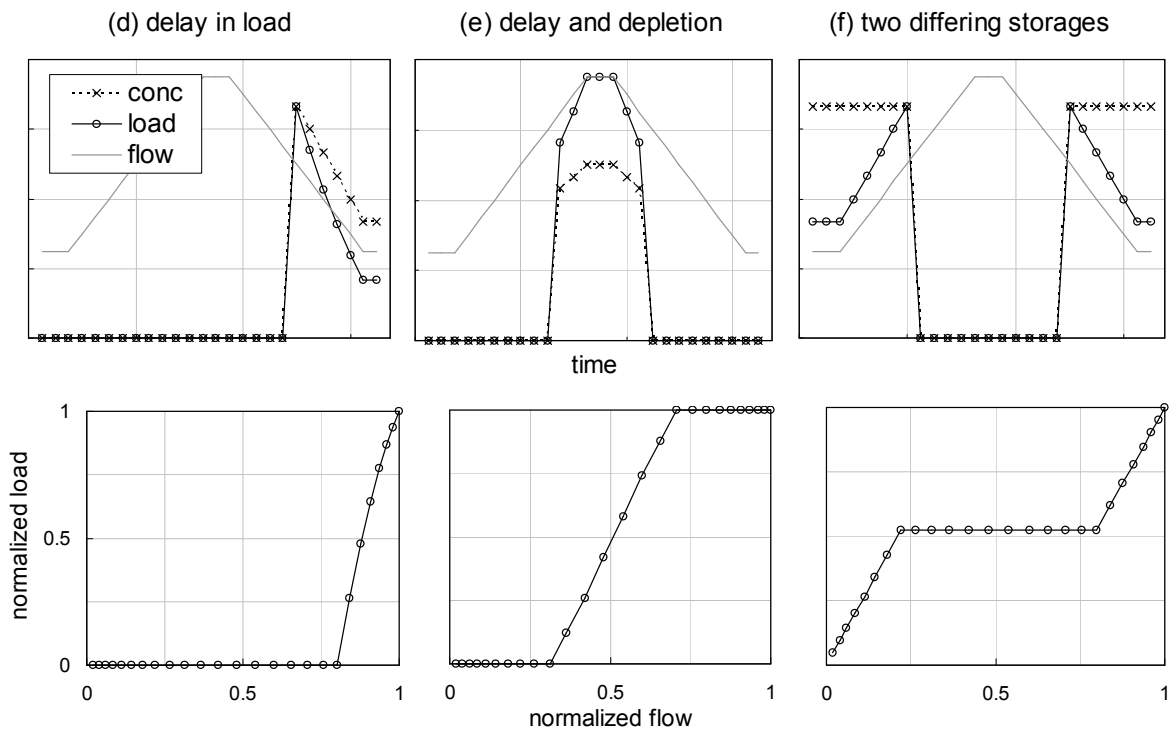


Figure 2-11: Resulting NCL-curves from scenarios d to f

- (d) *delay in load*: the load is delayed, which means that there is no (or hardly any) transport in the rising limb and in the peak of the flood; the NCL-curve is similar to (c), but the transport occurs at the end of the event, so it is not a first flush; true, if a storage needs time to become disposable for transport, example of a case where e.g. a crusted soil has to be broken up or if a covering layer has to be removed by erosion before.
- (e) *delay and depletion*: the beginning of the transport is delayed and the storage is limited, this is a combination of (c) and (d), the NCL-plot is equal to (c) or (d) but centred at 50% flow.
- (f) *two differing storages*: a following sequence of stored pollutants, one storage is easily and fast available for transport, the other after some time; the NCL-curve first increases, followed by a stagnation and a new increase similar to the first.

The concept of NCL-plots (normalized cumulative load against normalized cumulative runoff or flow) gives good insights in the variation of transport intensity in comparison to flow intensity during the preceding event. The ratio of load to flow gives an idea of the effectiveness or type of potential managing methods for these events on the basis of measured data.

### 2.2.5 Calculation of relative mass fluxes

Although they give a very good and condensed overview about the course of loadings over time, the NCL-plots are often difficult to interpret, because they are missing a direct reference to time, which would be needed to identify the periods of increased mass transport.

In order to compare different periods of the year or different periods within a flood wave in terms of their transport activity, the method of relative mass fluxes (RMF) have been developed. They can be calculated as the ratio of the percentage of a parameter in means of the total load and the percentage of flow in means of the total flow (Obermann et al., 2006):

$$RMF(X, t) = \frac{\int_{t=t_a}^t L(X, t) dt / \int_{t=t_0}^{t_e} L(X, t) dt}{\int_{t=t_a}^t Q(t) dt / \int_{t=t_0}^{t_e} Q(t) dt} = \frac{NCL(X, t)}{NCF(t)} \quad \text{EQ. 2-4}$$

in which

- $t_a$ : start of investigated time span, e.g. beginning of month [T]
- $t_0, t_e$ : start and end of total time span, e.g. beginning of the year [T]
- $L(X, t)$ : flux ( $X(t) \cdot Q(t)$ ) of parameter X at time t, if X is a concentration, L is a load in  $[MT^{-1}]$
- $Q(t)$ : water flow at time t  $[L^3T^{-1}]$
- $NCL(X, t)$ : normalized cumulative load of parameter X at time t [-]
- $NCF(t)$ : normalized cumulative flow at time t [-]

The relative mass flux at a specific time can be seen as the gradient of the NCL-curve at that time. In contrast to the method of plotting normalized cumulative loads, relative mass fluxes allow the direct comparison of transport activities in relation to flow activity for different periods, where a period can differ from minutes to years.

When comparing RMF curves of different parameters, it could be necessary to divide the values for RMF by the maximum of the regarded interval, which gives normalized relative mass flux curves (nRMF).

### 2.2.6 Indexes as classification methods for first flushes

Investigation of the relationship of flow rate and pollutant transport with the help of NCL-curves is an appropriate measure as outlined above. Nevertheless it is often helpful to characterise the strength of a first flush with a single value in order to compare different scenarios, catchments or events and to present strict criteria.

Therefore, many approaches have tried to construct a measure or a definition for a first flush (see Table 2-2).

One possibility is to calculate the integral of the NCL. In this case, an NCL-curve equal to the bisector would yield a value of 0.5, a greater value would indicate a first flush (a “perfect flush” would be 1) and a value below 0.5 would be a sign for a delayed reaction.

Other researchers defined the significance of a flush in terms of the load which was transported by the first x% of flow, e.g. Deletic (1998) for the first 25% ( $FF_{25}$ ) or Saget et al. (1996) for the

first 30% ( $FF_{30}$ )<sup>1</sup>. The maximum in these definitions (i.e. a “perfect flush”) would be 1 (or 100%) the minimum would be zero for no flush.

Geiger (1984) defined a criteria in terms of the maximum difference of the NCL-curve from the bisector. Figure 2-12 shows the course of this difference (Geiger criteria in the figure) for the six scenarios.

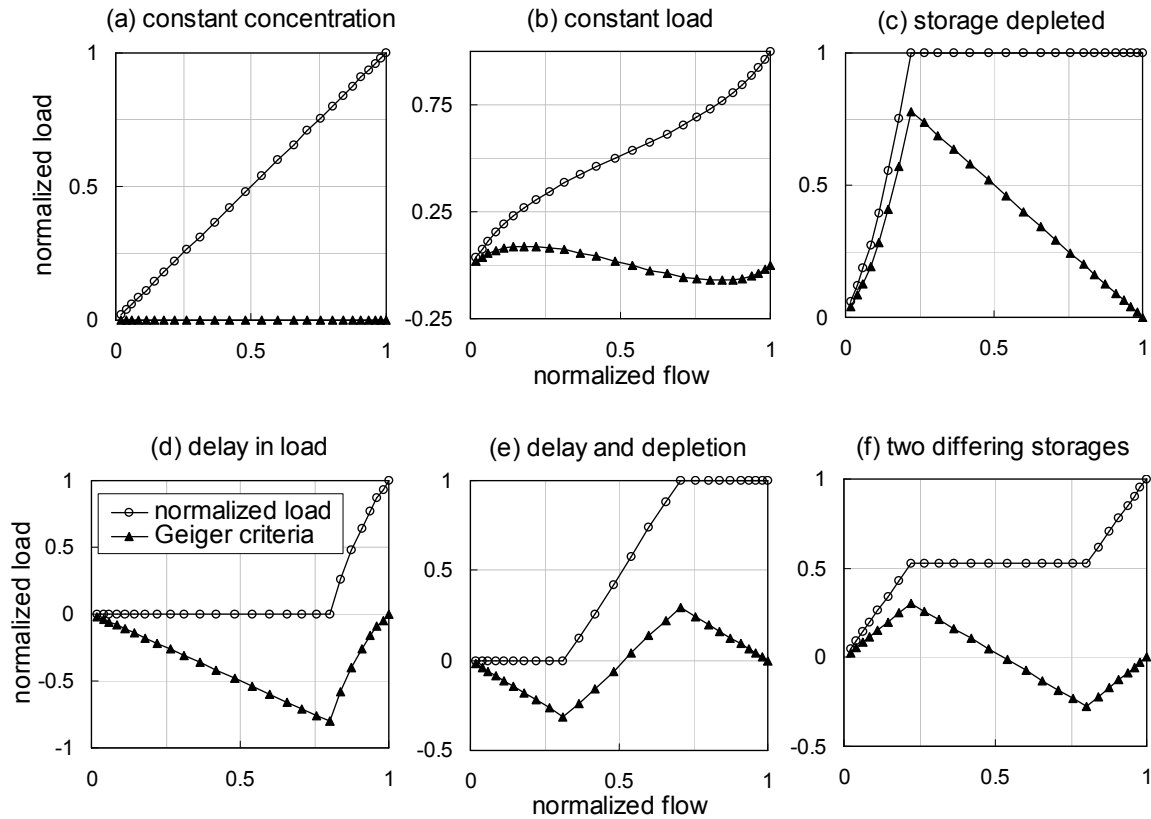


Figure 2-12: Resulting NCL-curves and the Geiger (1984) criteria as difference of normalized cumulative load from the bisector

The maximum of the difference is then the value of Geiger (1984). The highest possible value of 1 would again describe a perfect flush; zero would be the lowest (cp. Table 2-3).

Figure 2-13 shows an application of the three methods and one modification of the Geiger (1984) approach to the test scenarios explained earlier.

<sup>1</sup> The definition of or Saget et al. (1996) focuses on the applicability of the criteria in the dimensioning of stormwater treatment facilities and detention-settling tanks, the definition is very strict and was only satisfied by 1% of the events of the tested dataset in the study

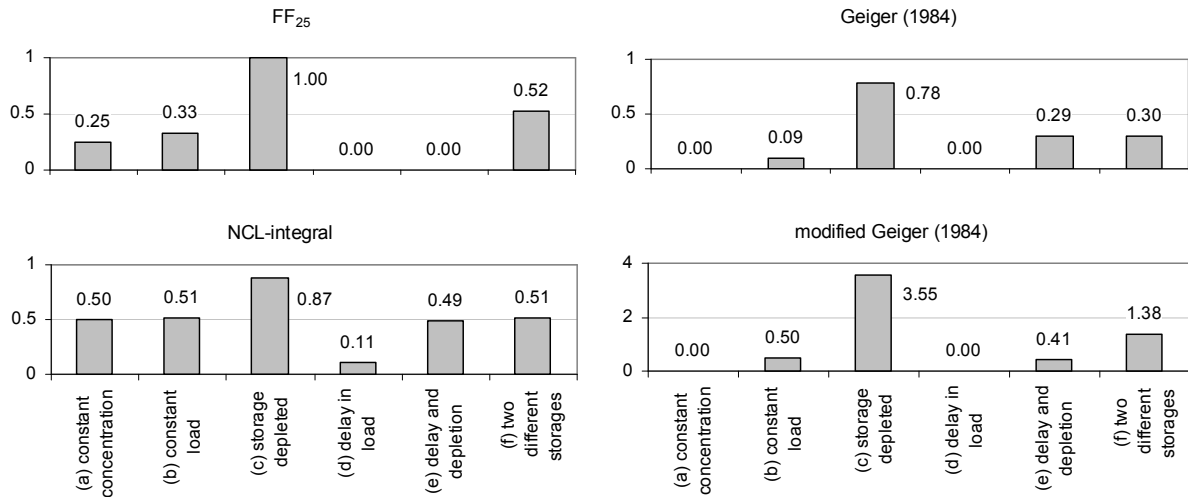


Figure 2-13: Comparison of "one-value" classifications for first flushes for the scenarios of Figure 2-11

In all approaches, scenario (c) yields the highest rating, which would have been expected by the study of the NCL-curves.

### *FF<sub>25</sub>-criteria*

The FF<sub>25</sub> criterion shows a good behaviour for (f). From a management point of view the first part of a flood could be treated separately, so this method is able to highlight this important differentiation from the other variants. The maximum of 1 at the case (c) does not include information about the situation before 25% of runoff, so a flush whose total load is even more condensed would have the same value and a distinction would not be possible.

### *Geiger's (1984) criteria*

As FF<sub>25</sub>, Geiger also yields a slightly higher value for (b) than for (a). In contrast to the FF<sub>25</sub>-method, (e) and (f) give nearly equal values. A rating index for flushes should be able to distinguish between these two cases. The criteria is usually limited from 0 (load is proportional to the flow) to 1 (perfect flush). In order to allow additional distinctions, the method could be extended to the range from -1 to 1, if negative maxima were allowed, like in case (d).

### *NCL-integral criteria*

The integral of the NCL-plot does only allow a gradation of the cases (c) and (d); the others are all in the same magnitude.

Although it is often implicitly included, the aforementioned definitions are all lacking a relation to the relative time after which a peak in the pollutograph appears. There is no coupling between the intensity of the flush and the time of its appearance.

### *Modified Geiger (1984) criteria*

To close this gap, a new approach was tested, which is based on the value derived from Geiger (1984). Geiger's value is divided by the normalized cumulative runoff, after which the maximum

of the difference of the NCL and the bisector occurs (see Figure 2-12), or in other words it is Geiger's (1984) value divided by its corresponding x-value.

The values on the x-axis are always between 0 and 1 for these plots, which means that if all mass is transported in the very last moment of the event (a perfect "inverse-flush"), the y-value will be 0, divided by the x-value of 1, the criteria will yield 0 (if minima would be also allowed, the y-value would be -1 and x would be 1).

On the other hand, if all of the pollutant was transported in the first instant of the event, the value of Geiger would be 1 and the position would be near or equal to zero, which means, that the value would go to infinity for a perfect flush.

### ***Limits of the classification methods for first flushes***

A summary of the boundaries of the presented approaches is given in Table 2-3.

Table 2-3: Boundaries of classification approaches for first flushes

Classification method	lower limit "late flush"	centre "constant conc."	upper limit "first flush"
FF <sub>25</sub>	0	0.25	1
Geiger (1984)	0 (-1)	0	1
NCL-integral	0	0.5	1
mod. Geiger (1984)	0 (-1)	0	$\infty$

### ***Applicability of the indexes***

Especially the method FF<sub>25</sub> proved to be valuable. It is easy to calculate and focuses on the beginning of the event. The integral approach and Geiger (1998) showed some limitations. The modified Geiger approach was found to solve some of these issues, but as the values can vary enormously and the calculation is comparably difficult, it was not applied further.

The FF<sub>25</sub> cannot be used instead of the measures as NCL and RMF-plots, but in combination with these, it is a helpful approach to easily compare different floods and to derive trends in nutrient fluxes from one event to another.

### 3 Modelling tools for temporary streams

---

In the following, a short introduction into the vast field of modelling computational fluid dynamics and the fate and transport of constituents is given. Later, there will be a comparison of the tested models HSPF, CASCADE. Finally the newly developed and applied tempQsim – STREAM model and its main enhancements will be shown.

#### 3.1 Classification of models

A model is a reproduction of a natural system or parts of a system, which is simplifying but sustains essential processes and basic principles. Of the two possible kinds of models in this context, physical and mathematical, only the latter will be considered.

Normally water quality transport models for rivers basins are a combination of a rainfall-runoff model, an instream transport model and one model solving the dynamic biological and chemical process equations. The water quality part is usually zero-dimensional and hands over source and sink terms to the hydrodynamic part, which transports the constituents in the water.

The discretisation in rainfall-runoff models is normally lumped or distributed. Lumped models are based on areas with similar hydrologic characteristics, often called Hydrological Response Units (HRU), distributed models can be based e.g. on grids or other finite elements. In the following, the focus lies on the instream parts of the models.

The transport model compartment can be either stochastic or deterministic. Only models of the latter type will be discussed herein. If every condition is a direct cause of a former state of the model, i.e. the result is always the same while calculating with the same boundary conditions, the model will be a deterministic model. Deterministic models can be either analytical or numerical.

Because it is only possible to find analytical solutions for linear or quasi-linear equations on simple grids, non-linear problems with complex boundary conditions on complex domains usually have to be solved numerically.

Solving a problem with the help of a deterministic, mathematical and numerical model in the context of hydrodynamics and water quality always implies the following three steps. First the governing equations have to be defined, in the second step the domain has to be discretised in time and space, i.e. the continuum of points has to be divided into grid points, areas or volume elements and the partial differential equations (PDE) have to be reduced to a system of algebraic equations (SAE). In the last step the SAEs are solved for all points and time steps (Zielke, 1999).

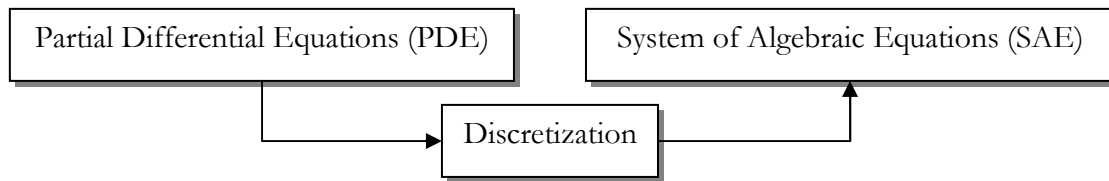


Figure 3-1: Concept of hydrodynamic-numerical models

There are three common methods for space discretisation:

- i) Method of Finite Differences (FDM)
- ii) Method of Finite Elements (FEM)
- iii) Method of Finite Volumes (FVM)

which will be shortly characterised in the following.

### ***Finite Difference***

To approximate the differential equations with finite differences the domain has to be covered with a grid of discrete points (normally orthogonally structured, but not necessarily equidistant), often called nodes.

### ***Finite Element***

As a major advantage of the FEM it can be applied in a totally unstructured way, i.e. with elements like triangles or prisms, which allows a very good approximation of complex boundary geometries. FEM-meshes can be refined easily.

### ***Finite Volume***

The Finite Volume Method (FVM) is based on the balance of fluxes in- and outflowing the control volume.

The methods of Finite Differences and Finite Volumes differ from a topological view. The former reduces the equations to points, the latter discretises them on volumes, thus the method of Finite Volumes is closer to the real flow regime than the method of Finite Differences (Malcherek, 2001).

Despite these differences, the FVM is a generalization of the FDM-scheme. The FVM can basically be applied on any grid structure and therefore has also the capability to replace the calculation time consuming and more instable finite element method in hydrodynamic calculations (Malcherek, 2001).

An additional advantage is the fact that FVM enforces conservation of quantities such as mass, momentum and energy by construction.



## 3.2 Flow routing

Starting from the Navier-Stokes equations, a number of equations can be derived including simplifying assumptions in order to enable a solution of water flow and solute transport. Three common equations in computational hydrodynamics are presented shortly below.

### 3.2.1 Dynamic Wave

The basic flow-governing equations are the dynamic wave equations, often referred to as shallow water wave equations or (in their one dimensional form) the Saint-Venant equations (Saint-Venant, 1871). These consist of the equations of continuity and momentum conservation for gradually varied unsteady flow (Borah and Bera, 2003).

These two parts can be expressed for open channel flow in prismatic channels as

$$\frac{\partial Q}{\partial x} + \frac{\partial A}{\partial t} + q_{source} - q_{sink} = 0 \quad \text{EQ. 3-1}$$

$$\frac{1}{A} \left( \frac{\partial Q}{\partial t} + \frac{\partial}{\partial x} \left( \frac{Q^2}{A} \right) \right) + g \frac{\partial y}{\partial x} - g (S_0 - S_f) = 0 \quad \text{EQ. 3-2}$$

(a)          (b)          (c)          (d)          (e)

where

Q:	discharge [L <sup>3</sup> T <sup>-1</sup> ]
q:	source or sink per unit width [L <sup>2</sup> T <sup>-1</sup> ]
A:	stream cross-sectional area [L <sup>2</sup> ]
y:	river depth [L]
g:	gravity constant [LT <sup>-2</sup> ]
S <sub>0</sub> :	bottom slope of channel [-]
S <sub>f</sub> :	friction slope [-]

The terms in EQ. 3-2 denote the local (a) and convective acceleration (b), the pressure gradient (c), the gravity term (d) and the friction term (e), see Tsai (2003).

There is no analytical solution of these equations available for most practical applications (Borah and Bera, 2003), but numerical approximations have been used in flood routing models such as Barkau (1993), Balloffet and Scheffler (1982) or Strelkoff (1970).

Derivation of the St. Venant equations uses the following basic assumptions:

- flow is essentially 1-dimensional
- stream length is many times greater than flow depth
- vertical accelerations are negligible and vertical pressure in the wave is hydrostatic
- water density is constant
- channel bed and banks are fixed
- channel bottom slope is relatively small (<15%)

The dynamic wave equations are normally not used in watershed models because of their computationally intensive numerical solutions.

However, some approaches as the non-inertia and kinematic wave use approximations of these equations, ignoring certain terms in the momentum equation.

### 3.2.2 *Non-inertia wave*

The non-inertia wave ignores both local and convective inertia terms in the momentum equation and is often called misleadingly diffusion wave. But the physical meaning of the diffusion wave is different. Because the term refers more generally to the wave whose induced disturbance in flow is analogous to the diffusion of particles or heat (Yen and Tsai, 2001) it should be avoided in this context. The non-inertia wave is a special case of the diffusion wave and can be obtained from EQ. 3-2 by ignoring both local and convective acceleration, which yields

$$\frac{\partial y}{\partial x} - (S_0 - S_f) = 0 \quad \text{EQ. 3-3}$$

In combination with EQ. 3-1 this forms the non-inertia wave.

As for the dynamic wave, there is no analytical solution.

### 3.2.3 *Kinematic Wave*

The kinematic wave equation is a further reduction of the non-inertia wave. It was first proposed by Lighthill and Whitham (1955a; 1955b) and it has subsequently been used in many rainfall-runoff simulation models. Due to its application in this work, it will be discussed in more detail than the approaches before.

In order to obtain the kinematic wave equation the first 3 components of EQ. 3-2 have to be dropped, reducing it to

$$S_0 - S_f = 0 \quad \text{EQ. 3-4}$$

This assumes that the momentum of the unsteady flow is the same as that of steady uniform flow in which discharge is a single-valued function of depth. Empirical formulas have been used to provide this functional relationship which takes the general form

$$A = \alpha Q^\beta \quad \text{EQ. 3-5}$$

in which

- A: cross sectional area [L<sup>2</sup>]
- $\alpha$ : function of channel geometry
- $\beta$ : empirical parameter

A well known example is the Manning-Strickler formula

---

$$\frac{Q}{A} = v = k_{st} r_{hy}^{2/3} S_0^{1/2} \quad \text{EQ. 3-6}$$

where

v: stream velocity [ $LT^{-1}$ ]  
 $k_{st}$ : Strickler roughness coefficient [ $L^{1/3}T^{-1}$ ]

The combination of EQ. 3-1 and EQ. 3-5 constitute the kinematic wave equation. Merged these give

$$\frac{\partial Q}{\partial t} + c \frac{\partial Q}{\partial x} + c(q_{source} - q_{sink}) = 0 \quad \text{EQ. 3-7}$$

where the parameter  $c$  is conventionally termed the celerity, with dimension  $LT^{-1}$ . The source and sink term has dimension  $ML^{-1}T^{-1}$ , or discharge per unit length of river. EQ. 3-6 demonstrates that the highest discharge, i.e. the peak of the flood wave, travels along the river with velocity equal to  $c$ , which is the velocity of the wave, not of the water. Parameter  $c$  is a function of  $Q$ , and EQ. 3-6 is non-linear. Due to the aforementioned simplifications, the kinematic wave is limited in its accuracy for some applications.

The theory is popular because it is simple, versatile, and reasonably accurate if the underlying assumptions are approximately satisfied but it is important that its limitations are properly acknowledged (Singh, 2001).

So it is well known, that it does not account for wave attenuation. Kinematic wave models assume a single-value relationship between stage and discharge, as well as they neglect backwater effects, but have found wide engineering applications (Tsai, 2003).

#### 3.2.4 Example of a numerical solution of the kinematic wave equation

There are several methods for a numerical solution of the kinematic wave equations.

The Muskingum-Cunge Methods, which are one possible branch of approaches, can be divided into two groups, (i) Variable Parameter Muskingum-Cunge (VPMC) methods and (ii) Constant Parameter Muskingum-Cunge (CPMC) methods. The difference lies in the calculation of the routing parameters: in an approach after the VPMC method, these are recalculated for each reach depending on local flow values, whereas a CPMC method only uses a single representative flow value which is kept constant during the computation time.

Four-point means in this context that the calculation is based on the conditions at all four grid points, two for the old time step and two for the new one, whereas three-point schemes are only based on information of the known grid points ( $Q_1, Q_2, Q_3$ , see Figure 3-2). Both approaches are normally explicit, but the first needs some iteration (Tang et al., 1999).

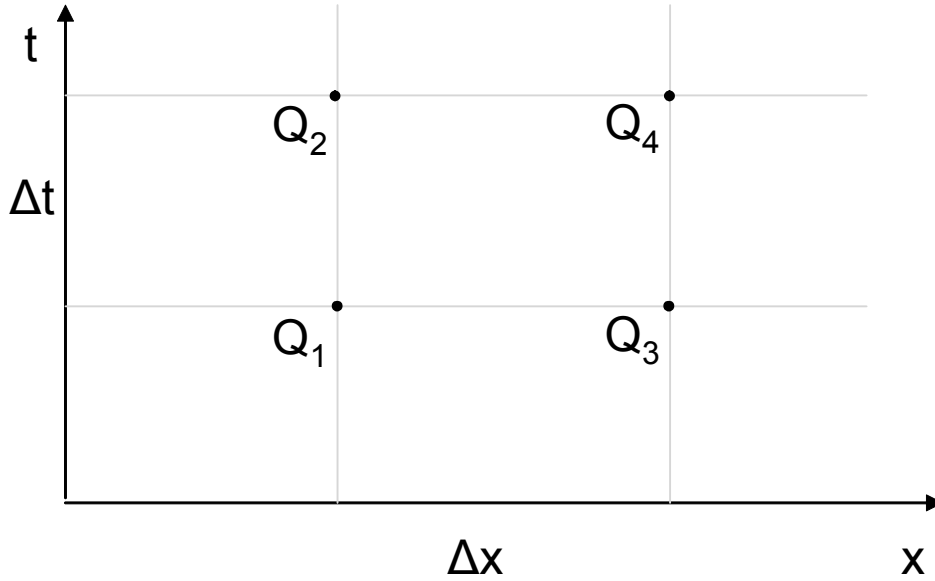


Figure 3-2: Common notation in solutions for the kinematic wave

For a time discretisation  $jDt$ ,  $j = 1, 2, \dots$  and a space discretisation  $iDx$ ,  $i = 1, 2, \dots$  discharge can be estimated using

$$Q_{i+1}^{j+1} = C_1 Q_i^{j+1} + C_2 Q_i^j + C_3 Q_{i+1}^j + C_4 \quad \text{EQ. 3-8}$$

The term  $C_4$  accounts for sources and sinks. The properties of this numerical scheme depend on the choice of  $C_1, \dots, C_4$ . For one particular choice, EQ. 3-8 is the Muskingum method (McCarthy, 1938), and for another the Muskingum-Cunge method (Cunge, 1969), which can accommodate hydrograph attenuation, essentially as a numerical error arising from the discretisation. The motivation for these two techniques comes through lumped storage routing, but they are essentially numerical solvers of the kinematic wave equation. The terms  $C_1, \dots, C_4$  may be written as

$$\begin{aligned} C_1 &= \frac{Dt - 2KX}{2K(1 - X) + Dt} \\ C_2 &= \frac{Dt + 2KX}{2K(1 - X) + Dt} \\ C_3 &= \frac{2K(1 - X) - Dt}{2K(1 - X) + Dt} \end{aligned} \quad \text{EQ. 3-9}$$

and

$$C_4 = \frac{\bar{q}_i Dx Dt}{2K(1 - X) + Dt} \quad \text{EQ. 3-10}$$

in which

$$\bar{q}_i : \quad \text{mean lateral inflow [L}^2\text{T}^{-1}\text{]}$$

In the above mentioned Muskingum-Cunge method K and X are chosen as

$$K = \frac{Dx}{\bar{C}} \quad \text{EQ. 3-11}$$

$$X = \frac{1}{2} - \frac{\bar{Q}}{2\bar{C}\bar{B}S_e Dx}$$

where

$$B: \quad \text{cross-sectional top width [L]}$$

$$S_e: \quad \text{energy slope [-]}$$

Both K and X are functions of Q and various approximations can be made in solving EQ. 3-8 to EQ. 3-11. In order to minimise numerical errors it can be required

$$Dt \leq \frac{T_r}{M} \quad \text{EQ. 3-12}$$

$$Dx \leq 0.5CDt \left[ \frac{Q}{BC^2S_0Dt} + 1 \right] + 1.5 \frac{Q}{BC^2S_0Dt} \left[ \frac{Q}{Q} \right]$$

Here  $T_r$  is the time to rise of the hydrograph, and  $M > 5$ .

This scheme was first proposed by Holden and Stephenson (1988).

### 3.3 Routing of properties using the kinematic wave equation

Water in natural rivers contains many constituents. In order to estimate their influence on the water bodies, their transport in the flow must be considered within water quality model. Routing of properties can be grouped into transport of soluble and particulate properties.

#### 3.3.1 Soluble properties

Following the transport equation describing the propagation of dissolved matter in a Newtonian fluid (incompressible, therefore  $\text{grad } \vec{u} = 0$ ) can be given as follows

$$\frac{\partial c}{\partial t} + \vec{u} \nabla c = D_{AB} \Delta([\vec{\varepsilon} + \vec{E}]c) \quad \text{EQ. 3-13}$$

in which

$$\vec{u}: \quad \text{fluid velocity vector [LT}^{-1}\text{]}$$

$$c: \quad \text{concentration of dissolved materials [ML}^{-3}\text{]}$$

$$t: \quad \text{time [T]}$$

$$\nabla: \quad \text{Nabla-operator}$$

$$\Delta: \quad \text{Laplace-operator}$$

$$D_{AB}: \quad \text{molecular diffusivity of substance A in fluid B [L}^2\text{T}^{-1}\text{]}$$

$\vec{\varepsilon}$ : vector of turbulent diffusivity [ $L^2T^{-1}$ ]  
 $\vec{E}$ : vector of dispersivity [ $L^2T^{-1}$ ]

Considering, that  $D_{AB} \ll \varepsilon \ll E$ , EQ. 3-13 can be rewritten in one-dimensional form as

$$\frac{\partial c}{\partial t} + u_x \text{grad } c = E_x \text{div}(\text{grad } c) \quad \text{EQ. 3-14}$$

or

$$\begin{array}{ccc} \frac{\partial c}{\partial t} + u_x \frac{\partial c}{\partial x} & = & E_x \frac{\partial^2 c}{\partial x^2} \\ \text{(a)} & \text{(b)} & \text{(c)} \end{array} \quad \text{EQ. 3-15}$$

Term (a) represents the change of concentration over time. The second term is the advection component and (c) considers dispersion, which is not considered in many approaches.

### 3.3.2 *Particulate properties*

Under the assumption, that particles are small, light and the concentration is low, so that the characteristics of the transporting fluid are not changed significantly, transport of particulates in the water phase is often simulated similar to the one of soluble materials. But due to their ability of settling and erosion, suspended solids have additional source and sink terms which must be accounted for.

Sediment transport processes result from the interaction of the flow regime and the bed morphology. The streaming fluid causes forces on the surface which result in entrainment of particles as well as their transport.

If the local transport capacity is higher than a critical concentration, particles will be resuspended from the bed. If the transport capacity is lower, formerly entrained matter will settle down.

The first steps are therefore the determination of

- i) the actual transport capacity (mainly as function of flow parameters) and
- ii) the critical transport capacity (mainly dependent on sediment properties).

Because of the different behaviour of sediment under changing stream intensities, a classification regarding the stream intensity is given below.

#### 3.3.2.1 Transport of individual particles

If a single particle is transported, it will only be influenced by the surrounding fluid.

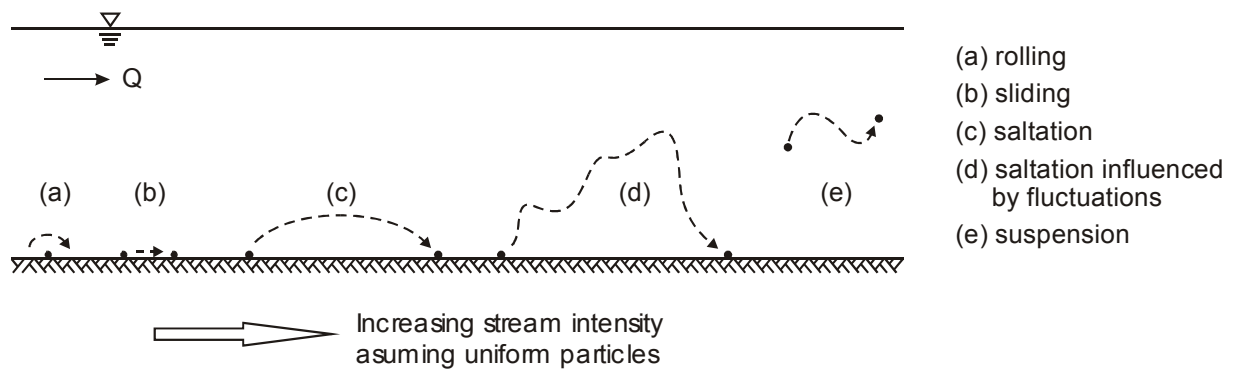


Figure 3-3: Classification of single particle movement, Bollrich (1989), modified

Figure 3-3 illustrates the different terms.

### 3.3.2.2 Transport of a continuum of particles

Regarding a cloud of particles, the amount of transported, undissolved solids in streams can be divided into three main groups:

- i) wash load,  $q_{s,w}$
- ii) suspended load,  $q_{s,s}$  and
- iii) bed load transport,  $q_{s,b}$

*Wash load* is composed of very fine particles (according to van Rijn (1993) smaller than  $50 \mu\text{m}$ ) transported by water but are not originated from the bed in the modelled sections. The wash load is mainly caused by land surface erosion and not by channel bed erosion.

*Suspended bed-material load* is the part of total load which is moving without continuous contact with the bed. The grains are entrained from the channel bed by eddies and are maintained in the flow by upward movements of the flow regime. The appearance of ripples will increase bed shear stress and thus the suspended load is related to the *total bed shear stress*.

*Bed load* transport is the part of the total load which is more or less continuously in contact with the bed. It is characterised by rolling, sliding or bouncing particle movements over the bed surface. The bed load is in close relation to the *effective bed shear stress* which acts directly to the grain surface.

Figure 3-4 provides an overview for the used terms.

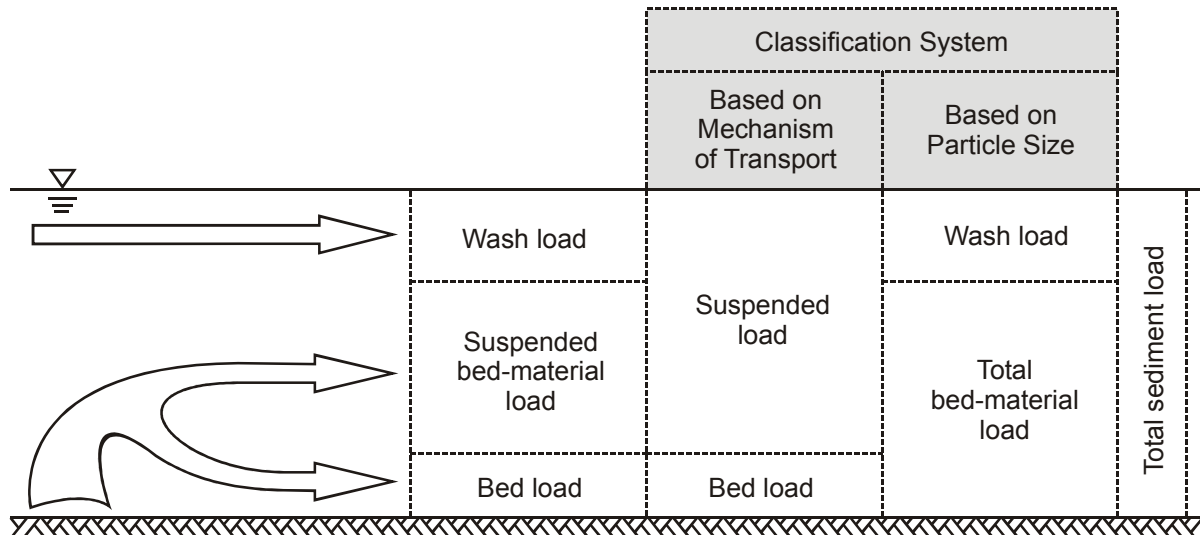


Figure 3-4: Classification of sediment transport

Normally, a sharp distinction between the conditions “suspended bed-material load” and “bed load” is not possible. For increasing flow intensity, the number of particles bouncing and rebounding increases until the cloud of particles becomes a suspension. The ratio of bed load to suspended load decreases.

Sediment transport is a complex topic where many relations are still unknown or too complicated to handle and require much input data. The beginning of sediment movement caused by the flow regime depends on different parameters. Influences can be sediment properties as well as stream properties. Often underestimated influences are e.g.

- *temperature*: Lane and Hansen (1949) found a difference near the factor 2 for measured sand transport rates in summer compared to winter ( $\Delta T \approx 15^\circ\text{C}$ ) due to different viscosity of the fluid,
- *high concentration of fine particles*: the presence of fine particles also increases the viscosity and density of the fluid/sediment mixture and therefore reduces the fall velocity of grains in suspension and leads to a higher transport capacity (van Rijn, 1993).
- *particle shape*: particles are considered spherical in most approaches, but the influence of the particle shape is interesting in the armouring process
- *cohesive forces*: the resistance of very fine particles, e.g. clay or silt, is high compared to their grain diameter respectively the weight; adhesional forces are reciprocal to the grain diameter in this magnitude (Raudkivi, 1982).

### 3.3.2.3 Actual shear stress

The shear stress is the force per unit area in flow direction on the bed. It is caused by the interaction of the streaming fluid and the bed. In a channel with a free surface, the shear stress  $\tau$  is zero at the surface and has its maximum at the bottom; it can be derived from a force balance.



### Forces causing fluid movement

Forces acting on a fluid volume with a length  $dx$  are (cp. Figure 3-5):

- i) forces caused by hydrostatic pressure ( $p_1$  and  $p_2$ ),
- ii) forces due to shear stress acting along the length  $dx$  and
- iii) the longitudinal component of the fluid weight force  $W_x$  for the volume.

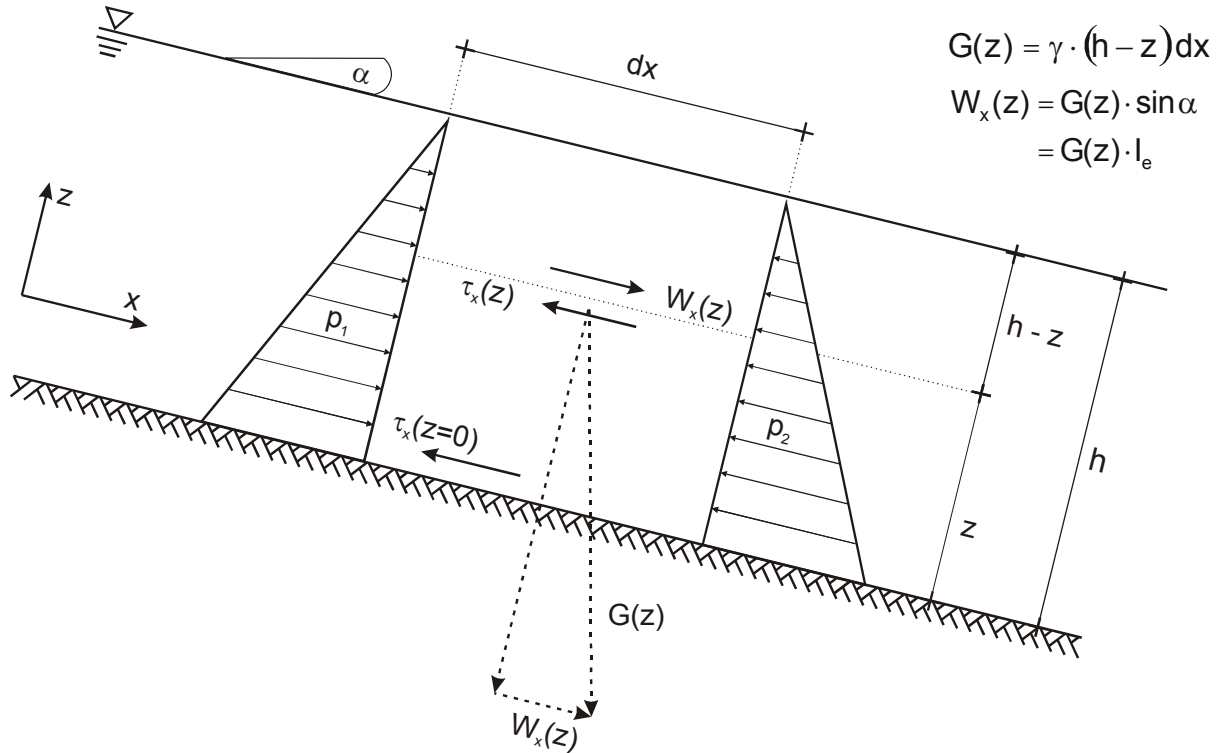


Figure 3-5: Shear stress on a control volume of the length  $dx$

Under uniform flow condition the energy gradient  $I_e = \tan(\alpha) = \sin(\alpha)$  and the hydrostatic pressure  $p_1$  equals  $p_2$ .

Therefore  $W_x$  must be counterbalanced by the shear force, which yields to

$$\tau_x(z) = \frac{W_x(z)}{dx} = \gamma (h - z) I_e = \rho g (h - z) I_e \quad \text{EQ. 3-16}$$

where

- $\tau_x(z)$ : shear stress in longitudinal direction at depth  $z$  ( $\text{N}/\text{m}^2$ )
- $\gamma$ : specific weight of water ( $\text{N}/\text{m}^3$ )
- $g$ : gravitational acceleration ( $\text{m}/\text{s}^2$ )

### The bottom shear stress

Based on the described relations the interesting bottom shear stress  $\tau_x(z=0)$  (often referred to as  $\tau_0$  or  $\tau_b$ ) can be given as

$$\tau_b = \rho g h I_e \quad \text{EQ. 3-17}$$

### Effective bed roughness

The total effective bed shear stress can be divided into two parts:

- i) on a microscopic scale represented by the *grain roughness*, related by particle shape and diameter and therefore depending on skin friction
- ii) on a macroscopic scale the shear stress is related to the *form roughness*, caused by pressure forces on the bed form, i.e. ripples and dunes.

Hence the total bed shear stress can be written as (cp. Figure 3-6)

$$\tau_b = \frac{F_s}{\lambda} + \frac{F_f}{\lambda} = \tau_b' + \tau_b'' \quad \text{EQ. 3-18}$$

where

- $F_s$ : skin-friction force
- $F_f$ : form related pressure force
- $\lambda$ : bed form length
- $\tau_b'$ : grain related bed shear stress
- $\tau_b''$ : form related bed shear stress

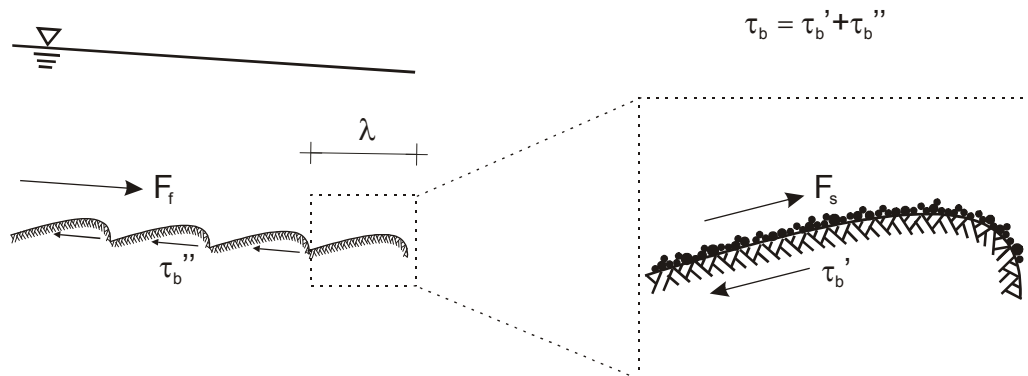


Figure 3-6: Shear stress, particle and bed form related

It can be stated, that  $\tau_b'$  mainly causes bed-load transport and  $\tau_b''$  is corresponding to the suspended load (suspended bed-material as well as wash load transport).

This can be explained by the fact that the grain related forces are restricted according to their range. The turbulences caused by the bed forms have greater influences in minor depth.

For the special case of a flat bed (e.g. regular channel) follows  $\tau_b = \tau_b'$ .

### 3.3.2.4 Critical shear stress

One central problem in the theory of sediment movement is the definition of the value of the critical shear stress for the inception of deposition and erosion. It can be either empirically derived from experiments or as the result of a calibration.

Because of the difficulties in finding an analytical expression of the forces entraining a sediment particle, Shields (1936) applied a dimensional analysis to determine the governing dimensionless parameters and established the so called shields diagram in Figure 3-7.

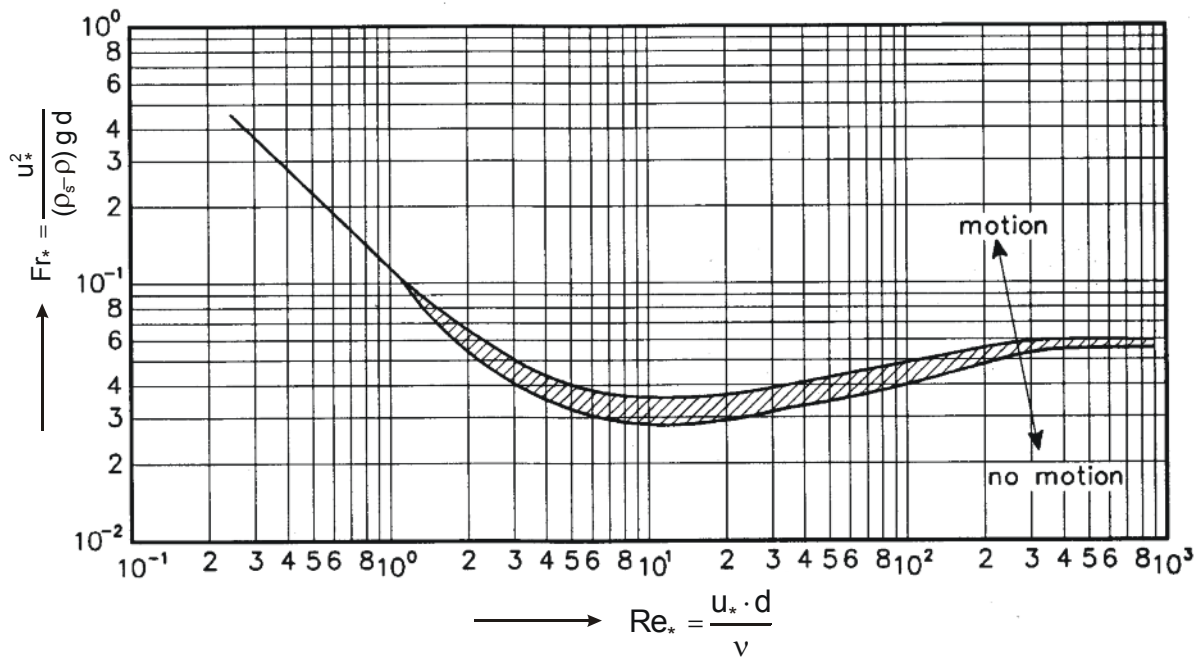


Figure 3-7: Shields (1936) diagram

Shields (1936) determined the grain Froude number and the grain Reynolds number as the most interesting dimensionless parameters in this correlation.

$Fr_*$  given as

$$Fr_* = \frac{u_*^2}{(\rho_s - \rho) g d_{50}} \quad \text{EQ. 3-19}$$

can also be transformed in the so called Shields- or mobility parameter.

#### *The mobility parameter*

$$\theta = \frac{\tau_b}{(\rho_s - \rho) g d_{50}} \quad \text{EQ. 3-20}$$

In the form of Figure 3-7 the shields diagram it is not suitable for computer programs. There are modified diagrams, e.g. proposed by Julien (1995) or van Rijn (1993). The latter is introduced in EQ. 3-21.

$$\begin{aligned}
\theta_{cr} &= 0.24 D_*^{-1} && \text{for } 1 < D_* \leq 4 \\
\theta_{cr} &= 0.14 D_*^{-0.64} && \text{for } 4 < D_* \leq 10 \\
\theta_{cr} &= 0.04 D_*^{-0.1} && \text{for } 10 < D_* \leq 20 \\
\theta_{cr} &= 0.013 D_*^{0.29} && \text{for } 20 < D_* \leq 150 \\
\theta_{cr} &= 0.055 && \text{for } D_* > 150
\end{aligned}
\tag{EQ. 3-21}$$

Based on this set of equations it is possible to give a better understandable form of the shields diagram, showed in Figure 3-8.

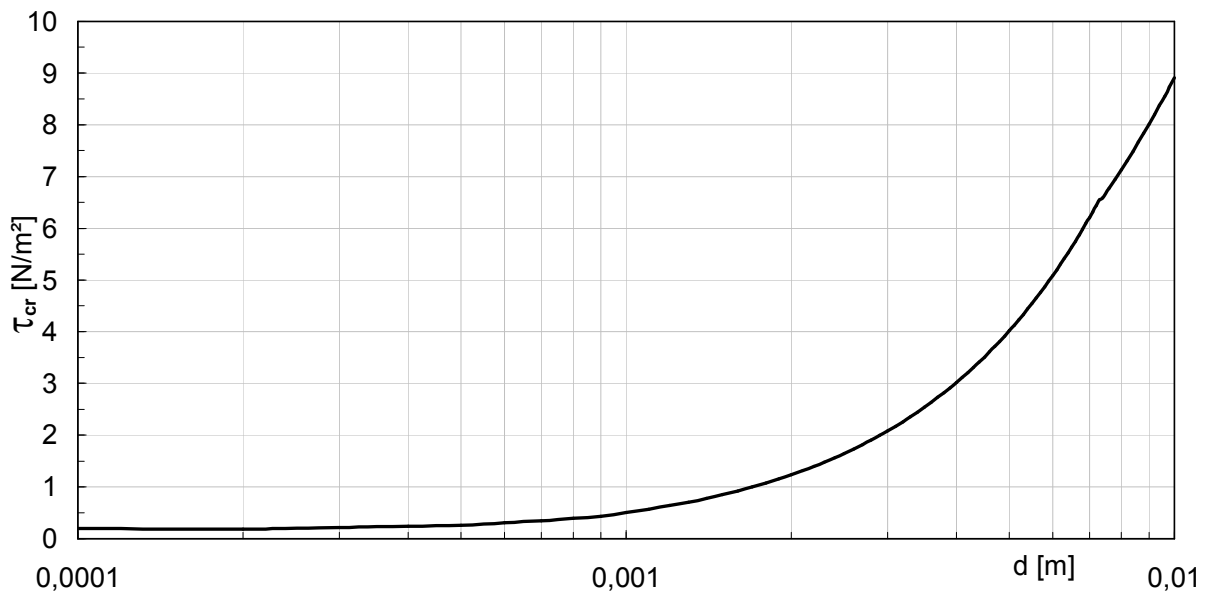


Figure 3-8: Approximation of the Shields diagram by van Rijn (1993)

Although the shields diagram offers a criterion for the condition of incipient motion, a clear distinction can never be given. As long as the sediment is considered as a cloud of comparable spheres (which is not true), there is some kind of a discretisation fault. On the other hand, the definition of “incipient motion” based on observations and measurements can only be derived subjectively. Some particles start their movement earlier, others are entrained later. Therefore, Shields never showed a *curve*, but presented a range (Bollrich et al., 1989).

### 3.3.2.5 Common approaches for sediment transport

Approaches for sediment transport can be divided into equilibrium and non-equilibrium ones.

The former, which are mostly used for the representation of bed load, are assuming that the actual concentration of particles in solution matches the maximal transport capacity of the stream. In these, the actual concentration is directly proportional to the actual transport capacity. Examples for these are e.g. Einstein (1950), Engelund and Hansen (1967), Ackers and White (1973) or Yang and Simões (2000).

Representations of the latter group are also considering the lag time in between the beginning of motion and the achievement of full transport capacity. Often these approaches are used for the simulation of suspended load. A typical couple are the formulas of Krone (1962) and Partheniades (1962) as given in EQ. 3-22 and EQ. 3-23 respectively.

$$D = \omega \cdot c \left( 1 - \frac{\tau_b}{\tau_{crit,d}} \right) \quad \text{EQ. 3-22}$$

$$E = M_e \left( \frac{\tau_b}{\tau_{crit,e}} - 1 \right) \quad \text{EQ. 3-23}$$

where

E, D:	Erosion and deposition flux [ML <sup>-2</sup> T <sup>-1</sup> ]
$\omega$ :	settling velocity [LT <sup>-1</sup> ]
c:	concentration of particulate substance [ML <sup>-3</sup> ]
$\tau_b$ :	actual bottom shear stress [L <sup>-1</sup> MT <sup>-2</sup> ]
$\tau_{crit,e}, \tau_{crit,d}$ :	critical shear stress for erosion and deposition [L <sup>-1</sup> MT <sup>-2</sup> ]
$M_e$ :	Erosion coefficient or erodibility [ML <sup>-2</sup> T <sup>-1</sup> ]

The values for D and E then function as an external source respective sink in the transport equation.

### 3.4 Reaction kinetics

But not only the flow alters concentrations in water bodies. Chemical elements are fate to many processes in natural environments. Elements are converted from one form to another by chemical and biological influences. To model the fate of substances in water quality models, the important reactions and their type must be known. Chemical reactions can be usually classified into zero-order, first order and second order reactions.

#### 3.4.1 Zero-order reactions

Zero-order reactions are independent of the concentrations of the reacting elements and the reaction rate is constant:

$$\frac{dc}{dt} = -k \quad \text{EQ. 3-24}$$

with

c:	concentration [ML <sup>-3</sup> ]
t:	time [T]
k:	zero order rate constant [ML <sup>-3</sup> T <sup>-1</sup> ]

So an increase of the concentration will not change the rate of the reaction. An example of this kind of reaction can be a photochemical reaction.

### 3.4.2 First-order reaction

If a reaction is only depending on the concentration of one reactant, then it will be called first-order:

$$\frac{dc}{dt} = -kc \quad \text{EQ. 3-25}$$

in which

k: first order reaction rate coefficient [ $T^{-1}$ ]

The higher the concentration is, the faster the reaction. An example of this reaction is the radioactive decay or the mortality of bacteria (excluding grazing processes).

### 3.4.3 Second-order reactions

If two constituents react to form one or more products, then the reaction will be called second-order.

The reaction rate depends on the concentration of both reactants and can be described by

$$\frac{dc_A}{dt} = \frac{dc_B}{dt} = -k c_A c_B \quad \text{EQ. 3-26}$$

where

$c_A, c_B$ : concentration of reactant A and B [ $ML^{-3}$ ]  
k: second order reaction rate coefficient [ $M^{-1}L^3T^{-1}$ ]

### 3.4.4 Michaelis-Menten kinetic

Another important kinetic, which is used in many models is the Michaelis-Menten kinetic (Michaelis and Menten, 1913). It is often used to represent the growth of biomass due to a substrate. It can be written as

$$\frac{dc_B}{dt} = \frac{\mu_{\max,B} \cdot c_S}{k_M + c_S} c_B = \mu_B \cdot c_B \quad \text{EQ. 3-27}$$

in which

$c_B, c_S$ : concentration of e.g. bacteria and substrate [ $ML^{-3}$ ]  
 $\mu_{\max,B}$ : maximum growth rate of bacteria [ $T^{-1}$ ]  
 $\mu_B$ : actual growth rate [ $T^{-1}$ ]  
 $k_M$ : half saturation concentration [ $ML^{-3}$ ]

The half saturation concentration corresponds to the concentration of the substrate, at which the growth of biomass is exactly half of the maximum possible rate. If there is no limitation in substrate, i.e. the concentration  $c_S$  will tend to be large compared to  $k_M$ , the growth tends to

$\mu_{\max,B}$ . In this case the kinetic acts like a zero-order reaction. On the other hand, if the substrate concentration is very low, the growth rate depends only on  $k_M$ , with reaction of zero-order.

The above shown formulas and approaches are part of many different types of models. Many currently used watershed or river models are a collection of smaller and former separated, more specific models, e.g. a rainfall-runoff model, a model for the instream routing of flow and constituents (often one dimensional) or a water quality model (often zero dimensional).

In the following, three current water basin models are presented and their main features are described.

### 3.5 HSPF

#### 3.5.1 *General*

The Hydrologic Simulation Program – FORTRAN, called HSPF, was developed by the U.S. Geological Survey (USGS) and the U.S. Environmental Protection Agency (EPA), and is capable of simulating hydrologic and water quality processes on land surfaces, streams, and impoundments.

Beginning in the early 1960's, the model was developed as the Stanford Watershed Model, later in the 1970's, water-quality processes were added and a FORTRAN version was developed, incorporating the following models:

- Hydrocomp Simulation Programming (HSP) (Hydrocomp, 1976; Hydrocomp, 1977)
- NonPoint Source Model (NPSM) (Donigian and Crawford, 1976b)
- Agricultural Runoff Management (ARM) Model (Donigian et al., 1977; Donigian and Crawford, 1976a)
- Sediment and Radionuclides Transport (SERATRA) (Onishi and Wise, 1979)

In the 1980's, preprocessing and postprocessing software, algorithm enhancements, and use of the USGS WDM system (Watershed Data Management) were added, which is the basic (binary) library to store, read and write time series in HSPF.

#### 3.5.2 *Framework of the model*

HSPF has been incorporated as a computation option into the USEPA Better Assessment Science Integrating Point Sources (BASINS) developed by Tetra Tech Inc. under a contract of the USEPA (Epa, 1998). The purpose of BASINS is the collection of features from different models in a comprehensive ArcView GIS pre- and postprocessor to ease the construction of input files and the analysis of the output in terms of TMDL standards and guidelines in the USA (Borah and Bera, 2003). Data for the USA can be directly assessed and downloaded from the internet.

Unfortunately, there is much more additional data needed within BASINS than what is needed for HSPF. This means for catchments outside the USA, a lot of data has to be produced and collected, which will not be included in the steering files. So the use of BASINS, which is normally meant to help and to accelerate the application, can sometimes be more time consuming than the direct setup of the HSPF project.

### *3.5.3 Programming philosophy*

The program is written in FORTRAN. The source code of the model version 12 was not available.

### *3.5.4 Input and Output*

Many software tools developed by the U.S. Geological Survey (USGS) are used by HSPF and BASINS to provide interactive capabilities concerning model input, data storage, input-output analyses and calibration such as WDMUtil (Hummel et al., 2001) and GenScn (Kittle et al., 1998). Steering files for HSPF can be either created by a text editor or by the use of the spatial and timeseries data provided in the ArcView GIS interface called BASINS.

For simulation with HSPF, the basin has to be represented in terms of land segments and reaches or reservoirs. A land segment is a subdivision of the simulated watershed. The boundaries can be established according to the user's needs, but generally, a segment is defined as hydrological response unit (HRU). For modelling purposes, water, sediment and water quality constituents leaving the watershed move laterally to a downslope segment or to a reach/reservoir. A segment of land that has the capacity to allow enough infiltration to influence the water budget is considered pervious, otherwise it is considered impervious. These two groups of land segments are simulated independently.

### *3.5.5 Flow routing*

In HSPF, the various hydrologic processes are represented mathematically as flows and storages. In general, each flow is an outflow from a storage, usually expressed as a function of the current storage amount and the physical characteristics of the subsystem. Thus the overall model is physically based, although many of the flows and storages are represented in a simplified or conceptual manner.

In pervious land segments HSPF models the movement of water along three paths: overland flow, interflow and groundwater flow. Each of these three paths experiences differences in time delay and differences in interaction between water and its various dissolved constituents.

Processes that occur in an impervious land segment are also simulated. Even though there is no infiltration, precipitation, overland flow and evaporation occur and water quality constituents accumulate and are removed.

The hydraulic and water quality processes that occur in the river channel network are simulated by reaches. The outflow from a reach or completely mixed lake may be distributed across several



targets to represent normal outflow, diversions and multiple gates on a lake or reservoir. Evaporation and precipitation are represented, but there is no instream infiltration, so a reach cannot dry up along the flowpath.

Routing is done using a modified version of the kinematic wave or storage-routing method. The model requires a function table for depth, volume and discharge relationships for each reach.

### 3.5.6 *Temporal scale*

HSPF has a standard input time step of 1h. Steering files created with BASINS and time series processed in WDM-database files with WinHSPF (the graphical user interface designed for Microsoft Windows) have a standard time step of 1h.

If available time series are different from that, WDM-UTIL will provide methods for disaggregation.

HSPF is suitable for long term simulations in the magnitude of years.

### 3.5.7 *Water quality*

HSPF simulates for extended periods of time the hydrologic and associated water quality, processes on pervious and impervious land surfaces and in streams and well-mixed impoundments. The determinants simulated by HSPF are summarized in Table 3-1.

Table 3-1: Considered state variables in HSPF

- |                      |                                  |
|----------------------|----------------------------------|
| o ammonium           | o pH                             |
| o nitrite-nitrate    | o dissolved oxygen               |
| o organic nitrogen   | o biochemical oxygen demand(BOD) |
| o orthophosphate     | o temperature                    |
| o organic phosphorus | o pesticides                     |
| o phytoplankton      | o conservatives                  |
| o zooplankton        | o faecal coliforms               |

### 3.5.8 *Particulate transport and benthic processes*

HSPF estimates sediment transport by the transport capacity approaches of Tofaletti (1969), Colby (1964) or by a user-specified power function of velocity for three different, non-interacting sediment fractions. This includes the following assumptions:

1. Sediment transport does not change the morphology and therefore has no effect on the hydraulic properties of the reach.
2. The deposition or scour of each fraction does not affect the availability of the other fractions.

3. The longitudinal movement of bed sediments is not implemented.
4. Sediment storage on the bottom is unlimited; resuspension is only a function of stream properties.

A problem with this process will occur, if the regarded element falls dry during the simulation.

### ***Accumulation in HSPF by the example of BOD***

In perennial streams one can assume, that the bed and the water phase of the stream are more or less in an equilibrium condition. Figure 3-9 shows some of the implemented processes in HSPF concerning the interactions of settled and suspended BOD.

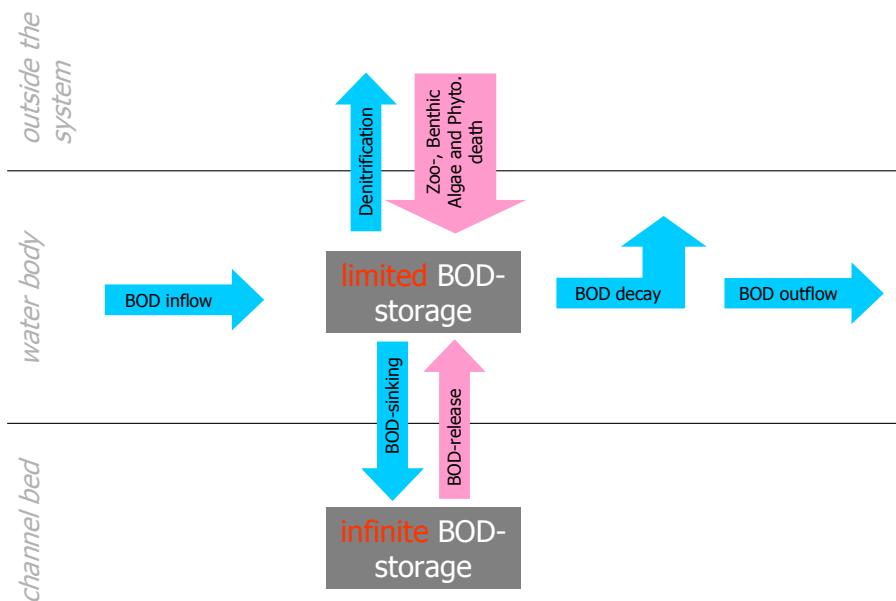


Figure 3-9 BOD release in HSPF

It becomes clear, that HSPF accounts for the mass balance of BOD, but assumes an infinite storage with a constant release rate from the bottom. This circumstance is not restricted to BOD, but also true for any other constituent, either solute or particulate.

An example of sediment transport was found by Gallart et al. (2003) in the Vallcebre catchments situated in the Spanish Pyrenees. It was observed, that high sediment transport activities occurs after summer even if most of the catchment does not contribute to the stream flow. Thus, a significant part of the entrained sediments must have been deposited in the channels before (during summer) and are later taken in suspension during wetter conditions (Gallart et al., 2003). The assumption of an infinite storage is a major limitation, because it neglects the processes of erosion and deposition. These are especially important especially in the context of temporary rivers.

## 3.6 CASCADE

### 3.6.1 *General*

Development of the CAtchment-SCAle DELivery model (CASCADE) started in the 1990's under the UK Natural Environment Research Council (NERC) LOIS (Land-Ocean Interaction Study) programme (Cooper and Naden, 1998; Leeks and Jarvie, 1998). The model was originally developed for use in humid temperate catchments with permanent water courses.

### 3.6.2 *Framework of the model*

The original CASCADE model comprised a delivery component only. This was linked to the QUESTOR in-stream water quality model (Boorman, 2003), which was itself derived from the QUASAR model (Whitehead et al., 1979). The delivery-only version of CASCADE was based on an HRU (hydrological response unit) conceptualisation of a catchment, with delivery by landscape class within HRU to a DEM-based stream network.

Later, a 1D variable parameter kinematic wave model using an improved four-point interpolation scheme proposed in Holden and Stephenson (1988) was developed for the instream routing of both water and constituents in the channels.

It was intended to be applied for catchment sizes of approx. 100-1000 km<sup>2</sup> with a daily time step for delivery to rivers, whereas the time step within the rivers is flow-dependent.

### 3.6.3 *Programming philosophy*

The program was established for research purposes and is written in FORTRAN 77. The code follows a traditional structure and is not easily readable. The source files were available within the tempQsim project since 2004.

### 3.6.4 *Input and output*

Being a research model, CASCADE does not have sophisticated pre- or post processors and no graphical user interface. All input data must be prepared with external text editors.

For full implementation including the instream- and the delivery-part, CASCADE requires geometric, process and input information to produce simulation results.

A stream network in geographic coordinates, an elevation grid as well as a landscape classification has to be available in order to derive the HRUs. If just the instream part is applied, only the first two are required.

Further, effective rainfall and other external sources of water quality variables have to be defined. Rate parameters for flow (roughness coefficient), sediment particle size distribution, water quality parameters for bed sediment as well as for the water phase have to be chosen in the steering files.

CASCADE has most recently been applied to phosphorus transfers and includes a range of processes influencing particulate phosphorus and dissolved phosphorus concentrations, both of them are related to suspended sediment properties and concentrations (Cooper et al., 2002b).

### 3.6.5 *Flow routing*

The instream component of the CASCADE model uses a numerical solution of the kinematic wave equation with advection. The solution takes account of lateral sources of water, and lateral sources of pollutants. It also includes source and sink terms, to represent internal processes.

Instream CASCADE uses a reduced river network derived from a full DTM river network. Contributions from the HRUs to the river network are estimated as daily discharges and loads. In principle, input from an HRU occurs all along a river reach, but in CASCADE it is treated as a point source at the most downstream point at which the HRU contributes to the river network. However, the daily input at each point is assumed uniformly distributed over the day. By construction, HRU point inputs are always at the top of a reach.

The model uses a fixed reach length, but adjusts  $\Delta t$  to ensure numerical stability of the solution algorithm. For each reach, the model simulates discharge through each day, with sub-daily time steps. The channel geometry and characteristics are estimated from DTM slopes, and empirical relationships between mean annual discharge and channel width. The roughness coefficient must be taken from tabulated values, according to the morphology of the stream.

Solution of the Muskingum-Cunge equation in CASCADE follows an implicit scheme (Holden and Stephenson, 1988). The model uses this numerical solution of the kinematic wave equation with advection, and has been applied successfully as such (Cooper et al., 2002b). It is necessarily limited in situations where the kinematic wave equation is a poor approximation to the major processes occurring.

There is a general weakness of this kind of models which use a comparable routing method based on fluxes through a FD discretisation. Problems occur with steep gradients and are caused by the fact that Variable Parameter Muskingum-Cunge routing methods are not volume conservative (as shown in Tang et al., 1999). This MC-routing method can also produce a leading-edge “dip” phenomenon in the outflow of a reach during the rise of the flow, where the outflow hydrograph can drop below the initial steady flow and can even be negative if this is allowed (Tang et al., 1999).

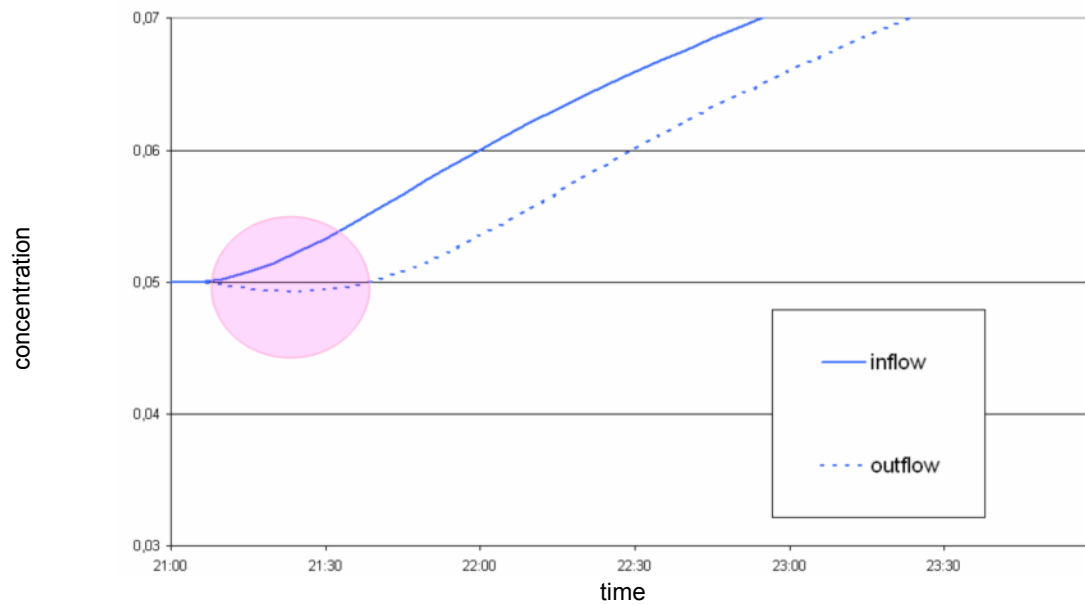


Figure 3-10: Leading edge dip phenomenon in Muskingum-Cunge flood routing

These phenomena are negligible under normal flow conditions with slowly varying discharges but not in this context of temporary waters. If the period of the reinitiation of flow is not modelled exactly, there will be big errors in solute transport and resuspension of particulates.

These issues will be explained further in chapter 7.7.

### 3.6.6 *Temporal scale*

In the beginning, CASCADE was developed with the daily output timestep; the internal stepping depended on the courant criteria for stability reasons. Although the output timestep was later reduced, CASCADE is still a model which has its strengths in the computation of longer periods than a couple of years.

### 3.6.7 *Water quality*

Measured point sources and estimated diffusive sources can be included as river inputs. Solute and suspended matter are then transported via advection. A velocity dependent model component accounts for suspended sediment exchange with bed sediment as well as adsorption-desorption. Process models for nutrients can define source and sink terms (Cooper et al., 2002a; Cooper et al., 2002b).

Possible in-stream variables are shown in the following Table 3-2.

Table 3-2: Possible state variables in CASCADE

- o discharge
- o conservative tracer
- o temperature – required for process-rate dependencies
- o nitrate
- o ammonium
- o soluble reactive phosphorus
- o soluble unreactive phosphorus
- o dissolved organic carbon
- o biological oxygen demand
- o particulate organic nitrogen (component of suspended sediment)
- o particulate phosphorus (component of suspended sediment)
- o particulate organic carbon (component of suspended sediment)
- o suspended sediment
- o bed sediment – as a source of entrainment (finite size)

### 3.6.8 *Particulate transport and benthic processes*

The traditional transport capacity calculation was replaced by the formulas of Krone (1962) and Partheniades (1962). The critical shear stress for erosion is calculated using the approach of Bagnold (1966), and the critical settling shear stress chosen to be 85% of the one for erosion as default.

The model is capable of exchanging particulate phosphorus, carbon and nitrogen with the bed but does not continue any processes on the bottom.

## 3.7 MOHID Water Modelling System and the tempQsim – STREAM model

### 3.7.1 *General*

The development of MOHID Water Modelling System started in 1985 and was initially a two-dimensional tidal model written in FORTRAN 77 (Neves, 1985). At this time it was focused on studying estuaries and coastal areas using a classical finite-differences approach. In the following years, two-dimensional eulerian and lagrangian transport modules were included in this model and the concept of a finite volumes approach was introduced to replace the FDM.

It is currently maintained and developed by the MARETEC (Marine and Environmental Technology Research Center) group of the Instituto Superior Técnico (IST) at the Technical University of Lisbon. Up to now, it has been constantly enhanced by additional features and modules.

Unlike the two models above, the MOHID Water Modelling System is based on a distributed approach, so it is discretised on a grid.

### 3.7.2 *Framework of the model*

There are three core tools: (i) MOHID Water, (ii) MOHID Land and (iii) MOHID Soil.

---

The first tool is the improved version of the original tidal model, the second one is a watershed model and the third one simulates water flow through porous media.

All models share the same framework of post- and pre-processors and can therefore easily be coupled or substituted by others. During the European project tempQsim, the river network part of MOHID Land was developed and enhanced further under the name tempQsim – STREAM model.

The tempQsim – STREAM model consists of a hydrodynamic model which can be coupled with a non-steady state water quality model and a benthic model.

### 3.7.3 Programming philosophy

The model was reorganised in 1998, using an object oriented conceptualisation in ANSI FORTRAN 95 as described in Decyk et al. (1997) and Miranda et al. (2000).

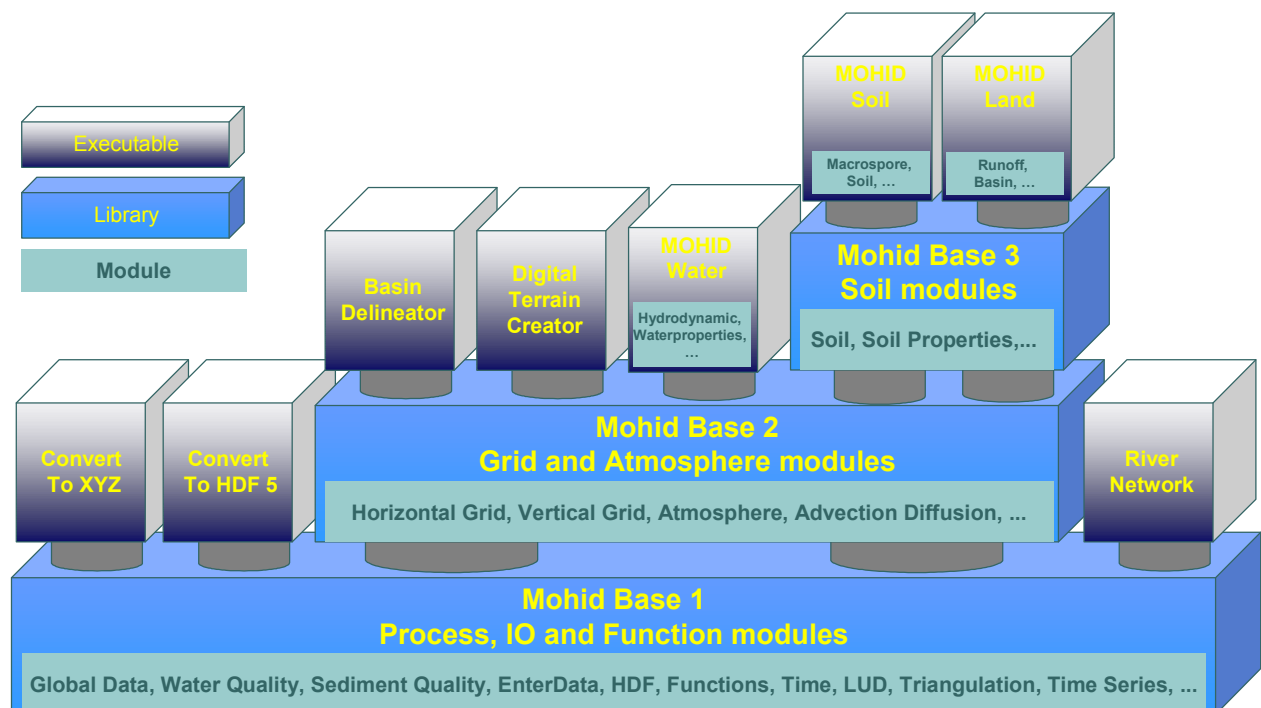


Figure 3-11: Internal structure of the MOHID framework (Braunschweig et al., 2004)

It is subdivided into several modules (classes) as shown in Figure 3-11.

### 3.7.4 Input and output

The tempQsim – STREAM model can produce results of two types: (i) time series at a given point and (ii) matrix data of the whole river system.

The TIME SERIES EDITOR, embedded in the front-end of the GUI, can be used for visualisation of input or output time series.

MOHID GIS allows formatting input files for the simulations, e.g. the delineation of the drainage network from a given digital terrain model. Furthermore, it can be used for the visualisation of matrix data (results varying in time and space) using the HDF format which is a platform

independent compressed binary file format storing matrix data in a hierarchical form (NCSA and Technologies, 2005).

The model needs time series of arbitrary time step of solar radiation, air temperature, cloud cover, relative humidity and wind speed for the computation period.

A drainage network has to be defined either manually or with MOHID-GIS, along with point discharges. For every point discharge the variable for flow, temperature or constituents can be given either constant or as external time series varying over time.

About 200 parameters (growth rates, half saturation constants etc.) for the water quality part can be either defined in the steering file or left to the default value preset in the program.

#### *3.7.5 Flow routing*

The hydrodynamics can be computed with the kinematic wave, non-inertia wave or the full Saint-Venant equations. The solution can be done implicit (with an approach similar to CASCADE) or explicit. In this study, only the explicit kinematic wave approach was applied.

Downstream boundary can be null gradient, a dam, or an imposed level at the outlet node.

#### *3.7.6 Temporal scale*

The calculation time step for the hydrodynamic can be chosen to be either constant, or in between a range. The time step is then adopted according to the courant criteria to guarantee numerical stability. Time steps of the water quality modules can be defined differently.

#### *3.7.7 Water quality*

The water quality module is a zero-dimensional ecological model which was developed based on WASP (Wool et al., 1993) and further enhanced. It now considers 18 state variables concerning water quality as shown in Table 3-3.



Table 3-3: Considered state variables in the tempQsim – STREAM model

- |  |                                   |
|--|-----------------------------------|
| o particulate organic nitrogen                               | o dissolved oxygen                |
| o dissolved refractory and non refractory organic nitrogen   | o biochemical oxygen demand (BOD) |
| o ammonium, nitrate, nitrite                                 | o temperature                     |
| o particulate organic phosphorus                             | o salinity                        |
| o dissolved refractory and non refractory organic phosphorus | o cohesive sediment (3 fractions) |
| o inorganic phosphorus                                       | o TSS and VSS                     |
| o phytoplankton  | o algae                           |
| o micro- and macrozoobenthos                                 | o heterotrophic bacteria          |

Water properties are routed by an advection diffusion equation including a settling and erosion term in case of particulate suspended matter. Diffusion is quantified by Fick's Diffusion Law.

The water quality part is subdivided into different parts, which can be turned on and off to fit to the respective situation.

### 3.7.8 *Particulate transport and benthic processes*

The benthos module has been developed to compute biogeochemical processes in the benthic zone at the water-sediment interface. Particulate phases can settle and deposit at the river bed where they will be subject to further conversion. Several processes can be computed, including:

- o algal mortality
- o particulate organic matter mineralization
- o biogenic silica dissolution
- o oxygen depletion
- o growth of heterotrophic bacteria in the river bed (often caused by point source inputs in dry phases where shear stresses are low).

The erosion algorithm is based on the approach of Partheniades (1962), deposition on the algorithm which was first proposed by Krone (1962) and later on modified by Odd and Owen (1972).

The approach was further modified to account for hiding ability of fractioned sediment within this study.

### 3.8 Conclusions of the model survey and extension of the tempQsim – STREAM model

The detailed model survey revealed some limitations in each of the tested software.

HSPF offers with no doubt the most complete collection of processes. Nevertheless, this complexity leads also to a limited applicability in cases, where the required data is not available. Furthermore, it was found that the model lacks some of the most important features needed for temporary rivers as shown above. However, as it was not meant to be directly targeted to semi-arid basins, it is with no doubt a very useful and widely accepted as well as applied model.

Being a research model with no intention of the developers to distribute it to a wide user community, CASCADE shows its main restrictions in the normal data handling. As it is even difficult to understand the idea behind well documented data structures (as in HSPF), a lot of time had to be spend to identify the needed input and its structure.

Based on the experiences during the model review and the data analysis during the project tempQsim, the MOHID Water Modelling System was chosen as a platform for the development of the tempQsim – STREAM model.

The tempQsim – STREAM model shares the graphical user interfaces and many of the core modules with the MOHID Water Modelling System. Its structure is based on a modern object oriented programming approach and exhibits superior data handling which eases its advancement and usability.

In the following, the extensions done in the tempQsim – STREAM model are shown, source code of the major changes can be found in chapter 7.10. The extensions done in the Cascade model and its limitations as representative for other commonly used approaches can be found in chapter 7.7.

#### 3.8.1 *Output of loads*

In the interpretation of results in terms of first flush dynamics, the changes in loadings over time are of great importance. In order to facilitate interpretation the tempQsim – STREAM model is now able to output loadings for every substance, if specified in the steering file.

#### 3.8.2 *Modification of post processor “timeseries editor”*

Because preparation of NCL-curves (see chapter 2.2.4) is time consuming, the postprocessor of MOHID has been modified. On the basis of a given interval and a flow timeseries, the postprocessor can now draw NCL vs. NCF-curves (normalized cumulative flow), NCL vs. time and RMF-curves (relative mass fluxes).

#### 3.8.3 *Bacterial growth in pools*

During the dry phases temporary rivers are often subject to greatly increased growth of bacteria downstream of point source inflows (cp. chapter 7.12). Due to the inputs of these sources (e.g.

---

WWTPs), small ponds or pools with very low stream velocity are forming in the river and an accumulation of organic matter can take place on the river bed and in the riparian zone. As it will be shown below (chapter 4), this accumulated matter can be responsible for increased loadings during the onset of early autumn floods.

### ***Bacteria dynamic in the benthic reactor***

In order to account for this accumulation, the tempQsim – STREAM model was extended following a simplification of the concept of the ASM3 (Gujer et al., 1999a; Gujer et al., 1999b).

Bacterial concentration has been defined as a particulate substance and is therefore enabled to sink to the bottom. On the river bed (represented by the module benthos in the model) the bacteria can continue growth by consuming particulate organic matter (POM, represented by PON) and dissolved non-refractory organic matter (DOMnr, represented by DONnr) as shown in Figure 3-12. Dead bacteria are then converted into refractory particulate organic matter (POMr, represented by PONr).

The dynamic of the heterotrophic bacteria is calculated via

$$\frac{\partial b_{bact}}{\partial t} = (\mu^{bact} - m^{bact}) b_{bact} \quad \text{EQ. 3-28}$$

in which

t:	time [T]
bact:	heterotrophic bacteria in [ML <sup>-2</sup> ]
$\mu^{bact}$ :	total growth rate of heterotrophic bacteria [T <sup>-1</sup> ]
$m^{bact}$ :	natural mortality rate of bacteria [T <sup>-1</sup> ]

Whereas the mortality is directly given by the user, the growth rate is -similar as in the aquatic phase- corresponding to the uptake:

$$\mu^{bact} = \mu_{DOM}^{bact} + \mu_{POM}^{bact} \quad \text{EQ. 3-29}$$

in which

$\mu_{DOM}^{bact}$ :	bacteria uptake of dissolved organic matter [T <sup>-1</sup> ]
$\mu_{POM}^{bact}$ :	bacteria uptake of particulate organic matter [T <sup>-1</sup> ]

The uptake of particulate organic matter is then realised through the Monod-Kinetic:

$$\mu_{POM}^{bact} = \frac{\psi(T) \cdot \mu_{max}^{bact} \cdot POM_{bottom,r}}{K_N^{bact} + POM_{bottom,r}} \quad \text{EQ. 3-30}$$

$$POM_{bottom,r} = \frac{POM_{bottom}}{h_{benthic}} \quad \text{EQ. 3-31}$$

where

$\mu_{\text{POM}}^{\text{bact}}$ :	bacteria uptake rate of POM [ $\text{T}^{-1}$ ]
$\psi(T)$ :	temperature limitation factor [-] as function of water temperature
$\mu_{\text{max}}^{\text{bact}}$ :	maximum bacteria uptake rate [ $\text{T}^{-1}$ ]
$\text{POM}_{\text{bottom}}$ :	concentration of POM at the bottom in terms of bottom area [ $\text{ML}^{-2}$ ]
$\text{POM}_{\text{bottom,r}}$ :	POM at the bottom in terms of the benthic reactor [ $\text{ML}^{-3}$ ]
$h_{\text{benthic}}$ :	depth of the benthic reactor [L]
$K_{\text{N}}^{\text{bact}}$ :	nitrogen half saturation constant for bacteria uptake [ $\text{ML}^{-3}$ ]

Because it was known that nitrogen is the main limitation in the catchment, a limitation of phosphorus was not considered within the bacteria growth until now. Phosphorus and nitrogen are coupled in the mass of organic matter via nitrogen to carbon and phosphorus to carbon ratios, which, if not defined in the steering file, were chosen according to Redfield (1934).

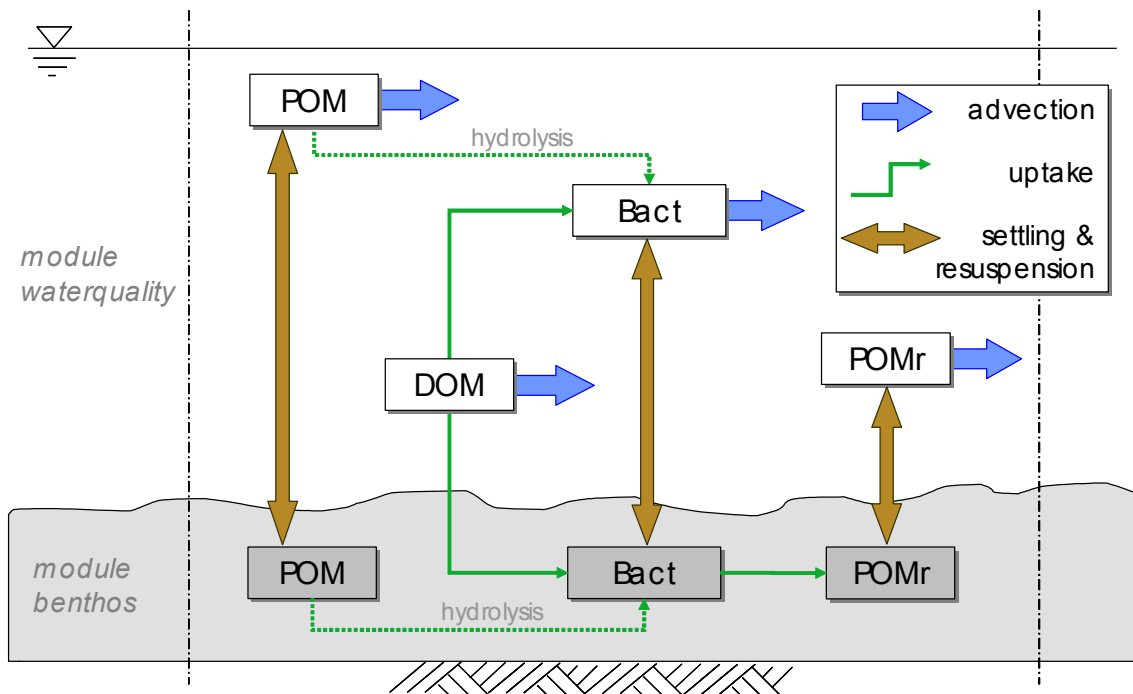


Figure 3-12: Scheme for processes of heterotrophic bacteria introduced in the tempQsim – STREAM model

The uptake rate of particulate organic matter is only depending on the amount of deposited material. Deposited POM is normally given as mass per area in the model. A problematic task was the determination of the availability of these particulate nutrients and to secure comparability with the uptake of the bacteria in the water phase. For this purpose, the deposited POM is converted to a concentration in terms of mass per volume. A benthic reactor depth was introduced, which can be given by the user in terms of the flow depth or by absolute values. A hydrolysis rate is currently only indirectly considered due to the high residence times in the pools.

The uptake rate of dissolved organic matter depends on the concentration of DON<sub>nr</sub> in the water phase, i.e. no vertical gradient is considered. Although this might be changed in future

version by the introduction of additional horizontal layers, this assumption seems reasonable, as the water depth in the period with the highest accumulation hardly exceeds 30 cm.

### 3.8.4 Fractioned sediment transport

Temporary rivers are characterised by highly varying stream velocities. Dry phases with hardly any movement alternate with flash flood events. In the original version of the model, cohesive mineral sediment was only considered as one fraction. In order to account for the great variability in velocity (which is one main driver of sediment transport capacity), the module was extended to include two additional sediment fractions. For each of the three fractions, parameters such as fall velocity, critical shear stresses for erosion and deposition, erodibility etc. can be chosen by the user in the steering files or will be computed independently.

### 3.8.5 Calculation of TSS and VSS

In order to simplify calibration and comparison with commonly measured parameters, the properties total suspended solids (TSS) and volatile suspended solids (VSS) were added (EQ. 3-32 and EQ. 3-33).

$$VSS = (\alpha_{N:C}^{phy} phyto + \alpha_{N:C}^{dia} diatoms + \alpha_{N:C}^{zoo} zoo + \alpha_{N:C}^{cil} ciliates + \alpha_{N:C}^{bact} bact + POM + POMr) / \alpha_{N:TS} \quad \text{EQ. 3-32}$$

$$TSS = \sum_i cohesive\ sed_i + VSS \quad \text{EQ. 3-33}$$

in which

VSS:	volatile suspended solids [ML <sup>-3</sup> ]
$\alpha_{N:C}^X$ :	nitrogen to carbon ratio of living substance X [-]
$\alpha_{N:TS}$ :	ratio of nitrogen to dry substance [-]
phyto:	phytoplankton [ML <sup>-3</sup> ]
diatoms:	diatoms [ML <sup>-3</sup> ]
ciliates:	ciliates [ML <sup>-3</sup> ]
bact:	heterotrophic bacteria [ML <sup>-3</sup> ]
POM:	particulate organic matter [ML <sup>-3</sup> ]
POMr:	particulate refractory organic matter [ML <sup>-3</sup> ]
TSS:	total suspended solids [ML <sup>-3</sup> ]
cohesive sed <sub>i</sub> :	i <sup>th</sup> cohesive sediment fraction [ML <sup>-3</sup> ]

VSS is the sum of all transported particulate organic living and dead matter and TSS is the sum of VSS and the mineral sediment fractions.

Organic matter and mineral sediment are normally based on different units in water quality models. In the tempQsim – STREAM model, the mineral sediments (cohesive sediment) are given in absolute masses or concentrations, living biota as phytoplankton or bacteria in mass of carbon (e.g. mg C/l) and dead organic matter in mass of nitrogen (mg N/l). As already implemented, every living variable can have its own nitrogen to carbon ratio defined in the steering file. So, a

major problem during the computation is the collection of the different ratios (nitrogen to carbon, carbon to dry mass etc.). Because there is no detailed data, the same ratio of nitrogen to dry substance had been defined for detritus (dead organic matter) and living organic matter to 224g N/2749g TS.

### 3.8.6 *New calculation of available erosion capacity for each fraction*

Each particulate fraction has a differing resistance to resuspension. So, if more than one fraction of particulate matter is considered, and if these fractions differ significantly in bottom concentration and erodibility, the total net erosion capacity of the stream flow has to be divided in some way on the fractions, to account for these differences.

Generally, the mass of mineral particulate matter is higher than the mass of organic particulate fractions. Normally this was done in the model by multiplying the calculated erosion rate with the ratio of the bottom concentration of the regarded particulate substance (e.g. PON) to the mineral sediment (called cohesive sediments in the model). The error introduced by this was considered to be negligible, because the concentration of cohesive sediment was assumed to be magnitudes higher than the concentration of particulate organic materials.

Due to the introduction of TSS in the model, it is possible to account for a better distribution of the available transport capacity. The erosion rate of each particulate substance is now depending on the proportion of this substance on the totally available particulate matter (TSS).

The erosion rate according to Partheniades (1962) has therefore been modified as follows

$$E [i] = M_e [i] \left( \frac{\tau_b}{\tau_{crit,e} [i]} - 1 \right) \cdot \left( \frac{substance [i]_{bottomconc}}{TSS_{bottomconc}} \right) \quad \text{EQ. 3-34}$$

where

$E[i]$ :	Erosion flux of particulate substance $i$ [ $ML^{-2}T^{-1}$ ]
$M_e[i]$ :	Erosion coefficient or erodibility [ $ML^{-2}T^{-1}$ ]
$\tau_b$ :	actual bottom shear stress [ $L^{-1}MT^{-2}$ ]
$\tau_{crit,e}[i]$ :	critical shear stress for erosion of substance $i$ [ $L^{-1}MT^{-2}$ ]
substance $[i]_{bottomconc}$ :	bottom concentration of substance $i$ [ $ML^{-2}$ ]
$TSS_{bottomconc}$ :	bottom concentration of TSS [ $ML^{-2}$ ]

This new approach was developed, to account for the situations in the accumulation pools. When there is a high inflow of nutrients, high concentrations of particulate organics will exist. These can temporarily reach up to the order of the mineral sediments. For temporary rivers with their capacity for mass retention and biomass accumulation, the assumption of the old approach was not valid.

Some other approaches, which mostly only account for mineral sediment fractions, define the available erosion capacity for each fraction by the spatial availability in combination with a hiding ability of smaller grain sizes between the coarser ones (Karim, 1998; Wu et al., 2000).

Due to the fact, that the differences in density are much higher, if a mixture of organic and mineral sediments is considered, an equal distribution over the bed area cannot be assumed here. Because there is no reliable assumption about the spatial distribution of particulate properties possible, the available erosion capacity of the current was divided in terms of mass.

This modified formula now allows the computation of different fractions of mineral sediment and will account better than the former approach for the varying flow conditions in temporary streams.

## 4 Water quality dynamics of Mediterranean rivers, data and results

Within the tempQsim project the methods for the characterisation of first flush dynamics as described in chapter 2 were applied to three catchments of different aridity: the river *la Vène* near the city of Montpellier in France, the *Mulargia* river on the southern part of the Italian island of Sardinia and *El Albuñón* in the Department Murcia, Spain. The Vène and the Mulargia are both comparable in size (about 67 km<sup>2</sup>) and in aridity, but the Mulargia seems to be a bit wetter. With a drained area of about 556 km<sup>2</sup>, Albuñón is nearly 9 times larger and has no clear annual discharge cycle.

All three are draining into larger basins of regional importance, the Vène and the Albuñón into lagoons at the Mediterranean Sea and the Mulargia river into the Mulargia Reservoir.

### 4.1 The basin of La Vène, France

#### 4.1.1 River characteristics

The Vène river is situated west of the City of Montpellier on the French Mediterranean coast. Its basin covers 67 km<sup>2</sup> rising from 2 to 323 m in elevation (as shown in Figure 4-1) and drains a part of the Thau lagoon catchment.

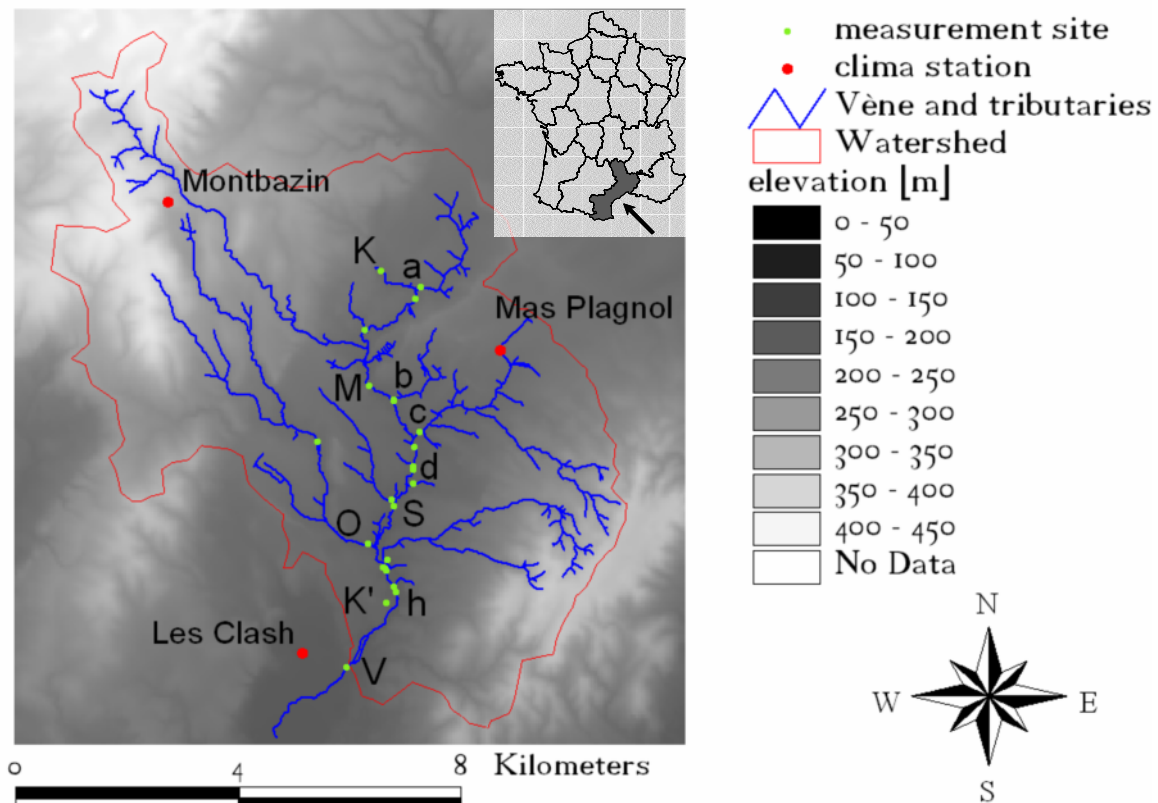


Figure 4-1: DEM and main field measurement sites of the Vène catchment



Fed by two main springs flowing out of a Jurassic karst (Cournonsec spring upstream and Issanka spring in the lower basin) the basin is also influenced by rainfall from outside the catchment. Its name is derived from the French word *avene*, which means cave, cavern or grotto and refers to its subterranean interconnection to the north.

The river has a 12-km course with a regular slope of 0.4% with cross sections about 3 to 5-meters wide and dense riparian vegetation, with abrupt banks (35%), straight walled banks (15%) or a mixed pattern.

Figure 4-1 shows the available rain gauges, the three waste water treatment plants (a, d and h) and the main sampling points at the karstic spring Cournonsec (K), the point S downstream Sanglier and the outlet of the catchment (V).

### ***General climatic situation and rainfall-runoff situation***

With an aridity index of  $AI \sim 0.46$  according to the UNEP (1997) classification (see Table 2-1), the basin of the Vène can be described as semi-arid.

Because there is no connected groundwater in the Vène catchment, the flow in the main river and the connecting tributaries decreases during spring and early summer, and is only partly sustained by domestic effluents. In this time, main parts of the river network dry up. In normal years, there is sufficient autumn and winter rain so that the river Vène starts flowing throughout its whole length every autumn.

The Vène may be therefore described as intermittent. Intermittent streams are dry for part of the year, but contain flow when the groundwater is high enough or during and after a storm event (Neitsch et al., 2002). Although there is no connection to groundwater, there are two main karstic springs which often retain flow during winter.

These springs can contribute significantly to the discharge, so that two kinds of floods can be identified: flash floods without any karstic influence at the outlet and karstic floods when one or both karstic springs are flowing.

Karstic floods are characterised by short rising period (less than one hour) but quite long lag time (about eight hours after the end of the rainfall event), and a very long recession period (from several days to several weeks). They occur with a return period of less than one year and only if more than  $\sim 120$  mm of rainfall are observed within less than a few days before. These floods always occur after one or several small floods (Froebrich et al., 2006).

### ***Soil and land-use situation***

The Vène catchment is characterised by sparse population; 12,400 inhabitants are distributed between three small villages. So only 3% of the total basin area is urban and 34% under agriculture of which 21% are vineyards (Figure 4-2). Natural vegetation covers almost all of the remaining area ( $>60\%$ ).

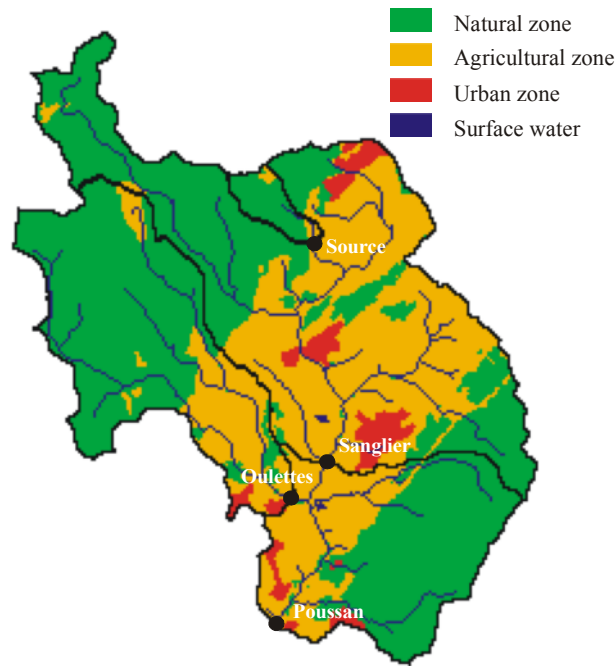


Figure 4-2: Land uses of the Vène catchment

### *Identified point sources*

Point-source pollutant inputs emanate from two wineries (b and c in Figure 4-1) and three waste water treatment plants (WWTP) that serve 9800 equivalent-inhabitants. The wineries only operate during summer and fall seasons. The effluents of the WWTPs have a strong seasonal variability due to the extensive lagooning treatment process (Figure 4-3).

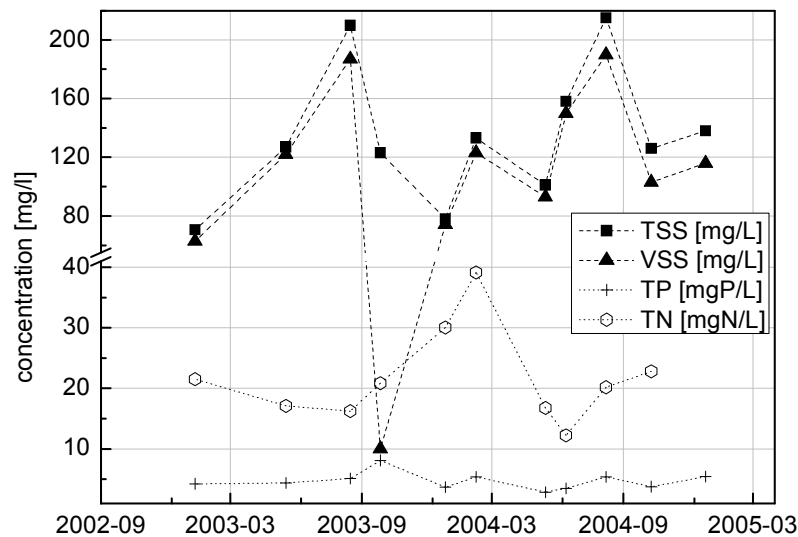


Figure 4-3: Effluent of the WWTP at Montbazin for selected constituents

Details of the site and instrumentation set up are described in Tournoud et al. (2005). Flow rates are derived from automatic measurements of flow depth over predefined rating curves with a time step of 5 minutes in the river. Water samples were taken manually in the middle of the flow section and were immediately filtered, preserved and analysed within less than 4 h. The samples

were analysed for total suspended solids (TSS), total phosphorus (TP), soluble reactive phosphorus (SRP), ammonium-nitrogen (NH<sub>4</sub>-N), nitrate and nitrite-nitrogen (NO<sub>x</sub>-N) and Kjeldahl nitrogen (KN) following the Standard Methods requirements (APHA et al., 1992).

#### 4.1.2 Relevancy of the dataset

Measurements in semi-arid or arid environments pose differing demands to equipment and campaign design than those in humid regions. The flow conditions are often strongly varying, and equipment has to resist extreme conditions. The executions of measurement campaigns might be restricted due to severe flooding events on the one hand, where the access to the river might be impossible, or on the other hand due to the absence of water in the stream network. This can lead to datasets, which only contain concentration measurements during some mean flow events, or measurement cumulated around big or characteristic events as e.g. first floods.

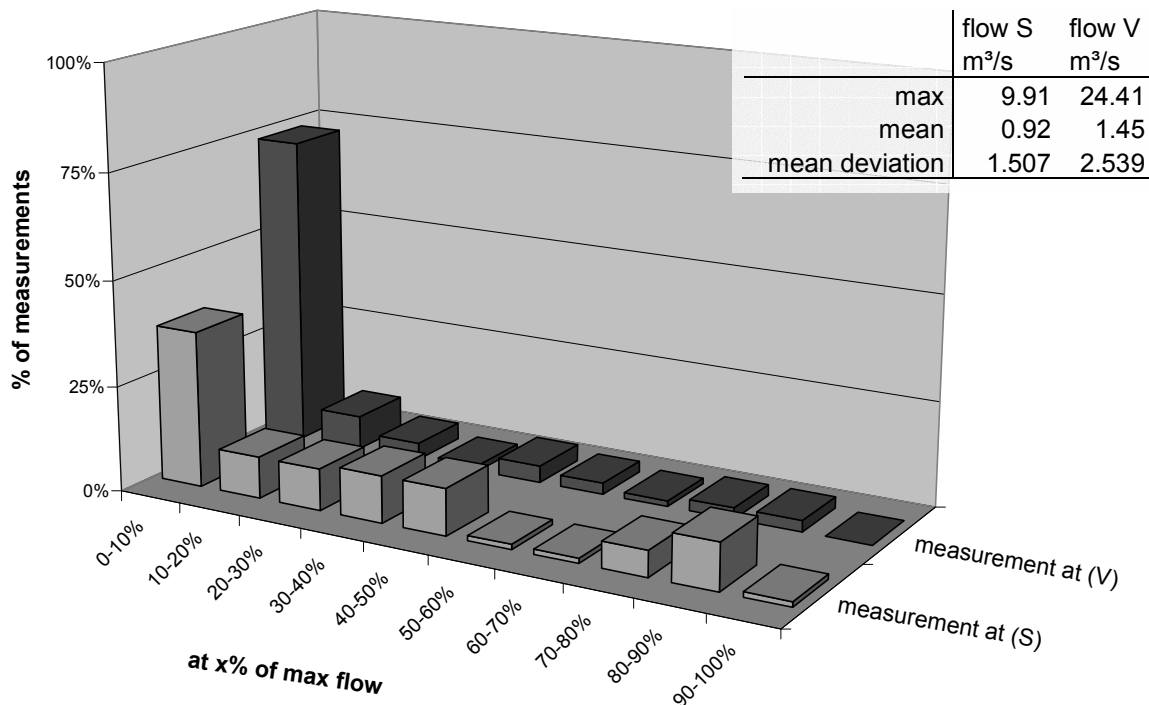


Figure 4-4: Distribution of measurements over flow condition at the Vène

Figure 4-4 shows a distribution of the available data points over the actual flow condition in relation to the maximum flow. Most of the measurements were taken during smaller events with lower flow intensity, so it seems unlikely, that the influence of a first flush flood on the overall transport regime will be overestimated just by the fact, that only big events are considered. However, most of the measurements were taken during September and October (up to 60 %).

#### 4.1.3 Annual cycle of transport – magnitude of months to years

As mentioned above, *Mediterranean climate* is characterised by intensive autumn and spring precipitation and summer droughts.

The sequence of wetting and drying favours a reoccurring cycle of increased transport followed by a period of accumulation with no or less transport through the outlet of the basin. Nutrients and pollutants can be retained within the system.

In the course of the year, between three main modes which alter nutrient concentrations can be distinguished (cp. Figure 4-5):

- i) accumulation
- ii) decomposition or other losses and
- iii) resuspension and transport

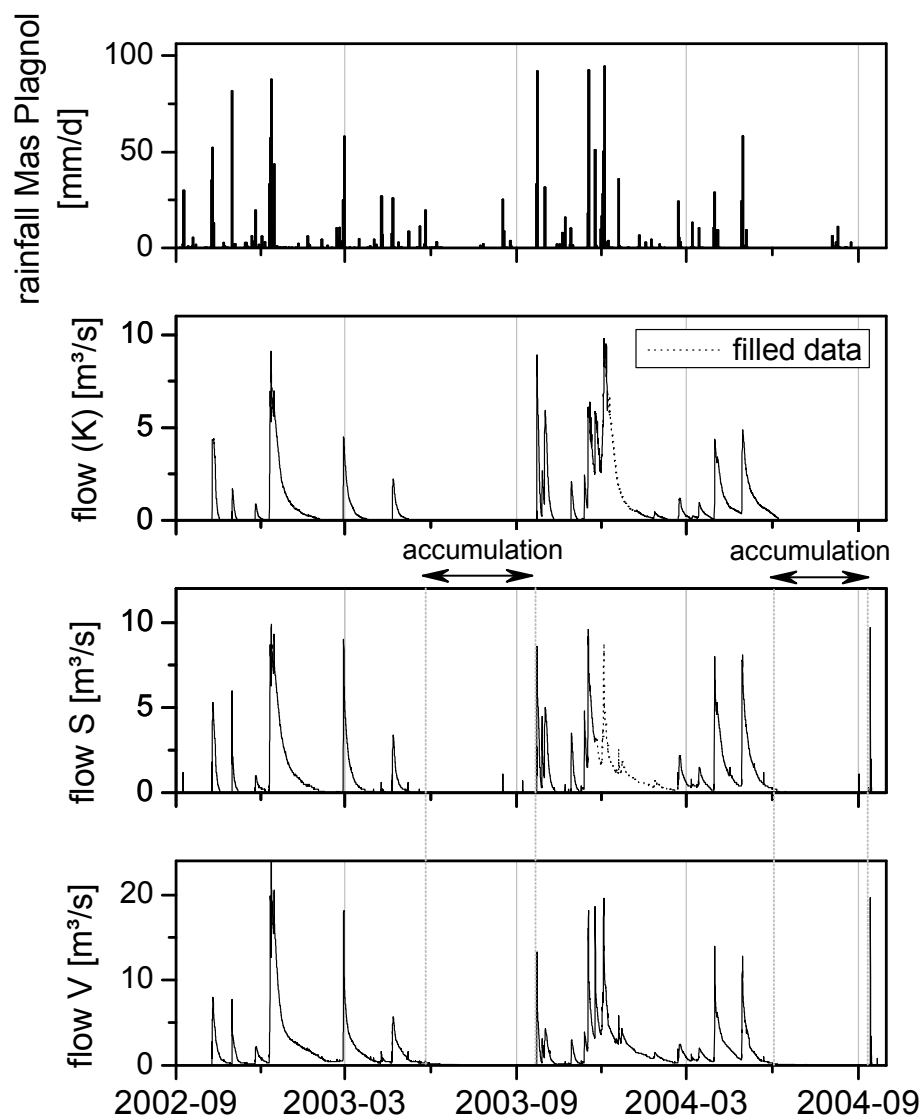


Figure 4-5: Hydrograph of stations K, S and V at the Vène

This annual cycle is typical for the semi-arid regions of the Mediterranean. For more arid regions (like e.g. in the south of Spain) the reoccurrence interval of rainfall and is much longer than a year and more unpredictable.

**Remark**

Unfortunately, during December 2003 and January 2004, there is no data of the stream gauge at S and for some period also not for the one at K. The probe at K was damaged by water intrusion and the one at S was even destroyed.

Due to this temporary failure, the flow at S had to be approximated for the following analyses. The data series of the flow measurements at S and V show a good coincidence (Pearson correlation coefficient of 0.93 and Nash-Sutcliffe efficiency of 0.70 (Nash and Sutcliffe, 1970), see chapter 2.1.2) and the station at V was fully operational. Hence, based on the last known measurement at S on 2003-11-26 up to the installation of a new probe at S on 2004-02-20, the course of flow at S was approximated by the following formula:

$$flow_S^t = flow_S^{t-1} + \frac{(flow_V^{t-1} - flow_V^{t-2})}{flow_V^{t-1}} flow_S^{t-1} \quad \text{EQ. 4-1}$$

in which

$flow_S^t$ : flow at station S [m<sup>3</sup>/s] at time t [h]

$flow_V^{t-2}$ : flow at station V [m<sup>3</sup>/s] at time t-2 [h], i.e. two hours before t

The formula in EQ. 4-1 considers the approximated transfer time for about one hour between the stations. Figure 4-5 shows these approximated data in a dotted line.

Because the karstic spring at K is fed by rainfall from another catchment to the north, it was not possible to make an approximation of the flow based on values from S or V for the missing period. Because the downstream gauging station at V did not record any major increase after the dysfunction of the probe at K, it was assumed, that it broke at the climax of the flood and that only an approximation of the falling limb was needed. The missing recession at K was therefore assumed by the recession which was measured at K from 2002-12-12 on and belongs to a flood of a similar peak value. The course was transferred to the missing period assuming, that the relative changes from point in time to another remain the same, i.e. in the same way as in EQ. 4-1.

#### 4.1.3.1 Distribution of precipitation

Figure 4-6 shows a mean distribution of precipitation in Hannover, Germany and Montpellier, France. In Hannover, the summer months bring most of the annual precipitation where in Montpellier rain falls mostly from September to November.

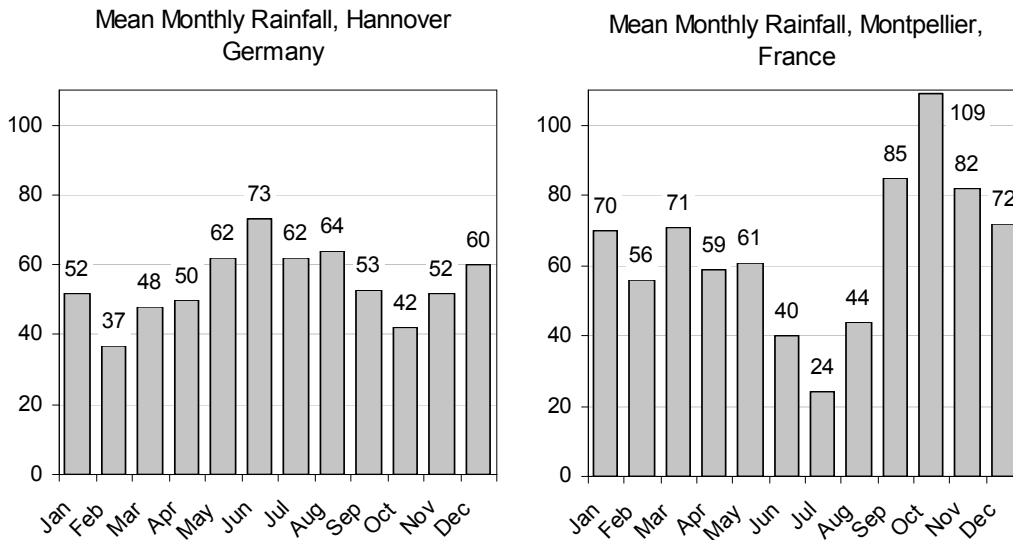


Figure 4-6: Mean Monthly values for precipitation in Hannover and Montpellier

Figure 4-7 shows the normalized cumulative rainfall and antecedent dry weather period for the weather stations “Montbazin” and “Mas de Plagnol” in the catchment. Normalized cumulative rainfall plots were derived by summation of continuous rainfall data up to each date and division by the total annual rainfall (cp. chapter 2.2.4). Antecedent dry weather days are the number of days which have past since the last occurrence of rainfall.

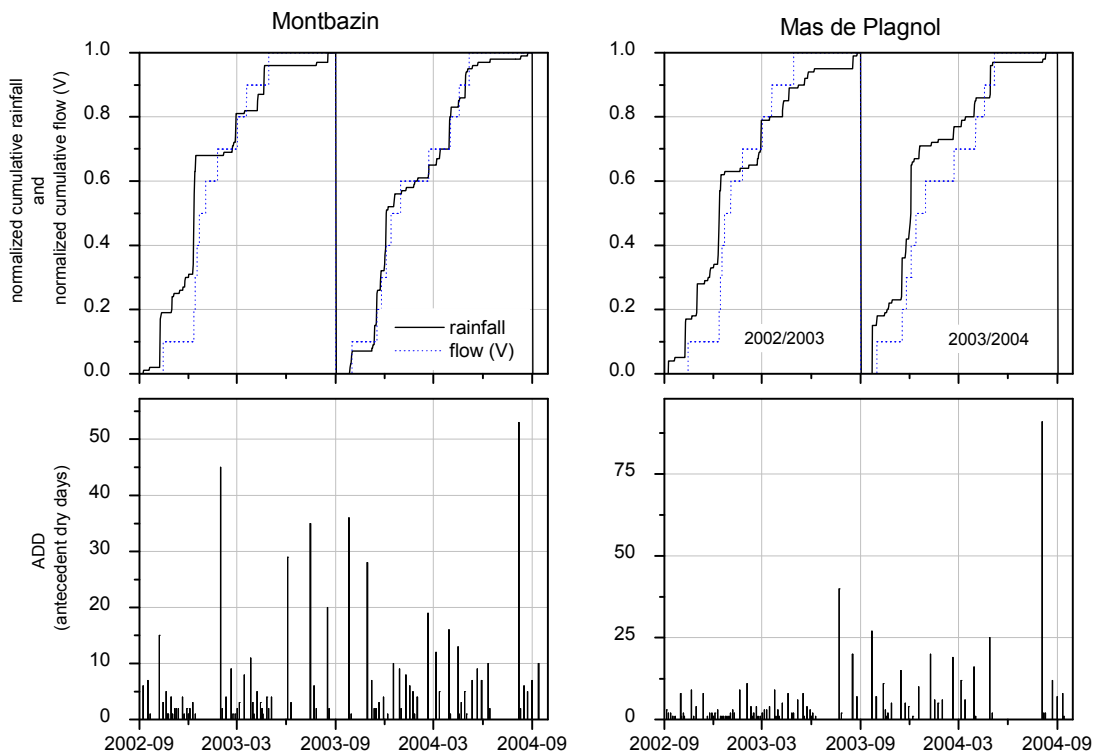


Figure 4-7: Normalized cumulative rainfall and antecedent dry period for three weather stations in the Vène catchment

In the first quarter of each of the investigated hydrological years (here starting from September 1<sup>st</sup> and ending at August 31<sup>st</sup>) normally 60-70 % of the total rain volume occurs (cp. Figure 4-7). After Tournoud et al. (1997), autumn storms can represent up to 75 % of the total annual rainfall.

#### 4.1.3.2 Relevancy of antecedent dry weather period

Even though many studies suggest a relationship between the antecedent dry weather period (ADWP) and the occurrence of a first flush, e.g. Larsen et al. (1998) or Gupta and Saul (1996), no strong relationship could be found on the basis of the data presented herein (see Deletic, 1998).

This may have different reasons:

- i) the measurements (excluding flow, conductivity, temperature) were not accomplished regularly, but on the basis of events, so that the choice of the time for a measuring campaign can influence a correlation negatively;
- ii) the spatial distribution of rainfall is, even though the catchment is quite small (67 km<sup>2</sup>), very inhomogeneous; it is not always possible to find one representative weather station for the whole catchment (as shown in Figure 4-7 the ADWP of weather stations in one catchment may differ enormously);
- iii) the ADWP does not consider the strength of an occurring event, only its appearance;
- iv) the ADWP does not exclude smaller events which occur after a longer dry period and can produce overland runoff, but are not sufficient to produce discharge in the river or respective parts of the river; it is not a proper indicator of the wet- or dryness of the system.

Deletic (1998) tried to correlate a lot of characteristics to the occurrence of a first flush (see above chapter 2.2.1), but finally came to the conclusion, that even complex multiple regression functions will not be sufficient to predict a first flush. Furthermore it was pointed out, that deterministic modelling approaches may be required, which are targeted to this specific purpose.

A reason, why no relationship was found between ADWP and a flush could also be the fact, that there was no distinction in terms of the sources of the flush. It became clear, that flushing effects caused in the Vène by a karstic spring flood and a prior accumulation due to biomass accumulation may happen independently from any rainfall in the catchment.

#### 4.1.3.3 Comparison of monthly rainfall

In terms of total annual rainfall, the year 2002/2003 can be considered to be a bit drier (about 731 mm/a) than 2003/2004 (ca. 824 mm/a). The tendency of increased autumn rainfall can be found in both years (see Figure 4-8), although the monthly distribution is different.

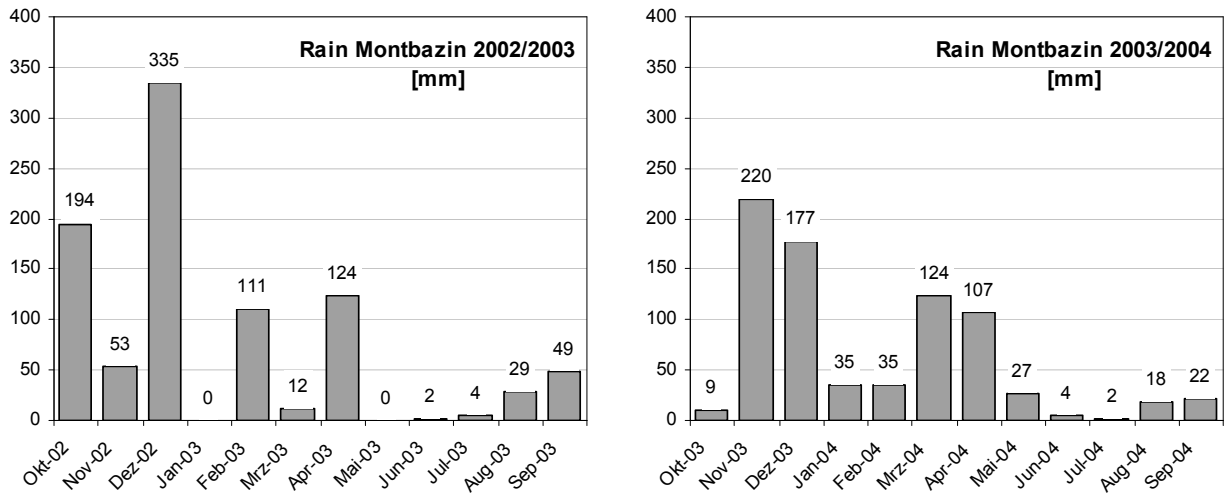


Figure 4-8: Rain at the station Montbazin for the hydrological years 2002/2003 and 2003/2004

In both years, the months of October, November and December contribute more than 50 % to the annual rain, the summer months from June to August less than 5 %. This means that there will be a time, where accumulation is favoured followed by a period of increased transport activity.

#### 4.1.3.4 Monthly discharges and loads for the year 2002/2003

The monthly summed values for flow in Figure 4-9 reflect the regime given by precipitation. Runoff is less than one percent of the annual total for July and August and the December has the highest mean flow. However, rainfall of one station and instream flow must be compared carefully, because the flow at the outlet of the catchment depends on the rainfall of the whole catchment as well as on the karstic springs, which also are influenced from outside the watershed.

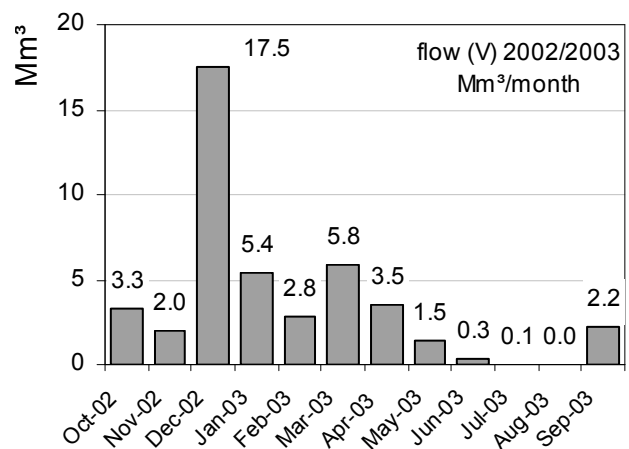


Figure 4-9: Monthly flow at the outlet of the Vène for the year 2002/2003

Due to the interaction of numerous processes (biological conversion, settlement, resuspension, infiltration of dissolved substances into the soil etc.) transport of pollutants and nutrients does not necessarily follow the scheme of rainfall and discharge, especially for organic matter as shown in Parks and Baker (1997).



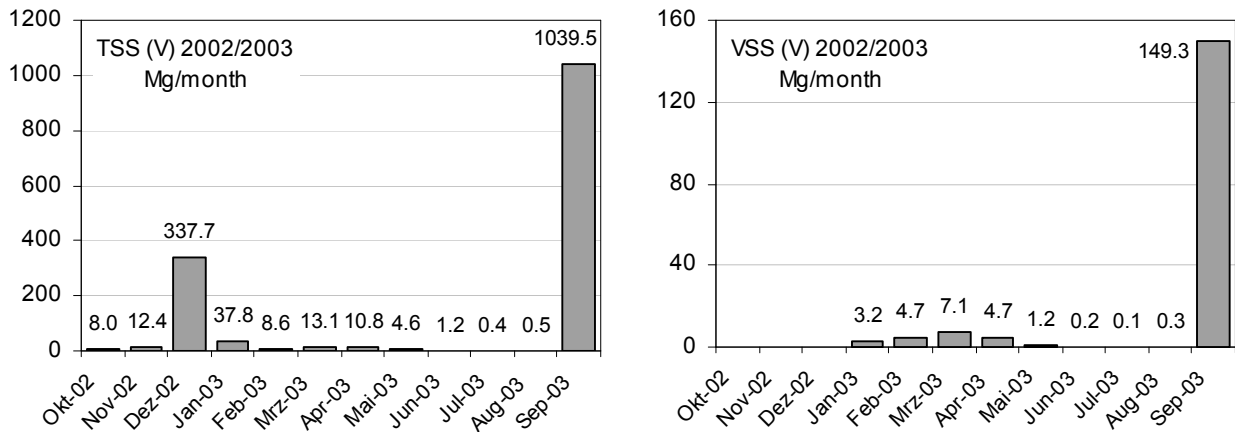


Figure 4-10: Monthly loads of total suspended solids (TSS) and volatile suspended solids (VSS) for 2002/2003

Only five percent of total annual flow in September is enough to transport 69 % of TSS (1039.5 t/month) and even 87 % of VSS (149.3 t/month, cp. Figure 4-10). December 2002 - which contains nearly 8 times more discharge than September 2002 - only contributes with 23 % to TSS, which is less than half of September, and hardly to any of the annual load of organic particulate matter (VSS).

The transport of phosphorus must be distinguished into dissolved and particulate transport. PP is less correlated to flow and rainfall than the soluble species (compare Table 4-1). The transport of particulate phosphorus depends much more on the prior conditions and on accumulation processes than the dissolved inorganic phosphorus (see also Figure 4-11).

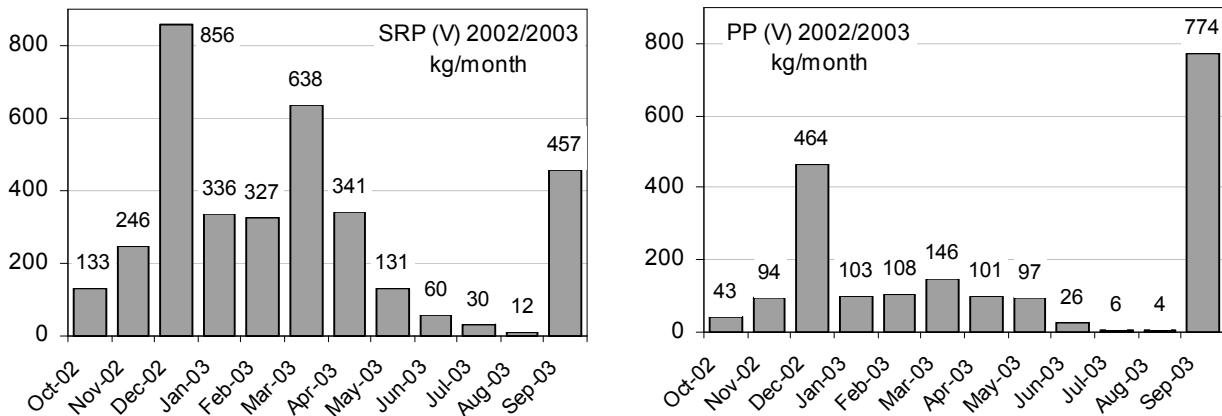


Figure 4-11: Monthly loads of soluble reactive phosphorus (ortho-phosphate or SRP) and particulate phosphorus (PP) for 2002/2003

Where the soluble phosphorus species have their maximum monthly load in December 2002 (856 kg/month), PP follows more the distribution for the other particulates with a maximum in September 2003 (774 kg/month), which is about 40% of the annual load.

Nitrogen transport in the river is dominated by nitrate, mostly brought in by the karstic springs (Figure 4-12).

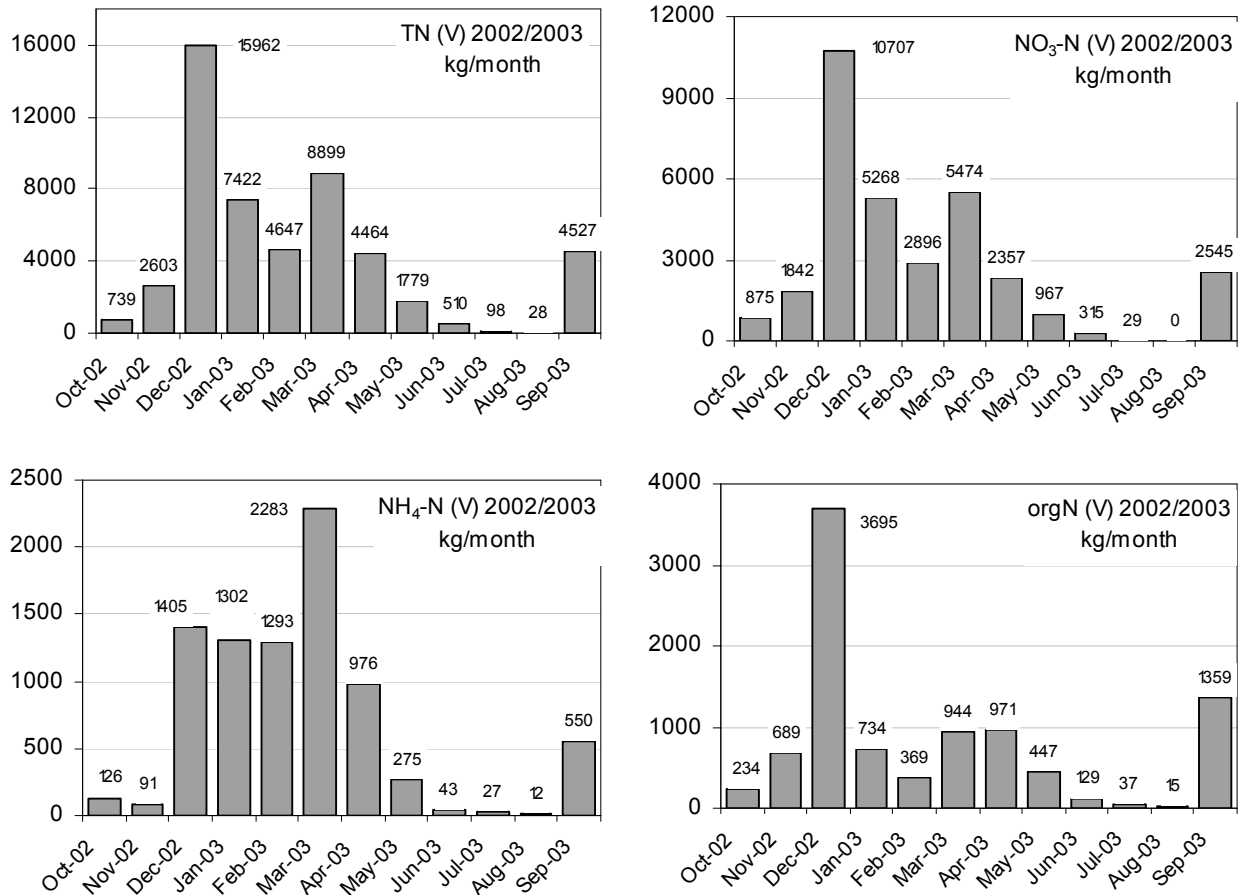


Figure 4-12: Monthly loads total nitrogen (TN), nitrate (NO<sub>3</sub>-N), ammonium (NH<sub>4</sub>-N) and organic nitrogen (orgN) for 2002/2003

Over one half (55%) of the total annual nitrate-nitrogen load is discharged from December to February, when the springs are very active. During this period, the load of nitrate is reducing from month to month, but ammonium nearly stays constant around 1300 kg/month (~16% of the annual amount). So, in contrast to the signal of nitrate, the load of ammonium seems to be more independent to the karstic spring, because it is mostly imported by domestic effluents. The values of ammonium load at V are therefore caused by two main drivers: the flow of the river and the efficiency of the WWTPs. Due to the reduced temperatures, the effectiveness of nitrogen removal in the extensive treatment is reduced (see Figure 4-3). The river is flowing through its whole length, so the ammonium can pass station V. In spring and summer, the combination of increased nitrification in the treatment plants together with the reduced instream flow causes the ammonium load at V to drop.

From the measured nitrogen species, organic nitrogen shows the highest fluctuation. About 39% of the annual load can be accounted for December 2002 and yet 16% to September 2003. Although the overall course resembles the one of nitrate, the high load of December is remarkable and a sign of an unknown source or process concerning organic nitrogen.

## 4.1.3.5 Monthly discharges and loads for the year 2003/2004

Compared to 2002/2003, December 2003 has low water flow, whereas November 2003 increased together with April and May. September 2003 makes out just one percent of the total annual flow, and this is only caused by one intensive event (shown below in Figure 4-23) with 155 mm in 4 hours.

July and August both contribute with even less than one percent as in the prior year. The small amount of precipitation in August is not sufficient to produce important discharge at the basin outlet.

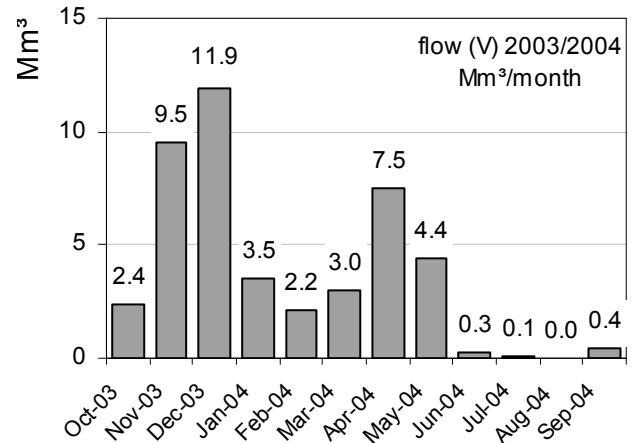


Figure 4-13: Monthly flow at the outlet of the Vène for the year 2003/2004

Transport of particulate matter is very intensive in September compared to the other months, although the effect is not as clear as in the year before. The absolute value of total suspended solids of about 330 t/month; so it contributes to the annual total load with 31 % (cp. Figure 4-14) and is mobilised by only one percent of the annual discharge.

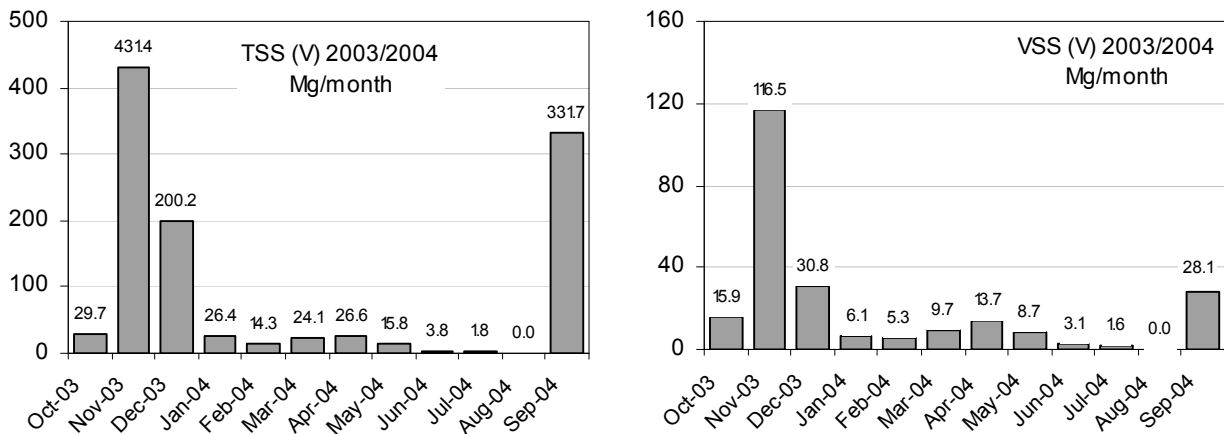


Figure 4-14: Monthly load of total suspended solids (TSS) and volatile suspended solids (VSS) for 2003/2004

A comparison of the relative impact of water flow on TSS for autumn 2003 shows, that discharge resp. runoff is more than 16 fold as effective in September in terms of resuspension than in November (31 % TSS for each percent flow in Sept. vs. 40 % TSS for 21 % flow in November).

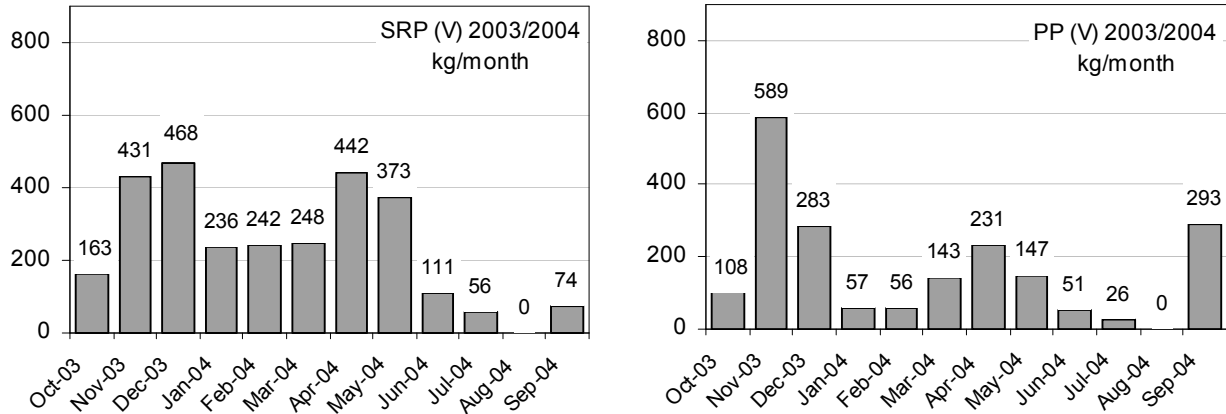


Figure 4-15: Monthly load of soluble reactive phosphorus and particulate phosphorus for 2003/2004

Compared with the previous year, November displaced December as the most transport-active month. The transport of phosphorus, at least for the particulate fraction, shows a similar pattern as VSS, 30 % of the annual particulate phosphorus accounts for November (~589 kg) and less than half of that, 14 %, on December (~283 kg).

In September 2004, relative mass flux is about 3 % of SRP for each percent discharge— which nearly matches the value of the previous year – and 15 % of PP for each percent discharge, which was only half in September 2003, but can be still considered to be in the same order of magnitude. On the other hand, November 2003 has only a relative mass flux of 0.71 % SRP per percent discharge and 1.43 % PP per percent discharge.

The transport pattern of organic nitrogen seems to follow the one of particulate organic matter (VSS); an exception is the month September. In November, most of the org N is transported (61 %) with a comparably high relative mass flux of about 2 % org N for each percent flow (cp. Figure 4-16).

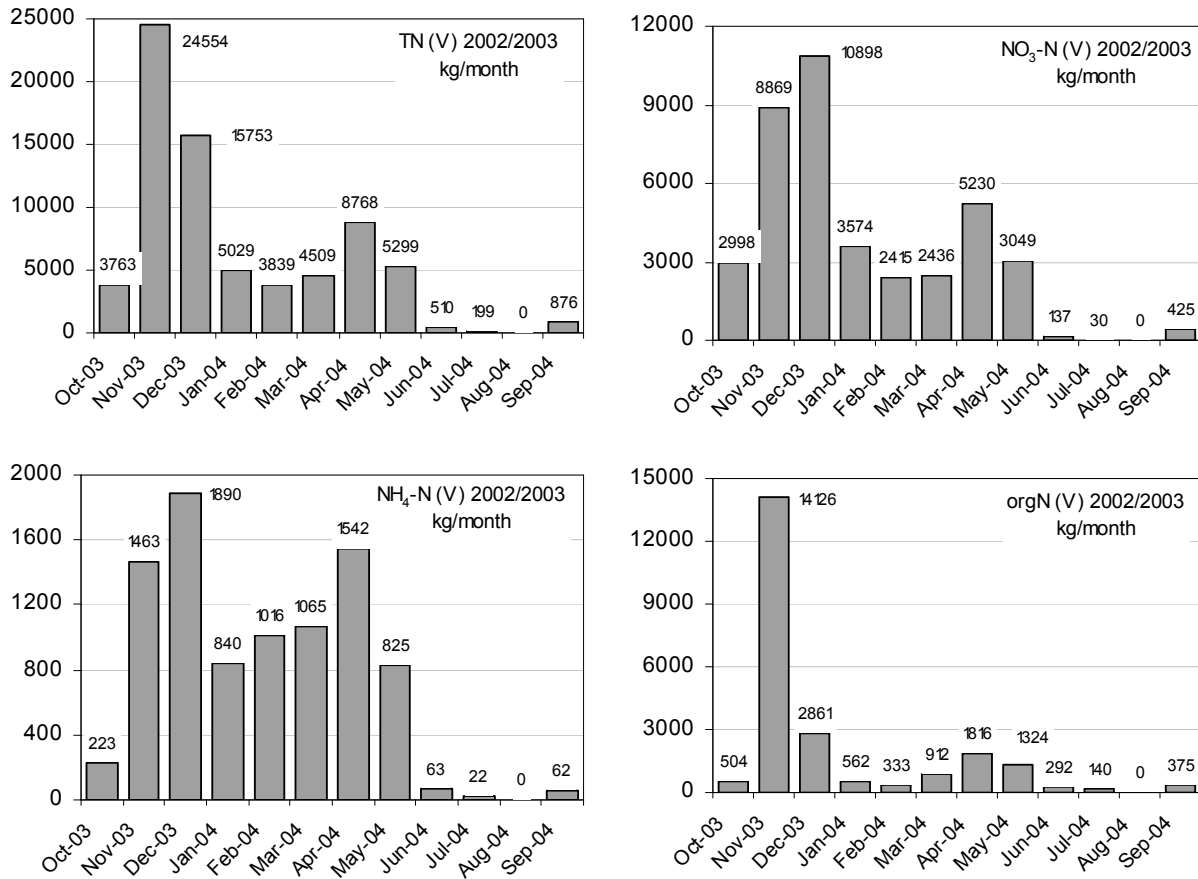


Figure 4-16: Monthly loads total nitrogen (TN), nitrate (NO<sub>3</sub>-N), ammonium (NH<sub>4</sub>-N) and organic nitrogen (orgN) for 2003/2004

This fits to the observation which was made earlier for the wash off effect. It is interesting, that the months with the highest orgN transport correspond to the month with the highest precipitation (compare Figure 4-8, Figure 4-12 and Figure 4-16).

#### 4.1.3.6 Correlation between flow, rain and the constituents

The correlation between the water flow and the constituents differ significantly. Whereas species as nitrogen or SRP show a Pearson correlation with flow of about 0.96 and 0.87, VSS or TSS are more independent from flow and only show values around 0.17 and 0.27 respectively.

This indicates that there are other important influences on the magnitude of transport of these constituents, e.g. accumulation processes.

Table 4-1: Pearson correlation between the constituents and flow resp. rain at Montbazin for monthly values for the period 2002-2004

	flow	TSS	VSS	TP	SRP	PP	TN	KN	NH <sub>4</sub>	NO <sub>2</sub>	NO <sub>3</sub>	orgN
corr. to rain	0.81	0.28	0.20	0.67	0.63	0.49	0.69	0.60	0.46	0.42	0.70	0.56
corr. to flow	1.00	0.27	0.17	0.83	0.87	0.53	0.86	0.65	0.73	0.68	0.96	0.56

There is also slightly higher correlation for rain than for flow in the particulate properties. Normally, the relation of the constituents to flow is more pronounced, e.g. for ammonium it is

0.68 for flow and only 0.42 for rain. The situation is not so clear for TSS and VSS, it even seems to be reversed.

If the impact of the rain is higher on VSS and TSS than on the other constituents, this is an indicator that the detachment of particulate properties during rain events from the landscape is important. Particulate phosphorus, however, seems to be more originated from instream, from this perspective.

#### 4.1.3.7 NCL-curves of the hydrologic years 2002/2003 and 2003/2004

Figure 4-17 and Figure 4-18 show NCL-plots for two successive hydrologic years starting October 2002. Water quality data was available from October 2002, so the most transport active month in the considered years (here September) is at the end of the abscissa.

Results for station S and station V are demonstrated for each investigation period considered.

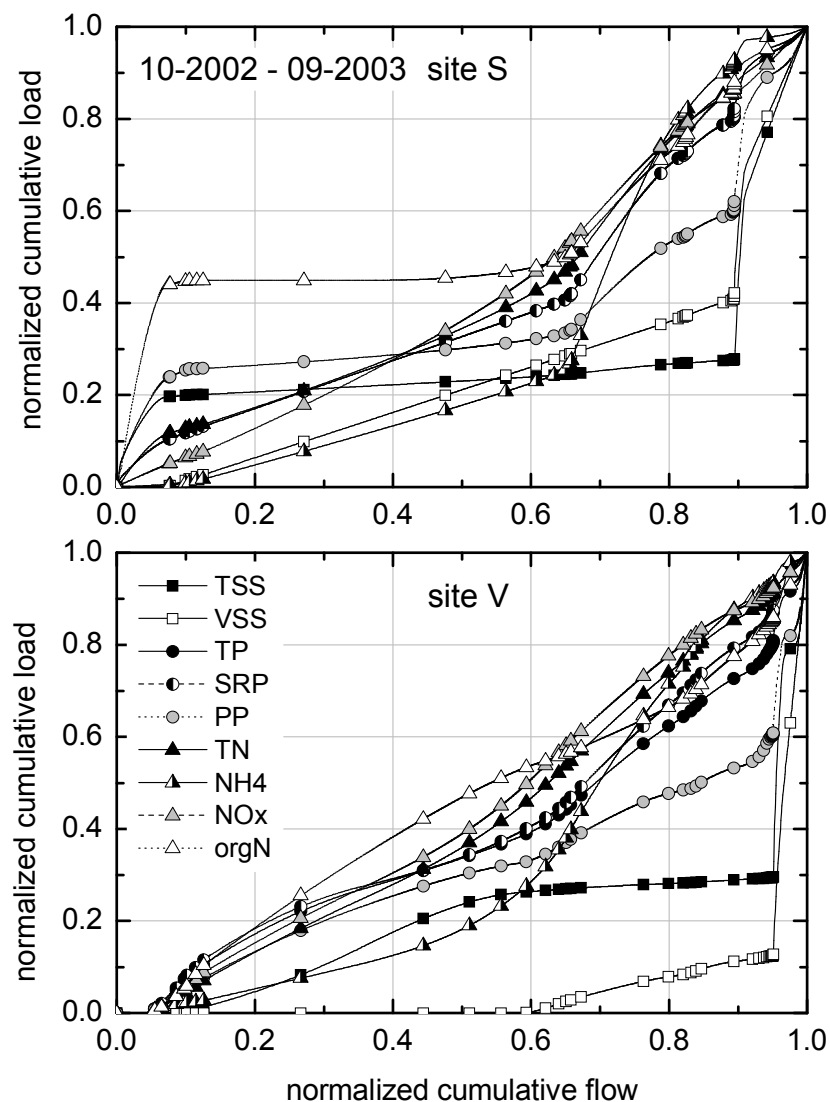


Figure 4-17: Normalized cumulative loadings in comparison to normalized cumulative discharge for the hydrologic year 2002/2003 in S and V starting in October

In the first year, Figure 4-17 indicate both for the stations S and V a significant disproportional increase for the normalized cumulative loads of volatile suspended solids (VSS), total suspended solids (TSS), and particulate phosphorus (PP) during the end of the cumulated discharge. In this year 2002/2003 the occurrence of first flush effects is more distinct at Station V. September 2003 only accounts for five percent of total annual flow but is enough to transport 69 % of the annual TSS (1039.5 t/month) and even 87 % of VSS (149 t/month). December 2002 contains nearly 8 times more discharge than September 2003 but only contributes with 23 % to the annual TSS load, which is a third of the load of September. December 2002 also hardly contributes to the annual load of organic particulate matter (VSS). This remarkably high transport activity is caused by a very intensive event starting 2003-09-22, which brought over 156 mm in only 11.5 hours in 3 showers. As found in Tournoud et al. (2005) a comparable storm of 167 mm with a duration of 72 hours in November 1999 brought up to 40 t of total nitrogen to the lagoon, which is about a quarter of the total annual load.

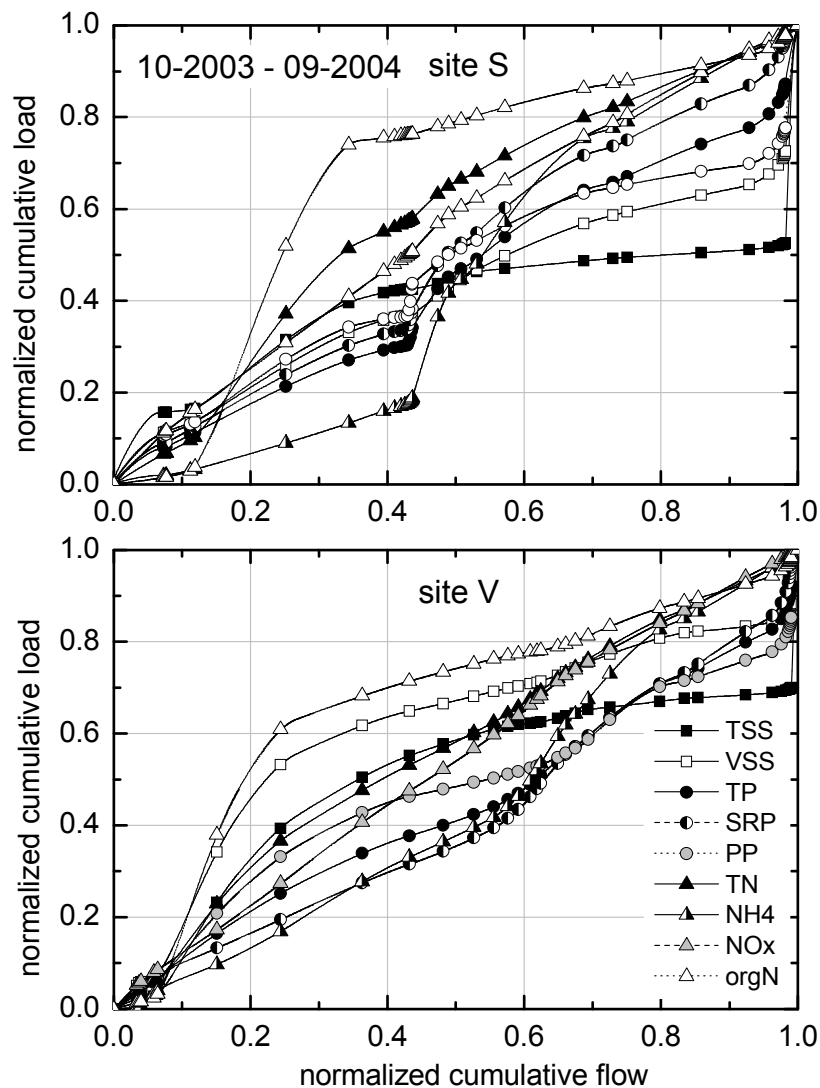


Figure 4-18: Normalized cumulative loadings in comparison to normalized cumulative discharge for the hydrologic year 2003/2004 in S and V starting in October

The second investigation period 2003/2004 (Figure 4-18) indicates a comparable regime. Even if the flush effects are smaller than the year before, transport of particulate matter is more intense in the end of the cumulated discharge (month September) again. The absolute value of total suspended solids at V of about 330 t/month contributes to the annual total load with 31 % and is mobilised by only one percent of the annual discharge.

In contrary to the antecedent year, now the flush of particulates is stronger at site S. Although there is some evidence in a current study concerning the event scale that the first flush diminishes downstream of the WWTP inflow, this could not be shown on the basis of the data presented here. Instead, the different spatial sequence of first flush intensity may indicate a stronger dependency to spatial distributed rainfall. During the first investigation period, precipitation causing the main flush event was concentrated in the north whereas it was concentrated on the urban zones during the following year's first flush flood.

The two above figures confirmed the commonly expected transport scheme for particulate matter in semi-arid and arid environments. For those constituents, the first month after the dry period (in this case September) plays a major role in the overall annual matter remobilisation, even if the years may be different in their distinctness.

It is difficult to indicate the presence for first flush effects for TP, SRP, NH<sub>4</sub>-N and orgN. Flush effects of these constituents seem to be more sensitive to the interpolation which has to be considered within the interpretation.

Judging from these two years, the relative strengths of first flood transport is TSS, VSS > PP > TP > SRP > TN > NO<sub>x</sub>, which was also concluded more or less in Lee et al. (2003).

#### 4.1.3.8 Relative mass fluxes

Figure 4-19 shows the relative mass fluxes for each month on a logarithmic scale, beginning in October 2002 until September 2004 (cp. Obermann et al., 2006).

Particulate substances like TSS and VSS show a clear seasonal trend with a maximum in September, although the order of magnitude differs between the years.

All forms of phosphorus show a similar behaviour, but it seems that the maximum appears before TSS and VSS, in August of each year. The relative mass fluxes reach 14.3 and 17.8 (respectively for TSS and VSS) for each percent of flow in September, while their reach 12.3, 13.7 and 8.5 (respectively for TP, SRP and PP) for each percent of flow in August. Nevertheless high values of PP are also observed during September.



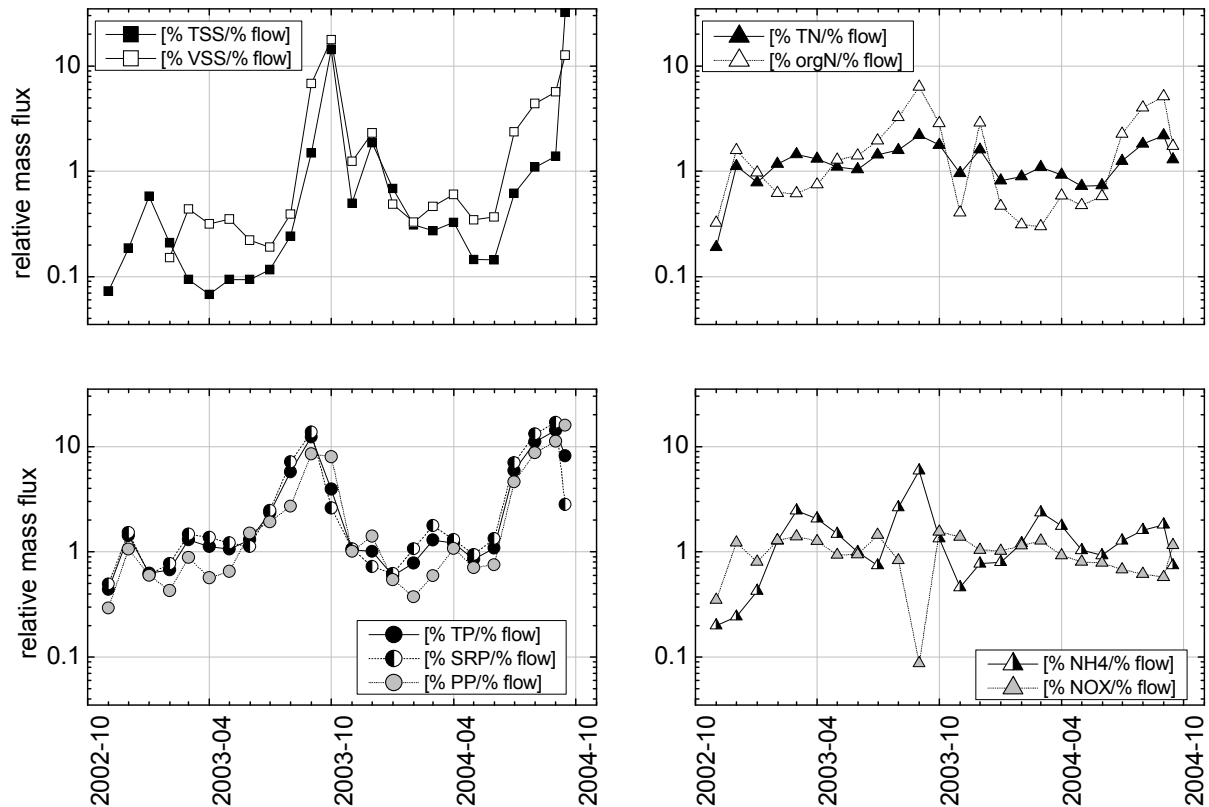


Figure 4-19: Relative mass fluxes for the measured parameters from October 2002 until September 2004 at site V

Within the forms of nitrogen, only nitrate follows a different transport pattern. Thus, the oscillation of  $\text{NO}_x$  is often inverse to the oscillation of ammonium during summer, due to the specific karstic inputs into the Vène River.

The particulate species (TSS, VSS and PP) tend to have their maximum in September, Nitrate around September to October. The other dissolved forms seem to reach the maximum relative mass flux in August.

The relative monthly flow values in Table 4-2 reflect the regime given by precipitation, runoff is less than one percent of the annual total for July and August. December has the highest mean flow. However, rainfall and in-stream flow must be compared carefully, because the flow at the outlet of the catchment depends on the rainfall of the whole catchment as well as on the karstic springs, which are also influenced from outside the watershed. So the relative mass fluxes as well as the NCL-curves were based on in-stream flow.

Table 4-2: Relative mass flux for October 2002 until September 2003

	% of total annual flow (V)	%TSS of total annual	%VSS of total annual	%TP of total annual	%SRP of total annual	%PP of total annual	%TN of total annual	%NH <sub>4</sub> -N of total annual	%NO <sub>x</sub> -N of total annual	%orgN of total annual
Oct-2002	7.5	0.5	-	3.3	3.7	2.2	1.4	1.5	2.6	2.4
Nov-2002	4.5	0.8	-	6.4	6.9	4.8	5.0	1.1	5.5	7.2
Dec-2002	39.5	22.9	-	24.7	24.0	23.6	30.9	16.8	32.2	38.4
Jan-2003	12.2	2.6	1.8	8.2	9.4	5.2	14.4	15.5	15.8	7.6
Feb-2003	6.2	0.6	2.7	8.2	9.2	5.5	9.0	15.4	8.7	3.8
Mar-2003	13.1	0.9	4.2	14.7	17.9	7.4	17.2	27.2	16.5	9.8
Apr-2003	7.9	0.7	2.8	8.3	9.6	5.1	8.6	11.6	7.1	10.1
May-2003	3.3	0.3	0.7	4.3	3.7	5.0	3.4	3.3	2.9	4.6
Jun-2003	0.7	0.1	0.1	1.6	1.7	1.3	1.0	0.5	0.9	1.3
Jul-2003	0.1	0.0	0.0	0.7	0.9	0.3	0.2	0.3	0.1	0.4
Aug-2003	0.0	0.0	0.2	0.3	0.3	0.2	0.1	0.1	0.0	0.2
Sep-2003	4.9	70.5	87.4	19.3	12.8	39.3	8.8	6.6	7.6	14.1

Due to the interaction of numerous processes (biological conversion, settlement, resuspension, infiltration of dissolved substances into the soil etc.) transport of pollutants and nutrients does not necessarily follow the scheme of rainfall and discharge, especially for organic matter as shown in Parks and Baker (1997).

The transport of phosphorus must be distinguished into the characteristics for dissolved and particulate transport. The amount of transported particulate phosphorus depends much more on the prior conditions than the dissolved inorganic phosphorus.

Compared to the year before, December 2003 has lower total flow and November 2003 increased in terms of 2002/2003. Compared to the total annual flow, September 2003 is very small, just one percent of total annual flow is brought to September by only one intensive event with 155 mm in 4 hours. July and August both contribute with less than one percent as in the prior year. The small amount of precipitation in August is not sufficient to produce important discharge at the basin outlet.

Table 4-3: Relative mass flux for October 2003 until September 2004

	% of total annual flow (V)	%TSS of total annual	%VSS of total annual	%TP of total annual	%SRP of total annual	%PP of total annual	%TN of total annual	%NH <sub>4</sub> -N of total annual	%NO <sub>x</sub> -N of total annual	%orgN of total annual
Oct-2003	5.4	2.7	6.7	5.6	5.7	5.4	5.1	2.5	7.5	2.2
Nov-2003	21.0	39.0	48.6	21.2	15.2	29.7	33.6	16.2	22.1	60.8
Dec-2003	26.4	18.1	12.9	15.6	16.5	14.3	21.6	21.0	27.2	12.3
Jan-2004	7.7	2.4	2.6	6.1	8.3	2.9	6.9	9.3	8.9	2.4
Feb-2004	4.8	1.3	2.2	6.2	8.5	2.8	5.3	11.3	6.0	1.4
Mar-2004	6.7	2.2	4.0	8.1	8.7	7.2	6.2	11.8	6.1	3.9
Apr-2004	16.5	2.4	5.7	14.0	15.5	11.7	12.0	17.1	13.1	7.8
May-2004	9.9	1.4	3.6	10.7	13.1	7.4	7.2	9.2	7.6	5.7
Jun-2004	0.6	0.3	1.3	3.3	3.9	2.5	0.7	0.7	0.3	1.3
Jul-2004	0.1	0.2	0.7	1.7	2.0	1.3	0.3	0.2	0.1	0.6
Aug-2004	0.0	0.0	0.0	0.0	0.0	0.0	0.0	0.0	0.0	0.0
Sep-2004	0.9	30.0	11.7	7.6	2.6	14.8	1.2	0.7	1.1	1.6

Although the effect is not as clear as in the year before, transport of particulate matter is more intensive in September 2004 compared to the other months. The absolute value of total suspended solids of about 330 t/month makes up 31 % of the annual total load and is mobilised by only one percent of the annual discharge.

### ***Importance of wash-off effects***

A comparison of the relative impact of water flow on TSS for autumn 2003 shows that September is more than 7 fold as effective in terms of resuspension than November (70.5% TSS for 4.9% flow in September vs. 39 % TSS for 21 % flow in November) and even more than 28 fold as effective than October.

October 2003 has only 5.4% of the annual flow volume and transports about 2.7% of the annual TSS load, so -compared to the following month and its predecessor- it has very low mass/flow-ratios.

Table 4-4: Comparison of transport activity for three autumn months 2003

Month	Mm <sup>3</sup> flow/ month	t TSS/ month	t VSS/ month	% TSS / % flow	% VSS / % flow
September 2003 <sup>2</sup>	2.18	1040	149	14.3	17.8
October 2003	2.42	30	16	0.5	1.2
November 2003	9.49	431	117	1.9	2.3

During October 2003 the discharge was similar to September 2003, but runoff from the catchment side was less, due to little rainfall. As shown in Figure 4-20 (left), during October 2003 precipitation was lower than in September 2003 at all weather stations. This does not match the annual distribution of instream discharge in Figure 4-20 (right), where September and October are comparable in terms of water flux.

<sup>2</sup> September 2003 and October 2003 are of different hydrological years, so relative values in Table 3 are based on different total flow values

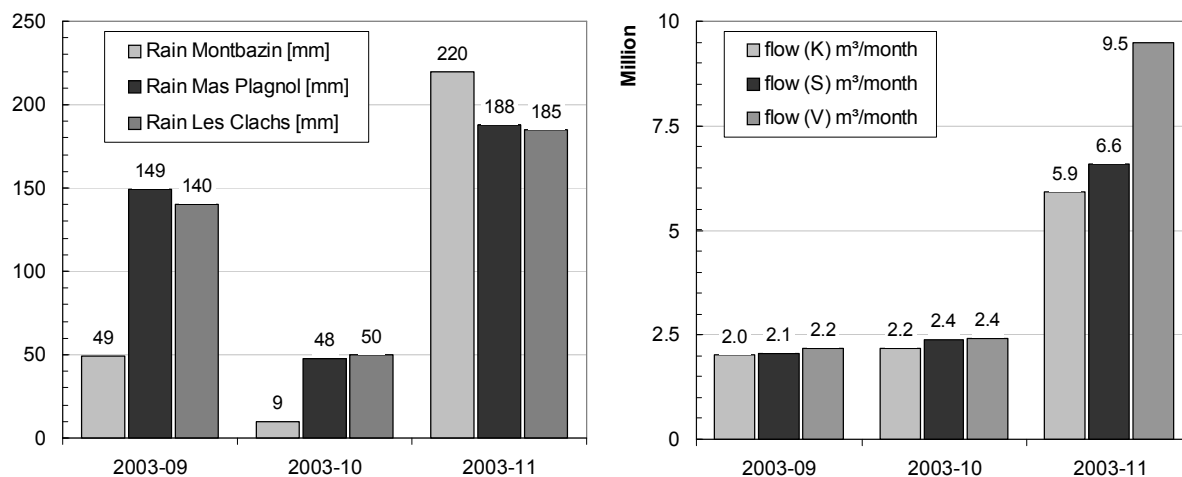


Figure 4-20: Rainfall for September, October and December of 2003

The importance of wash-off effects in the annual transport cycle and the magnitude of dry weather deposition on agricultural or urban areas underlies various influences and is difficult to quantify. However, there is still particulate matter left for transport in November, although the ratio of mass/flow is significantly lower than in September.

Evidence of the importance of these processes was already found above in chapter 4.1.3.7.

#### ***Composition of TP and TN at the catchment outlet (V)***

It is apparent that for each percent of annual discharge, 8 % PP and 2.6 % SRP are transported in September. Altogether, about 1060 kg TP was transported, of which 457 kg consisted of SRP. In December, which brings more than one third of the annual rain, this ratio is significantly lower for PP but stays more or less constant for SRP: each percent of discharge carries only 0.62 % PP and 0.59 % SRP.

The situation changes in late Winter and early Spring during the months of February, March and April, where SRP is excessively transported (1.47, 1.36 and 1.22 % transported for each percent discharge) compared to the particulate fraction (0.88, 0.57 and 0.65 % PP for each percent discharge).

As shown in Figure 4-21, during most time of the year, the greatest portion of total phosphorus (around 70 %) is transported as SRP, but not during autumn, where the particulate fraction can reach up to  $\frac{3}{4}$  of the total transported mass.

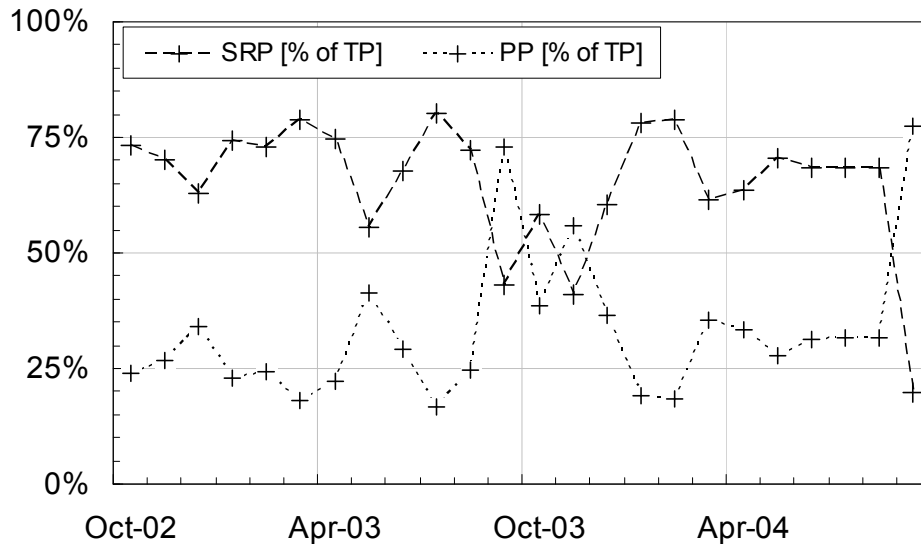


Figure 4-21: Distribution of phosphorus loads for the years 2002/2003-2003/2004, particulate phosphorus and soluble reactive phosphorus

This again could be an indicator, that there are storages of particulate matter (here represented by particulate phosphorus) in this case, which are reentrained during periods of increased flow intensities.

In contrast to the dynamic of phosphorus and TSS, nitrogen follows a different transport mechanism. The greatest proportion of total nitrogen normally consists of nitrates, followed by organic Nitrogen and ammonium (Figure 4-22).

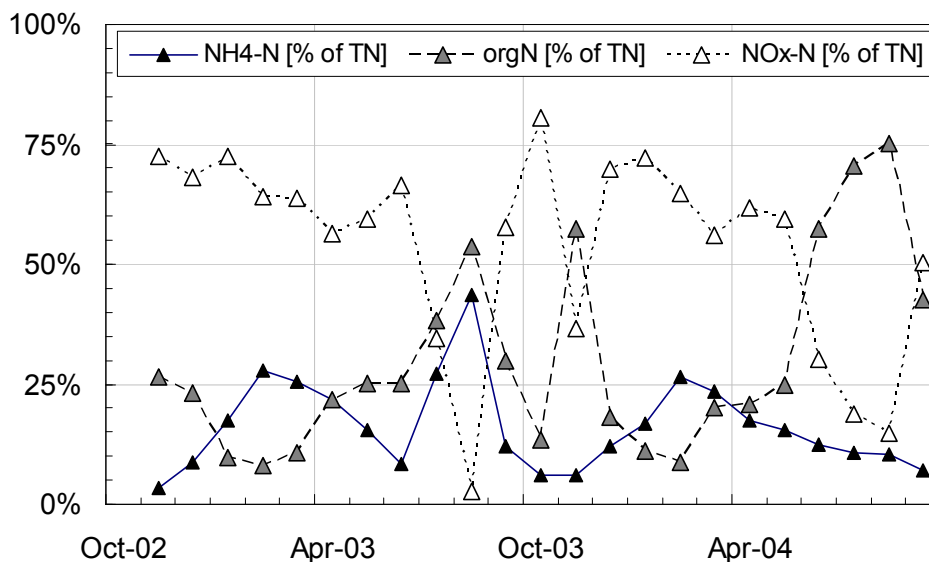


Figure 4-22: Distribution of forms of nitrogen loads over the years 2002/2003-2003/2004

Starting from January, there is a shift in the total nitrogen composition towards organic forms with a climax of 54 and 75 % of TN in August 2003 and 2004, respectively. This is the consequence of the ceased karstic springs (especially at K) during the summer, owing the fact that this is a main source for nitrate in the catchment. The transport activity of nitrate seems to

be following the discharge activity with a delay (between 2-4 weeks), which could be partly caused by the fact that the first events of the year rarely cause flow at the karstic spring but mainly surface runoff.

The overall in-stream transport in August is rather small compared to the other months. In the hydrologic year 2002/2003 it was less than one percent in terms of loads for all mentioned parameters.

Compared to water flow, organic nitrogen is transported in excess in August (6.3 and 5.1 % org N per percent flow for August 2003 and 2004).

#### 4.1.3.9 Conclusions

A reoccurring cycle of increased transport in late summer and early autumn exists for all parameters but is less clear for nitrogen. The strongest flushing effects are associated with sediment and sediment-linked nutrients. This is due to sediment stored in channels and new material brought in, solutes show weaker effects.

It was found that the first events in September can bring the major part of the annual particulate matter. Five percent of annual flow in September 2003 was enough to transport 69 % of TSS (1039.5 t/month) and even 87 % of VSS (149.3 t/month).

The highest relative mass transport rates normally occurs in August for dissolved and in September for particulate materials, because the flow intensity is too small for resuspension (of particulates) before. The relative strength of first flood transport was estimated in the order TSS, VSS > PP > TP > SRP > TN > NO<sub>3</sub>.

A comparison of the relative mass fluxes with flow and rainfall of October 2003 with the months before and after seems to bring up evidence of the importance of wash-off effects.

There is a strong correlation between nitrate and SRP with flow, but a poor relation between flow and the particulate properties TSS and VSS. This is due to the fact, that the processes erosion and deposition are very much related to the conditions before an event, so that the concentration of particulate substances is not so related to the actual flow concentration.

An alteration in the composition of total Phosphorus as well as total Nitrogen could be shown, which is most likely bound to the reoccurring annual flow variation. For TN this is mainly caused by the influence of the upstream karstic spring. If the spring is flowing nitrates prevail. During the flush season the balance is shifted towards organic forms, which seem to indicate a resuspension of formerly accumulated organic matter.

#### 4.1.4 *Examples for floods and flushes – magnitude of days to hours*

In addition to the annual fluctuation, data of two significant floods of the Vène were analyzed in terms of a first flush dynamic, one at 2003-09-22 and the second at 2004-09-13 (see Figure 4-23).

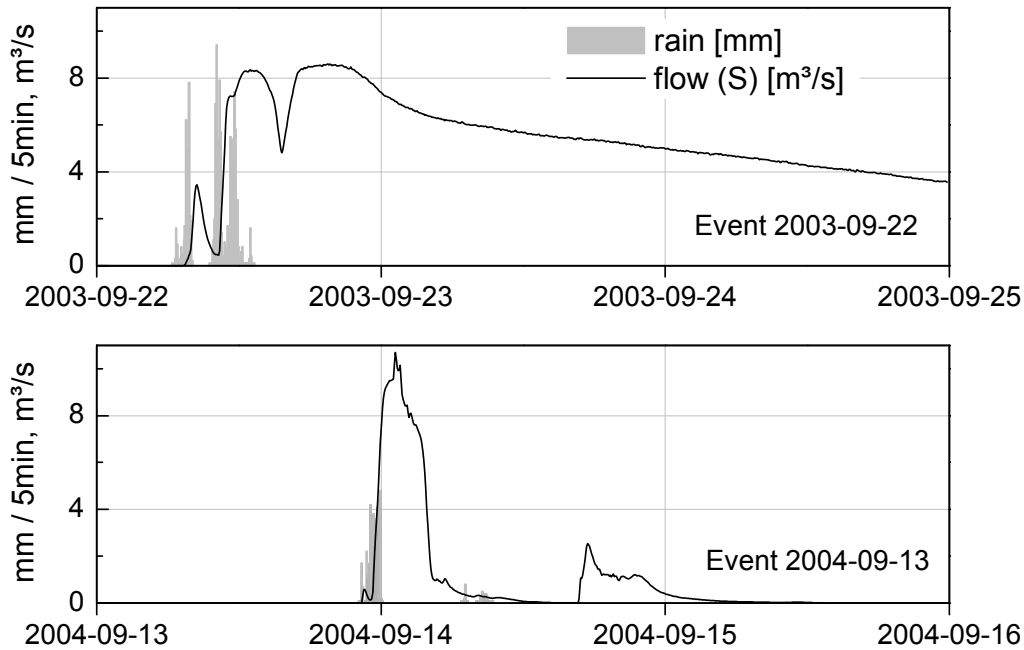


Figure 4-23: Rainfall at the weather station Mas Plagnol and flow at station S during two significant events in the Vène catchment

The event of 2003-09-22 can be divided into three parts. The very first initial part is comparably small and caused by a separated storm of  $\sim 1.5$  h. During this period, effects of surface runoff and wash off effects most likely prevail. The second stage follows after additional 1.5 h. The system is already wetted. In the later phase the upstream karstic spring at Cournonsec (site K) dominates the discharge regime, which is supplied by rainfall from outside the catchment (to the north), whereas the Cournonsec spring hardly has any flow in the 2004-09-13 flood. Judging from data of the available weather stations, rainfall was concentrated in the north for 2003 and in the south for 2004.

The fact that water originates from different sources at different times will have a significant influence on the pollutant mass transport in the course of the flood wave. Approximations show, that ca.  $3/4$  of the total phosphorus mass and approximately  $2/3$  of KN (which includes organic nitrogen) originates between K and S whereas most of the nitrate comes from the karstic spring. This will be explained in more detail below.

Although these events both were the first significant floods, they vary significantly in terms of maximum flow volume and rainfall, as summarised in Table 4-6 and Table 4-5.

Table 4-5: Basic flow data of the two floods

Flood	point	total flow volume [m <sup>3</sup> ]	peak flow [m <sup>3</sup> /s]
2003-09-22	S - Sanglier	1.262.587,67	8,56
	V - Outlet	1.409.769,00	13,27
2004-09-13	S - Sanglier	178.612,45	9,70
	V - Outlet	421.574,40	19,49

The period before both events was very dry and there was hardly any flow or rainfall for at least 3 months. However, the antecedent dry weather period (ADWP) indicates an extended dry period only for the event of 2003. This method does not take into account the overall wetness of the system, but only the period between rainfall events (although it is adjustable in the way that the rainfall has to reach a certain level to be counted). This may explain the reason why a strong relationship between the ADWP and the occurrence of a first flush could not be found (see also Deletic, 1998).

Table 4-6: Basic rainfall data for the two floods

Flood	point	total rainfall volume [mm]	maximum rainfall intensity [mm/h]	ADWP [d]
2003-09-22	Mas Plagnol	124.60	45.10	27
	Les Clachs	94.60	27.70	13
2004-09-13	Mas Plagnol	50.60	38.40	1 <sup>3</sup>
	Les Clachs	190.80	70.20	1 <sup>4</sup>

The event of 2004-09-13 is a very important event, because the previous rainfalls were only small (15-18 mm) and not sufficient to produce runoff in the whole length of the river.

A comparison of the normalized cumulative rainfall and the normalized cumulative flow in Figure 4-24 shows the higher rainfall gradients for 2004. Even though it was smaller in terms of total discharge, the event was more condensed than the one of 2003.

<sup>3</sup> there has been a small precedent event at 2004-09-10 of about 15mm which did not produce significant runoff and had a ADWP of 8d

<sup>4</sup> there has been a small precedent event at 2004-09-10 of about 18mm which did not produce significant runoff and had a ADWP of 9d



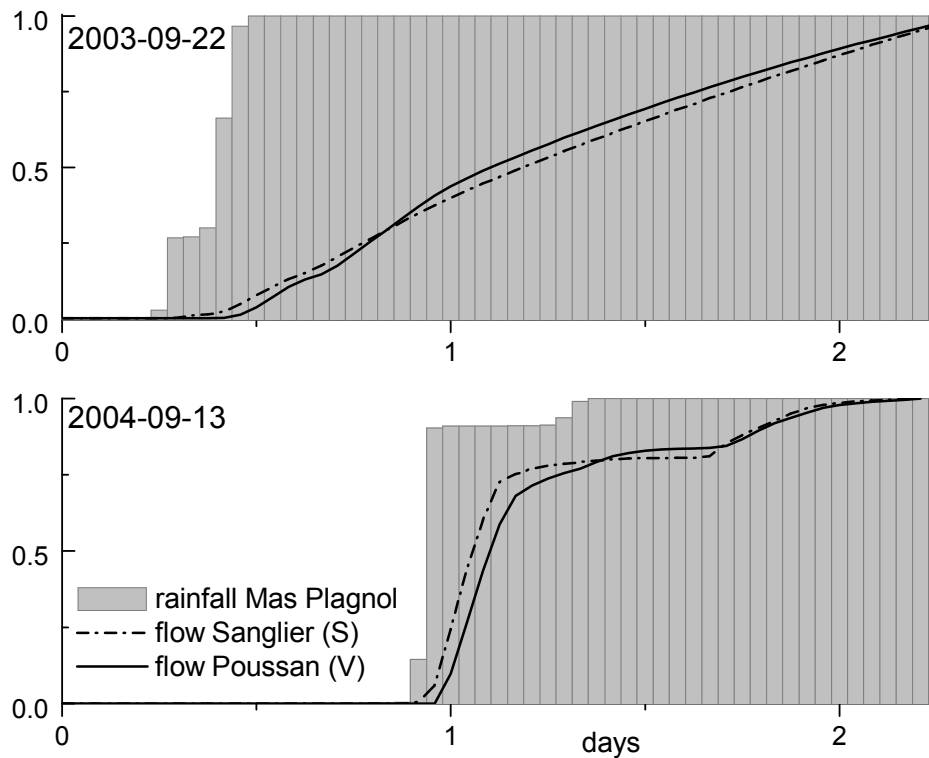


Figure 4-24: Normalized cumulative flow and rainfall for the two events

This is also reflected in the discharges, which are rising slower and continue a long time after the end of the rainfall event in 2003. Compared to this, the differences in the measuring stations in terms of their gradients are negligible, so the characteristic of the flow distribution over time does not change very much on the transfer from site S to V.

Table 4-7: Summary of the floods for the Vène at site S

site S	flow [m <sup>3</sup> ]	TSS [t]	VSS [t]	TN [kg]	TP [kg]	NO <sub>3</sub> -N [kg]
2003-09-22	1 262 588	446	45.0	2110	482	1 381
2004-09-13	178 612	178	15.6	462	222	230

An approximation of total loads for the site S is shown for both floods in Table 4-7. Only the mass of nitrate seems to have a direct correlation with the total flow, but the other elements are transported in a greatly higher amount than it could have been expected on basis of the flood volume for the first flush flood for 2004.

The two floods differ significantly from all other floods in both covered years in terms of mass transport scheme (see chapter 4.1.5) and runoff coefficient (see chapter 7.2), especially the flood of 2004-09-13, which had no karstic influence.

4.1.4.1 Mass balance and weighting of events for the sites K, S and V

When investigating the temporal distribution of loadings and concentration, the sources of the constituents are of importance.

Figure 4-25 shows a comparison of the sources for the flood of 2003-09-22 of the regarded parameters. The values for each station were derived from the total masses passing the station minus the total mass which passed the station upstream. So this means that for total phosphorus, 410 kg have their origin somewhere between site S and V. Major losses in between the stations can lead to odd results as it can be seen for the negative balance of nitrate for V. There is a great storage reservoir of about 18 000 m<sup>3</sup> before upstream point V. However, assuming a mean concentration of 1 mg/l of nitrogen, this will only retain 18 kg. Additionally, even with an optimistic infiltration capacity of 1 · 10<sup>-5</sup> m<sup>3</sup>/(m<sup>2</sup>s) the loss of nitrate-nitrogen will only sum up to approximately 16 kg for the event of 2 days.

Apart from these unresolved questions, Figure 4-25 gives an idea of the sources of the regarded constituents.

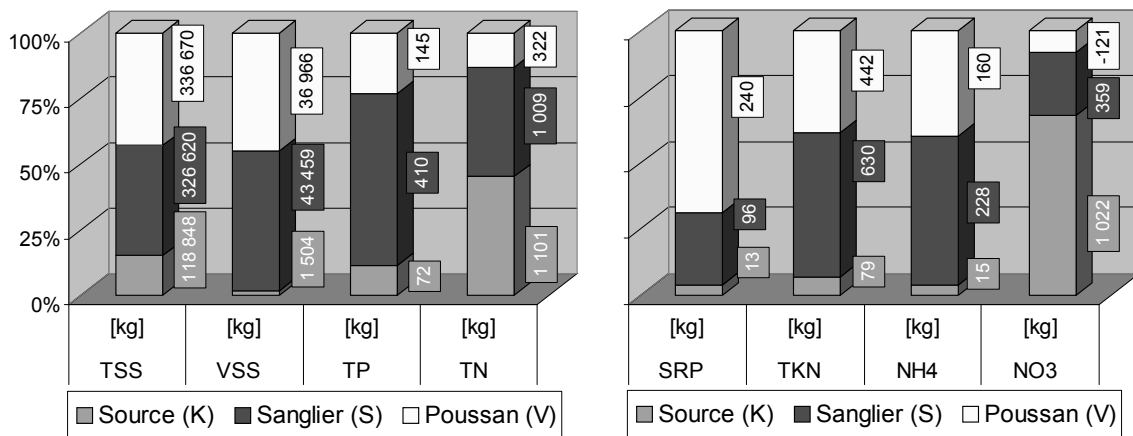


Figure 4-25: Weighting of the three sites K, S and V for the main parameters for the event 2003-09-22

The figure indicates, that the biggest contingent of nitrate (and with it also TN) in the flow is caused by the karstic spring at K. On the other hand, the biggest proportion of VSS, TP, KN and ammonium has its origin between K and S, and it can be assumed, that the waste water inflow upstream of S plays a major role in this dynamic. The net estimated drainage area for S is with about 35 Mm<sup>2</sup> (3 500 ha) slightly larger than the 32.2 Mm<sup>2</sup> (3 220 ha) for V. So the amounts for TSS seem reasonable, but the increased SRP production downstream S remains unclear.

4.1.4.2 Pollutographs of the event starting at 2003-09-22

**Particulate matter**

At the upstream point S, it seems as the most distinguished flush can be seen at the plot of particulate materials in Figure 4-26, especially for volatile suspended solids.

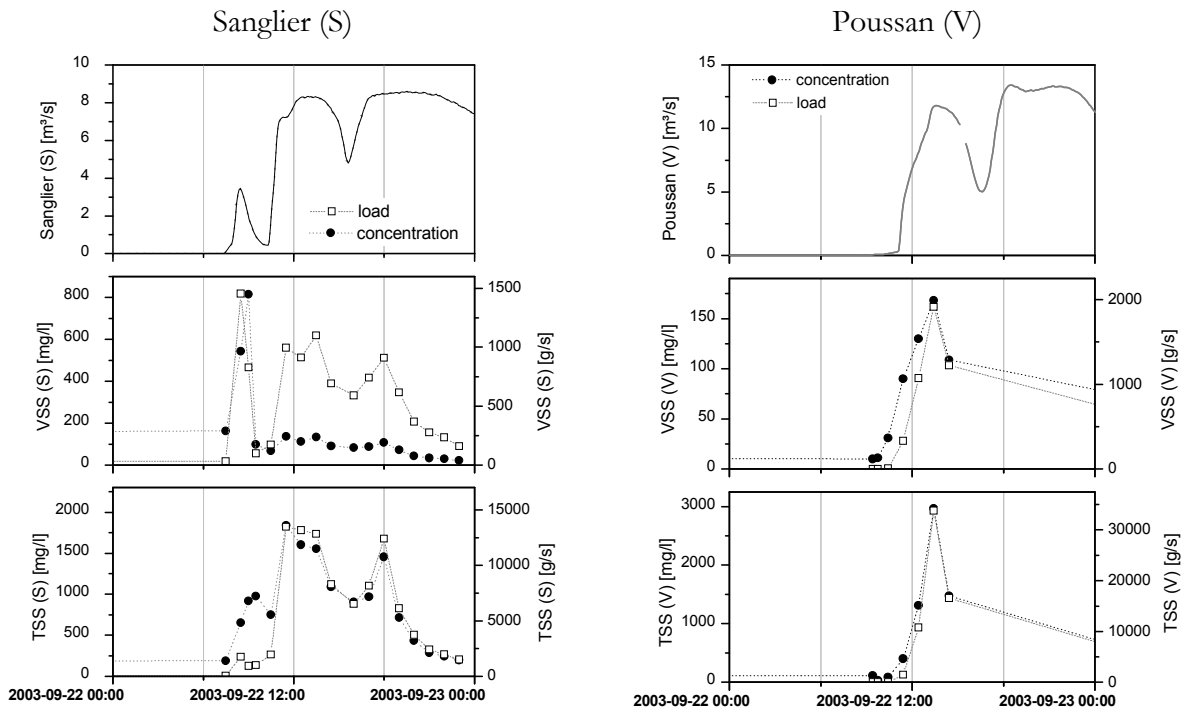


Figure 4-26: Concentrations and loads of particulate parameters of Sanglier (S) and Poussan (V) for 2003-09-22

The peak concentration at S is more than 4 times higher than average during the event and - especially at S - happens long before the peak of flow. This seems to be either caused by

- i) wash off from the surrounding agricultural areas or
- ii) is a result of a resuspension of deposited materials like partly decomposed leaves or branches and grown biomass at the bottom of the channel.

The latter would mean, that the first small peak would have had enough transport capacity to entrain all - or most of - the accumulated organic components. The storage of VSS seems to be exhausted after the peak at the beginning. There only seems to be transport of a base concentration, because there is -unlike in TSS- no clear reaction of the concentration to the flow rate any more.

Against the former possibility (i) militates the fact that the order of magnitude of the peak is higher at the upstream point S than in V ( $\sim 800$  mg/l vs.  $\sim 175$  mg/l). The clearly visible “pre-peak” at S cannot be found any more in V. This could mean that the impact of the instream resuspension decreases in downstream direction compared to the wash-off effect from the landside. It could be further evidence of the influence that the accumulation at S has on the mass flux regime of the whole system.

### ***Nitrogen***

Only total nitrogen shows some dilution effect caused by the flood, Nitrate is later in the event nearly constant at  $1000 \mu\text{g/l}$  which is the normal concentration of water coming from the karstic spring (see above).

Figure 4-27 shows a comparison of the loads and concentrations of nitrogen parameters for point S downstream a WWTP and point V which is near the outlet of the catchment.

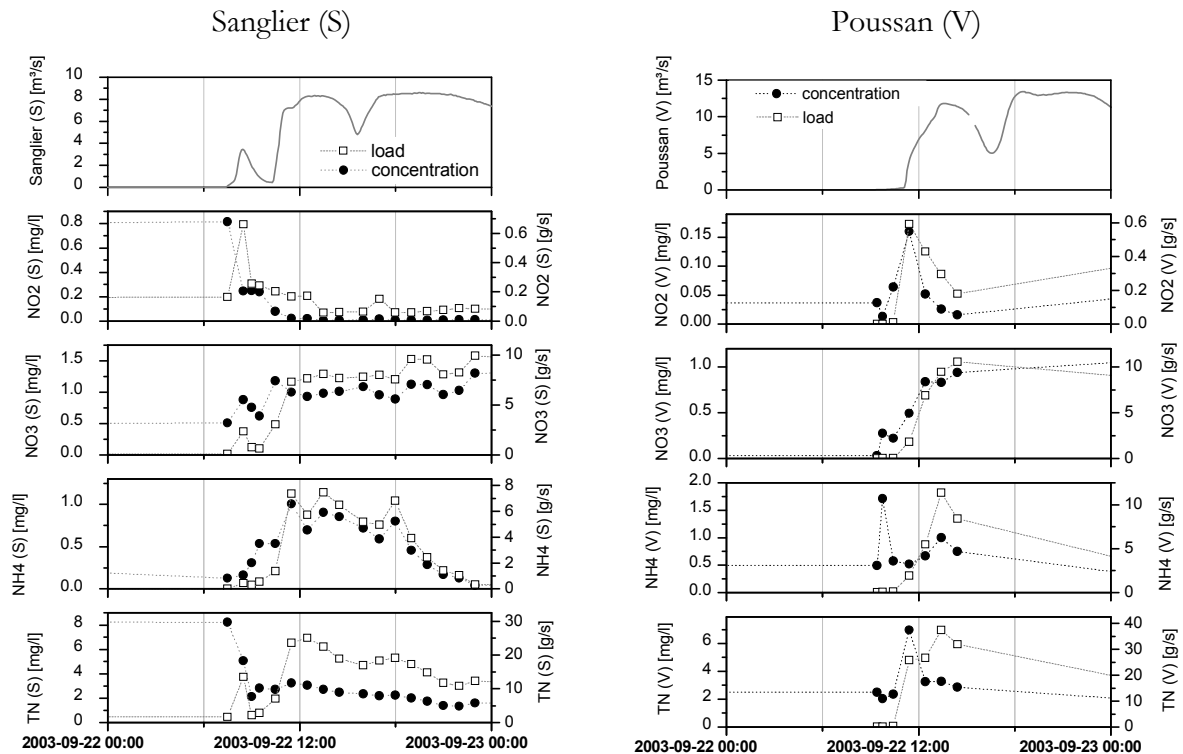


Figure 4-27: Concentration and loads of nitrogen parameters of Sanglier (S) and Poussan (V) for 2003-09-22

Due to the long retention time in the pools at S, most of the nitrate imposed by the point source upstream of S seems to be reduced in the period before the event. A lot of the nitrogen was converted to organic forms from the biomass at the riparian zone or was removed from the system through denitrification. As explained earlier, the karstic spring dominates this event in the later stage, so the concentration constantly rises up to the end at the level of the spring concentration.

Ammonium is not, as e.g. nitrite, transported in the first instant of the event, but there seems to be a limited storage, as indicated by the decrease when the karstic spring starts flowing. Possibly, the ammonium is originated from the agricultural surfaces, as ammonium ions can bind to soils, especially clays.

At the outlet point V there is a clear peak for concentration for nitrite, ammonium and total nitrogen.

Regarding a plot of the loads in Figure 4-27 for the event reveals an increased mass flux of nitrite and total nitrogen at station S at the beginning of the event, which could not be observed by the study of concentrations. The plot of ammonium in point V also reveals the misinterpretation, which could happen, if only the concentration was considered. The first peak of concentration does not contribute significantly to the overall mass flux, whereas the later – and much smaller – one coincides with the peak in loading.

It can also be seen that, even if there is a strong dilution effect in TN at the point S, the load remains at a higher level for a long time.

### *Phosphorus*

Only the pollutograph of total phosphorus at the outlet shows a peak in concentration as shown in Figure 4-28. Although at first there is a decrease in the concentration the later course may be caused by the release of a storage somewhere upstream.

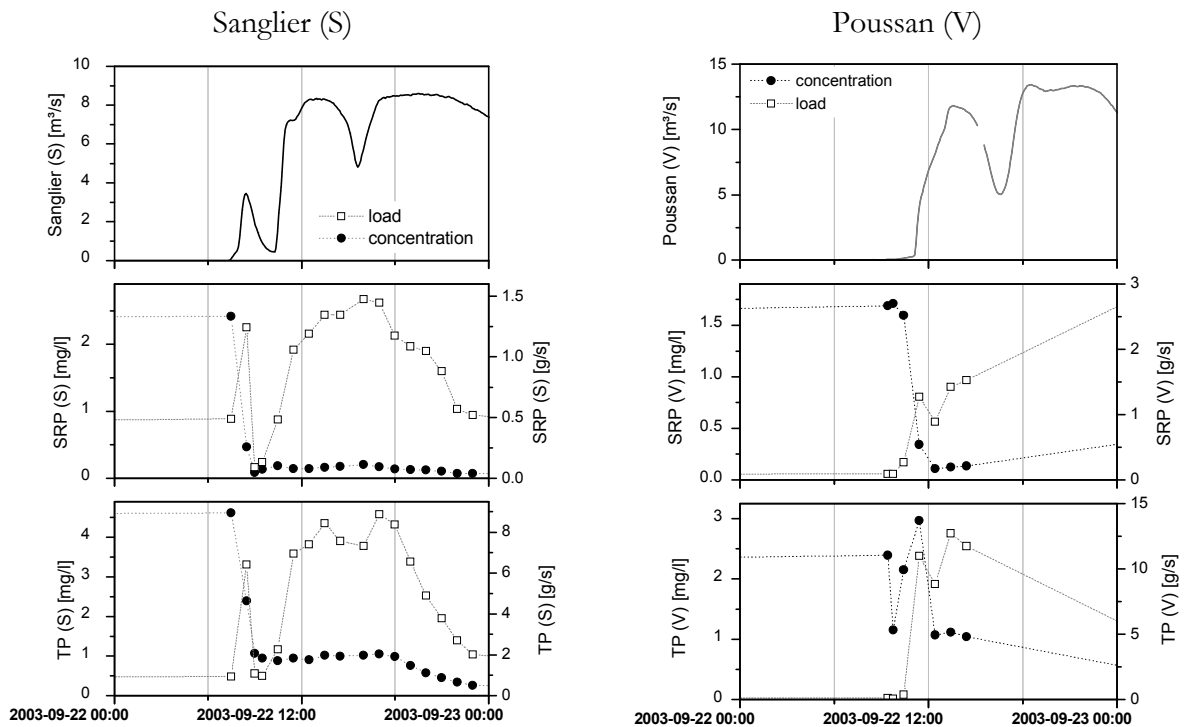


Figure 4-28: Concentrations and loads of phosphorus parameters of Sanglier (S) and Poussan (V) for 2003-09-22

Dilution effects prevail at S. However, if the mass flux is considered, there is a flush-like peak caused by the first small runoff maximum.

The plot of TP at S resembles the difference of the concentration of surface runoff (the first big peak) and the karstic spring (the second big peak).

#### 4.1.4.3 Pollutographs of the event starting at 2004-09-13

### *Particulate matter*

The fast decrease of total suspended solids in the first flood of 2004 could be a sign of a limitation in storage (Figure 4-29).

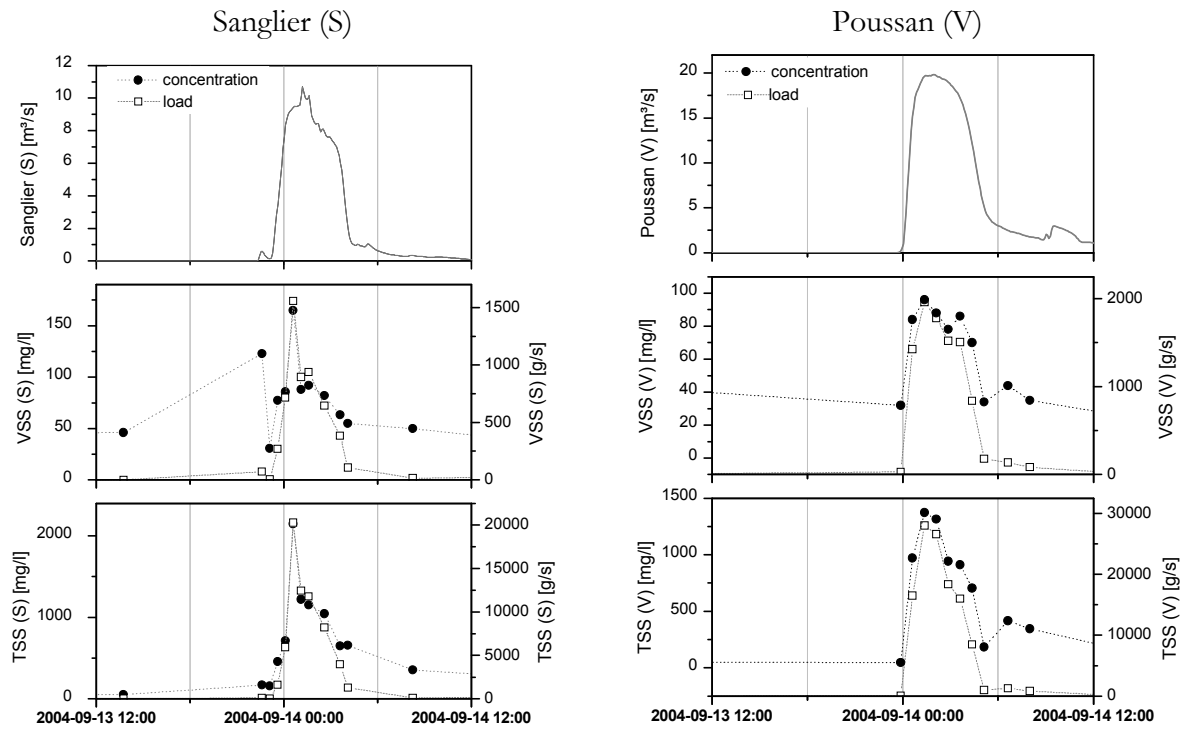


Figure 4-29: Concentrations and loads of particulate parameters of Sanglier (S) and Poussan (V) for 2004-09-13

In contrast to the event of September 2003, no preceding peak appears during the rising limb of the hydrograph in the loadings of VSS. The barycentre of mass flux seems to be shifted towards the beginning of the water flow, very distinctly visible in the point S.

### ***Nitrogen***

Nitrate shows a small peak of concentration during the rising limb of the flood of 2004-09-13 at S, but in terms of mass flux this is small compared to the amount transported in the later stages of the event. Ammonium and total nitrogen show a similar curve, with a peak at the beginning (which could not be very well documented by the measurements) and a dilution effect in the further progression.

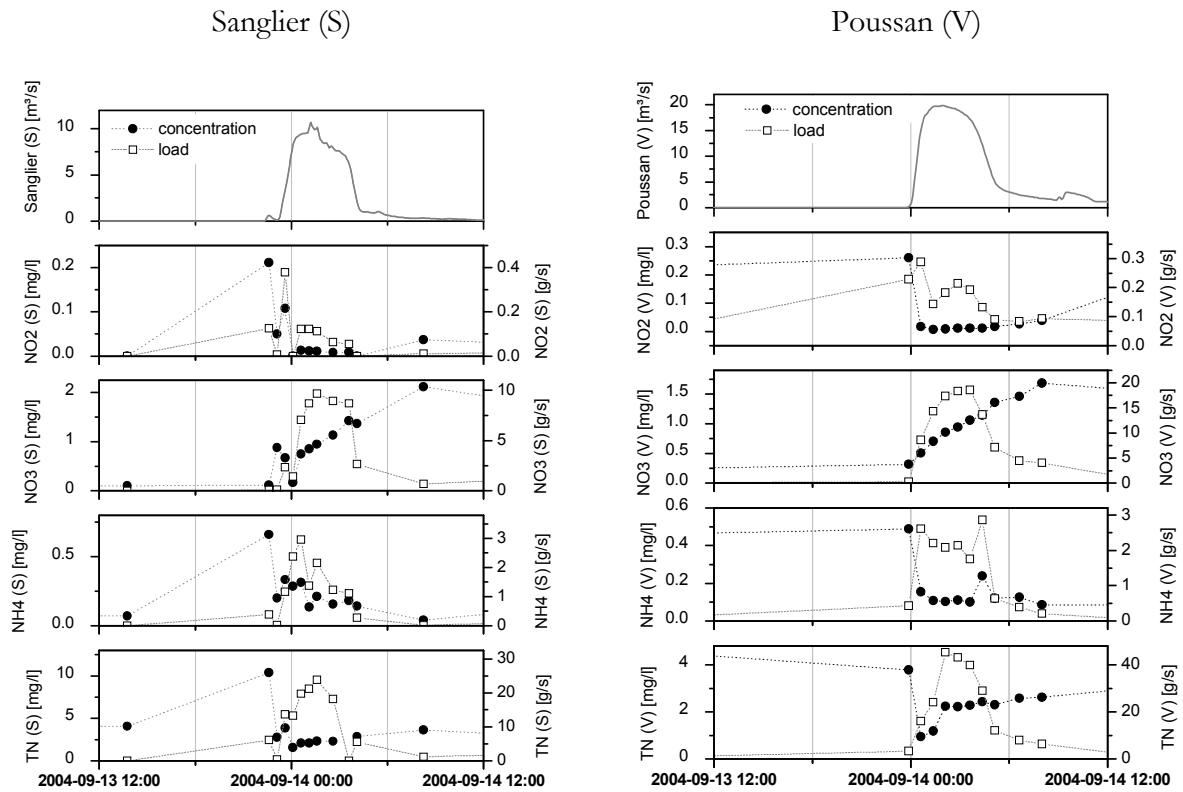


Figure 4-30: Concentrations and loads of nitrogen parameters of Sanglier (S) and Poussan (V) for 2004-09-13

Only the pollutographs of nitrite exhibit a significant flushing, which happens before the maximum. However, nitrite does not contribute significantly to the total nitrogen load of the event.

### *Phosphorus*

Soluble reactive phosphorus is diluted from the beginning and therefore the concentration decreases, but particulate phosphorus even seems to have two concentration peaks in 2004 at station S, and is only subject to dilution later, near the end of the event.

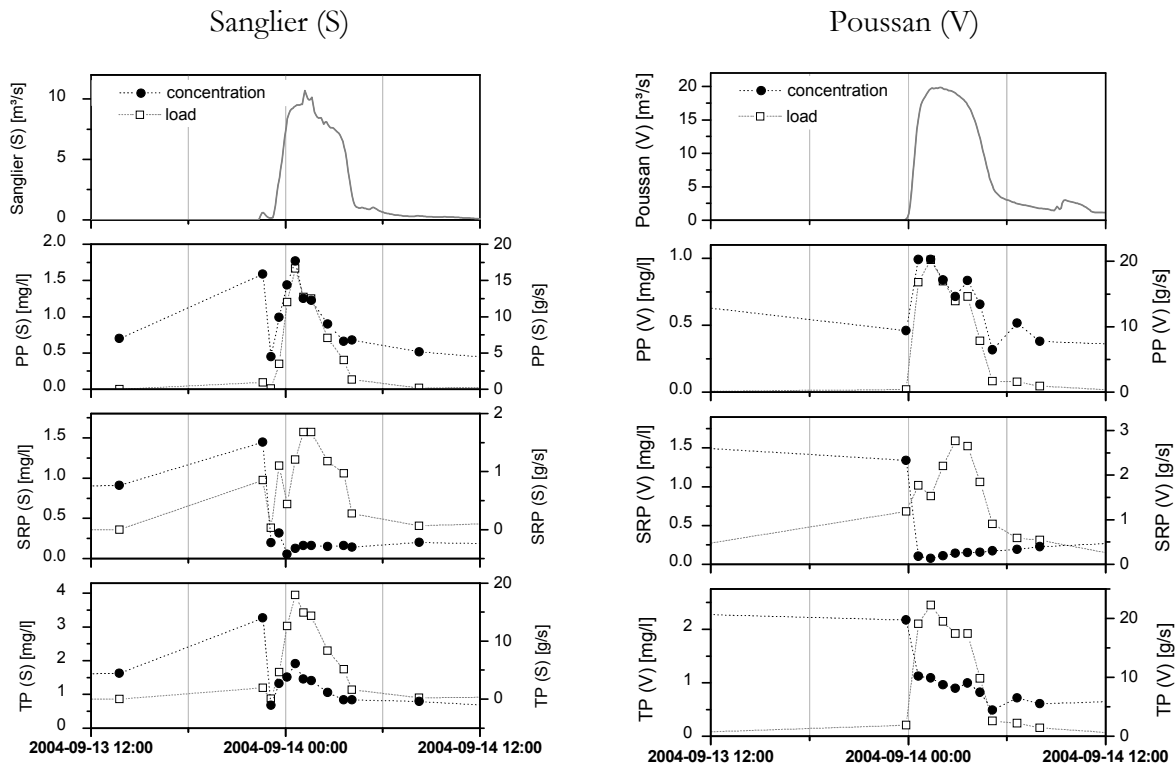


Figure 4-31: Concentrations and loads of phosphorus parameters of Sanglier (S) and Poussan (V) for 2004-09-13

This could also be a cause of an instream storage, especially, if the plots of PP and VSS are compared (Figure 4-32).

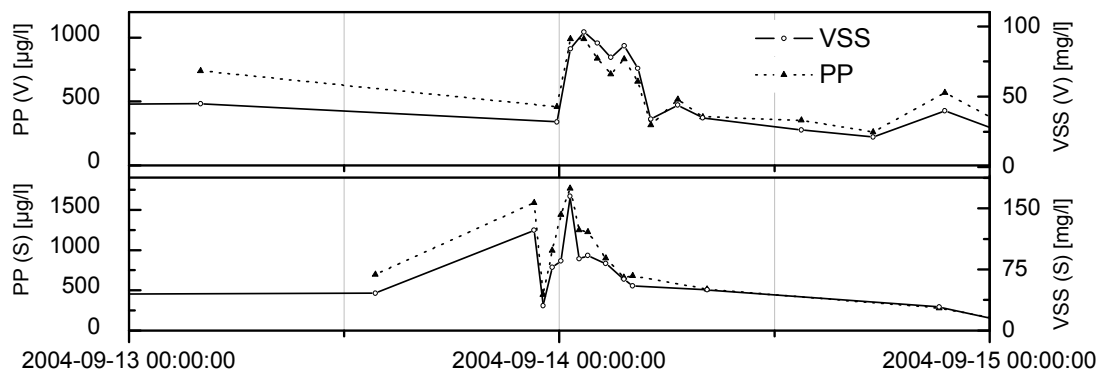


Figure 4-32: Comparison of concentrations of particulate phosphorus and volatile suspended solids for the flood of 2004-09-13

It seems that particulate forms of phosphorus are bound to the sediments (TSS respective VSS, which possibly contains an increased amount of small particles). Tournoud et. al. (2005) found that, due to alkaline pH-values of the water column (more than 7.5) and high calcium carbonate saturation indexes, co-precipitation of phosphorus and calcium-carbonates (House, 2003; Plant and House, 2002) occurred and this trapped phosphorus in the bed. In both points (S and V) the course of concentration of PP and VSS is similar, so that it can be suggested, that these two parameters are transported by comparable flow conditions.



## 4.1.4.4 NCL-plots of the event 2003-09-22

In analogy to chapter 2.2.4, plots of normalized cumulative loads versus normalized cumulative discharge were created for the two investigated sampling points as shown in Figure 4-33. Because the first water sample for an event is taken depending on changes in flow depth, it is possible, that the record starts after the beginning of the event. In this case, there is no sample available directly before the onset of the flood (as it happened in 2004). In order not to overestimate the flush effect, a special method was used to interpolate the concentrations which are needed to calculate the loadings. The concentration was assumed to stay constant from the last measured point before the event up to the first measured point within the event. The later concentrations were then linearly interpolated.

***Particulate matter***

The plot for (V) of Figure 4-33 must be interpreted with care, because the last part of the flood wave is not very well documented by measurements (see Figure 4-26).

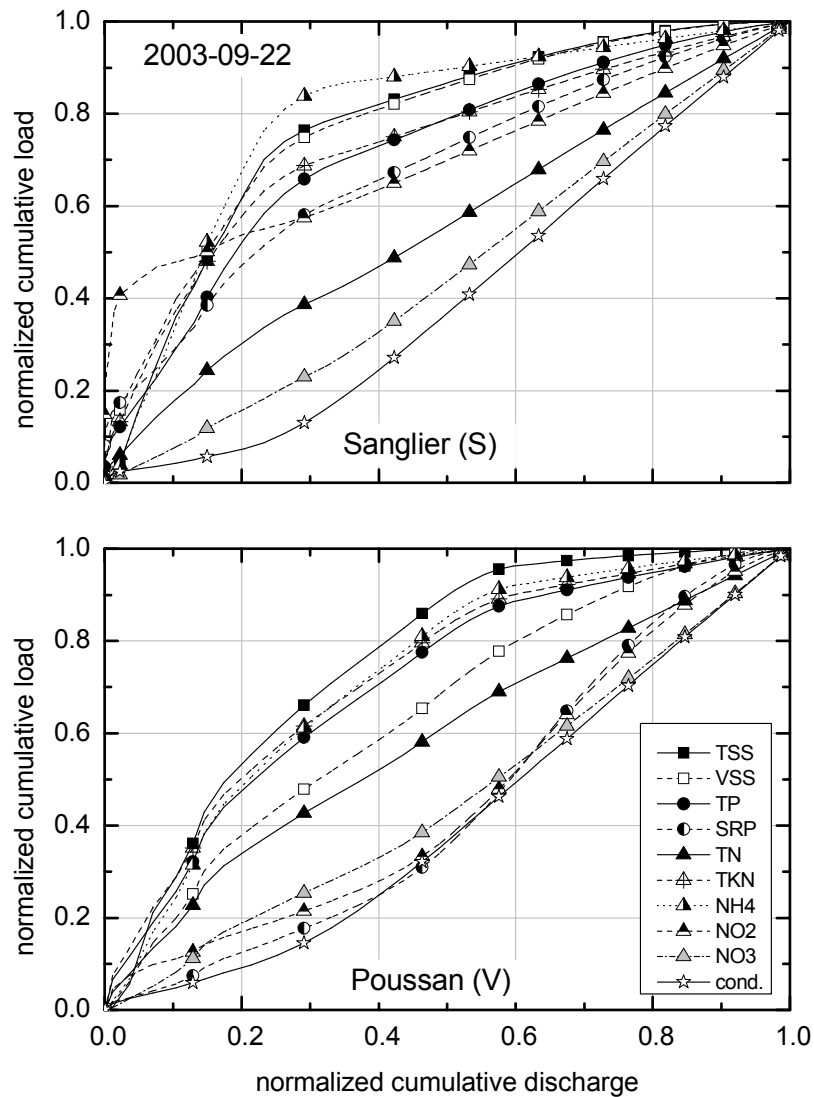


Figure 4-33: NCL-plot of 2003-09-22 for points S and V - normalized cumulative loads against normalized cumulative discharge

It could be that due to the later activation of the karstic spring, transport at this time is more intensive than estimated by the interpolation. However, for site S, where concentration measurements cover the whole regarded duration, particulate materials show an increased transport activity for the first 30% of the event discharge.

### ***Nitrogen***

It is remarkable that the nitrogen derivatives are very inhomogeneous in terms of their transport.

The previously denoted peaks in nitrite loads find their counterpart here only at S where nearly 50 % of the load is transported with only 10 % of discharge. The measurements end early at V, possibly the concentration (and therefore also the load) at S was assumed too high by the interpolation and the later part got too much weight.

The most extraordinary curve is the one of ammonium at S. For this flood, even the very strict criteria of Saget et al. (1995) is met, because  $FF_{30}$  is more than 83 %.

Nitrate is below the bisector in both points and because it is the dominating nitrogen species it has an important effect on total nitrogen.

The direct comparison of point Sanglier and Poussan shows, how the flush is disappearing along the 2.8 km from the accumulation spot of the WWTP at S to the point near the outlet V. This can have different reasons:

- i) inflow of less polluted rain water and subsurface flow,
- ii) worse data situation at V, overrepresentation of the later flood part,
- iii) the inflow of an additional karstic source between S and V and
- iv) possibly mixing within the flood wave.

### ***Phosphorus***

In terms of the normalized loading curves, the results are very diverse in S and V for soluble reactive phosphorus.

While total phosphorus'  $FF_{25}$  is above 60 % for both points, transport of the soluble part is delayed based on the regarded period. This is a cause of a high measured concentration after the end of the event at V (compare plot at V for SRP in Figure 4-33).

#### 4.1.4.5 NCL-plots of the event 2004-09-13

In comparison to 2003, for the flood of 2004-09-13 it seems as if the first flush effects are not so clear.

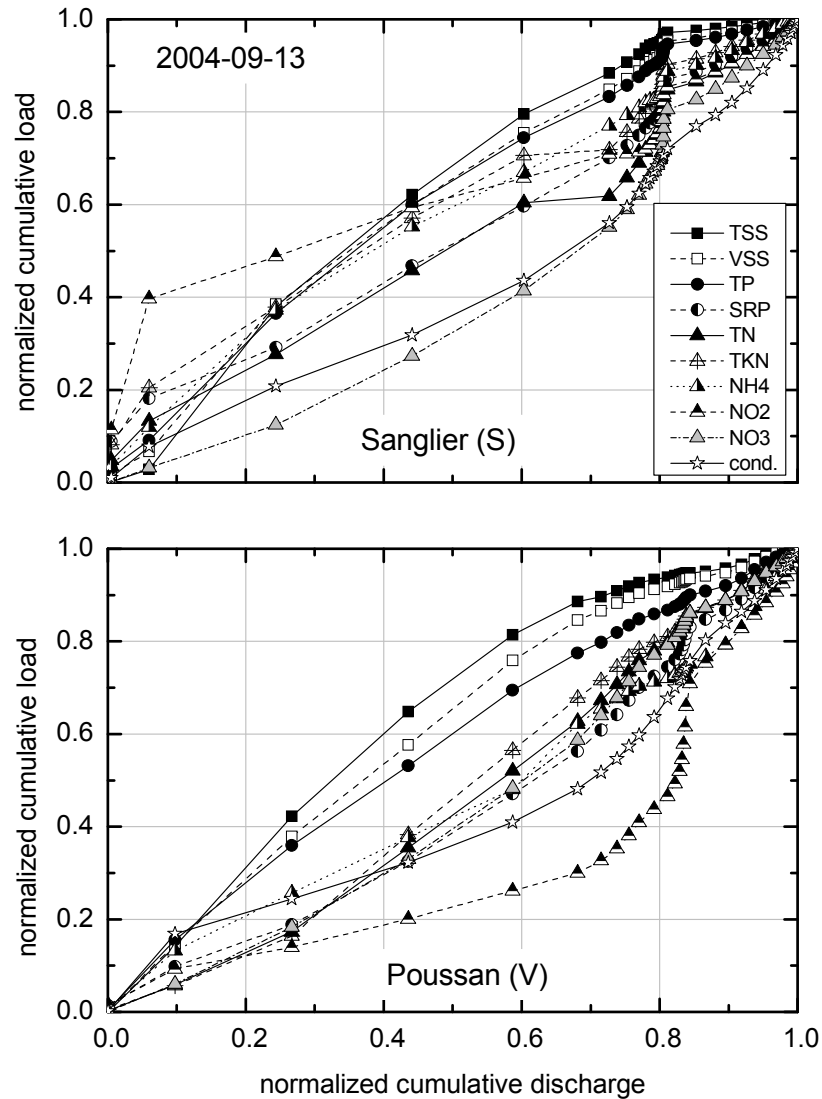


Figure 4-34: NCL-plot of 2004-09-13 for points S and V - normalized cumulative loads against normalized cumulative discharge

### *Particulate matter*

However, in terms of the normalized cumulative loadings, the particulate materials show at least a weak flushing behaviour at V compared to the other parameters (Figure 4-34).

Here the  $FF_{25}$  is about 42% for TSS which still meets the criteria of Vorreiter and Hickey (1994), which defined a first flush for a  $FF_{25}$  greater than 0.4 to 0.6 (see Table 2-2).

### *Nitrogen*

The fact that nitrite exhibit a significant flushing (as said before and indicated in Figure 4-30) is also very well represented in the NCL-curves of Figure 4-34.

Compared to the first flood in September 2003 the magnitude of flushes has decreased especially in S. Nitrate shows a very slow reaction to the flow condition in both sites, TN and  $NH_4-N$  are a bit above the bisector in S and a bit below in V.

### ***Phosphorus***

Apart from the beginning of the event, mass flux of phosphorus seems to follow the flow intensity.

Some explanations, why the flush effect is smaller in 2004-09-13 could be

- i) the small rainfall events before could have displaced and diffused most of the accumulated nutrients in the river; even if the water did not reach the receiving water, the pollutants are on one hand distributed in a smaller concentration over a longer stream section and on the other hand a great part of the material could have been settled downstream of site S,
- ii) the shape of the flood is more condensed and there is no small peak before the main peak, as in 2003-09-22; if this small first peak is capable of resuspending a great part of the accumulated matter, the transport activity of the flood is concentrated in the beginning.

However, the maxima of particulate matter concentrations are nearly equal for both floods, so they differ mainly in their total loadings and in the inter-event distribution.

#### 4.1.4.6 Measurements of conductivity

Conductivity was measured in 5-minute intervals and is therefore very helpful to determine the character of mass flows in rapidly changing flows.

In sites, where retention of water is possible in ponds or pools, i.e. at S or at the tributary Oulette (point O), the conductivity is coupled to the flow via an exponential regression (see Figure 4-35).

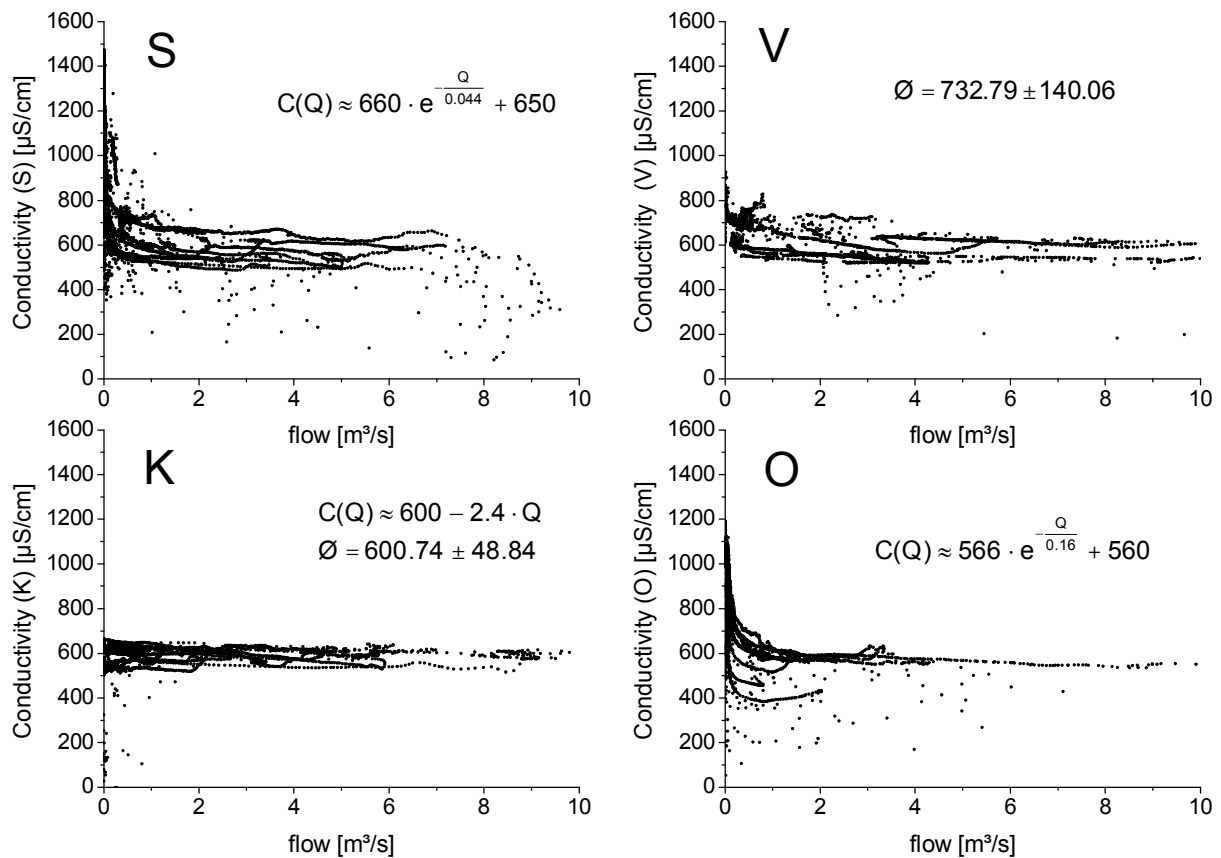


Figure 4-35: Conductivity against flow at four different sites of the catchment

Conductivity of the karstic source Cournonsec (K) can be considered as nearly constant around  $600 \mu\text{S/cm}$ . The comparably low standard deviation of about  $\sigma=49 \mu\text{S/cm}$  underlines, that it is nearly independent of flow. Station V, which lies close to the outlet also shows a more constant behaviour with a mean of  $733 \mu\text{S/cm}$  and a bigger standard deviation of  $\sigma=140 \mu\text{S/cm}$ . The reason, why the most downstream point may be better grouped with the most upstream point can be explained by a similar pattern:

- i) the flow passage through the karstic aquifer buffers and mixes the water;
- ii) on the way through the catchment, water from different origin (base flow, subsurface flow, overland flow and point source inflows) and with differing loadings of ions have time to mix and disperse, so that peaks are buffered;
- iii) during low flow, the upstream accumulation spots at e.g. S and O are not connected with V and the high concentration does not reach this station.

Judging only from the conductivity in  $\mu\text{S/cm}$  in Figure 4-36, it does not show a flush-like behaviour, no matter which one of the two floods or sampling points is considered.

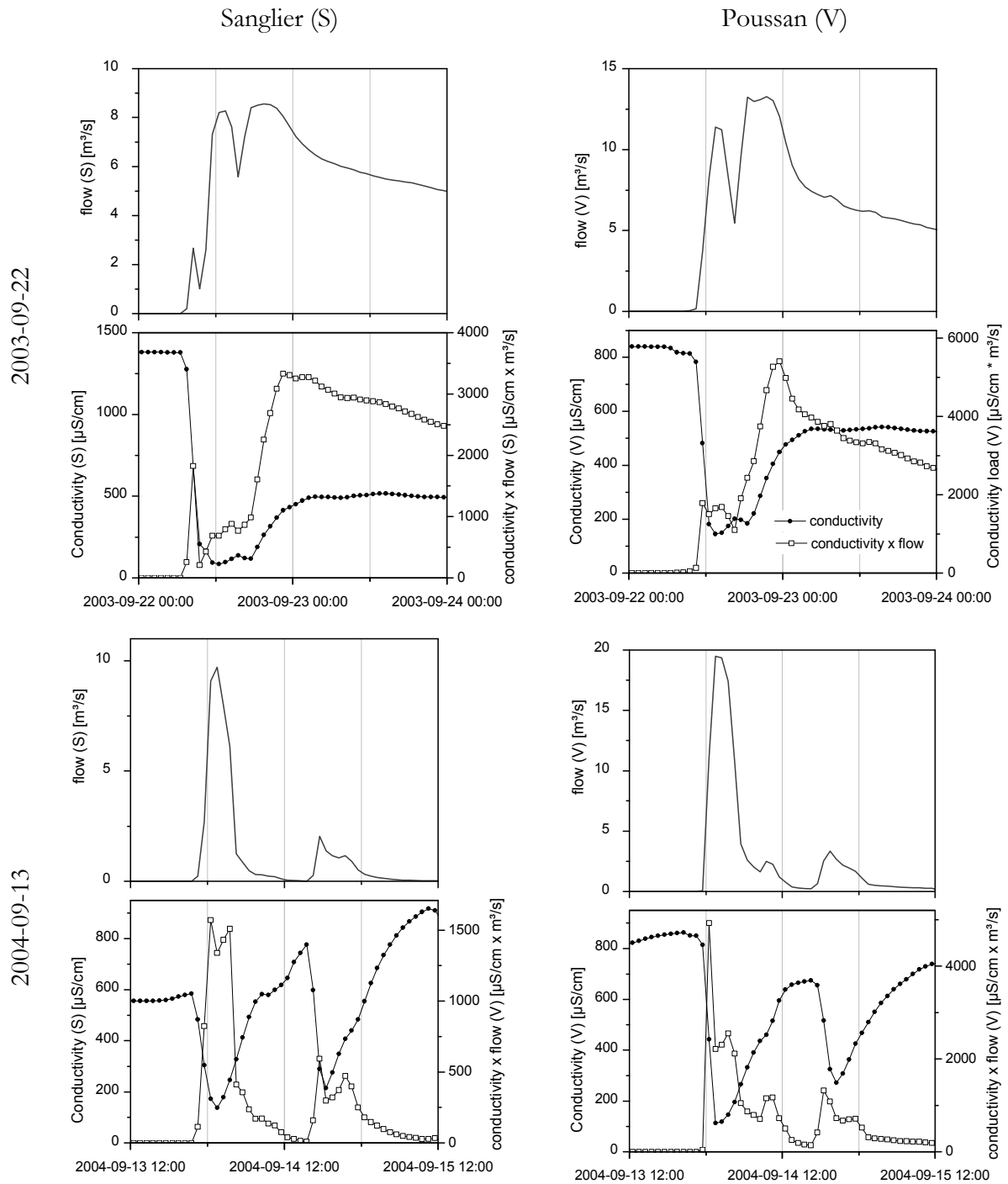


Figure 4-36: Conductivity for both floods at S and V

For constant flows above  $2 \text{ m}^3/\text{s}$  the conductivity is normally around  $600 \mu\text{S}/\text{cm}$  – which is the mean value for water originating from the karstic spring as mentioned above, whereas concentrations of up to nearly  $1300 \mu\text{S}/\text{cm}$  can be reached in the accumulation period, when the influence of steady inflows of point sources and evaporation prevails.

Apart from the conductivity, Figure 4-36 also shows the product of conductivity and flow, which can be interpreted as flux (load) of conductivity.

The load of conductivity shows a smaller flush for the flood 2003-09-22 only in S, and a peak in both points for the flood one year later.

#### 4.1.4.7 Application of rating methods for first flushes of each parameter

According to chapter 2.2.6, the indexes were applied to the two first significant flood events at site S as shown above.

The trend for all parameters in site S in Figure 4-37 is independent of the index method. The highest flush intensity in 2003-09-22 is therefore reached by ammonium, followed by the particulate properties TSS and VSS.

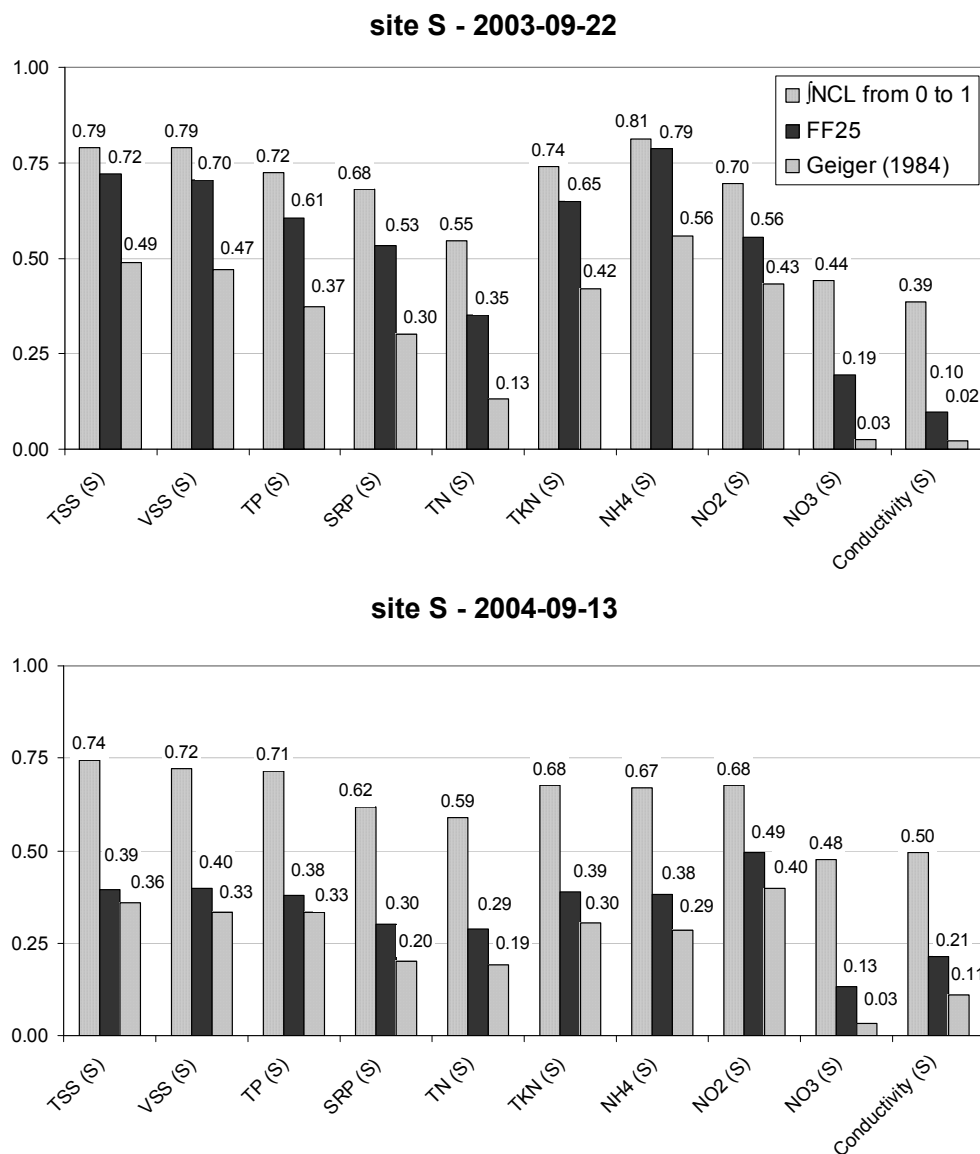


Figure 4-37: Rating of flushes for the site S on September 2003 and 2004 events

Apart from nitrate and conductivity, all parameters are transported in excess in the first 25% of the flood in 2003. This as well accounts for the flood of the following year, but clearly less pronounced.

In the flood of 2004-09-13 no flush of ammonium is happening, so that now TSS and VSS as well as TP prevail. The comparison of the two different floods makes one major limitation of the first method obvious: due to the integral calculation, the changes in the index values are not so clear as in the other methods (FF<sub>25</sub> and the index of Geiger (1984)).

#### 4.1.4.8 Conclusions

The first significant floods of the years 2002/2003 and 2003/2004 show a very different characteristic. The first flood of 2003-09-22 has three different peaks, which allows a distinction of different phases in the flood. It has a strong karst influence in the later part, which is not present in the flood of 2004-09-13.

There is a strong first flush effect at 2003-09-22 for VSS and TSS but also for solubles as ammonium and a very early one for nitrite. However, the flush of nitrite exists only downstream the WWTP at S. Whereas all constituents except nitrate and conductivity were transported in excess in the beginning of the event at S, the flush diminishes in downstream direction. At station V, only for TSS, VSS, TP and NH<sub>4</sub>-N occurs a notable flush effect.

The first significant flood of 2003/2004 did not show such clear flush events, which could have been caused by the small events before.

Two different relationships between flow and conductivity were identified: in places where accumulation is possible (S, O), the conductivity increases exponentially with decreasing flow. In spots without relevant and close upstream accumulation (K, V), the conductivity is nearly independent from the flow rate.

From the rating indexes for first flushes, the FF<sub>25</sub> proved to be the most valuable. The highest value was calculated from the 2003-09-22 flood for ammonium (0.79) followed by TSS (0.72) and VSS (0.70).

#### 4.1.5 *Regression of measured flow and water quality properties*

As said before, the course of the state of variables concentration and load is not coupled to flow with a simple relationship for most parameters. These relationships are studied in the following in order to investigate patterns for the regarded period in the Vène. Special focus is given to the following important events or parts of these events:

- (i) 2002-10-09 (1st part): first part of the flood from 2002-10-09 16:53 to 19:53
- (ii) 2002-10-09 (2nd part): second part of the flood until 2002-10-10 03:53
- (iii) 2003-09-22 (1st peak): the very first small peak of the event, from 2003-09-22 07:29 to 10:29
- (iv) 2003-09-22 (2<sup>nd</sup> & 3<sup>rd</sup> peak): the following two major peaks until 2003-09-22 22:59
- (v) 2003-10-01: the next following flood (flow maximum at 4.2 m<sup>3</sup>/s)



- (vi) 2004-09-13 (1<sup>st</sup> part): the first part of the flood until the flow maximum of 10.2 m<sup>3</sup>/s from 2004-09-13 13:35 to 2004-09-14 01:06
- (vii) 2004-09-13 (2<sup>nd</sup> part): the recession until 2004-09-15 05:11

In the following, the measurements will be grouped in terms of similar characteristics. The regressions of concentrations respective loads and flow rates will be investigated.

#### 4.1.5.1 Comparison of flow and concentration

Figure 4-38 shows the relationship between the concentration of TSS and the flow, both at station S for the period from October 2002 to September 2004.

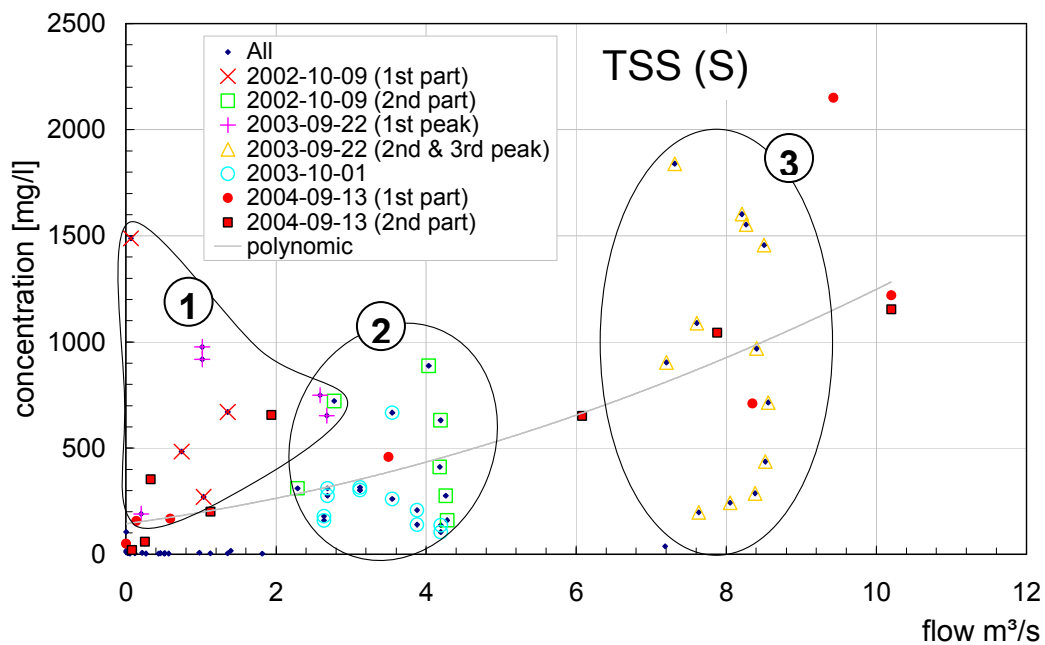


Figure 4-38: Relationship between flow and concentration of TSS at station S

It can be shown that there is a lower fluctuation in the concentration during medium flow (group 2). Here, the second event of 2003 as well as the second part of the first flood of 2003 can be found. During the onset of first significant floods in 2002 and 2003, there exists a wider spectrum of concentrations (group 1). The widest range of concentrations can be found for the flood of 2003-09-22, excluding the very first part (group 3). Although some groups can be identified, Figure 4-38 shows that there is no clear relationship between flow and concentration, even if the mean concentration is increasing with increasing flow intensity.

Another situation is found in the analysis of VSS (Figure 4-39). Only during the lower flow intensity at the beginning of the flood 2003-09-22 (data for 2002 was not available), there are extraordinary high concentrations. There is only a minor fluctuation in the other groups.

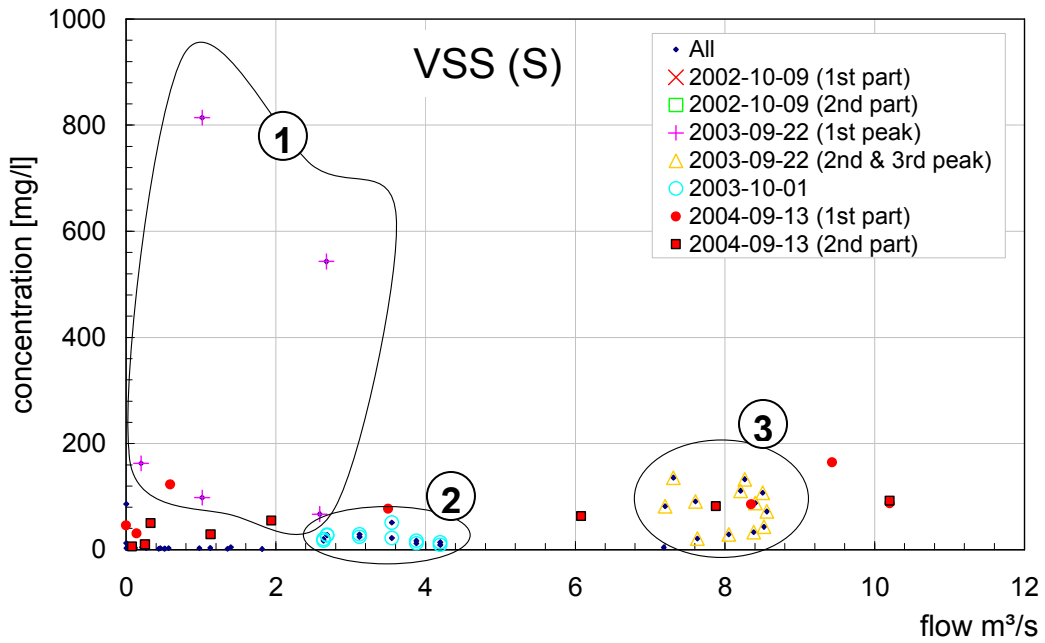


Figure 4-39: Relationship between flow and concentration of VSS at station S

The relationship seems to be clearer for TP in Figure 4-40. For this parameter, data for 2002 was also available. The distribution of concentration follows a logarithmic regression over flow for this dataset, the lower the flow, the higher the concentration.

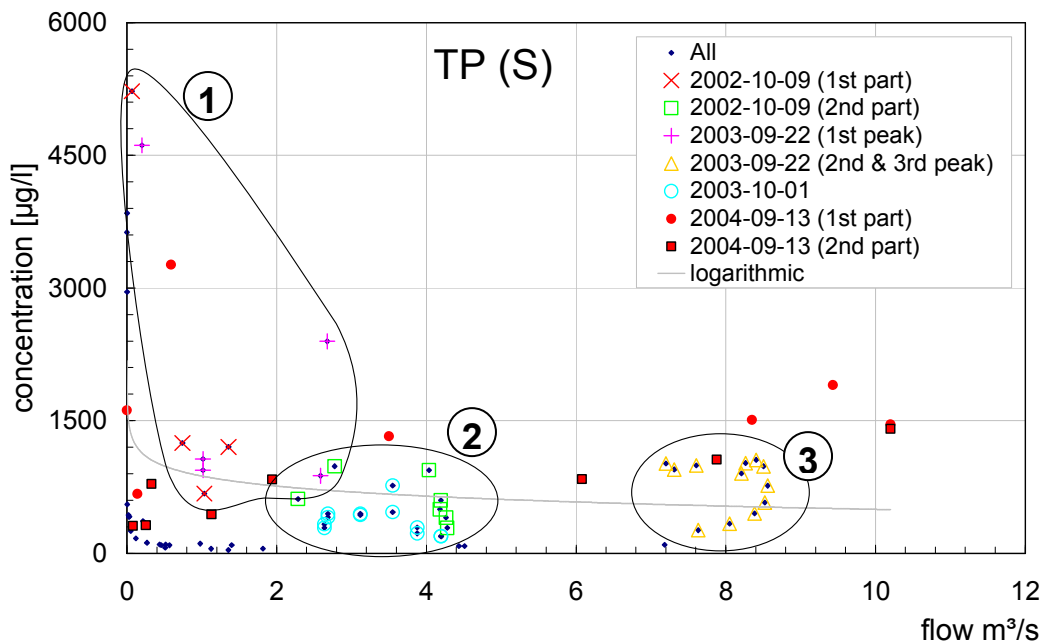


Figure 4-40: Relationship between flow and concentration of TP at station S

Only nitrogen again shows a differing characteristic as it can be seen in Figure 4-41. There are also some higher values during lower flow conditions as in the other parameters, but the magenta group (representing the onset of the floods) is lower than the blue one, where the floods are entering, when the system is already comparably wet.

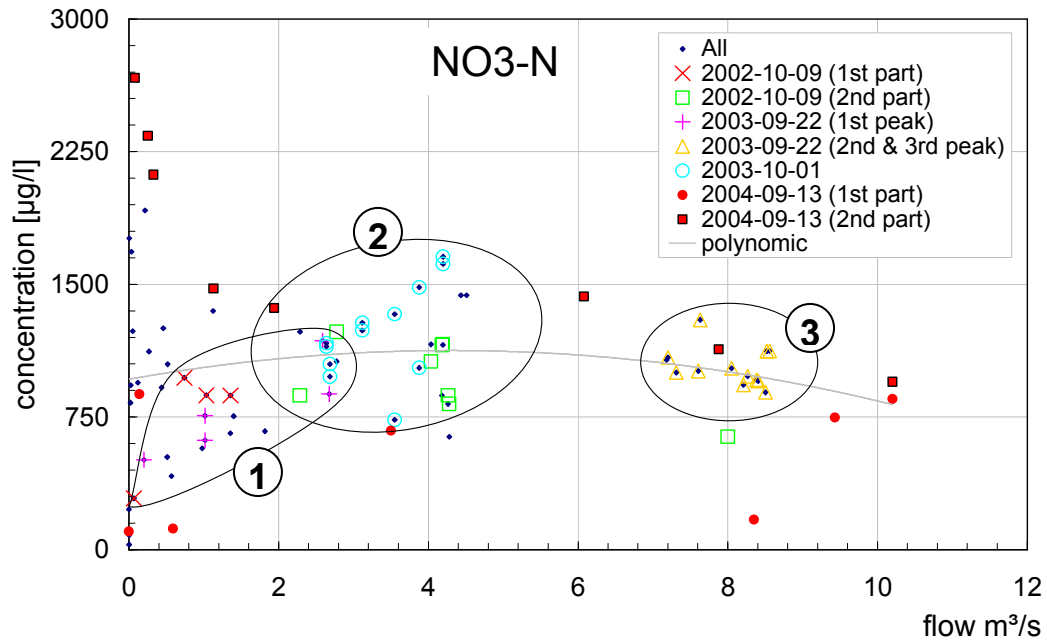


Figure 4-41: Relationship between flow and concentration of  $\text{NO}_3\text{-N}$  at station S

The concentration of nitrate seems to have a maximum in medium flow condition (blue ellipse in the middle).

For all the parameters shown above, values for the flood from 2004-09-13 could not be allocated to any group. They seem to follow a totally different pattern. Even the subdivision into two parts (rise and recession) did not bring any further clarification.

#### 4.1.5.2 Comparison of flow and load

The comparison of flow and load shows a much stronger relation (Figure 4-42).

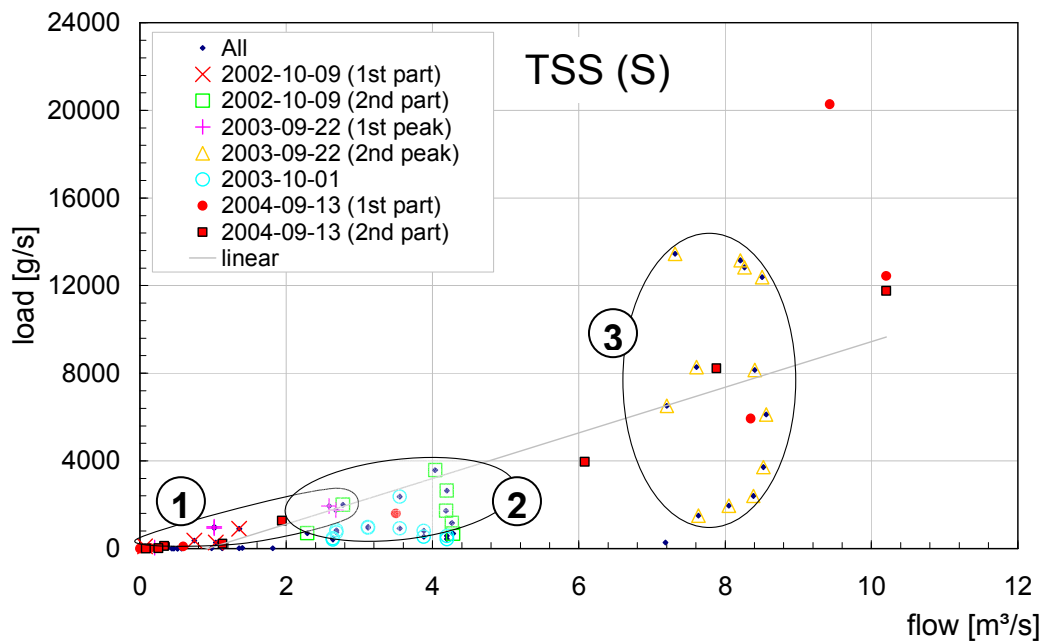


Figure 4-42: Relationship between flow and load of TSS at station S

Even though there is a growing deviation from the indicated linear regression, this is clearly visible for lower intensities. The linear regression curve indicates also a minimum flow, which has to be reached to produce a significant load, which seems to be around 0.9 to 1.0 m<sup>3</sup>/s.

As for TSS, there has to be reached a minimum flow in order to produce a significant VSS flux. This could be approximated by the linear regression to around 0.3 m<sup>3</sup>/s (Figure 4-43). As VSS is also a particulate substance, there is a comparable relationship as in TSS, but with important deviations in the magenta group during the beginning of the early rainy season rains in 2002 and 2003.

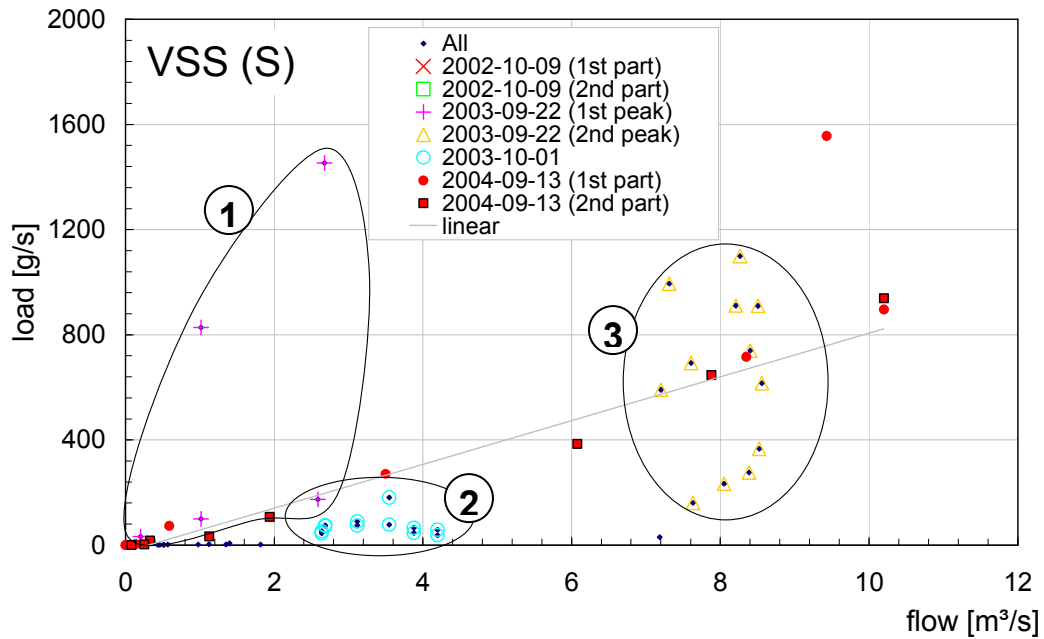


Figure 4-43: Relationship between flow and load of VSS at station S

Unfortunately, there are only two values available, which are extraordinary, so this trend cannot be generalised, but is possible as there are no such outliers in TSS.

Figure 4-44 clearly shows that the strongest relation exists between the load of nitrate and flow.

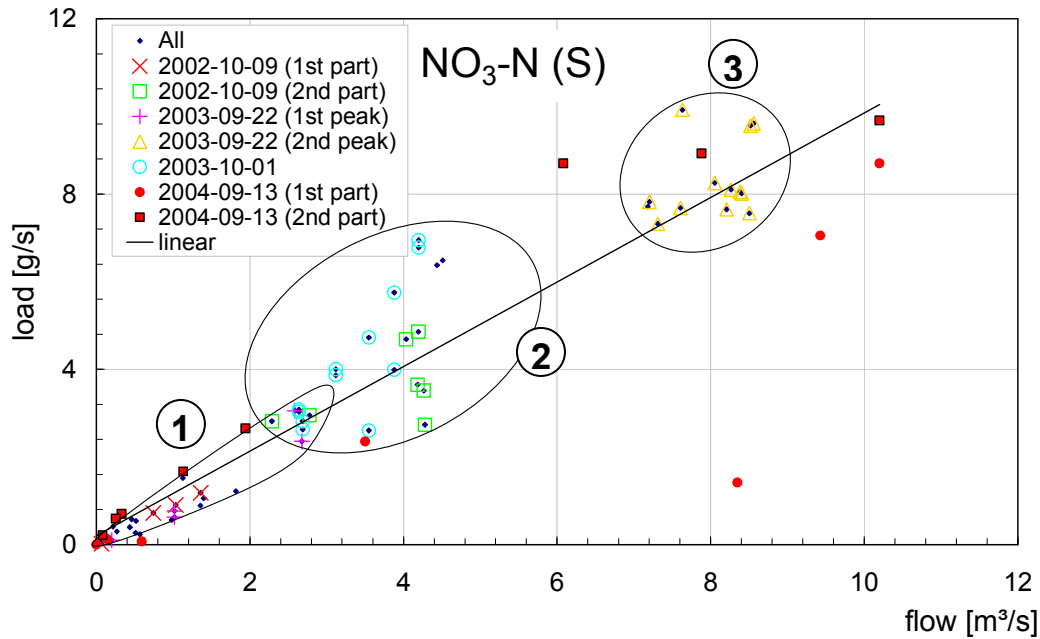


Figure 4-44: Relationship between flow and load of NO<sub>3</sub>-N at station S

As for the examples of concentration before, the event of 2004-09-13 could not be assigned to a group here. The best agreement exists in the regression of nitrate, but again there can be no distinction identified between the beginning of the flood and the later recession.

## 4.2 Selected examples in other catchments

In order to show some results from other regions and to investigate, whether some of the characteristics shown above are only specific for the dataset of the Vène, two other catchments were also analysed in the following, The Mulargia river and the Albujión river.

### 4.2.1 *The Mulargia River, Sardinia, Italy*

#### 4.2.1.1 River characteristics

The island of Sardinia is a typical Mediterranean region, characterised by a dense network of temporary rivers and streams that play a crucial role in feeding water bodies such as reservoirs, lagoons or coastal areas.

The temporary river Mulargia is located in the south-eastern part of Sardinia (Figure 4-45) and flows into the Mulargia reservoir.

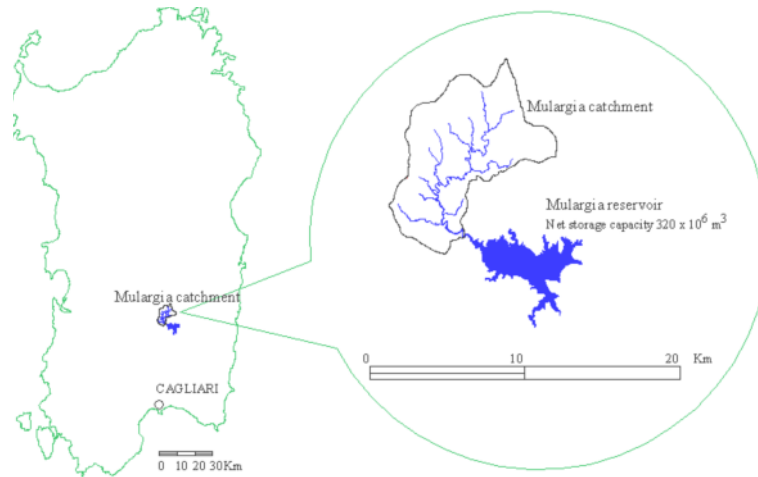


Figure 4-45: Location of the Mulargia catchment on the Island of Sardinia

The stream is the main tributary of the dam which plays a major role in the water distribution network of Southern Sardinia for various civil, agricultural and industrial purposes.

The studied catchment area has an extension of about 66 km<sup>2</sup>, an average elevation of 480 metres spanning from 250 to 750 m above sea level. The river network has an overall length of around 44 km, while the distance from the origin of the stream to the outlet in the reservoir is 17.6 km.

**General climatic situation and rainfall-runoff situation**

The catchment’s main hydrological characteristics are summarised in Figure 4-46. The maximum temperature in summer is around 40°C and minima seldom reach below 0°C. According to the United Nations definition of aridity (UNEP, 1997), the Mulargia River lies in a dry-subhumid zone (AI~0.57 at the outlet to the reservoir, see Table 2-1). The climate in this area is characterised by an average annual rainfall of around 445 mm mostly concentrated in autumn and winter with usually very dry summers.

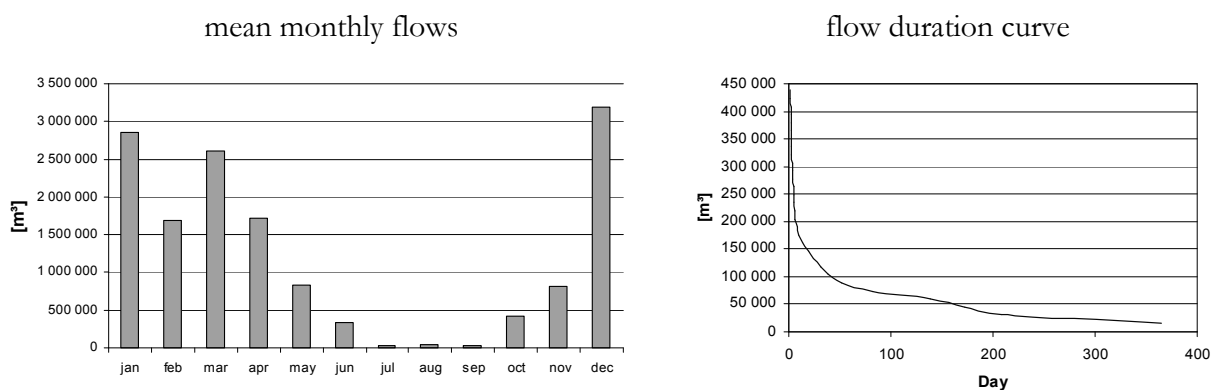


Figure 4-46: Mulargia stream flow statistics of the years 1992-2004

As a typical temporary river, the Mulargia stream is completely dry during hot season except for some wet parts affected by wastewater discharges from treatment plants.

### ***Soil and land-use situation***

The geomorphology is characterised mainly by shaly rocks and the entire zone shows small permeability resulting in very low transmission losses through infiltration and consequently high runoff coefficients.

Land use is mainly influenced by grazing: natural pastures have great extension to satisfy large sheep requirements, so cultivated lands are mostly dedicated to the production of pasture for breeding with a small amount of arable land (mostly vineyard).

### ***Identified point sources and sampling points***

There are three small villages in the catchment, with a total population of around 4500. Wastewater is treated in two treatment plants (all up to a secondary stage) that discharge into the river network upstream of B (Froebrich et al., 2006).

Industry is largely absent in the catchment, although there is one cheese factory and one slaughter-house, which are both situated near the villages in the north of the catchment.

Automatic sampler connected with flow-loggers and online probes for the detection of pH, temperature, dissolved oxygen and conductivity have been installed in two points -at an upstream site (B) and at the outlet into Mulargia reservoir (D)- together with rain gauges for continuous precipitation record (see Figure 4-47).

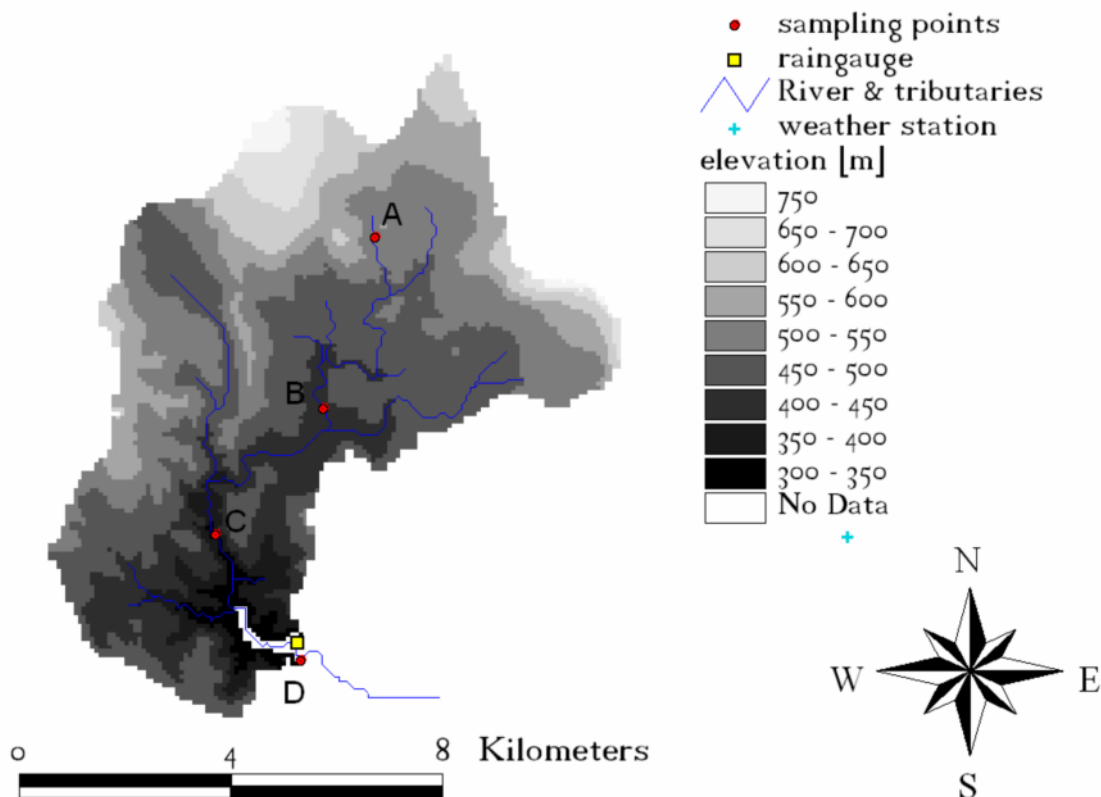


Figure 4-47: Elevation, point sources and weather stations in the Mulargia catchment

During high intensity rainfalls, water level-switched automatic samplers allow the collection of numerous and frequent water samples within the storms.

## 4.2.1.2 Relevancy of the dataset

Measured water quality data in the Mulargia was available in detail for the period from September 2003 until June 2004. As in the Vène catchment, the measurements in the Mulargia are concentrated on low flow conditions in the regarded period (see Figure 4-48).

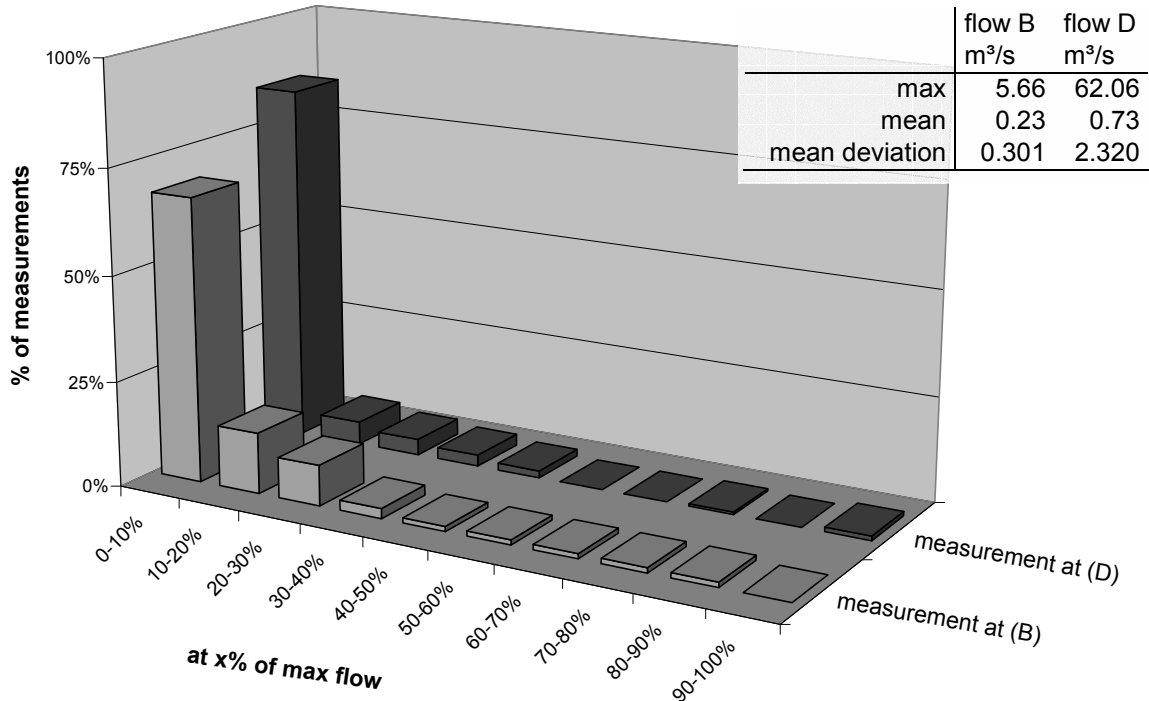


Figure 4-48: Distribution of measurements over flow intensity in the Mulargia

Although there is a bigger difference between mean and maximum values for flow than in the Vène, these flood events seem to be more unlikely. Judging from the available datasets, there is generally less fluctuation in flow. This can be either seen in the lower mean deviation in Figure 4-48, which is only 3.7% of the maximum (10.4% in the Vène, see Figure 4-4) and also in the fact, that 99% of the flow measurements in D (93% in B) are smaller than 10% of the maximum flow in the regarded period.

## 4.2.1.3 Annual cycle of transport – magnitude of months to years

***Distribution of precipitation***

For the hydrological years 1991-1998, the rainfall regime is even more distinct Mediterranean than in the Vène. Figure 4-49 shows that nearly one third of the annual precipitation falls in August and September.



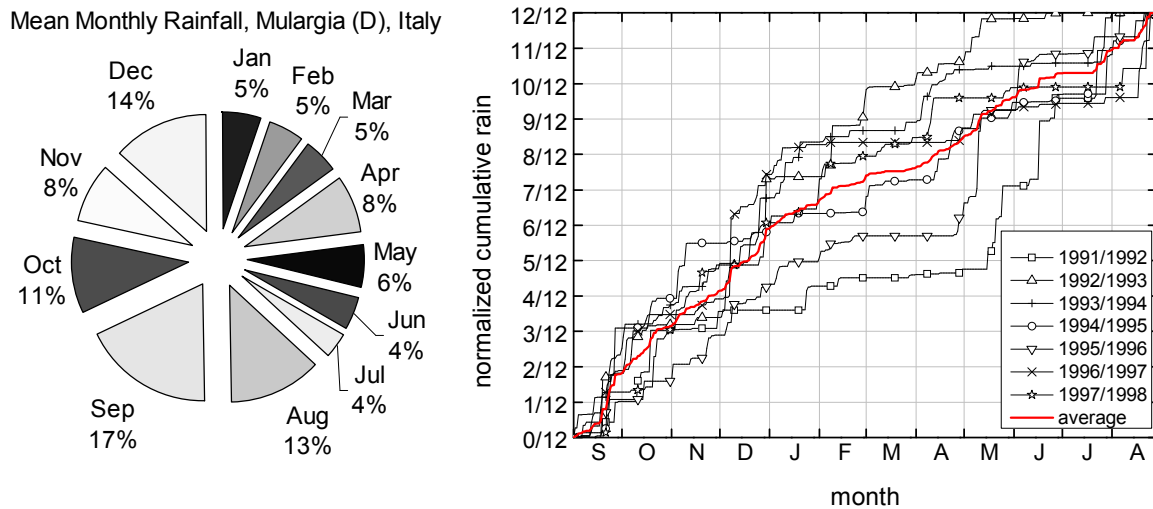


Figure 4-49: Mean monthly and normalized cumulative precipitation on basis of data from September 1991 to August 1998 at the Mulargia

Due to the fact, that the available water quality data record at the Mulargia is shorter and does not cover a whole hydrological year, an analysis in terms of an intra-annual variation as in the Vène was not done.

The following shows the more detailed data of the flood events in the available period.

#### 4.2.1.4 Examples for floods and flushes – magnitude of days to hours – site B

##### ***Pollutographs of the event 2003-10-17 and 2003-10-22***

The two events allow the comparison of two directly following flood events at the beginning of autumn. Note that the recession limb of the second flood had to be approximated in order to calculate loadings due to a failure of the measuring device. Therefore, the relative decrease per timestep of the recession of the former flood was adopted from 2003-10-22 05:00 to 2003-10-24 00:00. The investigation of the courses of concentration supports the chosen progression of water flux, and the assumption seems reasonable.

##### *Particulate matter*

The particulate properties shown in Figure 4-50 reveal an interesting feature of the system. The floods are comparable in their maximum peak flow (1.75 for the first and 1.57 m<sup>3</sup>/s for the second) and the first has even nearly the double amount of total flow (about 70 000 m<sup>3</sup> and 39 000 m<sup>3</sup> respectively), the magnitude of concentration especially for TSS is over tenfold higher in the second flood (deviating from the following parameters here not shown on the same scale).

Although it is hard to make a general statement with this little data, the higher load in the second flood can possibly be caused by increased bank erosion in the channel, which was already wetted before and finally lost its stability.

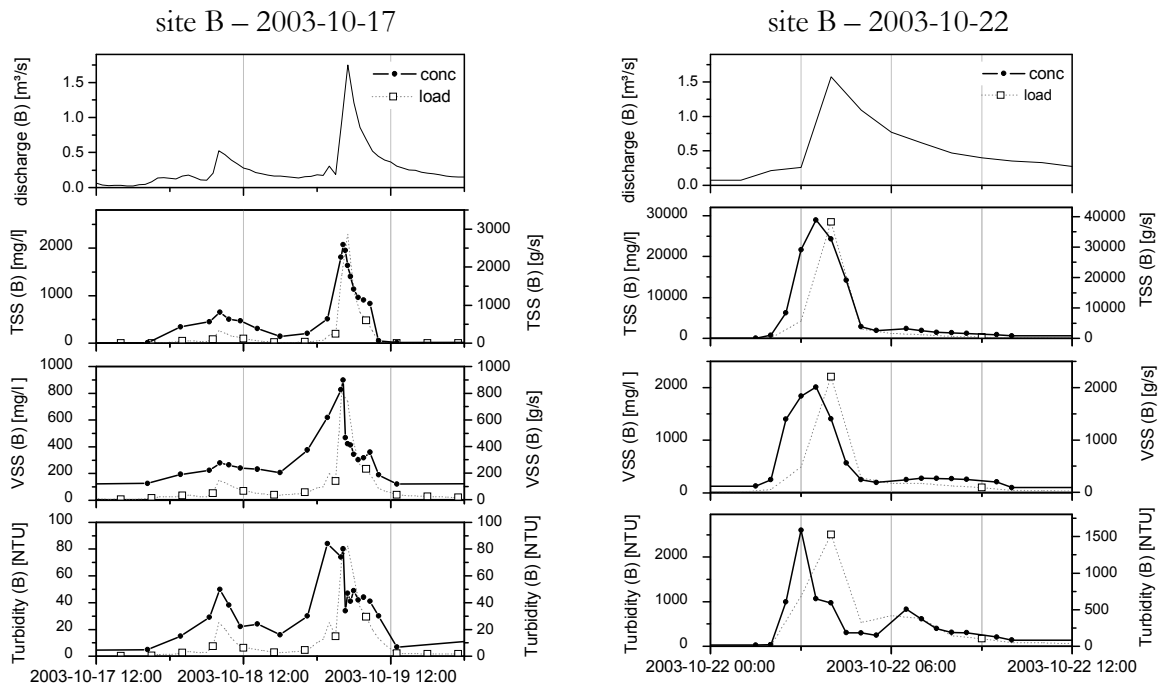


Figure 4-50: Pollutographs at site B of the events 2003-10-17 and 2003-10-22 for particulate properties

The spatial distribution of precipitation is very heterogeneous and varying (Froeblich et al., 2006). It could also have been the case that the rainfall affected different parts of the catchment for the floods, enabling also differing erosion capacities.

### Carbon

The big difference of the above particulates is not found for parameters related to carbon. On the contrary, the floods seem to behave in quite an analogue manner, with peak values for POC around 184 mg/l for the first and 160 mg/l for the following flood (see Figure 4-51).

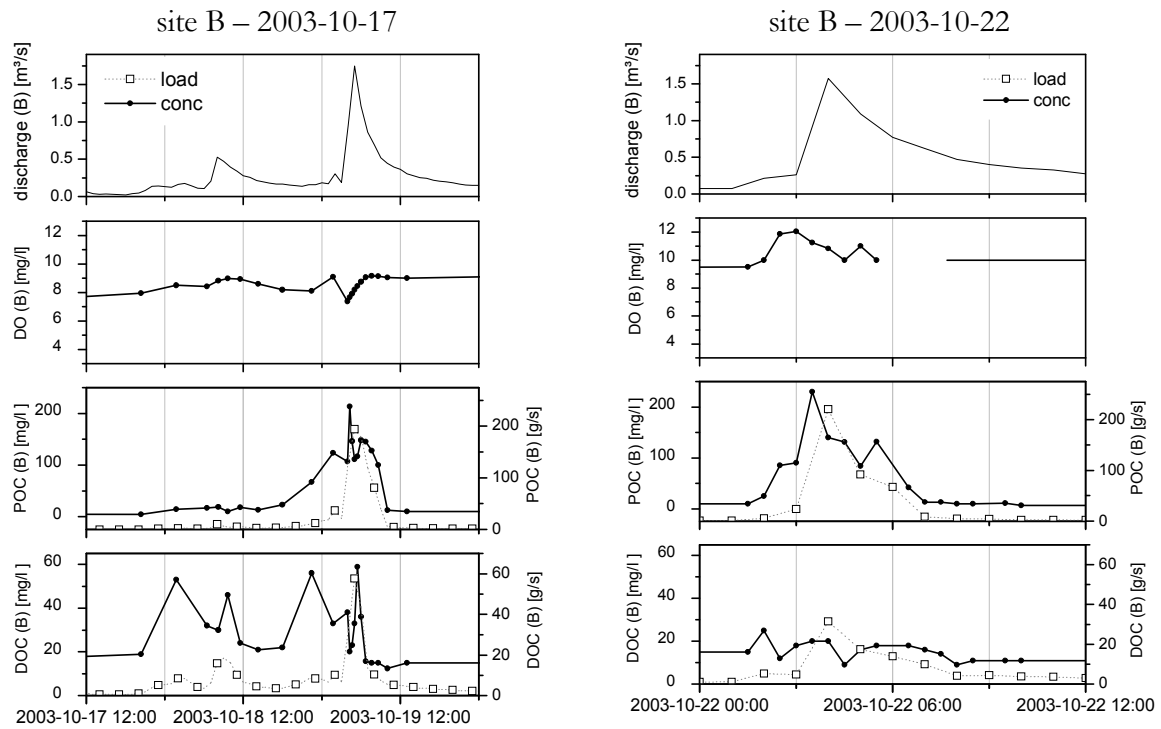


Figure 4-51: Pollutographs at site B of the events 2003-10-17 and 2003-10-22 for properties associated with carbon

Dissolved oxygen (DO) is following the superimposing influences of nutrient content (as sink) and stream velocity (as source) and is generally a bit higher in the second flood. Dissolved organic carbon (DOC) is very sensible during the onset of the flood, pending around 30 mg/l for the flood of 2003-10-17 and is later reduced to around 11 mg/l.

### *Nitrogen*

Total nitrogen (TN) in Figure 4-52 also shows increased concentrations in the second flood (85 to 54 mg/l respectively).

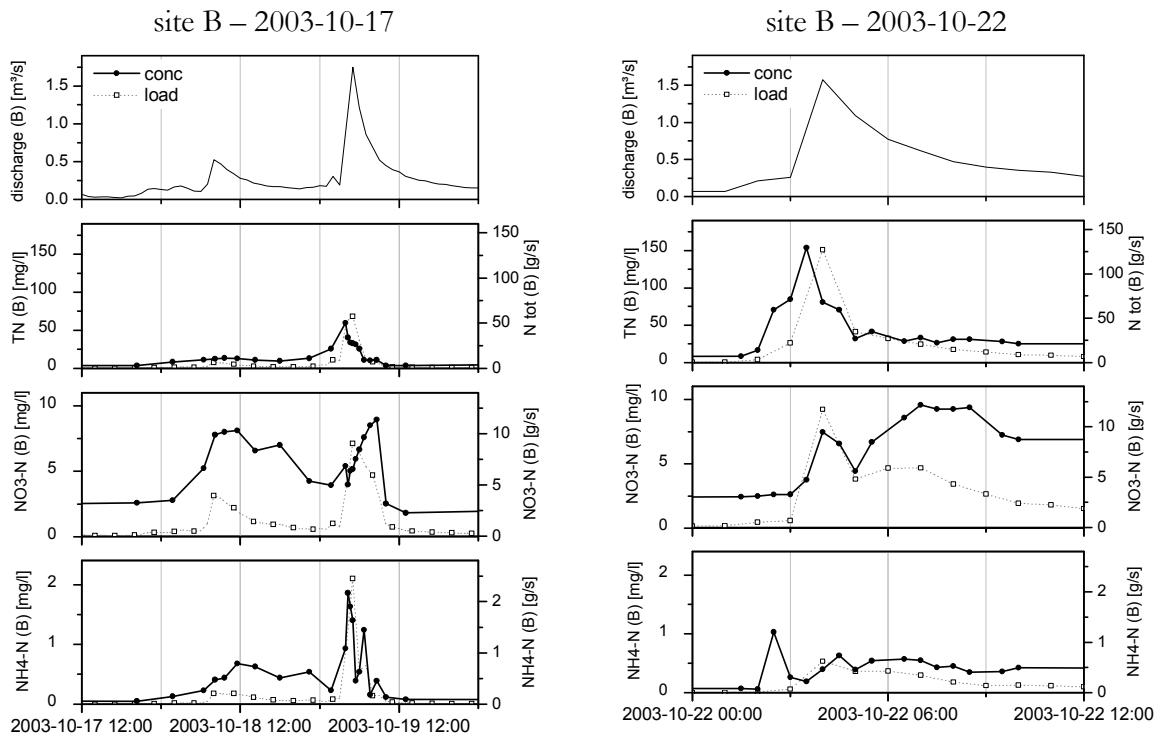


Figure 4-52: Pollutographs at site B of the events 2003-10-17 and 2003-10-22 for properties associated with nitrogen

In contrast, nitrate-nitrogen is only marginally higher in 2003-10-22, but the concentrations seem to slowly increase.

Ammonium is subject to fast dilution for both floods after a small flushy increase in concentration.

Following these information it can be concluded that the organic part of nitrogen is causing the higher values of TN in the later flood.

#### *Phosphorus*

As before, total phosphorus encounters a stronger transport activity in the second flood.

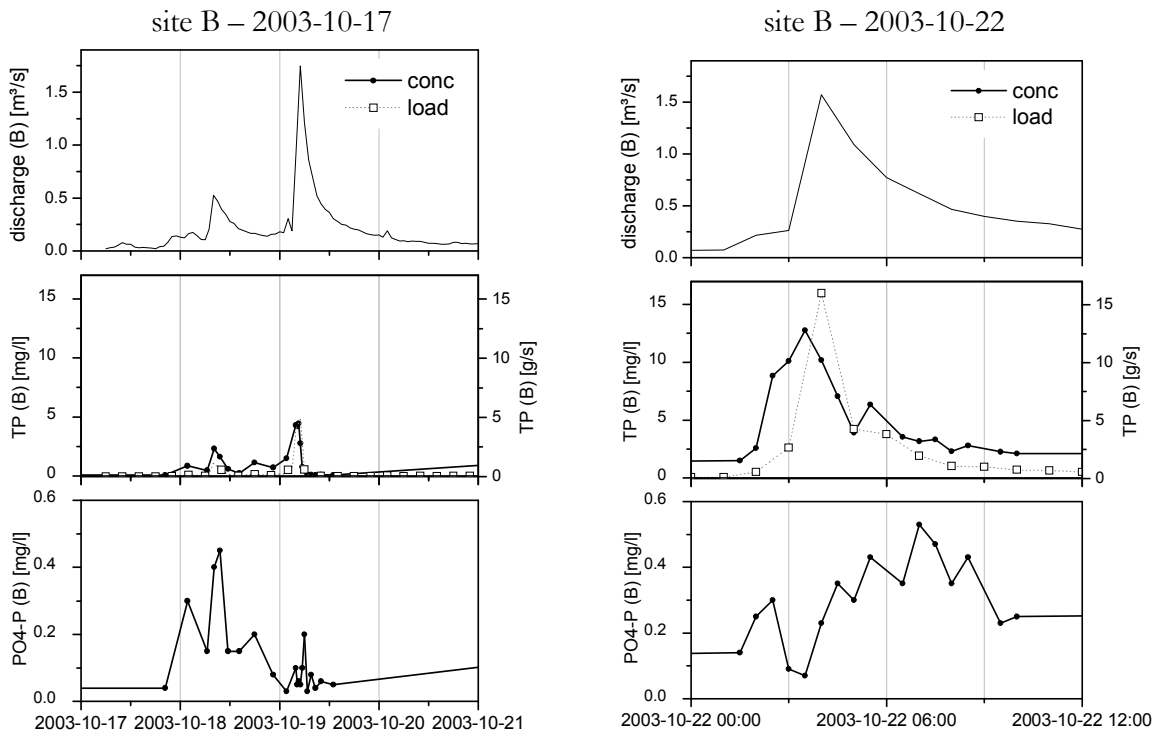


Figure 4-53: Pollutographs at site B of the events 2003-10-17 and 2003-10-22 for properties associated with phosphorus

Figure 4-53 also documents an increasing concentration of  $\text{PO}_4\text{-P}$  in the progression of the second event, but the magnitude is similar for both.

#### *Temperature, pH and conductivity*

The temperature is nearly the same for both floods and -except the sudden increase in the end of the first one- regular around 7 to 8 °C. The value of pH is a bit higher in the second one, around 8, but conductivity is decreasing from the first to the second event, which is a reference of the declining export of ions from the soils or instream storages.

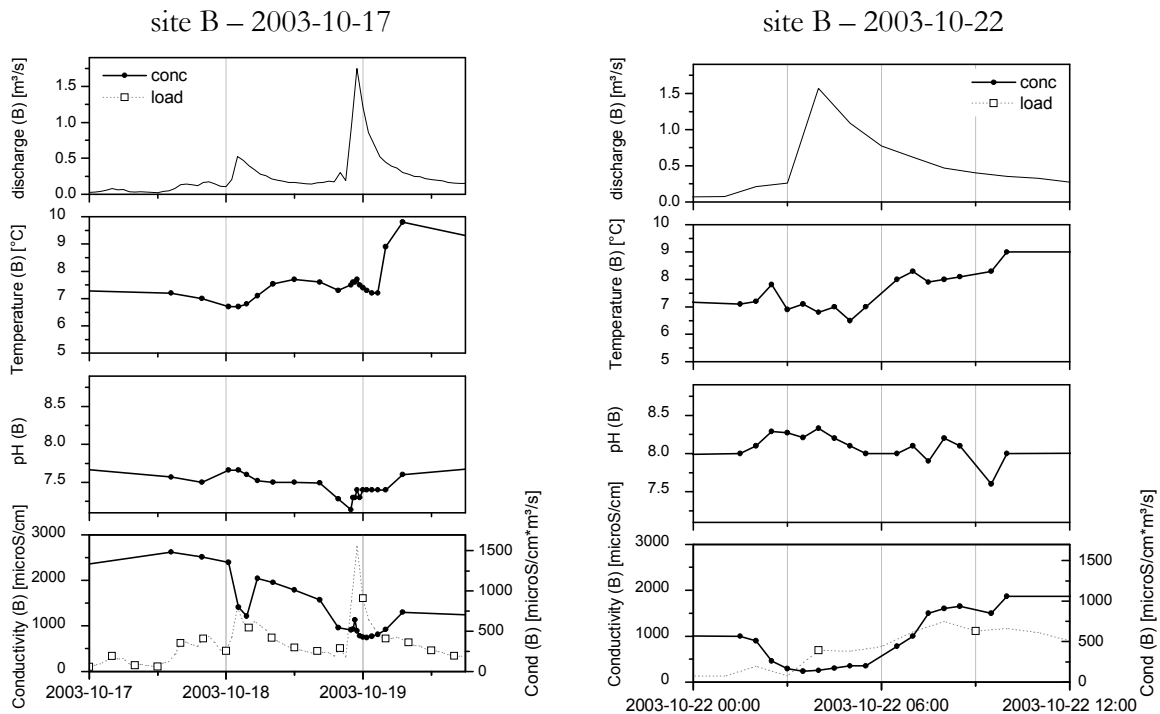


Figure 4-54: Pollutographs at site B of the events 2003-10-17 and 2003-10-22 for properties associated with phosphorus

After the discussion of the other available parameters, the strong increase of TSS for the second flood is still rare. It is possible, that there was an increased effluent from the slaughter house or the cheese factory during the second flood.

For carbon nitrogen and phosphorus, the increase of concentration is visible in the organic species, which backups the course of VSS. The extraordinary concentrations for TSS can be also caused by destabilised soil texture or a failure in the collection or analysis.

The data for the downstream station D is limited for these two events, so a detailed analysis was not done.

### ***Pollutographs of the event 2003-11-20***

Compared to the aforementioned floods, the one of 2003-11-20 is characterised by higher peak flow ( $2.93 \text{ m}^3/\text{s}$ ) and total flow ( $88\,240 \text{ m}^3$ ) and a shorter duration of only 32 hours.

#### *Particulate matter and phosphorus*

Even though the event is more condensed and therefore intense, the concentration of VSS is even smaller than in both precedent events (Figure 4-55).

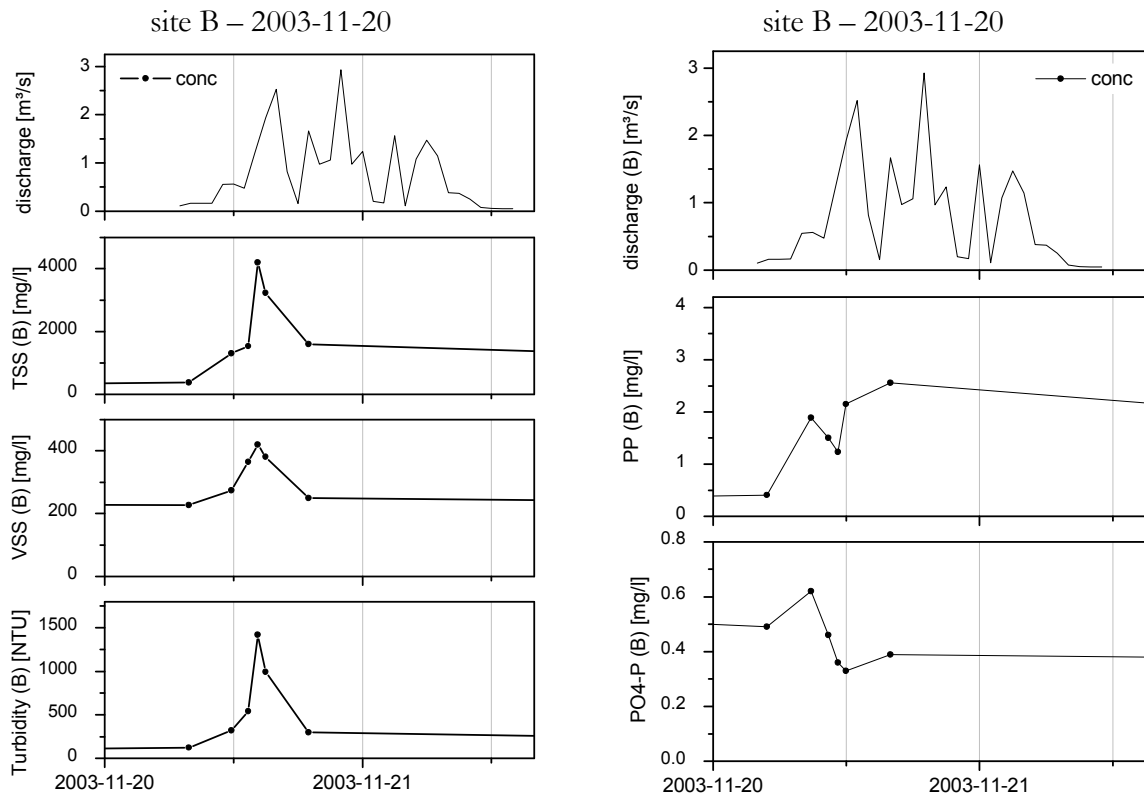


Figure 4-55: Pollutographs at site B of the events 2003-11-20 for particulate and phosphorus properties

Unfortunately, the record ends after the first peak, so a comparison of the course at a later stage of the concentration is impossible.

*Nitrogen, temperature, pH and conductivity*

There is some evidence of a concentration based flush, to be seen in Figure 4-56 for ammonium, conductivity and pH.

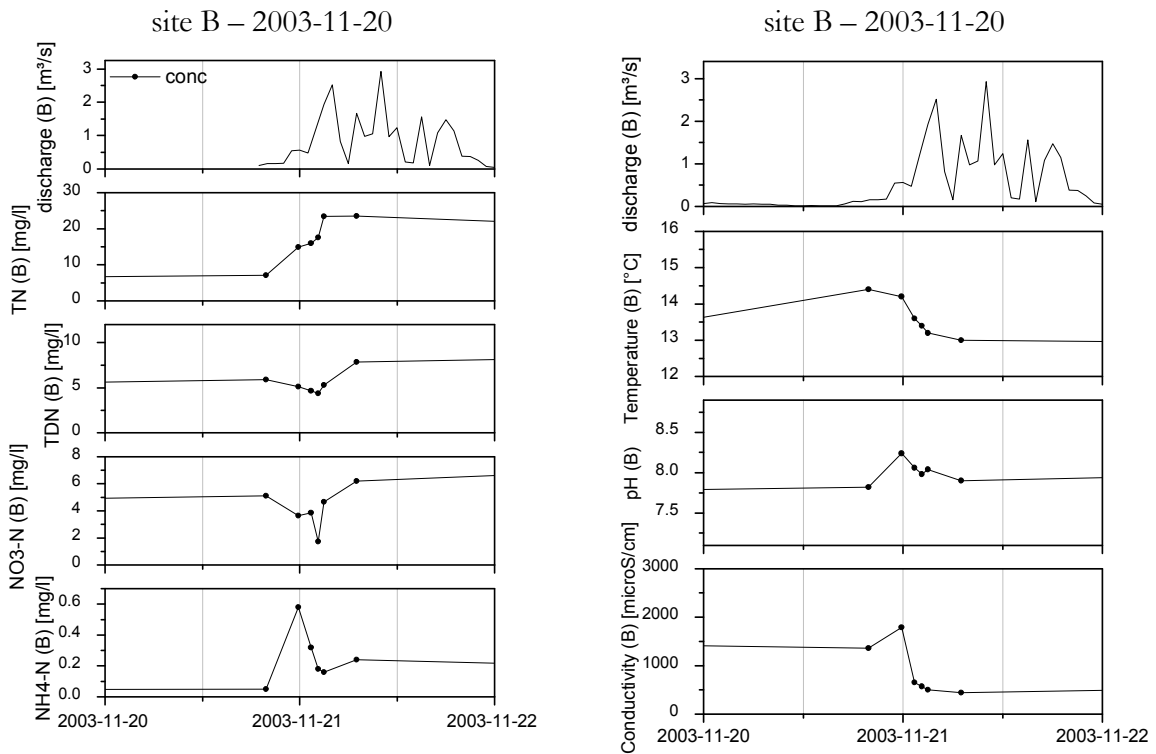


Figure 4-56: Pollutographs at site B of the events 2003-11-20 for Nitrogen, temperature, pH and conductivity

Nevertheless, the overall tendency is a reduction of both peak and mean concentrations in comparison to the floods before.

***Pollutographs of the event 2003-11-27***

With a duration of less than 8 hours and a peak value of 4.6 m³/s (55 000 m³/s in total) this is the most intense event measured.

*Particulate matter and phosphorus*

Unlike flow, the peak concentration of TSS of around 900 mg/l is the lowest of all events (Figure 4-57).



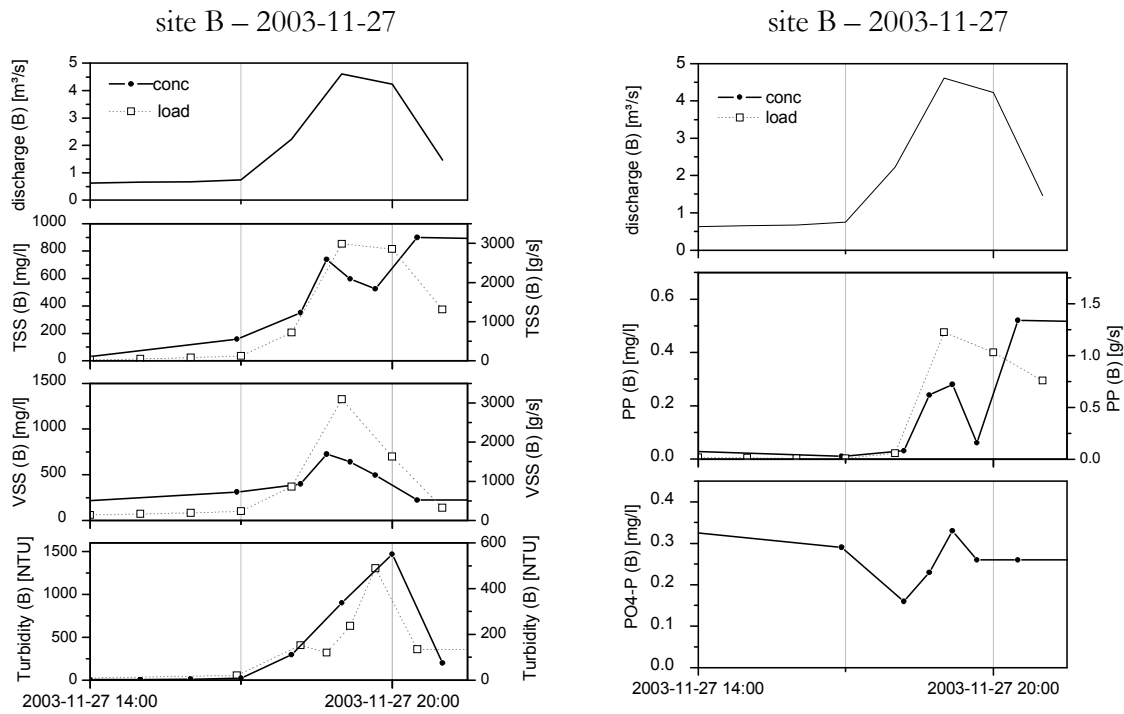


Figure 4-57: Pollutographs at site B of the event 2003-11-27 for particulate and phosphorus properties

VSS shows less fluctuation, but is still much lower, than it could be expected for a flood of his magnitude. A shortage of storage within the catchment to this later stage of the flow period lies near.

For the first part of the flood, VSS makes the greatest part of the total suspended solids.

#### 4.2.1.5 Examples for floods and flushes— magnitude of days to hours – site D

For site D near the outlet of the Mulargia River into the reservoir, frequent flow data was available, but the chemical analysis was not done in the intensity of site B.

#### ***Pollutographs for the flood of 2003-11-27***

On the way downstream, the flood gained much strength compared to B, the peak flow is increased fourfold and nearly reaches  $20 \text{ m}^3/\text{s}$ , with a transfer time between B and D of 30 mins two an hour. There was even a second peak measured of about  $25 \text{ m}^3/\text{s}$  which is indicated in Figure 4-54, but there were no samples taken in the sites.

#### *Particulate matter and phosphorus*

Due to the much higher carrying capacity of the stream, the concentration of TSS is higher at D but VSS reaches nearly the same level as at B.

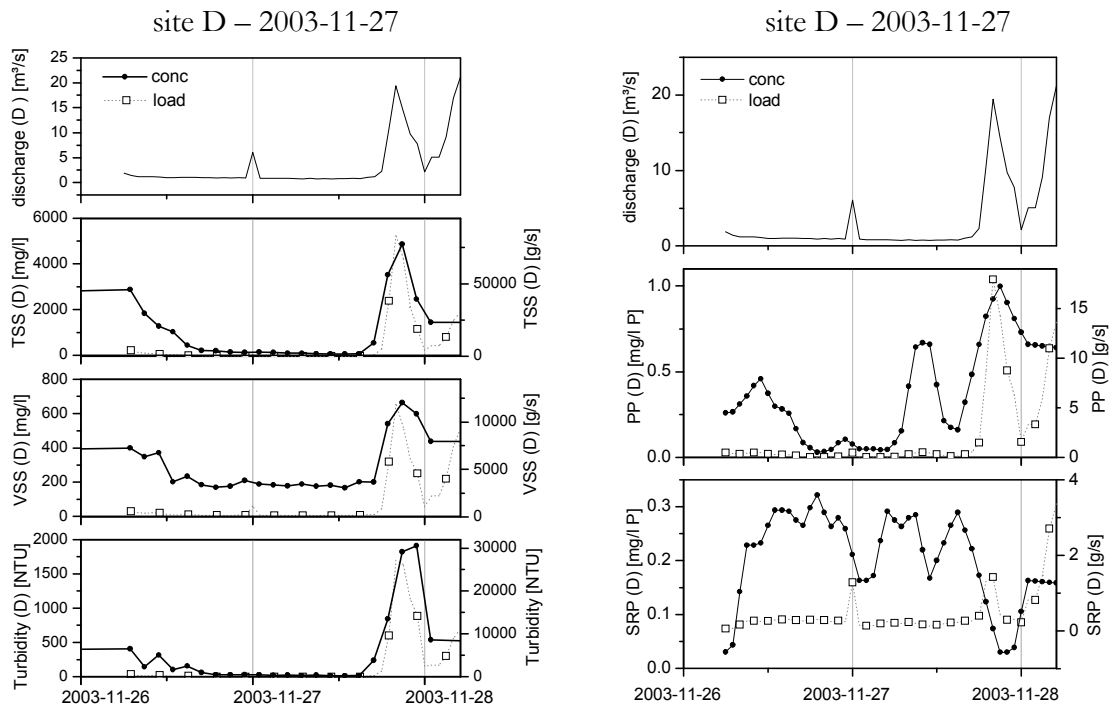


Figure 4-58: Pollutographs at site D of the event 2003-11-27 for particulate and phosphorus properties

The curves of particulate phosphorus and soluble reactive phosphorus show in Figure 4-58 an opposing trend and reflect the differences between particulate properties, which can be stored more easily within the system, and solubles, which are often diluted. The overall level of pollution is low in terms of phosphorus.

#### *Nitrogen, temperature, pH and conductivity*

As usual, the reaction of nitrate is slow, but the concentration shows higher values than for the Vène. Ammonium is only present in a small amount, so nearly all of the total dissolved nitrogen (TDN) is available as nitrate (Figure 4-59).

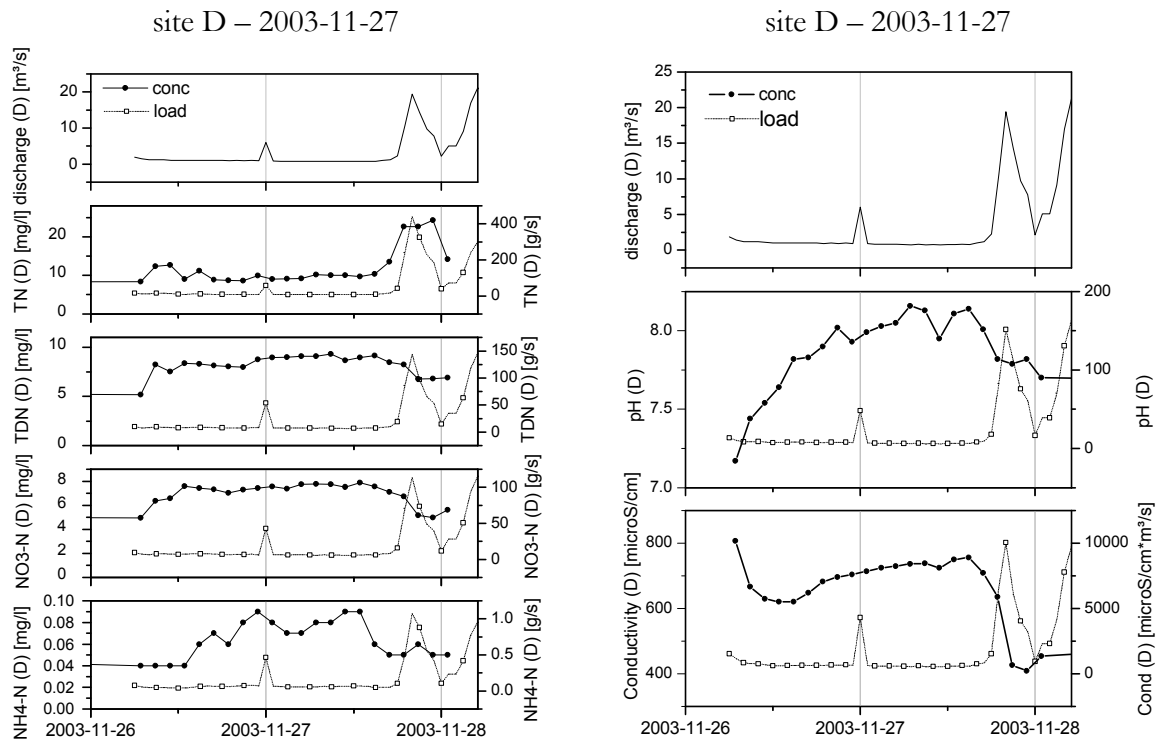


Figure 4-59: Pollutographs at site D of the events 2003-11-27 for Nitrogen, temperature, pH and conductivity

Even if the particulate phosphorus values are low, there must be a significant particulate organic nitrogen fraction to explain the higher values of total nitrogen (TN) during the flood, which is not diluted, but seems to be resuspended from a storage.

#### 4.2.1.6 NCL-plots

In analogy to chapter 4.1.4, NCL-plots of the floods have been constructed for site B to investigate the differences of subsequently following floods on the mode of transport.

#### *NCL-plot of the flood of 2003-10-17 and 2003-10-21*

Above, there was already discussed the difference between this flood and the following. The first flood of October 2003 had much lower concentrations than the following, especially for particulates and total nitrogen.

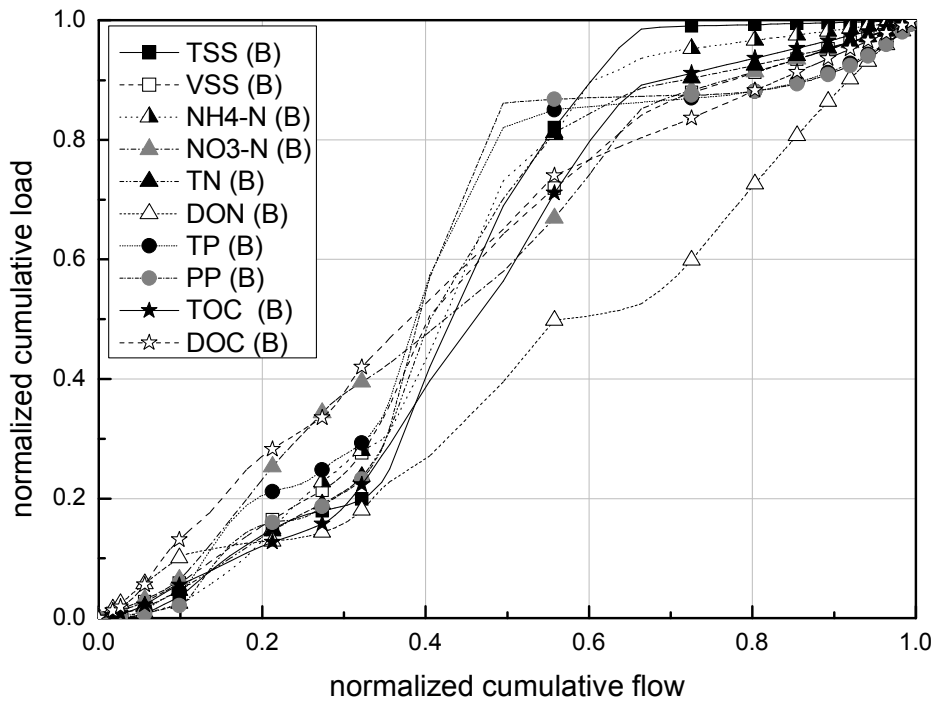


Figure 4-60: NCL plot for the period from 2003-10-17 06:00 to 2003-10-21 14:00 for site B

But not only the level of concentration, but also the mode of transport is very different. Figure 4-60 shows clearly, that there is no first flush. On the contrary, all properties, even the particulates as VSS are transported with a very slow reaction to flow. This situation changes greatly later.

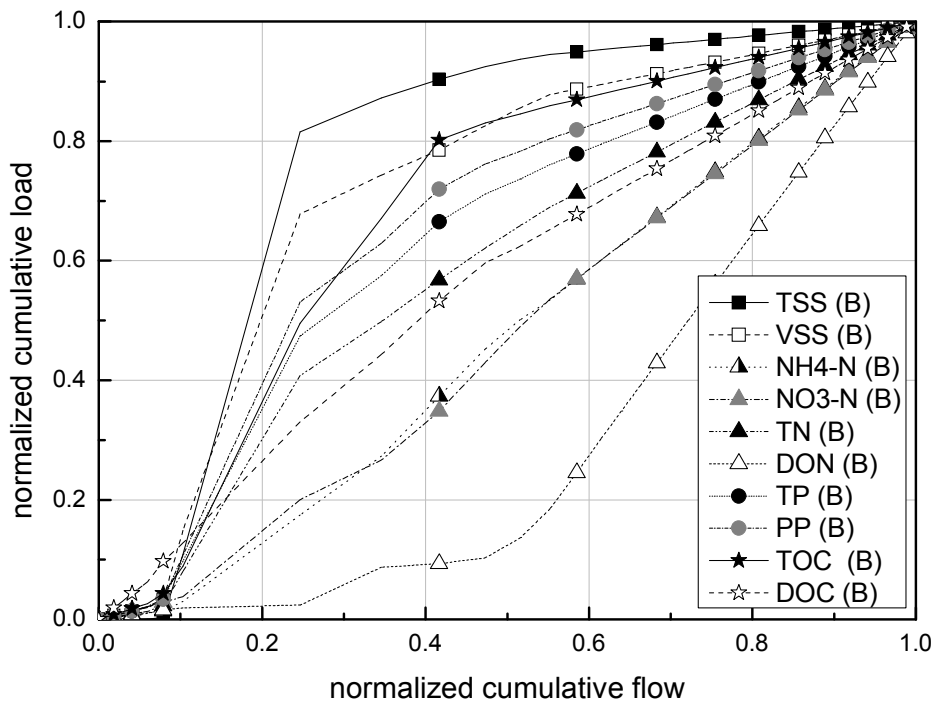


Figure 4-61: NCL plot for the period from 2003-10-21 14:00 to 2003-10-24 00:00 for site B, recession limb approximated

The flow event of 2003-10-21 (in Figure 4-61, note that the flow values of the recession limb is an approximation) is characterised by the typical flush of particulates like TSS and VSS which show a  $FF_{25}$  of 0.82 and 0.68 respectively. Only nitrogen, especially the dissolved organic fraction, needs a long time to develop and react to the changing stream conditions. Unlike in the Vène, carbon has been directly measured here and it shows, that the differences between the particulate and soluble species are situated somewhere between phosphorus and nitrogen.

#### *NCL-plot of the flood of 2003-11-20*

Later in the year in November, constituents are transported proportionally to stream flow (Figure 4-62) or even less (Figure 4-63).

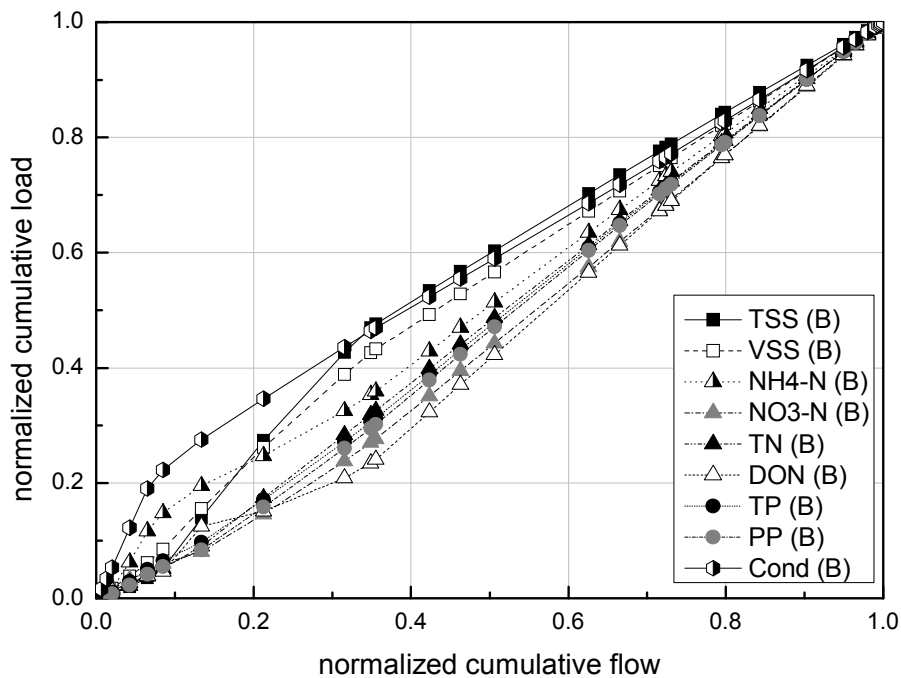


Figure 4-62: NCL plot for the period from 2003-11-20 19:00 to 2003-11-22 02:00 for site B

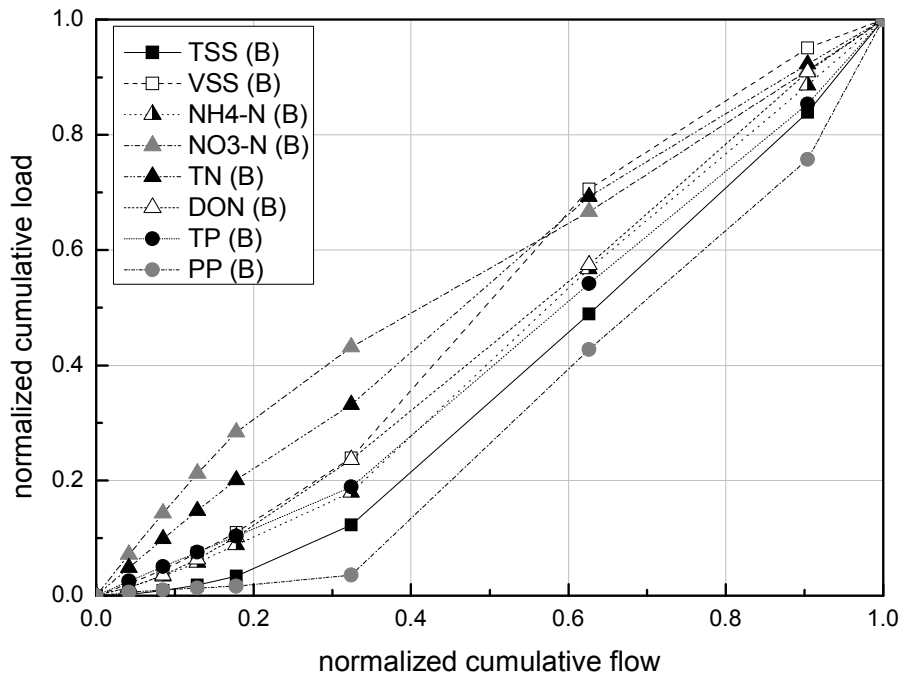


Figure 4-63: NCL plot for the period from 2003-11-27 13:00 to 2003-11-27 21:00 for site B

The latest recorded flood of the period in Figure 4-64 shows that there is even a reversed trend in the “flushyness” of the constituents.

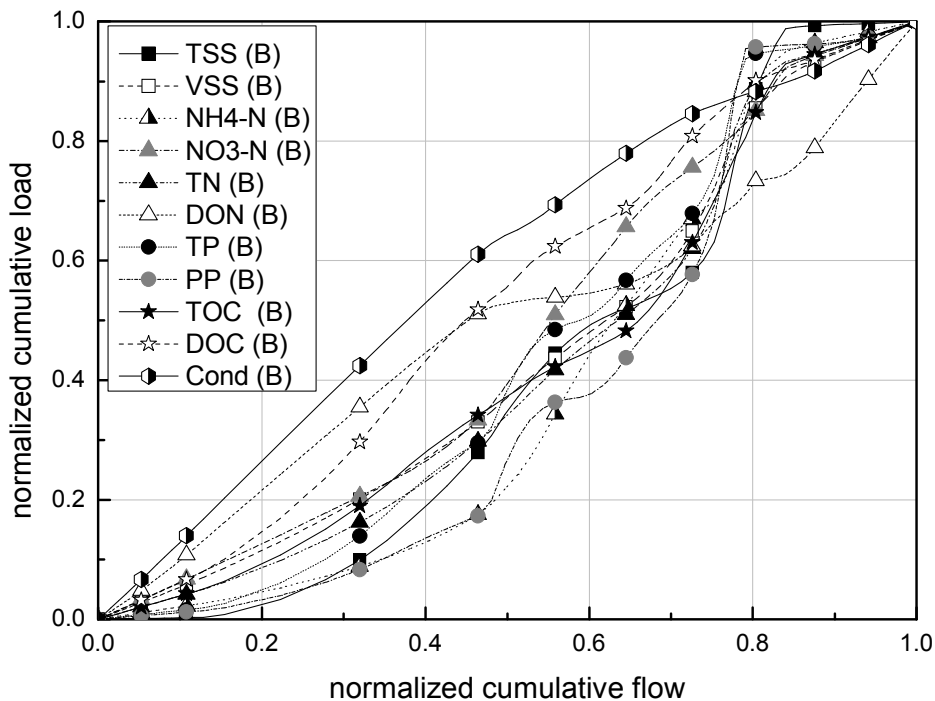


Figure 4-64: NCL plot for the period from 2003-12-03 10:00 to 2003-12-06 04:00 for site B

Properties showing a strong flush at the beginning of the flow period like TSS, VSS or PP need much more time developing than properties which are normally subject to dilution as conductivity or DON. This means that the fact, which normally leads to an increased transport in the onset of the flood, also causes the particulate properties to give a delay in reaction later.

Particulate properties can be accumulated more easily in the river bed, at the riparian zone or in small tributaries near the main channel. As soon as this storage is exhausted during a storm event, additional particles can be perhaps picked up from the overland passage. The circumstance that the detachment and transport needs more time in this phase explains the delay of the reaction.

#### 4.2.1.7 Conclusions

The comparison of subsequent floods of one hydrological year showed that for the Mulargia, it is not necessarily the first flood, which carries the first flush. Table 4-8 summarises the  $FF_{25}$  values for the above discussed events.

Table 4-8:  $FF_{25}$  for the all events at station B

$FF_{25}$	2003-10-17	2003-10-22	2003-11-20	2003-11-27	2003-12-03
TSS	0.17	0.82	0.33	0.08	0.05
VSS	0.19	0.68	0.31	0.17	0.15
TN	0.17	0.41	0.21	0.27	0.12
TP	0.22	0.47	0.21	0.15	0.08
TOC	0.14	0.50	-	-	0.13

The trend for all shown properties seems clear: the first event has no first flush. The system seems to need some wetting first, to produce significant flushing, which then occurs at the directly following second flood. Later, the values are declining continuously.

#### 4.2.2 *El Albuñón River, Murcia, Spain*

##### 4.2.2.1 River characteristics

As last example, the Albuñón River in Spain will be shown, which is very important for the downstream Mar Menor. The Mar Menor is a hypersaline (42 to 47 ‰) coastal lagoon located in the southeast of Spain. It is one of the largest coastal lagoons in the Mediterranean as well as in Europe, and is also one of the most important wetlands in Spain.

The lagoon supports commercial fisheries and along with the surrounding wetlands, it is also an important location for nesting, roosting and wintering of migratory birds (Froeblich et al., 2006).

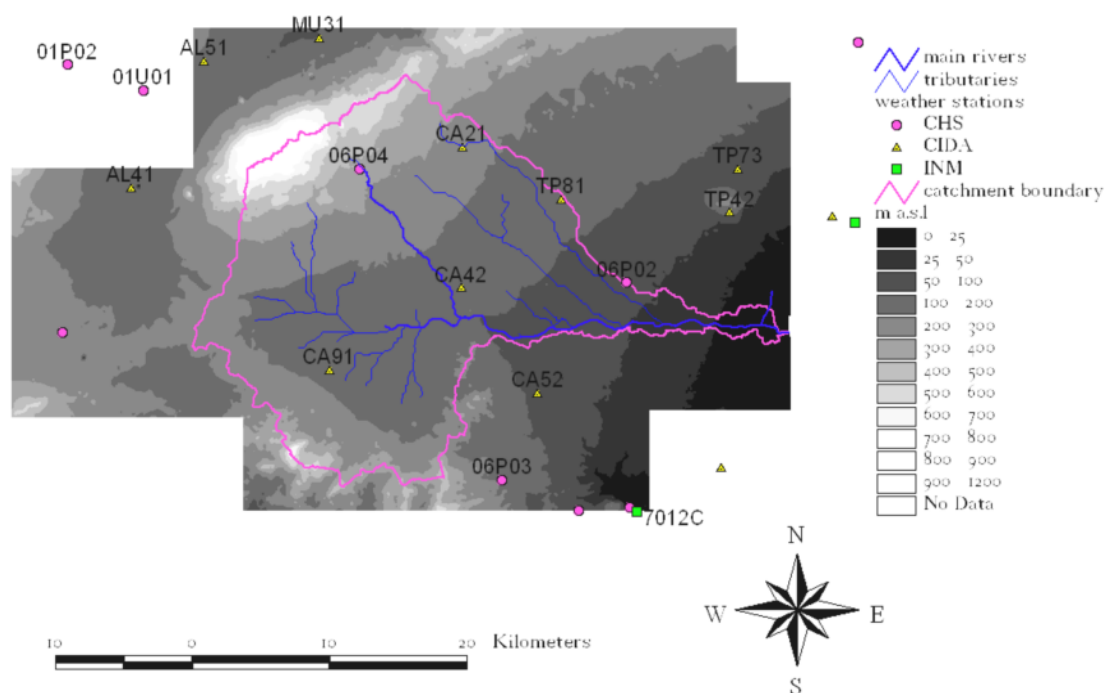


Figure 4-65: Digital elevation and weather stations at the Albuñón

The Rambla del Albuñón runs from west to east as shown in Figure 4-65, flowing into the Mar Menor and draining an area of 556 km<sup>2</sup>, so the catchment is one magnitude larger than the former two examples.

#### ***General climatic situation and rainfall-runoff situation***

With an aridity index (UNEP, 1997) of about 0.19, the Albuñón catchment can be declared as arid. Although it has no distinct periodic annual rainfall variation, most of the precipitation is concentrated in intense storm events in autumn and spring, with generally dry preceding conditions. Precipitation events and their effective runoff are very irregular in time and space.

The Albuñón is an ephemeral stream throughout its course, and contain water during and immediately after a storm event and is dry for the rest of the year (see Neitsch et al., 2002).

Except the last 5 to 8 km, it only flows after a rainstorm, where flow is seasonally sustained by groundwater exfiltration, fed by leached irrigation waters. Intensive rainfall events during dry periods produce around 0.5% runoff with lag times of around 5 h at the outlet. There is also runoff from urban areas and localised Hortonian runoff from agricultural areas (Froeblich et al., 2006).

#### ***Soil and land-use situation***

Although the region is mainly agricultural, it is also an important area for tourism.

For the Rambla del Albuñón investigations of total loads flowing to the Mar Menor showed that under continuous flow conditions 55% of nitrate (and 49.5% of 249 t/year of dissolved inorganic nitrogen) originates from agricultural sources.



### ***Identified point sources and sampling points***

In contrast, 70% of the total phosphorus (51 t/year), 74.6% of soluble reactive phosphorus and 91% of total organic carbon comes from urban point sources (García-Pintado et al., 2006).

Sampling points and continuous flow measurements have been sited in the last 4 km of the river, where the channel slope averages 8.9 m/km.

#### 4.2.2.2 Relevancy of the dataset

In the available data, no annual reoccurrence in the rainfall could be identified, although it is obvious, that there must be a relation on a long term perspective.

During the three years of studies, only 3 substantial discharge events were recorded, which will be shown below.

#### 4.2.2.3 Examples of a first flush – magnitude of days to hours

During the study period, the following floods have been recorded:

- i) 2003-10-17 00:00 until 2003-10-17 11:28,
- ii) 2003-11-19 01:10 until 2003-11-19 19:10 and
- iii) 2004-04-15 20:00 until 2004-04-16 11:20.

They are comparable in their magnitude ranging from a total flow volume of about 58 to 130 Mm<sup>3</sup>. For details see Table 4-9.

Table 4-9: Summary of the floods for El Albujón

	flow [m <sup>3</sup> ]	TSS [t]	NO <sub>3</sub> -N [kg]	NH <sub>4</sub> -N [kg]	TP [kg]	TOC [kg]
2003-10-17	130 347	739	590	23.5	575	786
2003-11-19	57 707	81.2	426	17.3	220	504
2004-04-15	79 920	33.8	987	50.1	131	293

### ***The flood of 2003-10-17***

Figure 4-66 shows the measured constituents at the outlet of the catchment, where the Albujón is flowing into the lagoon.

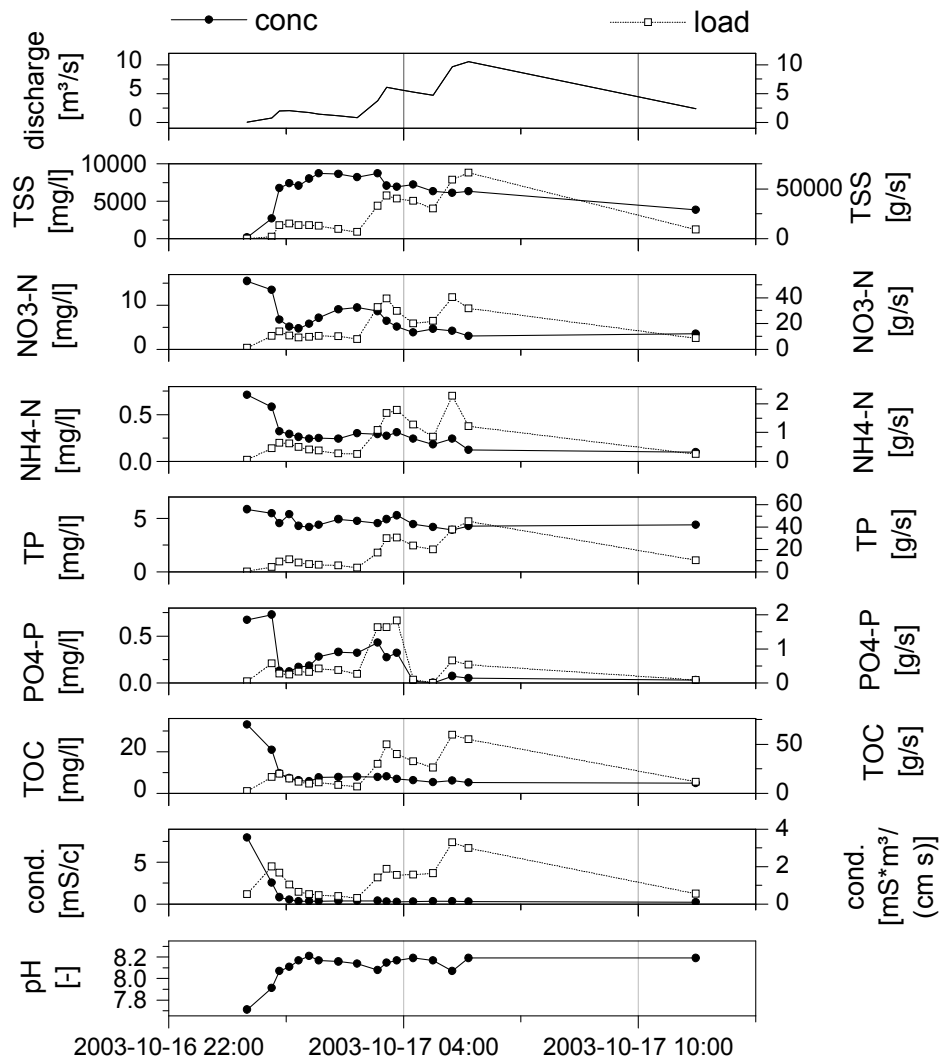


Figure 4-66: Pollutographs of the flood of 2003-10-17

The level for total phosphorus is relatively high for this flood and it is not significantly diluted like e.g. TOC or ammonium. Nitrate-nitrogen is high at the beginning of the event ( $\sim 15.5$  mg/l) but is also quickly diluted. The concentration of TSS reaches its maximum before the climax of the flood, which could be a sign, that the catchment has a minor influence in comparison to the instream resuspension.

However, the NCL-plot in Figure 4-67 shows, that only  $\text{PO}_4\text{-P}$  is characterised by a distinct first flush, the other parameters are only transported insignificantly higher in the beginning of the flow.

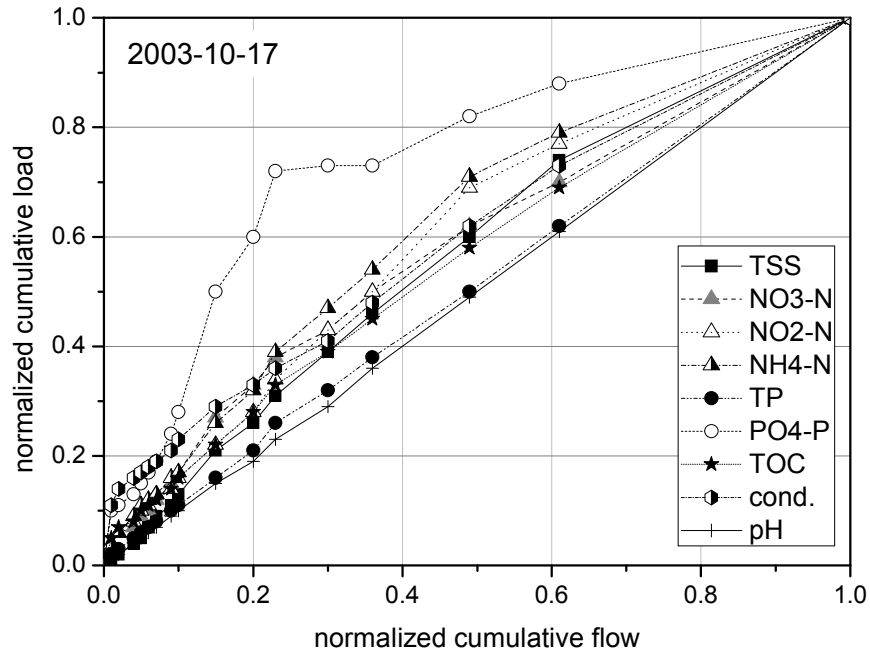


Figure 4-67: NCL-plot of the flood of 2003-10-17

This fact is owed to a certain degree also to the available water quality measurements, which are not so detailed during the period with the most discharge.

During the last 5 hours of the flood, the concentration of  $\text{PO}_4\text{-P}$  is much lower, than for the other constituents.

### *The flood of 2003-11-19*

With a maximum TSS concentration of about 2600 mg/l, this flood has a lower impact on the erosion due to the lower peak flow of only 2.65 m<sup>3</sup>/s (10.5 in the event before). Unusually, TSS has its minimum at the flow peak.

Interestingly, this smaller flood has also a negligible influence on nitrate-nitrogen or TOC, but produces a significant peak of TP of over 12 mg/l this time (see Figure 4-68).

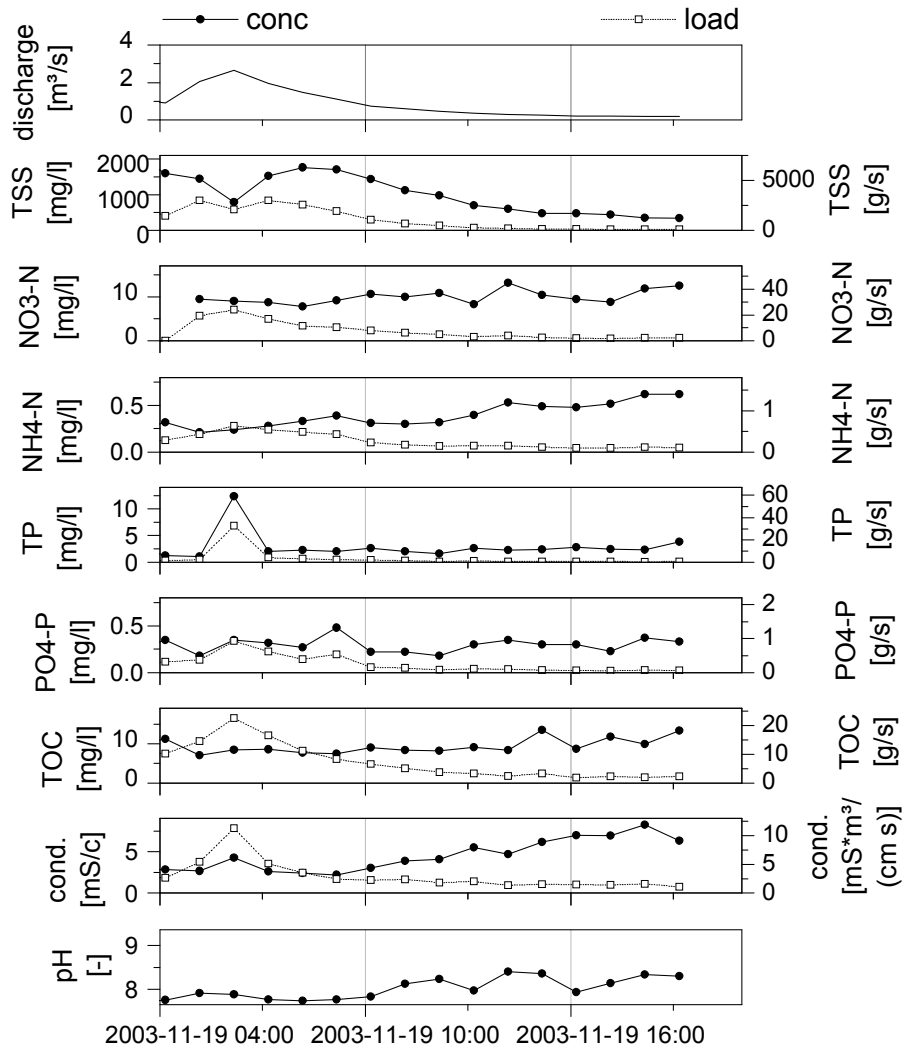


Figure 4-68: Pollutographs of the flood of 2003-11-19

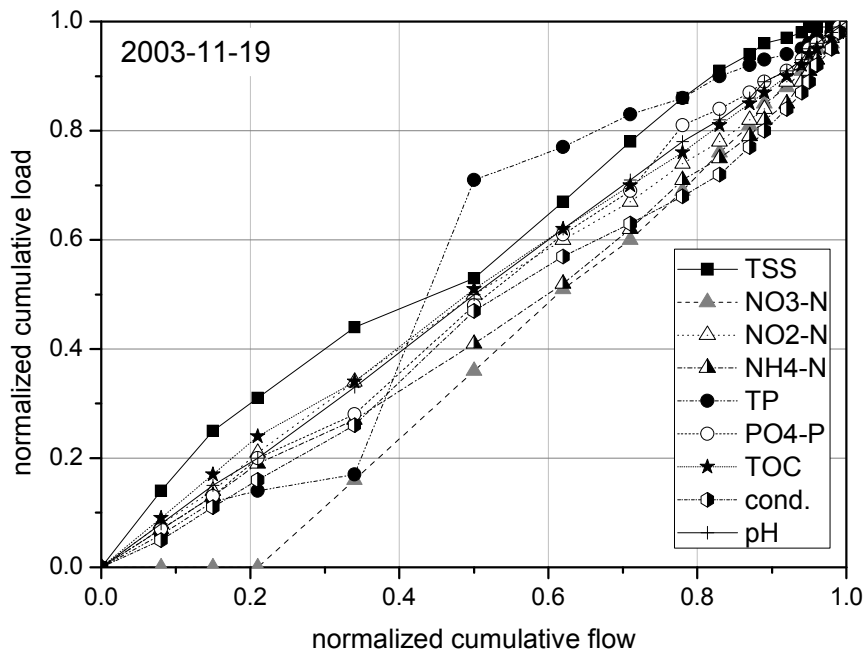


Figure 4-69: NCL-plot of the flood of 2003-11-19

Again, there is no flush visible (Figure 4-69). Only the  $FF_{25}$  of TSS lies with 0.35 slightly higher.

### *The flood of 2004-04-15*

The last measured flood event does not show any flush-like behaviour. In contrary, there is a strong dilution during the flow event (Figure 4-70).

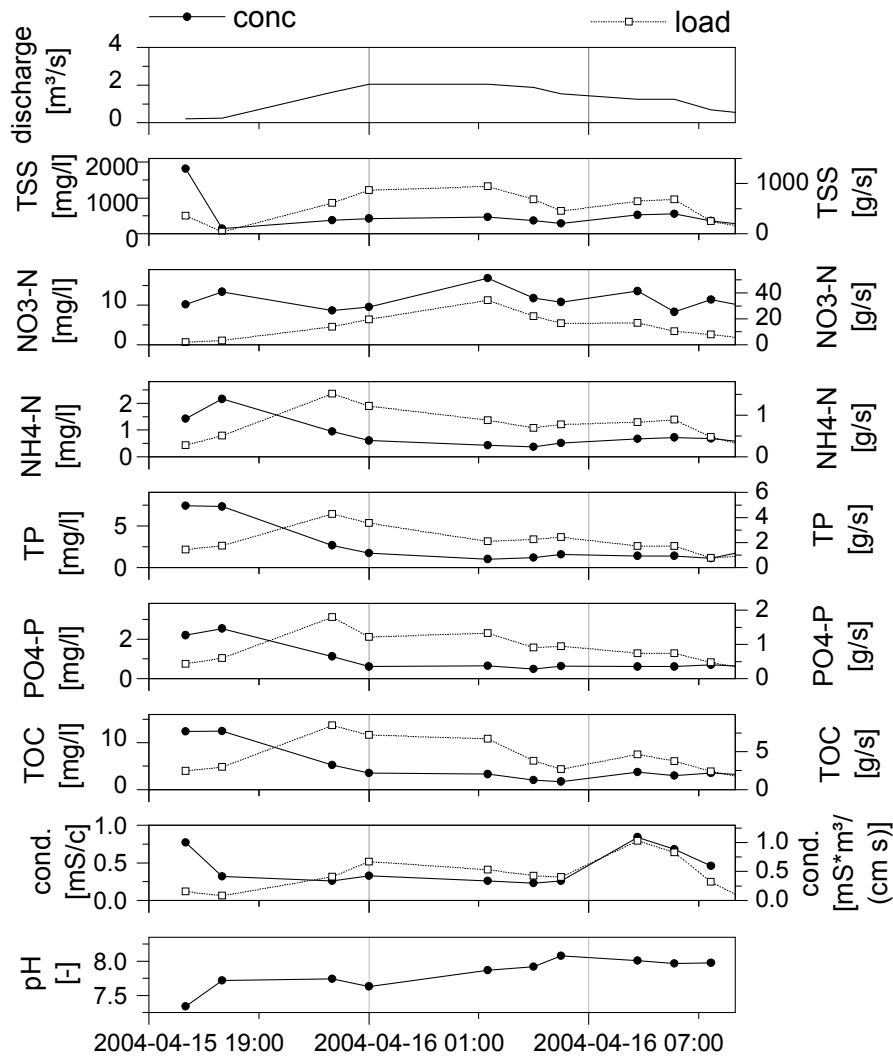


Figure 4-70: Pollutographs of the event at 2004-04-15

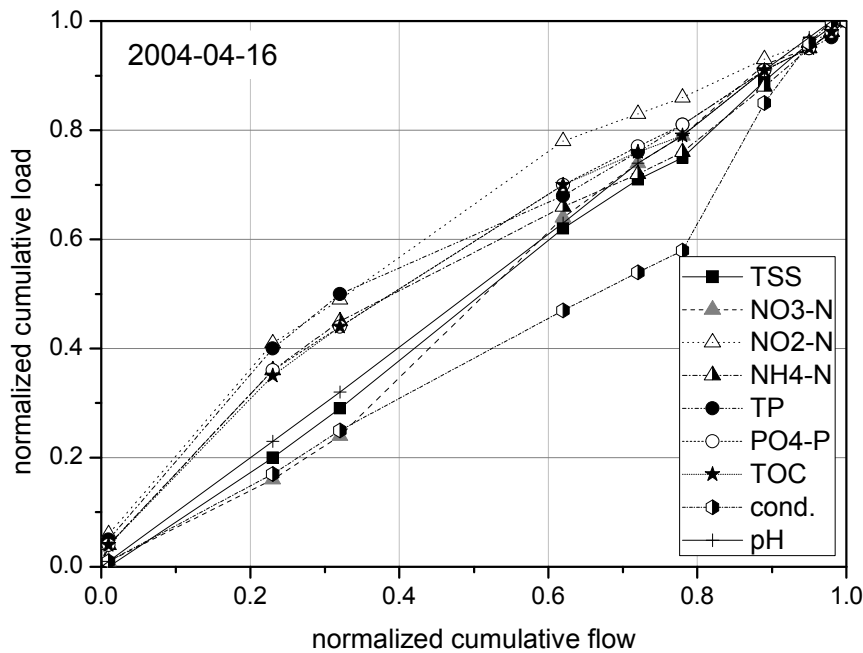


Figure 4-71: NCL-plot of the flood of 2004-04-16

#### 4.2.2.4 Conclusions

The catchment of El Albuji3n is very large and strongly influenced by human activity. Flow and rain events are very rare and only 3 were available, so a general behaviour could not be derived. Nevertheless, the export of nutrients to the lagoon seems to be quite high.

A general annual trend of the nutrient loadings can only be guessed on the basis of this data, but it seems as if the transported amount of nutrients is more correlated to the time of the year, than to the strength of the flood. From October 2003 to April 2004, the total loads of TSS, TOC and TP constantly decreased, although the total flood volume of the second flood resides between the two flanking floods (Table 4-9). Only nitrogen ( $\text{NO}_3\text{-N}$  and  $\text{NH}_4\text{-N}$ ) shows the opposite trend and is increasing over the period.

### 4.3 General conclusions of the data analysis

It could be shown for the V3ne, that there exists an important cycle of nutrient transport activity which is related to the seasons. During late summer and early autumn, mass transports are increased for all constituents except for nitrogen. Flushing effects are most intense directly downstream accumulation spots and show a trend to diminish in downstream direction. In general, the intensity follows  $\text{TSS} > \text{TP} > \text{TN}$ .

Especially for sediment or sediment-linked nutrients, most of the annual load is transported by the first significant events after the dry period. About 2/3 of the annual TSS and VSS can be transported in September.

But not only the absolute loads are increased. In comparison to the water flux, the load of particulates is enormously increased. For each percent of annual flow, 18% of the annual VSS

load was transported in September 2003. That means, that the transport of VSS was 18 times more intensive than the water flow on an annual perspective.

Further, during the first flush flood of this month, 72% of the VSS load is transported by the first 25% of the flow.

There is a stronger correlation between the loads of soluble constituents (e.g.  $\text{NO}_3\text{-N}$  or SRP) and the flow than between the particulates (TSS and VSS) and the flow. This means, that the latter are heavily influenced by accumulation and resuspension processes.

The analysis of two other catchments revealed some additional characteristics.

In the catchment of the Mulargia river is comparable to the Vène in terms of surface area and aridity. Detailed data from following floods of one flow period was available. It was shown that not the first flood carried a flush effect, but the directly following one. After this second flood, the  $\text{FF}_{25}$  values decrease continuously for every following event.

The driest and biggest of the three basins finally showed no significant flush event, although this could be owed to the fact, that data is very scarce in this catchment.

In order to get deeper insights into temporary rivers and to investigate the sensitivity of these systems to changes, one catchment was chosen for the application of the tempQsim –STREAM model in the following.

## 5 Application of the tempQsim – STREAM model to the Vène

The tempQsim – STREAM model was intensively tested and modified in the context of temporary rivers. Due to the good data situation at the Vène, this site was chosen for the application. The model was applied for the period from October 2002 to September 2004. The calibration was found to be very challenging, and some issues are demonstrated in chapter 7.3. The simulations were analysed in two differing scales: on a continuous annual scale as well as at the event scale. The methods of investigation are pollutographs, relative and absolute monthly loadings and normalized cumulative loads, which were explained above.

Some approaches for further enhancements of the simulation are shown in the chapter 7.11.

### 5.1 Spatial discretisation

The Vène catchment has already been discussed in detail in chapter 4.1. In the modelling, only the main branch of the river between points K (karstic spring Cournonsec) and V are considered.

Based on the spatial discretisation of the DEM (Digital Elevation Model) consisting of a regular orthogonal grid with a side length of 50 m, a river network was delineated. The network has 360 reaches with element lengths from 50 to  $50\sqrt{2}$  m and trapezoidal cross sections of 3 to 6 m width.

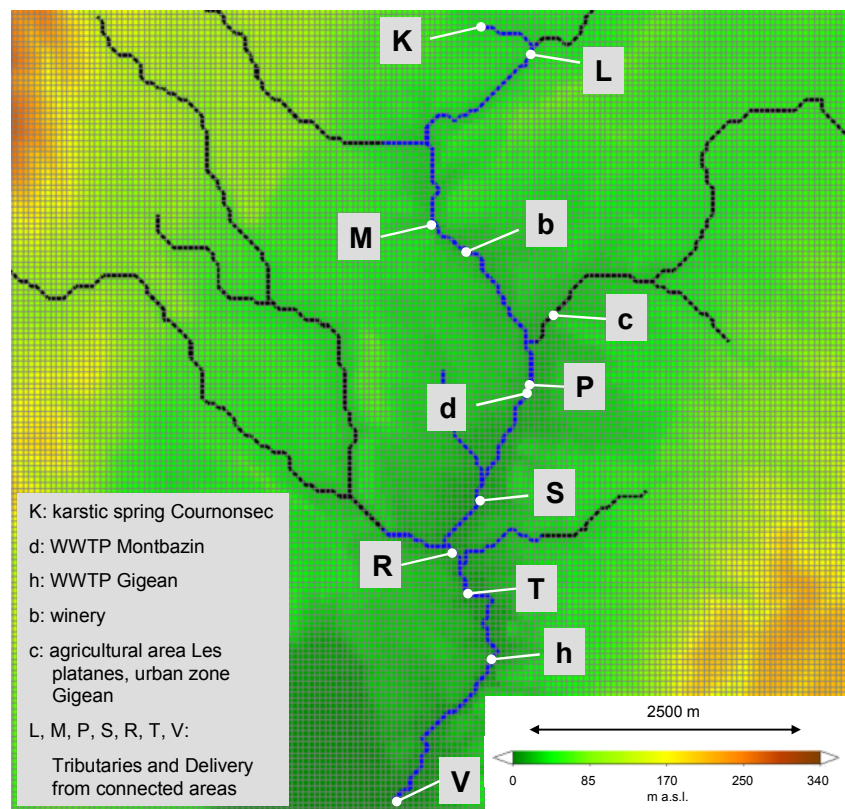


Figure 5-1: Spatial discretisation and DEM of the Vène in MOHID-GIS, grid width 50m



The model of the river has 5 main point source inflows: the karstic spring Cournonsec (K) at the top of the river, a winery (b), an agricultural area and the connection to the urban area of the village Gigean (c) as well as the two wastewater treatment plants for Gigean and Montbazin (d and h). The rainfall-runoff part of the model was calculated with the French model MERCEDES and a simple storage cascade and is handed over to the simulation via defined inflow points at L, M, P, S, R, T and V.

For the inputs of the WWTPs and the karstic spring at K, the water quality parameters are variable over time, if available by continuous measurements, if not (as e.g. for the overland flow), they were chosen constant.

## 5.2 Calibration of the system

The system was calibrated on the basis of the hydrological year 2002/2003 and later validated on the year 2003/2004. The calibration followed the methodology shown in Figure 5-2. A detailed calibration was done for the instream part, the delivery of the rainfall-runoff model was taken as a boundary condition and concentrations were chosen or modified when necessary. First, the concentration was checked, in a second step the load. This was necessary because low fluxes of constituents with a long duration can have an influence on a long-term analysis which is comparable to medium scale events.

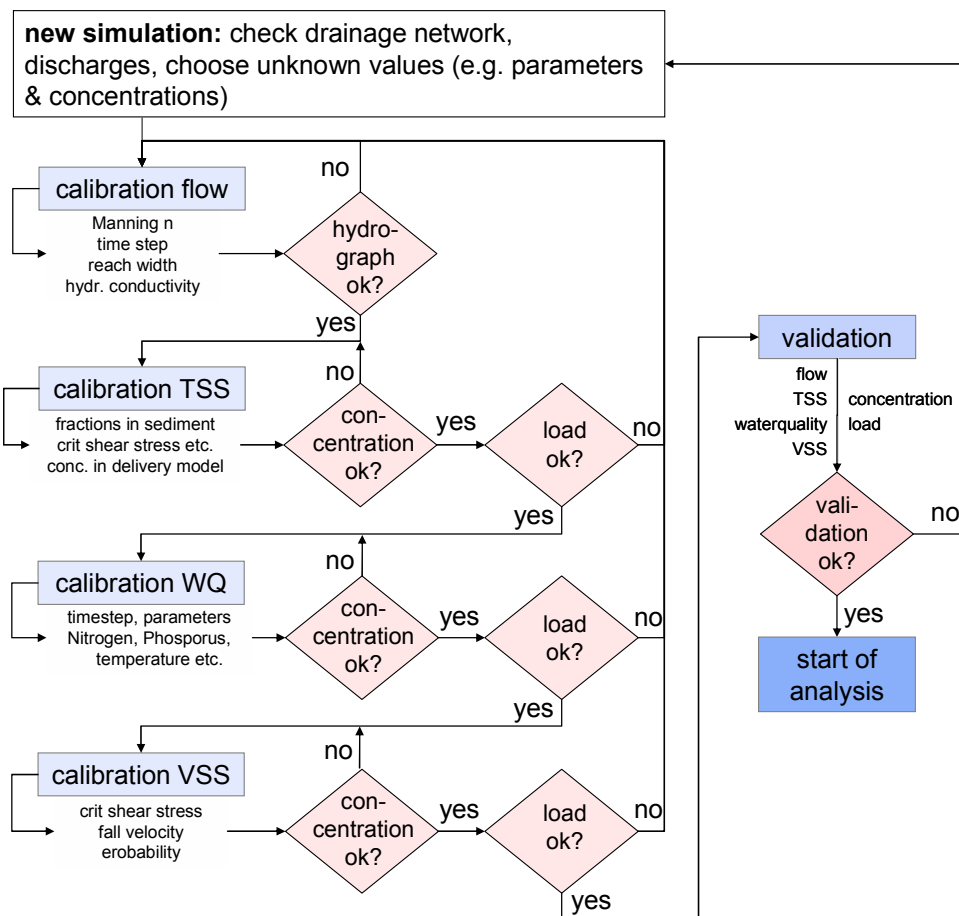


Figure 5-2: Methodology for calibration and validation of the model

The calibration of VSS was done as the last step, because it depends on the concentrations of the soluble as well as particulate nutrients.

A special focus was given to the first flush events on 2003-09-22 and 2004-09-13. These important events cause a major part of the pollutant export to the lagoon, but especially the one of 2003-09-22 is different than the other (smaller) floods measured in this year. Furthermore, the first floods of the years 2002/2003 and 2003/2004 have very different origins (one is dominated by the influence of the karst at K the other depends mainly on overland runoff, see chapter 4.1), which complicates the validation.

More details and some examples for the calibration and the sensitivity of the model can be found in chapter 7.3.

### 5.3 Scenarios for the modelling

The aims of the following modelling exercise are the definition of critical processes as well as their sensitivity. This was done in order to derive background information on dominant pollution pathways and starting points for future management options. The focus herein was on the process of organic accumulation and resuspension expressed by volatile suspended solids (VSS).

The following 11 scenarios have been constructed as shown in Table 5-1. In each of these cases, at least one main process is turned off or altered in order to get deeper insights into the influence of this process on the overall result.

Table 5-1: Scenarios applied to the Vène

no.	scenario	setting
1	all	the parameterisation uses all processes explained in chapter 3.8
2	no transmission losses	the main instream transmission loss, the infiltration, is turned off, i.e. there is no infiltration in the bed
3	no bacteria	inflow and growth of bacteria is turned off in the water phase as well as in the benthos
4	no benthos	the calculation in the benthos module is turned off, no processes occur at the river bed, but settling and resuspension are still possible
5	no fraction	instead of three sediment fractions, only one is calculated with a comparable parameter set and similar concentration in the inflows
6	double WWTP	concentrations of organic properties are doubled in the two WWTP effluents
7	no WWTP	concentrations of all properties of the WWTP effluent are set to zero (except temperature)
8	no delivery	concentrations of all properties of the delivery model are set to zero (except temperature), but the water inflow remains
9	no karst	concentrations of all properties of the karstic spring at K (Cournonsec) are set to zero (except temperature), but the water inflow remains as in 8)
10	no processes	all parameters are considered to be conservative, so they are only subject to advection, diffusion and settling or resuspension, but not to reactions in module waterquality
11	variable delivery WQ	an approach was used to increase the runoff concentration with increasing dry days, i.e. the longer the dry period, the higher the concentrations; if a rainfall event occurred, concentrations were reduced up to a defined base level

This analysis may give indications for the importance of this process in terms of the management of the watershed. Future measurement campaigns will also benefit from this kind of analysis as it shows the main drivers of the system, so that processes with the highest impact may be measured in detail.

Every scenario was executed on the same spatial discretisation for four periods: the hydrological years 2002/2003 and 2003/2004 (starting at October, see chapter 4.1.3) and two notable first flush events at 2003-09-22 and 2004-09-13 including the prior accumulation period of 5 and 3 months respectively.

The scenario 1 (“all”) was calibrated using September 2003 data. The results of the chosen parameterisation were later compared with the measurements of the whole period, with special emphasis on September 2004.

The boundary conditions and parameter sets of the other scenarios are all based on scenario 1.

## **5.4 Annual simulation and results**

The simulations were carried out for the two hydrological years 2002/2003 and 2003/2004. Specially focused investigations were done for the period of the accumulation period and the following flushing in September of each year.

### *5.4.1 Pollutographs for 2002-2004*

Figure 5-3 shows results for flow, particulates (TSS and VSS) and inorganic dissolved nitrogen (NH<sub>4</sub>-N and NO<sub>3</sub>-N) of the simulation with the scenario “all” which includes all processes. The approximated values for measured flow are shown in light grey.

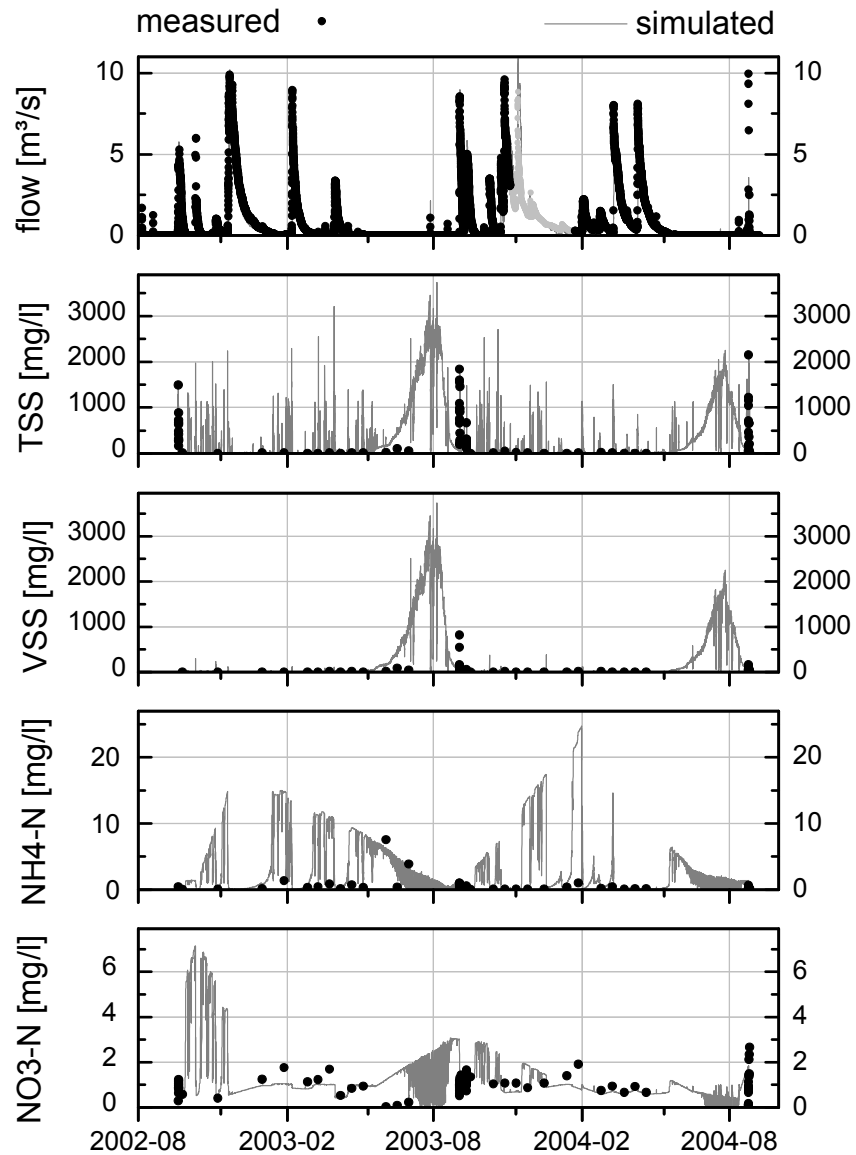


Figure 5-3: Measured and simulated concentrations (scenario 1, “all”) at site S for the years 2002-2004 for particulates and dissolved inorganic nitrogen

Because the measured results for particulate phosphorus (PP) and organic nitrogen (orgN, both shown in Figure 5-4) were not calculated in the model, they are compared with simulated particulate *organic* phosphorus (POP) and *particulate* organic nitrogen (PON). As most of the organic phosphorus and nitrogen amount is available in particulate form, the comparison seems reasonable.

From this temporal scale the performance is hard to judge. A regression analysis of the measured flow data and the simulated flow data (variant “all”) for the two investigated years 2002/2003 and 2003/2004 shows a Pearson's correlation coefficient of 0.97 or 0.84 and a Nash-Sutcliffe efficiency (Nash and Sutcliffe, 1970) of 0.90 or 0.65 respectively (see Table 5-8).

The values in the dry phase are very sensible, as it can be seen e.g. for ammonium or soluble reactive phosphorus (Figure 5-4).

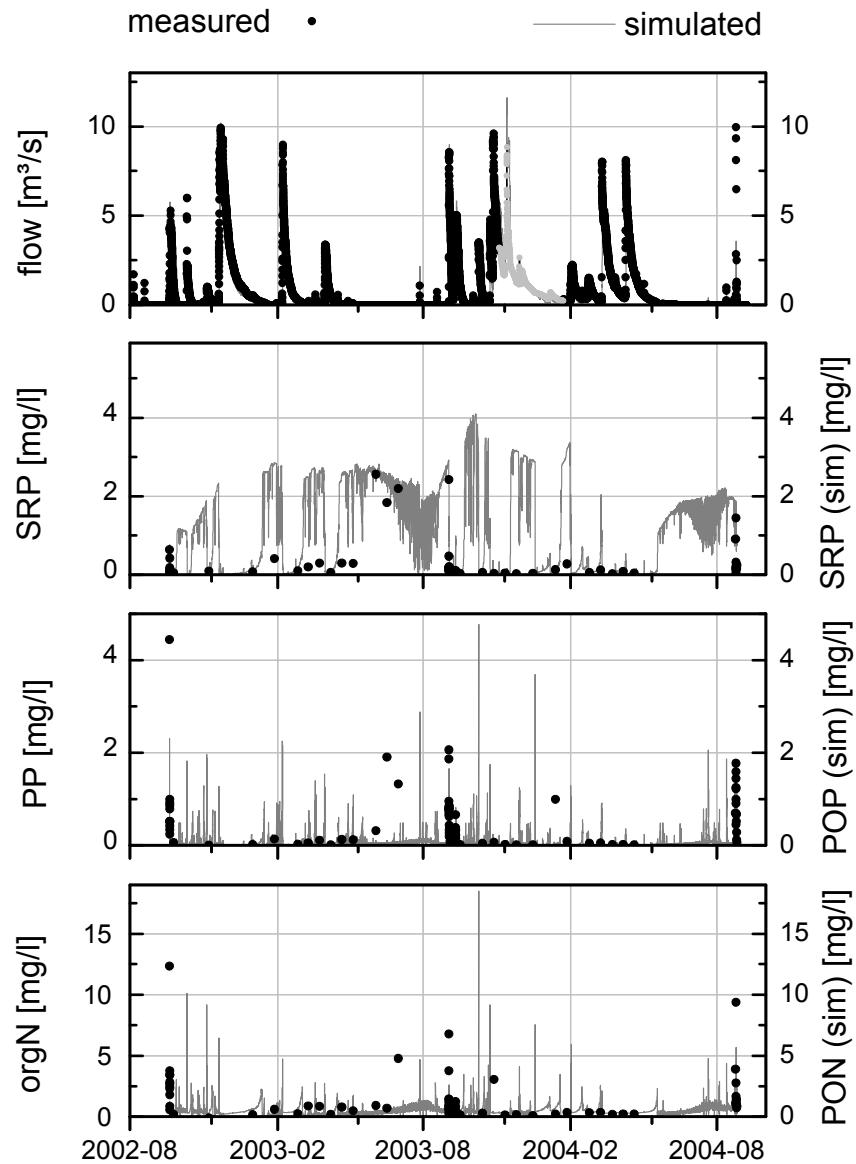


Figure 5-4: Measured and simulated concentrations (scenario 1, “all”) at site S for the year 2002-2004 for inorganic phosphorus, particulate (organic) phosphorus and (particulate) organic nitrogen

These soluble parameters show the typical behaviour when they are measured in a pool of the river. The trend of the concentration follows the superimposition of the boundary conditions. These are given by the point source inputs, the conversion processes (e.g. nitrification or remineralisation) as well as the climatic situation. This trend is interrupted from time to time by small disturbances caused by the inflow of less contaminated water imported by a rainfall event (the disturbances are not so pronounced for nitrate, because water from the overland flow caused by precipitation has a concentration of about 1 mg/l). If these fluctuations are very frequent, in most cases, regression analyses such as correlation coefficients or a Nash-Sutcliffe analysis will fail for water quality parameters in temporary rivers (see chapter 7.6 for details).

The fluctuations at the end of the accumulation period in  $\text{NH}_4\text{-N}$ ,  $\text{NO}_3\text{-N}$  or SRP are not caused by instabilities of the model, but through the growing influence of the rising organism concentration manifested in the VSS concentration, whose turnover rates strongly depend on the

daily cycle of light availability and temperature. This accumulation of the biomass is of great importance for the system and poses great demands on the involved water quality algorithms.

#### 5.4.2 *Accumulation of organic matter in the river bed and importance of events during the dry phase*

Recent investigations concluded an estimated accumulation of about 29 kg/m<sup>2</sup> of organic matter in summer at point d downstream the Montbazin WWTP (Kretschmer et al., 2006). Figure 5-5 shows that the simulated results hardly reach 10 kg/m<sup>2</sup> at this point (a value of about 30 kg/m<sup>2</sup> is reached more upstream in the catchment at point b).

It is difficult to extrapolate the punctual measurements to the whole river reach and to estimate the exact amount of settled VSS at the moment before the flood. Observations showed that the thickness of organic layers varies significantly depending on the local flow depth and bottom sediment composition (protection of finer sediment by coarser material), the location in the river cross section (riparian zone or in-stream) and the flow velocity.

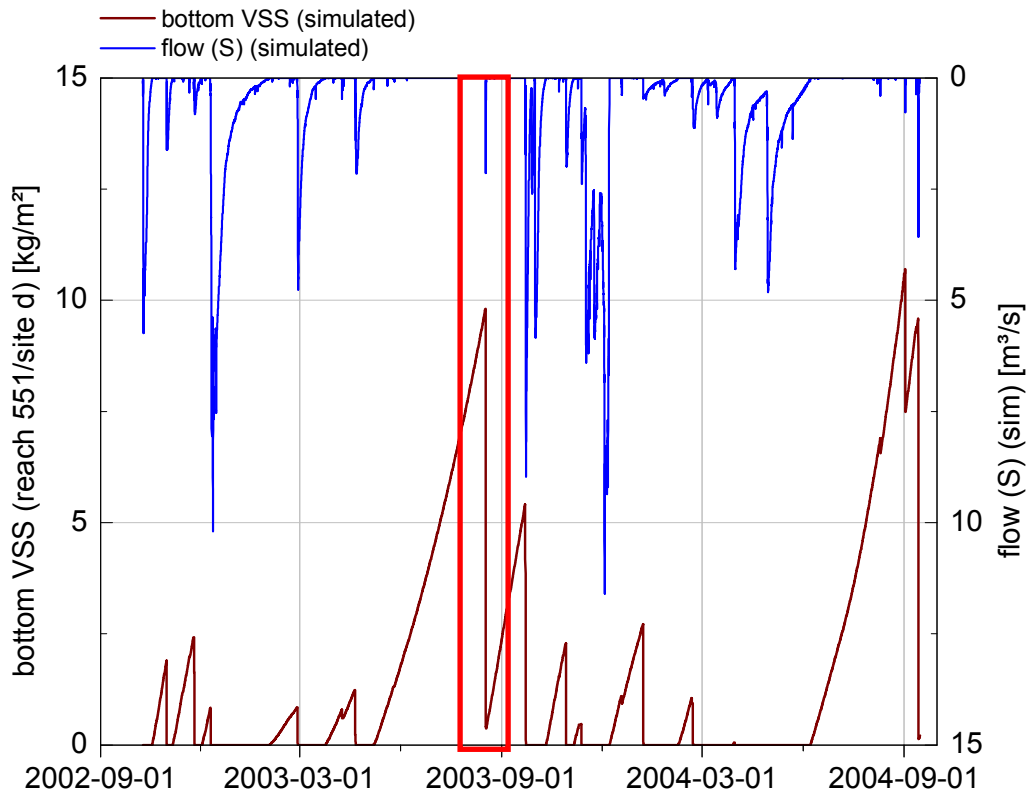


Figure 5-5: Accumulation of VSS downstream the outlet of a WWTP at site d

Furthermore, a closer investigation of the simulation in terms of the accumulated matter also reveals the importance of events during the dry period. The event of 2003-08-17 is comparably small with maximum flow of about 2 m<sup>3</sup>/s and an estimated volume of 36 000m<sup>3</sup> (highlighted in Figure 5-5), but it enters the system in a state of high pollution potential and transports, compared to its magnitude, a highly contaminated discharge. About 95% of the stored VSS is resuspended in the event.

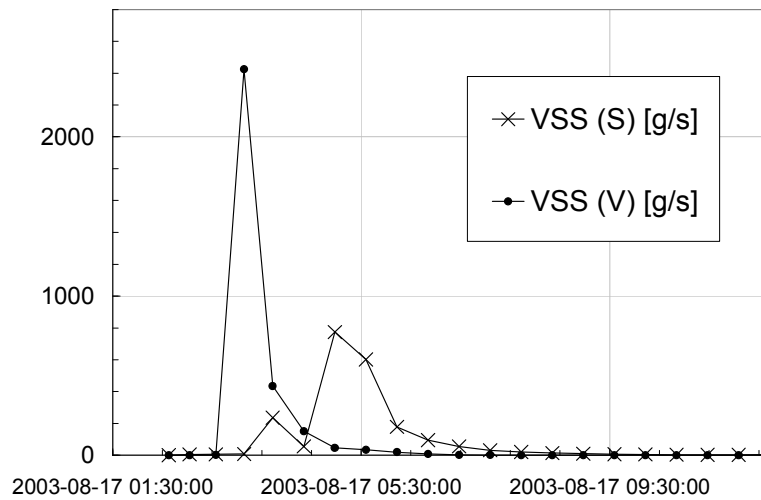


Figure 5-6: Loadings during the event of 2003-08-17 for VSS in sites S and V

The load also reaches the outlet and is not only a displacement within the riverbed from one point to another (see Figure 5-6), so that about 7.8 t of VSS are released from the accumulation site at S, which is nearly 10% of the annual load.

If a highly loaded flow like this reaches the Thau Lagoon, it will contribute to a further degradation of the already tensed situation at the end of summer and may finally be the last straw which leads into a dystrophic event (Malaïgue).

#### 5.4.3 Monthly VSS loads for 2002/2003

Pollutographs of the concentration as shown above are a good measure to judge the performance and to get an overview of the behaviour of the system. The concentration as such only reveals the state of the measured water body, but contains just limited information of the consequences for downstream water bodies. The impact of the transport of the regarded constituent can only be evaluated by using the fluxes or loadings.

Consequently, in the following, absolute as well as relative loadings for VSS were compared on the basis of months for the years 2002/2003 and 2003/2004 for the scenarios and measurements (For more parameters and additional graphs, see chapter 7.3.3).

As already explained above, the system reaction in terms of particulate transport is very sensitive to even small rain and discharge events during the dry phase (chapter 4.1.5). Thus, an important deviation to the measurements occurs in the simulation for August 2003, since the flow of the event at 2003-08-17 has been recorded by an automatic flow logger, but it was not subject to a measurement campaign, because it was comparably short in duration and started during the night between Saturday and Sunday. By lack of data, the representation of the measurements is not exact of August (cp. Table 5-2).

Table 5-2: Absolute monthly loadings of VSS for the year 2002/2003 at site S

VSS (S) [t/month]	meas.	all	no trans- mission losses	no bacteria	no benthos	no fraction	double WWTP	no WWTP	no delivery	no karst	no process	variable delivery WQ
10-2002	2.7	5.3	5.4	5.2	5.3	5.3	6.5	4.2	4.9	1.7	7.2	5.2
11-2002	1.8	2.5	2.4	2.4	2.4	2.5	3.7	1.3	2.3	1.4	4.8	2.4
12-2002	26.2	20.1	20.0	19.9	20.0	20.1	21.2	19.0	19.1	2.2	23.0	19.7
01-2003	5.2	5.1	5.1	5.1	5.1	5.1	5.9	4.3	5.1	0.9	8.1	5.1
02-2003	3.0	3.0	3.1	3.0	3.0	3.1	3.4	2.7	2.7	0.8	5.2	2.9
03-2003	6.9	6.1	6.3	6.0	6.1	6.1	6.4	5.8	6.1	0.4	9.8	6.1
04-2003	3.8	2.8	2.6	2.7	2.7	2.8	3.5	2.0	2.4	1.2	6.7	2.6
05-2003	0.6	0.4	0.5	0.4	0.4	0.4	0.5	0.2	0.3	0.2	1.4	0.4
06-2003	0.1	0.4	0.1	0.1	0.4	0.4	0.4	0.4	0.4	0.4	0.0	0.4
07-2003	0.1	3.2	0.1	0.2	3.1	3.2	3.2	2.8	3.2	3.2	0.0	3.2
08-2003	0.7	16.0	2.3	3.5	15.7	16.1	18.9	12.1	15.8	15.9	11.0	16.1
09-2003	69.5	14.0	12.6	12.3	13.8	13.9	16.2	11.9	13.7	4.0	13.7	14.3
t/year	121	79	61	61	78	79	90	67	76	32	91	78

Though it cannot be finally resolved, there is some evidence, that the organic matter transport and bacteria inflow in August 2003 had a greater influence on the quality of the lagoon.

#### ***Comparison of scenario “all” with other variants***

The consideration of instream infiltration increases the accumulation potential during June to August, but also leads to slightly higher VSS loads during the wetter period from October to May. During the dry months the reduction of the flowing water volume reduces the transport capacity of the river, causing a higher settling of particulates, so that an event during this phase has a much higher impact. On the other hand, if there is more transport capacity during the wet months, the flow will loose a minor fraction of its VSS to the bottom due to deposition.

Disregarding heterotrophic bacteria causes a significant reduction of VSS in August from 16 to 3.5 t/month, but also in July and September. Not only the absolute values change, but also the dynamics of the annual flux when ignoring bacteria: relative monthly transport of VSS is reduced from 20.2 to only 5.8% in August 2003 (cp. Table 5-3).



Table 5-3: Monthly percentage of VSS loads in terms of the year 2002/2003 at site S

VSS (S) [% of annual]	meas.	all	no trans- mission losses	no bacteria	no benthos	no fraction	double WWTP	no WWTP	no delivery	no karst	no process	variable delivery WQ
10-2002	2.3	6.8	8.9	8.6	6.8	6.7	7.2	6.3	6.5	5.1	7.9	6.6
11-2002	1.5	3.2	3.9	4.0	3.1	3.2	4.1	1.9	3.1	4.5	5.3	3.1
12-2002	21.7	25.4	33.1	32.8	25.6	25.4	23.6	28.4	25.2	6.8	25.3	25.1
01-2003	4.3	6.5	8.5	8.3	6.6	6.5	6.6	6.5	6.7	2.8	8.9	6.5
02-2003	2.5	3.8	5.1	4.9	3.8	3.9	3.8	4.0	3.5	2.4	5.7	3.7
03-2003	5.7	7.7	10.4	9.9	7.8	7.7	7.1	8.7	8.0	1.3	10.8	7.8
04-2003	3.2	3.5	4.3	4.4	3.5	3.6	3.9	3.1	3.2	3.8	7.4	3.3
05-2003	0.5	0.5	0.9	0.6	0.5	0.5	0.6	0.4	0.5	0.7	1.5	0.5
06-2003	0.1	0.5	0.2	0.2	0.5	0.5	0.5	0.5	0.5	1.3	0.0	0.5
07-2003	0.0	4.0	0.2	0.3	4.0	4.0	3.5	4.3	4.1	9.8	0.0	4.0
08-2003	0.6	20.2	3.8	5.8	20.1	20.4	21.1	18.2	20.8	49.3	12.1	20.6
09-2003	57.7	17.8	20.9	20.2	17.7	17.6	18.0	17.8	18.0	12.3	15.1	18.3

Due to the lagooning process, the WWTP has highly varying effluent quality over the year, but relative changes in the effluent of the WWTP –as it is a doubled organic substrate concentration in “double WWTP”- does not have a high impact on the annual fluctuation of VSS (Table 5-3). The relative annual loadings only vary from 18.2% (“no WWTP”) to 21.1% (“double WWTP”).

Comparing absolute masses, the changes of the WWTP are more pronounced. The values range between 18.9 t/month with doubled and at only 12.1 t/month without any WWTP substrate loading.

If the concentrations in the karst are set to zero, nearly 50% (15.9 t) of the annual VSS load accounts for August. Ignoring the karst causes a reduction of the VSS load in the wet period. But during months without a strong karst influence (e.g. in the drier period with only short floods), the values nearly match the ones of the first scenario. Due to this, the total annual VSS load of 32 t/year is the lowest of all variants.

Treating the constituents as conservative parameters increases VSS fluxes during months with high discharges and decreases VSS fluxes in months with small discharges or after the accumulation period (June-September). Interestingly, this variant generates the highest annual VSS flux, followed by “double WWTP”. It seems as if the hindered remineralisation in the water phase is responsible here: from October to May, when there is a regular water flow in the river, the load of VSS is always higher than in “all”. But in the dry period –and also slightly in the flushing month September- VSS is always lower.

The last variant with a variable delivery component seems to cause a minimal increase of the bandwidth of annual fluctuation. The overall annual mass remains nearly unchanged.

In the chosen parameter sets, the variants “no benthos” (in the case, that there are no transformations considered), “no fraction” and “no delivery” do not have a major impact on VSS

transport in this parameter setting. But especially the impact of the delivery should be further investigated, as the influence seems to be underestimated (see below).

#### 5.4.4 Monthly VSS loads for 2003/2004

In contrast to the prior year, in 2003/2004 the overall VSS transport seems to be overestimated especially in the months December and January when the values are doubled, and also during the dry period in July to September (Table 5-4). There was a failure in the gauging station at S during that time (see above in chapter 4.1.3). So the deviation here must not only be searched in the modelling. It seems that the approximation on the basis of measured data might be too small: during the period when S is out of service, flow in the simulation is higher than in the approximation (chapter 4.1.3), so the load is probably higher in reality than assumed. The load might be even higher than calculated by the model because there was data for the station K missing in this period as well. The event which led to the destruction of the probes can be assumed to transport a great quantity of load.

Table 5-4: Absolute monthly loadings of VSS for the year 2003/2004 at site S

VSS (S) [t/month]	meas.	all	no trans- mission losses	no bacteria	no benthos	no fraction	double WWTP	no WWTP	no delivery	no karst	no process	variable delivery WQ
10-2003	13.3	13.5	13.4	13.3	13.4	13.5	14.7	12.3	13.4	1.4	13.4	13.4
11-2003	22.5	24.4	24.3	24.2	24.4	24.4	25.4	23.3	23.8	1.9	24.3	24.1
12-2003	8.8	17.2	17.6	17.1	17.2	17.3	17.6	16.9	16.7	1.0	17.2	17.0
01-2004	1.9	3.9	21.2	3.8	3.8	3.8	5.3	2.6	3.8	1.5	3.8	3.9
02-2004	5.8	3.0	3.0	3.0	3.0	3.1	3.8	2.2	3.0	1.0	3.0	3.0
03-2004	7.9	4.2	4.2	4.1	4.2	4.2	5.1	3.3	4.0	1.2	4.2	4.1
04-2004	12.0	12.9	12.8	12.7	12.9	12.9	13.7	12.1	12.5	1.3	12.9	12.7
05-2004	9.3	12.7	12.6	12.5	12.7	12.7	13.4	11.9	12.6	1.0	12.6	12.6
06-2004	1.9	1.0	0.8	0.8	1.0	1.0	1.1	0.8	0.9	0.4	0.7	1.0
07-2004	0.2	1.9	0.1	0.1	1.8	1.9	1.9	1.6	1.9	1.9	0.0	1.9
08-2004	0.1	6.3	1.5	0.5	6.3	6.7	6.6	5.6	6.3	6.3	0.4	6.3
09-2004	0.1	5.7	4.2	4.6	5.3	5.1	10.0	1.3	5.3	5.6	4.0	6.0
t/year	84	107	116	97	106	106	119	94	104	24	97	106

Further sources for the aberration are the early flushing months. The first flood of September 2004 was mainly driven by surface runoff without any karstic influence. This means, that for this month, the influence of the overland runoff in terms of nutrient import into the river is higher, than in September 2003, where the karstic influence was strong. So an underestimation of available organic matter on the delivery part of the model will even have a higher relative importance than in the year before.

Even though the overland runoff has slightly more influence, the general regime of this year is comparable with the prior one in terms of the impact of the scenario.

## 5.5 Event scale analysis and results

Apart from the fluctuation on the annual timescale, there is also an important inter-event dynamic as explained earlier (chapter 4.1.4). The representation of this fluctuation will be shown in the following chapters at the two events of 2003-09-22 and 2004-09-13.

### 5.5.1 Pollutographs for the event at 2003-09-22

Figure 5-7 and Figure 5-8 show the results of the first scenario (“all”) in comparison to measured values for some of the output parameters at S on the first flush flood in September 2003.

In comparison to the long-term calculation of the whole year 2002/2003, this flood could not be represented with the same accuracy. The correlation reaches 0.86 and the Nash-Sutcliffe 0.68.

The measured behaviour of the system is only partly represented in the simulation (see also chapter 7.11.1), which is a cause of the complex and still unknown rainfall-runoff relationship.

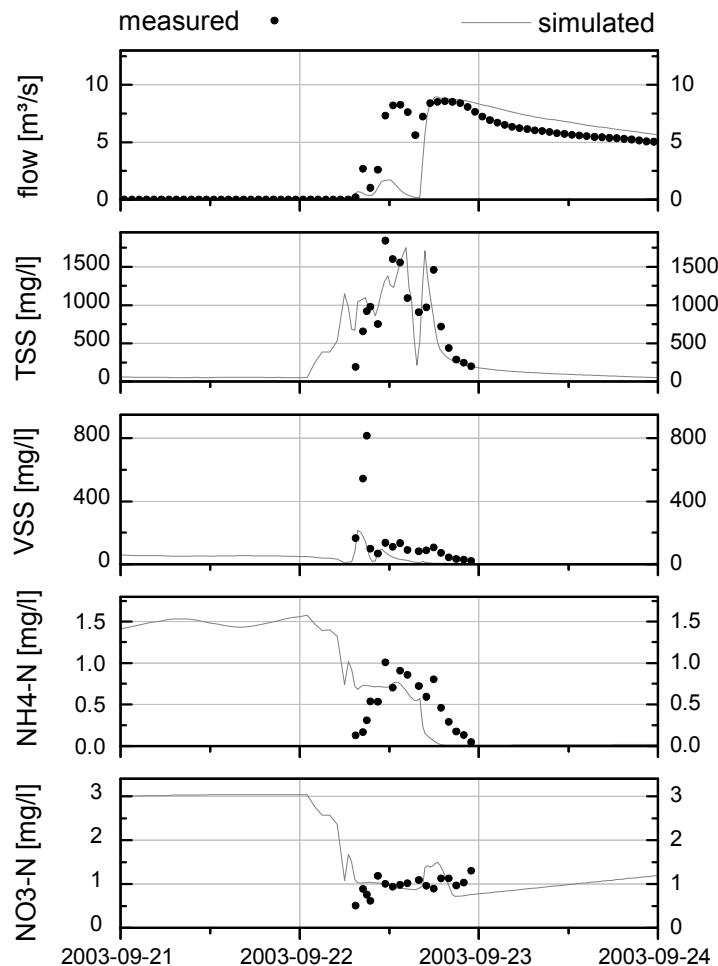


Figure 5-7: Measured and simulated concentrations at Sanglier (S) for 2003-09-22, Scenario “all” for particulates and dissolved inorganic nitrogen

Estimations revealed a runoff coefficient of about 6 %, which was normally 1% for other floods ((Perrin, 2006), compare also chapter 7.2). Due to this, the first major peak in the flow, which is assumed to be caused by instant runoff at the start of the rain event, cannot be modelled exactly.

Nevertheless it must be noted that about 90-99% of the flow at S is contributed by the karstic spring at K during this event ( $(\text{flow}_S - \text{transmissionloss}_{K-S}) / \text{flow}_K$ ). This means that it depends on the parameter, whether this lack of compliance is serious for the overall mass transport or negligible. For example, nitrate-nitrogen is mostly transported by the karstic spring with comparably high fluxes, whereas VSS or other organic compounds emerge from other sources or are build up in the pools. The effect on nitrate-nitrogen will be much smaller than on VSS in terms of the overall event load.

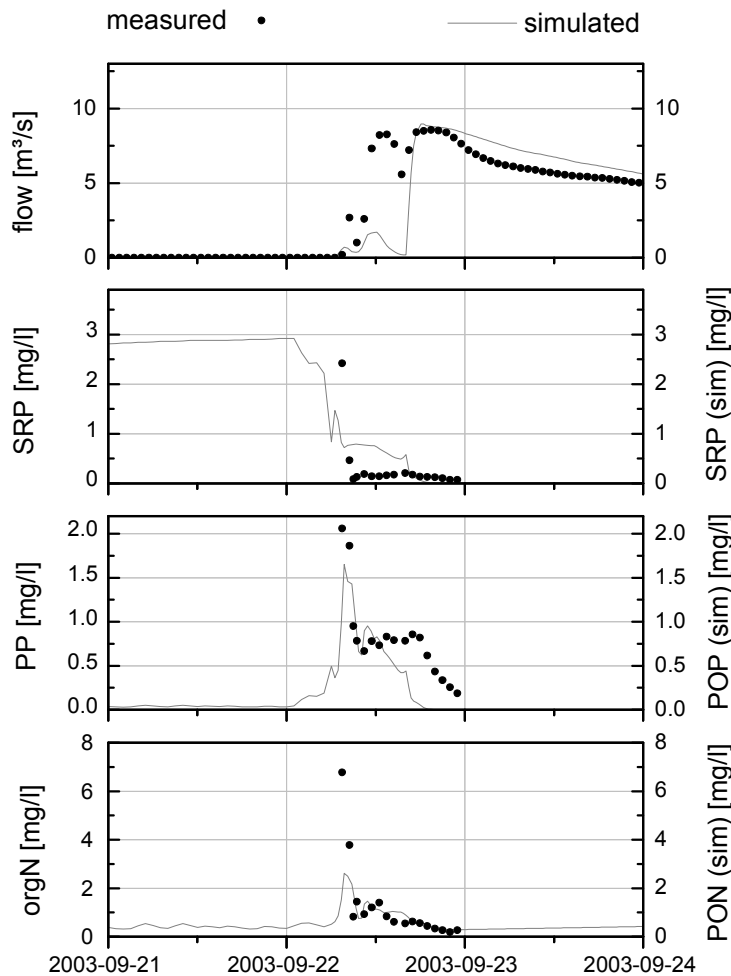


Figure 5-8: Measured and simulated concentrations at Sanglier (S) for 2003-09-22, Scenario “all” for inorganic phosphorus, particulate (organic) phosphorus and (particulate) organic nitrogen

Results at V were not included here. One main source, the Issanka spring at site K’ could not be included in the model, because it is not possible to measure the volume of the contribution of this very diffuse spring.

A peak for VSS at S could be reproduced, but there still seem to be additional sources of organic matter in the reach apart from the instream bacteria growth. This may be caused during the floods by an overflow of the waste water treatment plants or by the surrounding vegetation which is importing organic matter in the form of leaves and small branches and other detritus.

The courses of the other parameters seem in the range of normal applications. In the measurements, ammonium is slightly less concentrated in the beginning (Figure 5-7). Maybe the

nitrification is more intensive than specified in the model. Particulate organic phosphorus along with particulate organic nitrogen is well approximated, only the peak is smaller in the simulation as it happened also with VSS (Figure 5-8).

### 5.5.2 Pollutographs for the event at 2004-09-13

This flood is only caused by overland runoff. A limited replication of the rainfall-runoff part will be even more obvious than before.

The correlation and Nash-Sutcliffe were calculated to 0.88 and 0.37 resp. for the flood of 2004-09-13, but the water flux is underestimated in the simulation of this flood as shown in Figure 5-9.

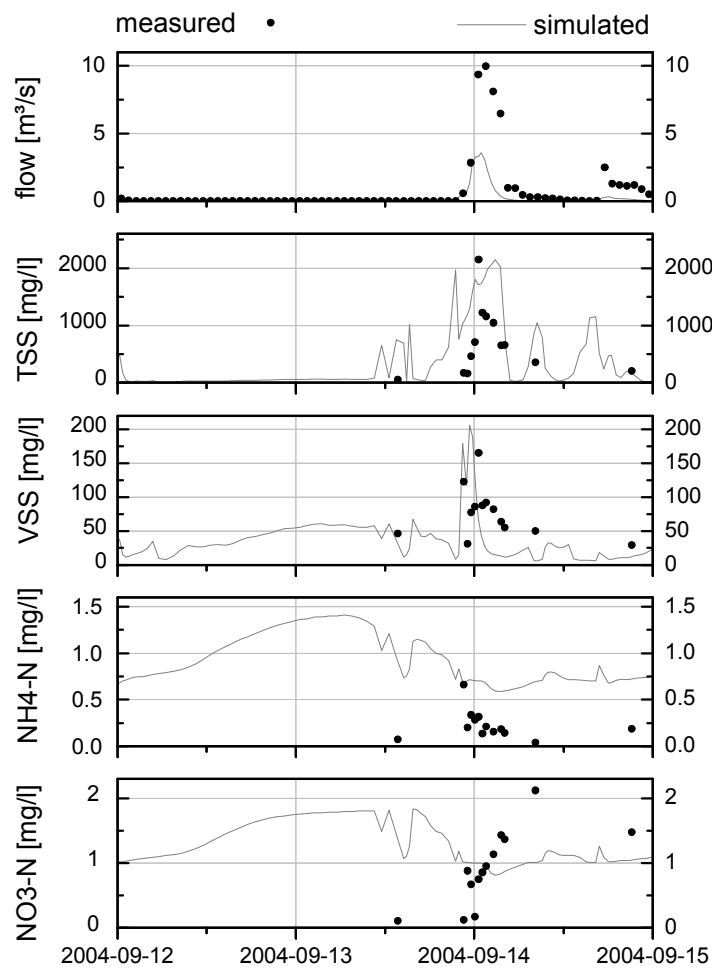


Figure 5-9: Measured and simulated concentrations at Sanglier (S) for 2004-09-13, Scenario “all” for particulates and dissolved inorganic nitrogen

This fact will have minor influence on the concentrations of solubles, as long as they are governed by the inflows, but it leads to an underestimation of the loadings charged to the receiving lagoon. If a particulate substance as TSS or VSS is considered, the complexity caused by the interacting processes of resuspension and deposition will add an additional error source, especially when flows are not calculated correctly.

The concentrations of TSS are therefore underestimated, either due to an underestimation in the inflows or by the missing transport capacity.

Ammonium underlies an early flushing followed by a fast dilution in the measurements, which is not reproduced by the model in this extend. The lacking dilution effect of rain on the overland runoff needs to be accounted for.

Furthermore, the reason for the increase of the nitrate concentration in the falling limb of the hydrograph in the measurements remains unclear. Either this is a cause of some delayed flows from instream nitrate storages in upstream pools or more likely by nitrate leaching from the soils.

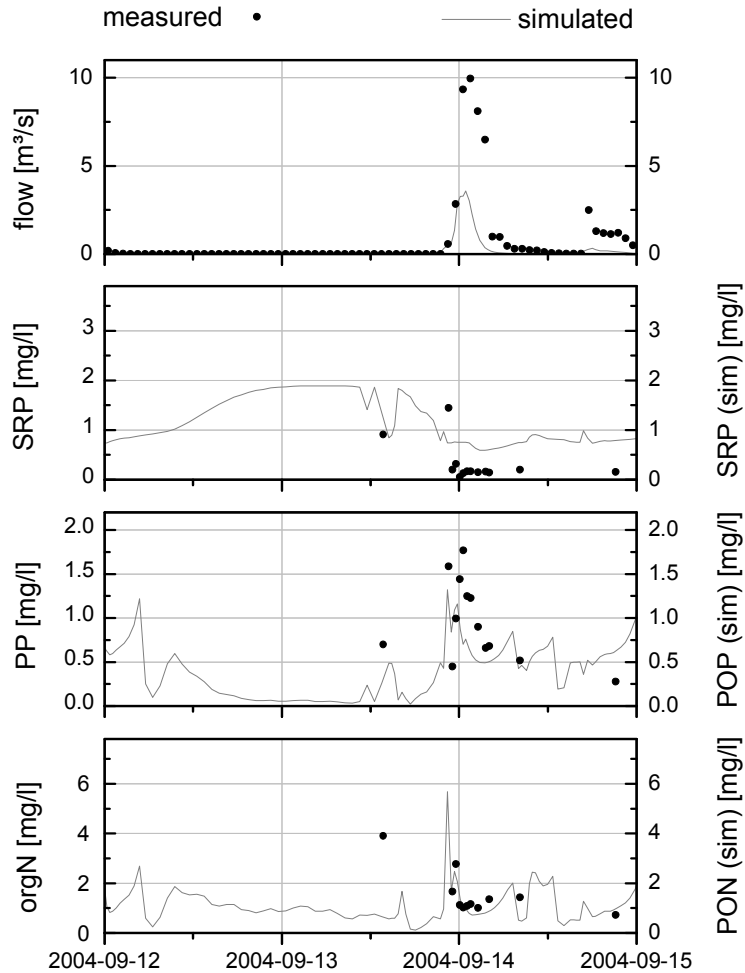


Figure 5-10: Measured and simulated concentrations at Sanglier (S) for 2004-09-13, Scenario “all” for inorganic phosphorus, particulate (organic) phosphorus and (particulate) organic nitrogen

The course of POP and PON is better as it can be seen in Figure 5-10. There is a lot of fluctuation especially in the particulate phosphorus (PP) measurements, so the model’s performance is in an acceptable range. As with ammonium, the dilution caused by the rainwater in the later stage of the flood was not accounted for (the delivery part is run with constant concentrations), so the concentrations are overestimated. An attempt to include this effect will be done below (chapter 7.11.3).

### 5.5.3 Sensitivity of the processes in the flushing months September 2003 and 2004

During each of the two regarded years, the main first flood events occur in September. For all variants, total flow and load are compared in detail for these months in the years 2003 and 2004 for VSS, TSS and nitrate.

In terms of flow, disregarding infiltration in scenario 2 caused an increase in total flow of 4% for September 2003 respective 43% for September 2004. Due to the lack of karstic flow in 09-2004, the total values for this month are significantly lower, so that transmission losses achieve greater importance.

Table 5-5: Loads of VSS for September 2003 and 2004 at site S, total values and percentages in terms of scenario 1

	all	no trans- mission losses	no bacteria	no benthos	no fraction	double WWTP	no WWTP	no delivery	no karst	no quality	variable delivery WQ
VSS (S) [t/month] 09-2003	14.02	12.64	12.28	13.84	13.89	16.16	11.90	13.69	3.97	13.75	14.30
VSS (S) [%] 09-2003	100%	90%	88%	99%	99%	115%	85%	98%	28%	98%	102%
VSS (S) [t/month] 09-2004	5.68	4.20	4.60	5.32	5.15	10.01	1.29	5.27	5.65	3.99	6.03
VSS (S) [%] 09-2004	100%	74%	81%	94%	91%	176%	23%	93%	99%	70%	106%

As a result of the flow increase in scenario 2, the load of VSS is reduced by 10 to 26% (cp. Table 5-5). This is mainly caused by higher stream velocities and erosion.

Bacteria are an important factor in the build-up of organic matter because up to 19% of VSS is caused by uptake of substrates (see 09-2004, “no bacteria”), but the benthic bacteria growth only accounts for 1 to 6%.

Transport and build up of VSS is strongly influenced by the biota. If all constituents in the simulation are considered to be conservative (scenario “no quality”), the total VSS flux is reduced by 30% in September 2004. So, the smaller the input from the karst, the greater the influence of the biological conversion processes becomes. If the karst is dominating, the built up organic matter will be negligible (2% in September 2003).

If the substrate of the heterotrophic bacteria is doubled in concentration in the WWTP inputs, then the total load will be increased by 76%. Here, the influence of the karstic spring is once again more obvious, as it does not allow a proper accumulation instream in September 2003: the effect of higher organic substrate concentrations is much lower than in the year 2004, where there is hardly flow coming from site K. The situation is reversed in the variant without substrate inflow by the WWTPs (scenario 7, “no WWTP”), because here the additional loading of the spring becomes dominant and not, as in the case before, the additional erosion (and with it a reduction of accumulation potential) caused by the spring flow.

In the simulation, the delivery part of the model only accounts for 2 to 7% of VSS flow, whereas, if the karstic input of particulates and solubles is turned off, VSS is reduced by 72% for September 2003.

The last variant with changing input concentrations for the delivery model did not yield major changes in total, but slightly increased the loadings.

The changes in results for TSS are not as numerous as for VSS (see Table 5-6).

Table 5-6: Loads of TSS for September 2003 and 2004 at site S, total values and percentages in terms of scenario 1

	all	no trans- mission losses	no bacteria	no benthos	no fraction	double WWTP	no WWTP	no delivery	no karst	no quality	variable delivery WQ
TSS (S) [t/month] 09-2003	297.64	291.91	295.90	297.46	357.20	299.82	286.59	212.14	98.94	283.58	297.93
TSS (S) [%] 09-2003	100%	98%	99%	100%	120%	101%	96%	71%	33%	95%	100%
TSS (S) [t/month] 09-2004	69.57	69.22	68.50	69.21	73.38	73.86	64.58	14.39	62.56	63.93	69.93
TSS (S) [%] 09-2004	100%	99%	98%	99%	105%	106%	93%	21%	90%	92%	101%

Major variations are caused by the new fractional sediment transport approach. The total load of TSS is increased by 20% for the year 2003. The total net erosion capacity will be lower, if fractioned sediment is considered, because e.g. the availability of the fine fraction on the river bed is limited due to the other two fractions (see EQ. 3-34). The interpretation of this is that some finer sediment is not mobilised because it is held in the interstices between immobile coarser material, i.e. that there is a hiding ability of the finer sediment fractions (see also e.g. Wu et al., 2000)).

In the comparison of variants “double WWTP” and “no quality” the influence of VSS on TSS can be estimated as between 1 and 8%.

The most significant influences are attributable to the karstic spring at K as well as for the delivery model. If the flow regime is dominated by the spring, as in 09-2003, the TSS load is reduced by 2/3, if the karst concentration is set to zero. On the other hand, if the delivery model dominates, the influence on the TSS load can be 79%.

However, the variations not only influence loadings of particulates. Table 5-7 shows nitrate loads, and it can be seen that during seasons of small flow volume, ~60% of the nitrate may be lost to the groundwater due to infiltration.



Table 5-7: Loads of NO<sub>3</sub>-N for September 2003 and 2004 at site S, total values and percentages for scenario 1

	all	no trans- mission losses	no bacteria	no benthos	no fraction	double WWTP	no WWTP	no delivery	no karst	no quality	variable delivery WQ
NO <sub>3</sub> -N (S) [kg/month] 09-2003	2 310	2 439	2 311	2 310	2 310	2 310	2 290	2 272	62	2 312	2 313
NO <sub>3</sub> -N (S) [%] 09-2003	100%	106%	100%	100%	100%	100%	99%	98%	3%	100%	100%
NO <sub>3</sub> -N (S) [t/month] 09-2004	53.24	84.15	53.38	53.25	53.24	53.24	49.88	4.43	52.88	53.38	54.86
NO <sub>3</sub> -N (S) [%] 09-2004	100%	158%	100%	100%	100%	100%	94%	8%	99%	100%	103%

The WWTP play a minor role in the nitrate transport in the catchment, only 1 to 6% of the total load can be assigned to the WWTP at site d. The karstic spring at the top of the catchment contributes most of the nitrate in the stream, up to 97% in September 2003.

#### 5.5.4 NCL-plots for the scenarios

In the following, some NCL-plots of the scenarios are compared with measured ones for the flood of 2003-09-22 to check, whether the modelling reproduces a similar load distribution. As the regarded timescale differs from the plots shown in Figure 4-33, the values of the measured plot may differ from the ones above.

For TSS there is a good correspondence with the NCL-plot derived from the measurements (see Figure 5-11), the FF<sub>25</sub> is about 65% for all variants (cp. chapter 7.5).

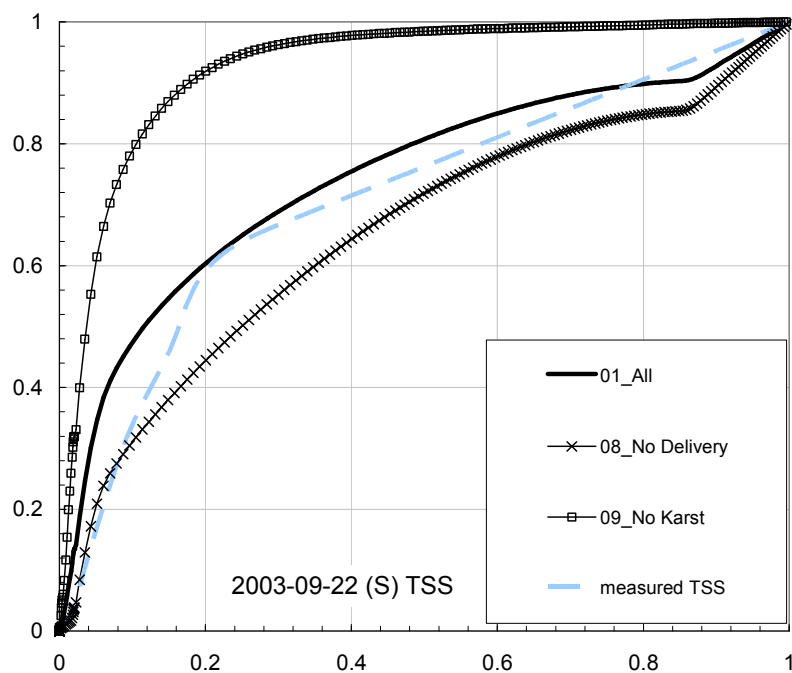


Figure 5-11: Comparison of normalized cumulative loads of measured TSS and all scenarios at S for 2003-09-22

The simulation for VSS shows some deviations in comparison to the measurements. The flush occurs earlier in most of the scenarios, except in the variant without WWTP inflows and consideration of conversion processes (“without quality”). Nevertheless, the interval of the measurements at the very beginning of the flood is too long and in the values of the simulation also the very first, very intensive parts are included. The gradient of the measured curve matches the ones from the simulations at the beginning of the flood.

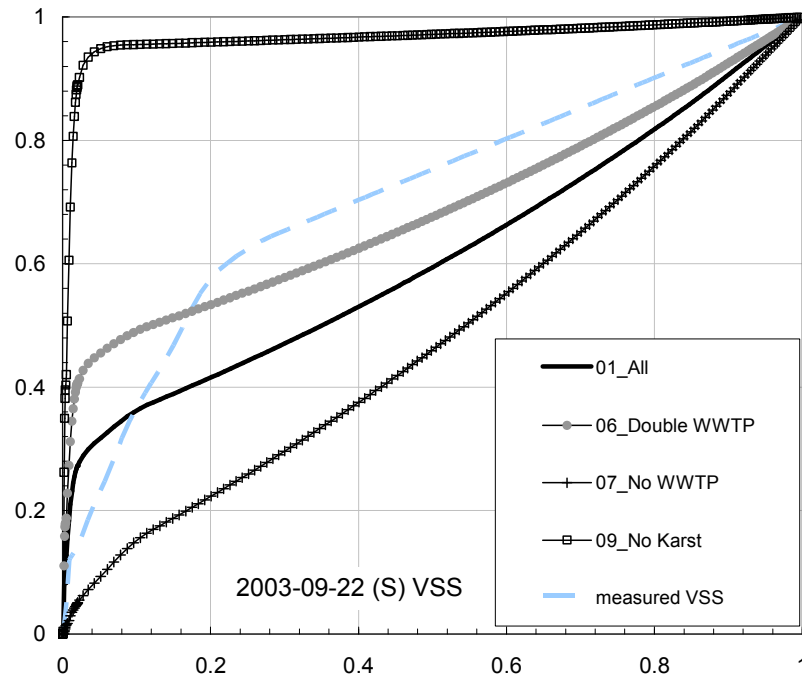


Figure 5-12: Comparison of normalized cumulative loads of measured VSS and all scenarios at S for 2003-09-22

As already found in Figure 5-11 for TSS, it can be seen that the karstic spring at K attenuates the first flush.

The measurements at the Karst effluent showed concentrations of VSS between 25 and 200 mg/l for the event. This data was included as a boundary condition.

The Karst at K can not be measured directly, but a few meters downstream the zone, where it is emerging. A ditch from a small vineyard is directly flowing in this zone. The rainfall of the event of 2003-09-22 is mainly concentrated in the north (see above), and this is causing very high surface runoff on this parcel, which brings this VSS loads.

Obviously, if the karst is considered to contain only perfectly clean water, as it is the case in scenario 9 (“no karst”), the flush will be only caused by the amount of stored mass in the system prior to the event.

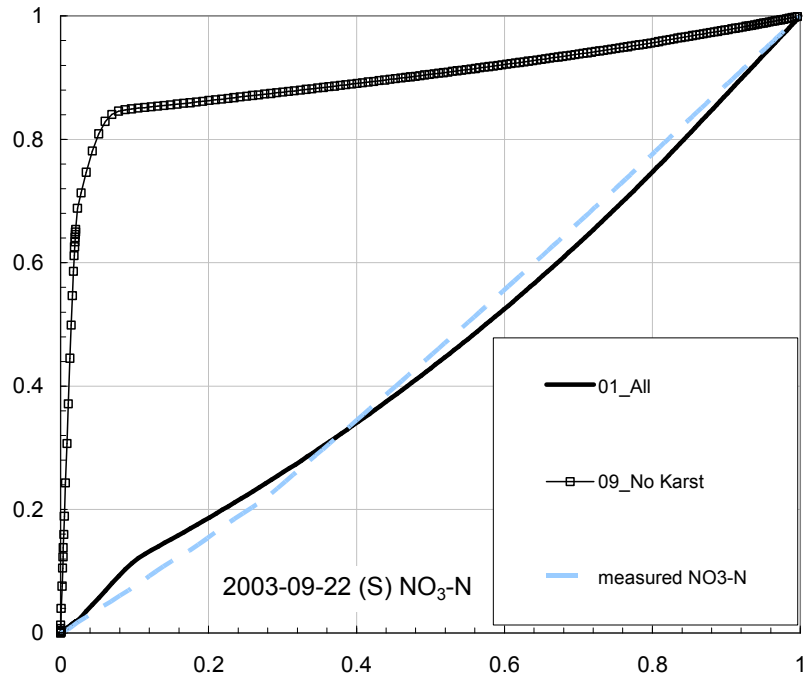


Figure 5-13: Comparison of normalized cumulative loads of measured NO<sub>3</sub>-N and all scenarios at S for 2003-09-22

Clearly the karstic spring heavily influences the nutrient transport in the catchment, especially for nitrates. Owing to the accuracy of the measurements at the spring which were input in the model, there is a strong agreement between the simulation and the sampled data (cp. Figure 5-13).

The comparison of the measured NCL-plots and the ones of the scenarios demonstrates that the general dynamic of the transport intensity of different types of properties as volatile suspended solids or nitrate can be reproduced successfully.

## 5.6 Regression of simulations and measurements

Figure 5-14 shows a regression analysis of the scenario “all” for site S for the period of 2002-2004.

The output of the simulation was interpolated on the timestep of the measurements. In the analysis, points were only included, if a measurement existed, all simulation data without measured data were discarded.

Whereas the flow values seem to be reasonable in general, data for the water quality parameters show some deviations. In order to identify the sources of these deviations, similar groups as in chapter 4.1.5 were formed. Especially for VSS, also the two available measurements in July 2003 (green triangles) are important, where the simulation overestimates the concentration. During the whole month the flow was very low, normally less than 1 l/s. Only in some pools downstream the WWTP inflows water still remains and there is a lot of organic accumulation due to high temperatures and excess of nutrients. Small disturbances in the flow rates of the simulation at the two days are enough to resuspend them and to cause these high overestimations, which are not relevant in terms of the overall VSS transport (see chapter 7.6 for further explanations).

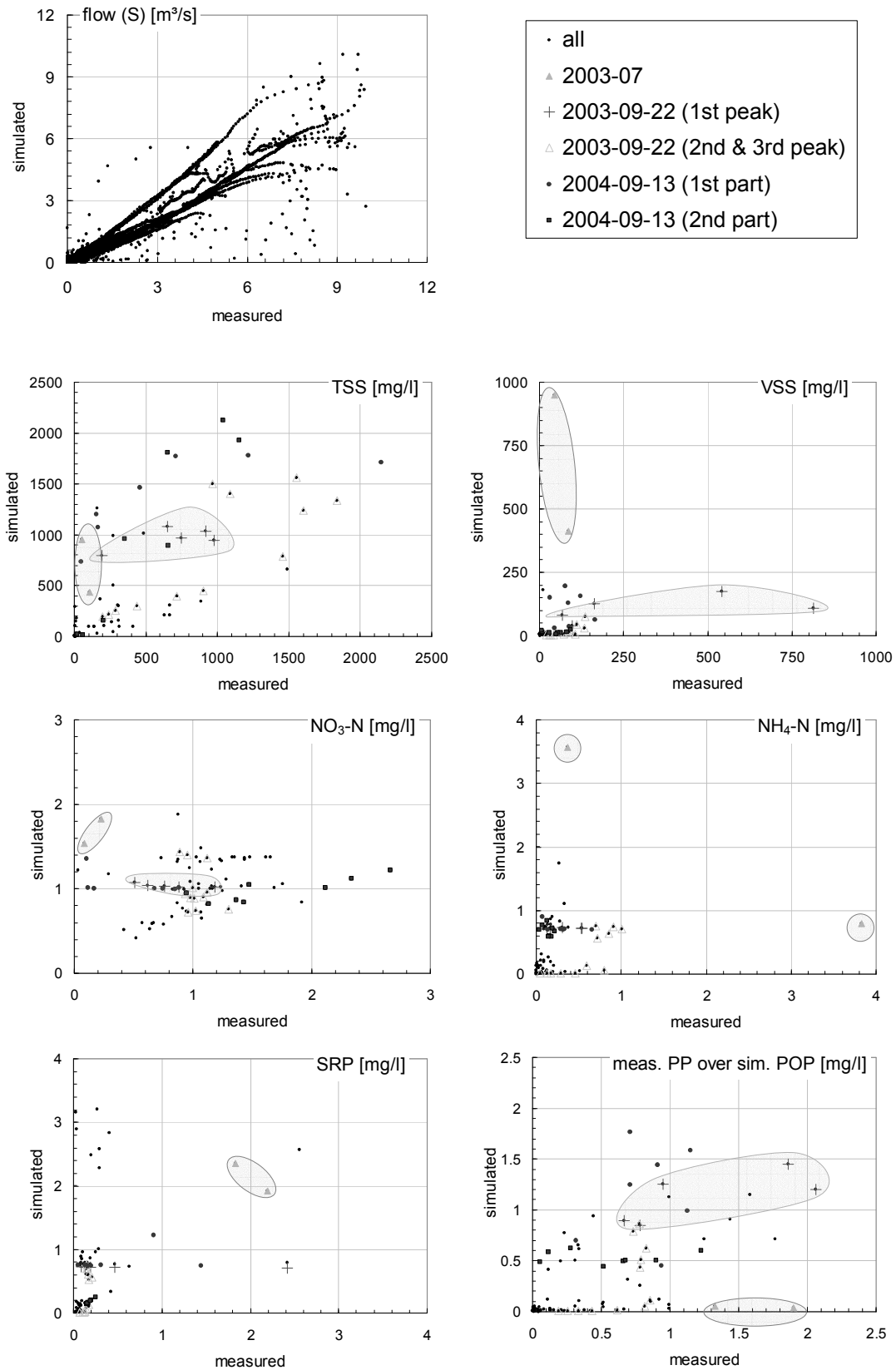


Figure 5-14: Data simulated with variant "all" over measured data

The other main deviation happens during the onset of the 2003-09-22 flood. Especially during the maximum flow of the very first peak (the two points most to the right), the concentrations are underestimated.

How sensitive the system is during the low-flow condition can be seen best in the difference in the behaviour of the two points in July 2003. It is not possible to make any reliable prediction during this time.

Concentrations of VSS and PP were found to be underestimated in the falling limb of the event of 2004-09-13 and overestimated in the rising limb. As this event is only caused by the deliver part of the model, either the resuspension in the model is overestimated, or the concentrations of the delivery model underlie greater changes, so that the assumed constant concentrations induced by the rainfall-runoff model are not valid.

Table 5-8: Correlation simulated and measured concentration at the Vène catchment for the years 2002-2004, point S

variable	Pearson correlation 2002-2004	Nash-Sutcliffe efficiency 2002-2004
flow	0.90 (0.97,0.85)	0.78 (0.90,0.65)
TSS	0.70	0.20
VSS	0.19	-0.78
NH <sub>4</sub>	0.21	-20.27
NO <sub>3</sub>	0.07	-0.29
PON/orgN	0.50	0.12
SRP	0.41	-20.6
POP/PP	0.71	0.37

Table 5-8 summarises the correlations of simulated and measured concentrations at site S for the years 2002-2004 (values for the years 2002/2003 and 2003/2004 in parenthesis).

The correlation for the particulates (TSS, PON, POP) seems to be better than for solubles (NH<sub>4</sub>-N and NO<sub>3</sub>-N).

If the most dominant outliers (2003-07 and 2003-09-22 1<sup>st</sup> peak) are disregarded, the coefficients would change to 0.41 and -0.33 respectively. If it would be possible to simulate these periods with an error of about 75% (reducing the RMSE from 147 to 95), the values would be even better: 0.95 for the Pearson correlation and 0.25 for Nash-Sutcliffe.

This means, that frequently used automatic calibration tools will most likely fail, if they are applied unchanged to the case of temporary waters, due to their inability to distinguish between the *uncertainty noise*, which is always present in measured data and the natural *temporary river noise*, caused by the fast and irregular fluctuation in concentration during short termed dry period storms.

During the analysis of data, especially in temporary rivers but also in perennial ones, it must be kept in mind that, in addition to all other uncertainties and assumptions, timeseries of

measurements often do not possess the same properties as timeseries of continuous simulations. Some features, which can be modeled, are normally not measured in campaigns done in natural rivers.

As mentioned before, concentrations were often not found to be a reliable parameter for the analysis as they do not contain any information about the downstream propagation of nutrients. Because it was now found that the concentration is also more affected by small disturbances investigations of loads should normally be favoured in the analysis.

## 5.7 Conclusions of the modelling

On the long time perspective of the two simulated years, the model shows good coincidence with the reaction of the natural system. The Nash-Sutcliffe efficiency for flow yielded 0.78 and the Pearson correlation coefficient was 0.90 for the whole regarded period, but there are still remaining limitations in the event scale.

The calibration was especially successful for particulate constituents. It was found, that the system is very sensitive to even small changes in flow rate during the dry period. A major limitation is the missing knowledge of the processes of nutrient wash-off from the land-side in combination with the high degree of uncertainty concerning the spatial variability of rainfall.

The results of the simulation indicate, that there are additional sources within the catchment, which are still unknown. These are responsible for the under-representation of VSS concentrations in some of the events. They can be caused by overflows of the WWTPs as well as wash-off of organic matter brought in by the surrounding vegetation.

Hence, the model calculations could substantiate the importance of the interaction between rainfall-runoff caused delivery of materials and the karst-induced instream resuspension processes, which have already been indicated during the data analysis.

Accumulation processes due to the biomass growth downstream the WWTP inflows have been modelled successfully, even if a verification is difficult, because the extent of accumulation underlies greater differences in the bed and on the banks than it is the case for suspended or soluted matter concentration in the water phase.

It was shown through the simulation, that events during the dry period may contribute to a great extent to the annual VSS transport. A comparably small event in August 2003 was able to release about 7.8 t of VSS (10% of the annual load) from the accumulation site at S.

The simulation revealed, that events of this type during summer can be of great importance to the nutrient export to receiving waters of temporary rivers. They may be small in volume, short in duration and therefore difficult to measure, but due to their great impact, they should be included in any measurement and management programme.

## 6 Summary and conclusions

---

Temporary rivers are difficult terrains for hydrologists and engineers. Often not recognised in their importance, there are not many studies concerning the modelling of water quality in drylands. Their fluctuating nature makes great demands on the design of measurement campaigns as well as on the equipment. Water quality models to be applied to these systems must be characterised by extended features in terms of stability, mass conservation and have to consider some key processes (transmission losses, mass retention etc.) of importance in temporary rivers.

This work deepens the knowledge in water quality processes in temporary rivers on the basis of two methods:

- i) the analysis of real data and the application of new approaches (RMF, NCL) to identify fluctuations in mass transport, and
- ii) a detailed scenario analysis with the help of a modern water quality model (tempQsim – STREAM) which was adopted for temporary rivers.

### *Development of new methods for the data analysis*

Within this work definitions of the first flush phenomena and related terms were specified and important issues for the investigation of temporary rivers have been discussed. The method of normalized cumulative loads (NCL) was reviewed and applied in a new context not only at an event scale, but also for hydrological years. It proved to be a most valuable method, but a limitation was found in the identification of periods with increased proportional mass transport. This led to the development of the relative mass fluxes (RMF). This method is able to relate the transport of constituents to the water flow at each point in time and is especially useful for the analysis of longer periods (Obermann et al., 2006).

Along with two already known methods ( $FF_{25}$ , Geiger (1984)), two new indexes to quantify flushes were introduced and discussed (NCL-integral criteria and a modified Geiger (1984) method). All these methods showed comparable trends, but especially the  $FF_{25}$  method proved to be valuable. The approach classifies the extent of a first flush by the percentage of cumulative load at 25% of cumulative flow. It does not share the negative feature of the NCL-integral method, which shows only small differences between varying floods. As a further advantage it is easier to apply than the Geiger (1984) method or the modified Geiger method. The  $FF_{25}$  approach gives the most descriptive parameter and was therefore found to be the most applicable.

### *Data analysis and first flush characterisation*

Data of three catchments of the three Mediterranean rivers La Vène in France, Albuñón in Spain, and Mulargia on the Italian island Sardinia was analysed for the years 2002/2003 to 2003/2004 and the methods described before were applied.

The application of NCL-plots for the hydrological years revealed in the Vène River a severe increase of mass transport at the beginning of the autumn rain period. The relative strength of these phenomena –caused to a great extent by accumulation in pools downstream of wastewater inflows– could be observed by means of the NCL-plots to TSS, VSS > PP > TP > SRP > TN > NO<sub>x</sub>.

An application of the developed RMF-plots clearly demonstrated the reoccurring cycle of increased transport in late summer and early autumn. For particulates like total suspended solids (TSS) or volatile suspended solids (VSS) the maximum of relative mass transport occurs in September. Over 70% of the annual TSS load and even more than 87% of VSS was transported by only about 5% of the annual flow in September 2003, which means that 17.8 times more of the annual amount of VSS than of water volume is transported in this month. Other parameters, mainly belonging to the group of solubles, as ammonium (NH<sub>4</sub>-N), soluble reactive phosphorus (SRP) or organic nitrogen (orgN) tend to have their maximum RMF even earlier in August. From the delay of the particulates it can be assumed, that the easier a substance can be resuspended, the earlier the peak of the relative mass flux will occur. Only nitrate (NO<sub>3</sub>-N) does not show this trend. On the contrary, it seems to follow a reciprocal tendency with minima in August, presumably caused by nitrification processes during summer as well as due to strong inputs of karstic springs, which deliver most of the NO<sub>3</sub>-N during the rain period.

A comparison of flow, rainfall and transport activity of TSS and VSS indicated the importance of wash-off effects at the example of October 2003. That month had similar flow volumes as September 2003, but less rainfall. The relative mass flux of VSS was over 12fold higher in September than in October and still 1.6fold higher in November. It was found that the correlation between flow and e.g. nitrate is strong (0.96), but that it is poor for particulate substances as TSS and VSS (correlation of 0.27 and 0.17). This means, that there must be great storages within the system. Further, there is an indication that the correlation of particulate substances is stronger to rainfall than to instream flow, which further underlines the importance of the rain-caused wash-off effects.

An analysis of the composition of total nitrogen (TN) and total phosphorus (TP) in terms of their different species revealed a reoccurring pattern mainly influenced by the beginning of the flow season. In general, up to 70-75% of TP is available in the form of SRP, but during periods with increased mass transport and import from the landside -as in September and November 2003- particulate phosphorus (PP) reaches up to 74%. A similar tendency can be observed with TN, where normally nitrate and nitrite (NO<sub>x</sub>-N) make up about 60-70%, but not during August, when the organic forms (orgN) can reach a proportion up to 75%.

On the event scale, important flush effects especially for particulates have been shown in the NCL-plots as well as through the application of three indexes: FF<sub>25</sub> values for TSS and VSS reach up to 0.72 respective 0.70. The highest flush occurred for ammonia in the course of the flood of 2003, where 79% of the NH<sub>4</sub>-N event load was transported by the first quarter of flow.



On the basis of very detailed measurements in a 5-minute interval, it could be shown that there are two different relationships between conductivity and water flow. In river sections that are not influenced by or far away from possible accumulation pools, the relationship is nearly linear. In sites where an accumulation is possible the conductivity is constant for higher flows, but increases exponentially with a reduction in flow rate. This means that during low flow, the conductivity is generally higher, indicating a higher potential of nutrient retention in these sites.

At the example of the Mulargia River a comparison of several subsequently following floods was done. It was found in this case that not the very first flood starting at 2003-10-17 contained a flush, but only the second flood at 2003-10-22, which followed shortly after. It was concluded that the system might need some wetting before it is able to produce a flush, but not too much, as the values for  $FF_{25}$  are constantly falling with proceeding autumn and winter after that.

As to its arid nature, data at the Albuñón River was very scarce, so a general trend could not be derived. It seems as if the transported amount of nutrients is more correlated to the time of the year than to the strength of the flood.

### ***Development and modification of the tempQsim – STREAM model***

From the great variety of models, two were chosen to be evaluated: HSPF and CASCADE. The source code of HSPF was not available and limitations in the mass balance have been identified for the finite difference discretisations combined with the variable parameter Muskingum-Cunge approach used in CASCADE.

Based on the gained experiences a lot of additional processes have been implemented in the newly developed tempQsim – STREAM model. It was modified to calculate fractioned sediment transport and to include the parameters TSS and VSS as output variables. In this context the approach of Partheniades (1962) was enhanced. The newly implemented formula considers the availability of each settled particulate substance on the bed in the calculation of the erosion rate. This helps in the simulation of highly varying stream conditions as it is common in temporary rivers. In addition, a more differentiated consideration of POM dynamics and its storage in the benthic zone during the dry period have been introduced. Heterotrophic bacteria was included as a particulate substance, which is able to settle down on the streambed thus forming a great quantity of the VSS in pools maintained by point source inputs.

### ***Application of the tempQsim – STREAM model***

The tempQsim – STREAM model was applied in the Vène catchment. It was calibrated for the hydrological year 2002/2003 and validated for the year 2003/2004, with a special focus on the transport of particulates for the first significant flood events of these years.

The model was thoroughly tested for 11 scenarios in order to test the extensions and to make a sensitivity analysis of the processes. It was applied in accordance to the prior investigation of the data for an event and an annual scale. For the long-term simulation, the model shows generally good coincidence with the measured values, which are in the range of other model applications.

It was found that the system reaction is very vulnerable during the drier phase to even small rain events. If there is no relevant water flow in the river, and the existing pools are maintained by point source inflows, the concentration of nutrients is usually high. If small waves of relatively uncontaminated rainwater frequently enter the system, this leads to many small disturbances, letting the concentration constantly fluctuate between the one of the rainwater and the one provided by the point sources. This circumstance, which was observed in the simulation but will happen in nature as well, complicates the calibration and validation as it e.g. inhibits the use of conventional automatic calibration tools.

The accumulation of thick layers of organic matter on the channel bed, which was observed in the Vène River, could be modelled successfully in the range of about 10-30 kg/m<sup>2</sup>. The calibration was difficult because the available approximations of settled biomass were done in discrete points whereas the model outputs are mean values for the regarded reach.

The model considers a simplified transformation of substrates into bacterial biomass following the ASM3 concept. This was done in order to account for cases where accumulation of organic matter is caused by effluents from less treated or untreated waste water with high residence times in pools within the river network, which is common in the Mediterranean and in particular in the MENA region. It was found through the modellisation, that the resuspension capacity of events during the dry period can be very important for the annual VSS balance. Even though comparable small, an event during August 2003 was capable to release over 95% of the stored bottom VSS and transported nearly 10% of the total annual load. The simulation showed, that these events can have a severe impact on the downstream lagoon. Hence, great care should be taken in order to include these short-lived events during the summer in measurement programmes for temporary rivers.

The comparison of the scenarios was done for absolute values as well as for relative monthly loads and in terms of NCL-plots, in detail for VSS but also for TSS, NH<sub>4</sub>-N and NO<sub>3</sub>-N. It showed that bacteria play a main role in the build-up of the stock of VSS in the river. If no bacteria were considered, the transported mass during August 2003 would be reduced by 85%.

The importance of the wastewater inflows became mostly obvious in periods with little karstic influence. A total prevention of wastewater inflows was found to reduce the VSS load in S (the site downstream the WWTP inflow) by 25% during August and by 15% during September 2003, whereas a doubled concentration of organic nutrients leads to an increase of 24.4% resp. 15.7%. In September 2004, when karstic spring was not flowing at all, the monthly load was even increased by 76% for the double WWTP concentrations and reduced by 77%, if the concentrations in the WWTPs were zero.

The karstic springs are of extreme importance for the total annual loads as well as for the annual distribution. If the nutrient input in the springs was disregarded, the months with minor flow would gain influence. So in this variant, nearly 50% of the annual VSS load was transported by August 2003 but the total annual load was reduced by nearly 60% to 32 t/a.

The comparison of the calibrated simulations with the measured values exposed, that there seems to be a general underestimation of VSS transport in September 2003 and an overestimation in September 2004.

It was concluded, that there are additional sources within the system, which are still unknown. These may be either caused by overflows of the WWTPs during some floods as well as by continuous accumulation of organic matter on the landside by the vegetation within the catchment.

It was found that especially the first peak of the event in September 2003 and the whole event of September 2004 were underestimated. They were both caused by overland runoff and had no karstic influence. Neither in the calibrations with data produced by the delivery model MERCEDES nor with a newly developed delivery model a reasonable parameter set could be found to reach the peak flows.

### ***Application of variable runoff concentrations***

In order to investigate the influence of this deviation on the transport of properties, a simulation was done with an idealised delivery inflow. This constructed flow enabled a significant improvement for the computation of TSS, but the values for VSS load or concentration could still not be met. At the beginning, the concentrations entering the river with the overland runoff were chosen to be constant in the modelling, without any consideration of the former conditions. This might be one cause of the underestimation, because surrounding vegetation seems to import great quantities of organic matter into the stream.

Hence, two approaches were tested, to link the concentration of the delivery model to the dryness of the system and to simulate increasing storage of organic matter on the landside during dry periods. Very good improvements for the flood of 2003-09-22 and even acceptable results for 2004-09-13 could be demonstrated with one of the approaches.

### ***Conclusions of the model performance***

The tempQsim – STREAM model has been found to be most valuable to identify critical periods for the mass transport in temporary streams. Due to its ability to be mass conservative in any flow condition, the stored organic matter within the riverbed could be reproduced.

The scenario analysis gave deeper insights in the functioning of the system of the Vène. This is beneficial for future management, identification of areas for further improvements of applied models as well as for the planning of measurement campaigns.

The strengths of the model were most visible in the transport of particulate substances as VSS, TSS, POP and PON. The more river-based constituents could be better represented.

Limitations in the simulations were mainly caused by missing knowledge of processes and sources and not by the general construction of the model. Many of the remaining issues can be e.g. solved by a coupling to an enhanced rainfall-runoff model with an advanced consideration of the urban zone (as in Grillot, 2006).

---

### ***Future perspective and outlook***

Future work is recommended to improve the link to delivery models for semi-arid river basins. Further, supporting tools to help with the calibration and the filling of data gaps have to be developed.

The current work shows many proofs for fluctuations in transport activity. It deepens the understanding of water quality dynamics in dryland rivers and its modellisation. The derived knowledge enables advanced measurement campaigns and management options, which are tailored for the specific needs of comparable dryland rivers.

Enhancements presented within this work will be part of future releases of the MOHID Water Modelling System and will be used within a greater community as basis for further investigations and advancements.

Measurements in the catchments are still done in the framework of current European and national projects. As it was already done in the Albuji3n catchment, the inclusion of radar data for runoff prediction seems to be a good measure for a better consideration of the highly variable spatial variation of rainfall. The work done in the V3ne catchment concerning the identification of the accumulated bacteria biocenosis can provide a better representation within the model in the future.

With additional information, especially on the landside part and on the reaction of the waste water treatment plants during storm events, the simulations can be further enhanced. This would enable a step towards a joint investigation of the river system including downstream basins, reservoirs or lagoons. The above proposed further developments may enable to determine the impact of predicted flood events on receiving waters in terms of their resuspension potential in real time, so that suitable management measures can be derived and implemented.

## 7 Annex

### 7.1 Additional formulas concerning transport of particulate materials

#### 7.1.1 *Fall velocity of single, spherical particles*

In a non-moving fluid, the terminal fall velocity of a single suspended particle is only influenced by gravity force, the buoyant force and a drag force.

Hence, the terminal fall velocity for a spherical particle can be derived from

$$\underbrace{\frac{1}{2} C_d \rho \omega_0^2 A_s}_{\text{drag force}} - \underbrace{\rho_s g V_s}_{\text{weight force}} + \underbrace{\rho g V_s}_{\text{buoyant force}} = 0 \quad \text{EQ. 7-1}$$

where

- $C_d$ : drag coefficient
- $\rho, \rho_s$ : density of water and sediment (kg/m<sup>3</sup>)
- $\omega_0$ : terminal fall velocity of a single particle (m/s)
- $A_s$ : area of the particle in vertical direction (m<sup>2</sup>)
- $g$ : gravitational acceleration (m<sup>2</sup>/s)
- $V_s$ : volume of the particle (m<sup>3</sup>)

Rearranging and assuming spherical particles with

$$A_s = \frac{\pi}{4} d^2 \quad \text{and}$$

$$V_s = \frac{\pi}{6} d^3$$

EQ. 7-1 can be written as

$$\omega_0 = -\sqrt{\frac{4 g d}{3 C_d} (s-1)} \quad \text{EQ. 7-2}$$

in which

- $s$ : specific density of sediment (-)
- $d$ : particle diameter (m)

#### 7.1.2 *Drag coefficient $C_d$*

There are different approaches to determine the drag coefficient, e.g.

$$C_d = \frac{24}{Re} \quad \text{for } Re < 1 \quad \text{Stokes (1851), for spherical particles}$$

$$C_d = \left( \left( \frac{24}{Re} \right)^{2/3} + 1 \right)^{3/2} \quad \text{for } Re < 1 \cdot 10^4 \quad \text{Cheng (1997), for natural sediment}$$

Hence, with the Particle-Reynolds number

$$Re = \frac{\rho \omega_0 d}{\mu}$$

where

$\mu$ : dynamic viscosity of water (Ns/m<sup>2</sup>)

the calculation of the terminal fall velocity in water leads to an iteration process.

**Remark:**

Outside the STOKES region (where  $Re > 1$ ) there is no simple expression for the drag coefficient. The  $C_d$ -value decreases rapidly outside this region and becomes nearly constant for  $10^3 < Re < 10^5$  yielding the fall velocity proportional to  $d^{0.5}$ .

**Empirical formula**

Therefore, there are also some empirical formulas, e.g. those of Gibbs et al. (1971):

$$\omega_0 = 10 \frac{-30v + \sqrt{900v^2 + g d^2 (s-1)(0.003869 + 2.480 d)}}{0.011607 + 74405d} \quad \text{EQ. 7-3}$$

where

$v$ : kinematic viscosity of sediment (m<sup>2</sup>/s)

**7.1.3 Fall velocity of a cloud of particles**

In a continuum of sediment the settling velocity of a single particle is affected by the motion of surrounding particles. A thick suspension has a slower fall velocity than a single particle, and the fall velocity decreases with increasing sediment concentration. This effect is called *hindered settling*.

Van Rijn (1993) recommended estimating the fall velocity of a suspension from

$$\omega_s = (1 - 2.15 c_s)(1 - 0.75 c_s^{0.33}) \omega_0 \quad \text{EQ. 7-4}$$

in which

$c_s$ : volumetric sediment concentration (-)

Gibbs et al. (1971) was validated for nearly spherical particles from sizes of 50  $\mu\text{m}$  to 5 mm.

Some empirical formulas, like the one of (Zhang and Xia, 1995) already include factors for the hindered settling:

$$\omega_s = \sqrt{\left(\frac{13.95 v}{d}\right)^2 + 1.09\left(\frac{\rho_s}{\rho} - 1\right) g d} - 13.95 \frac{v}{d} \quad \text{EQ. 7-5}$$

$\omega_s$ : terminal fall velocity of a suspension (m/s)  
 $\rho, \rho_s$ : density of water and sediment ( $\text{kg}/\text{m}^3$ )  
 $g$ : gravitational acceleration ( $\text{m}^2/\text{s}$ )

Due to the often inadequate data basis and the sums of assumptions involved with the approaches above, the fall velocity is often subject to calibration and can therefore be directly defined in many water quality models.

#### 7.1.4 Occurrence of suspended load transport

In general, transport in suspension is regarded as advanced state of bed-load transport. Exceeding a critical condition causes the formerly bed-near transported particles to loose the contact to the bed.

The occurrence of suspended load transport is not necessarily coupled with bed-load transport because the finer particles may be entrained when there is no bed movement. Anyway, in many approaches suspended load starts at a defined condition of bed-load transport.

Several researchers developed a criterion for the inception of transport in suspension. As the governing parameter most of them used the ratio of the shear velocity  $u_*$  and the fall velocity of a single particle  $\omega_0$ .

Chanson (1999) suggests as a first approximation

$$\frac{u_*}{\omega_0} < 0.2 \dots 2 \quad \text{EQ. 7-6}$$

## 7.2 Runoff coefficients in the Vène

Figure 7-1 shows the runoff (delivery  $S$ ) over the rainfall at station Les Clachs. The runoff was calculated by the difference of the flow measurements at  $S$  subtracted by the flow at the karstic spring  $K$  including a lag time of one hour. Each point in Figure 7-1 represents the data for one event, where the duration of the event was defined by the rainfall duration.

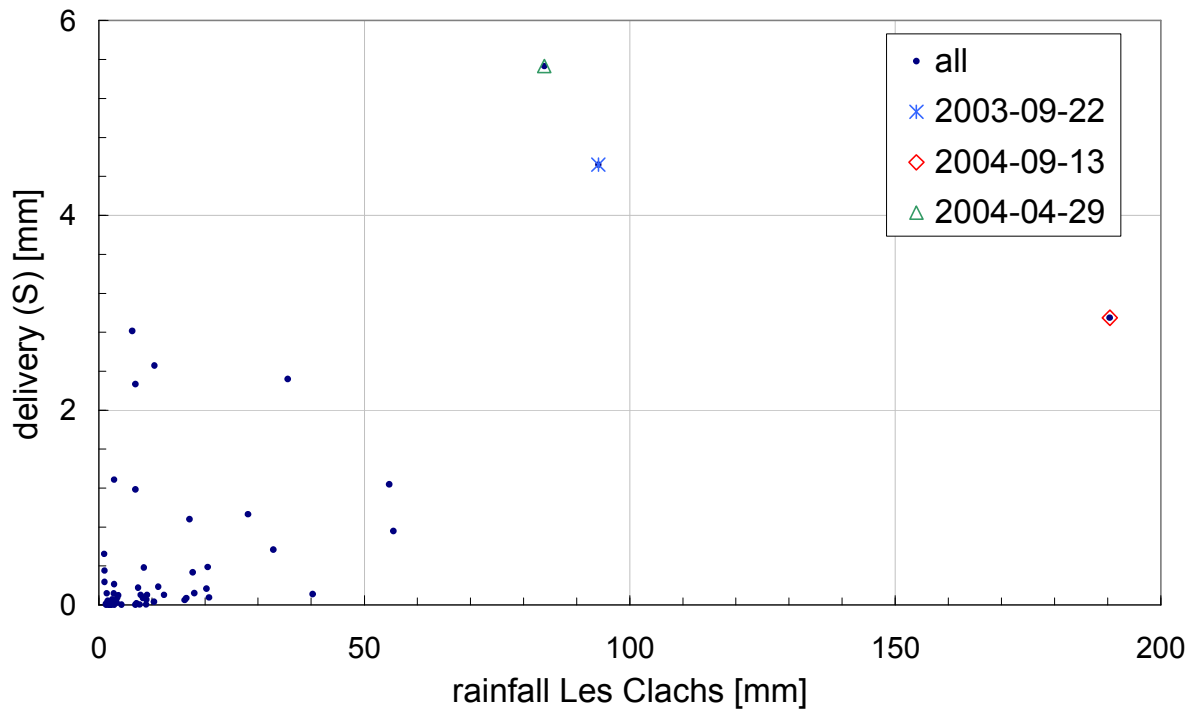


Figure 7-1: Runoff over rainfall for the events from 2002-2004

The figure shows that the two floods occupy an outstanding position. They are the biggest events during the regarded period and the event of 2004 has even the double total rainfall amount than the event of 2003. Due to the subtraction of the karstic influence in the flood of 2003-09-22, the both runoff coefficients can be compared: a coefficient of about 4.8% could be calculated for the event of 2003, and only 1.5% for 2004.

There are quite high values of the runoff for comparably low rainfall values. Additionally, there is a deviation for the event of 2003 to (Perrin, 2006). This might be explained by the fact, that the rainfall is very locally condensed for some events and it is therefore impossible to find one representative rain station for all events. So the choice of the station or an eventual interpolation between some stations has great influence on the results of the derived rainfall-runoff relationship.



### 7.3 Calibration and sensitivity analysis

In the following, the effort spent on the calibration and the problems involved will be demonstrated on few examples without going into detail.

#### 7.3.1 Sensitivity of the Manning Coefficient

Figure 7-2 shows a variation of the Manning coefficient for site S. The hydrograph is only met during the later stage of the flood. The first major peak, as explained earlier, is caused by the overland runoff, which is normally faster and more direct, and the second peak with the longer recession limb can be assigned to the karstic spring at Cournonsec.

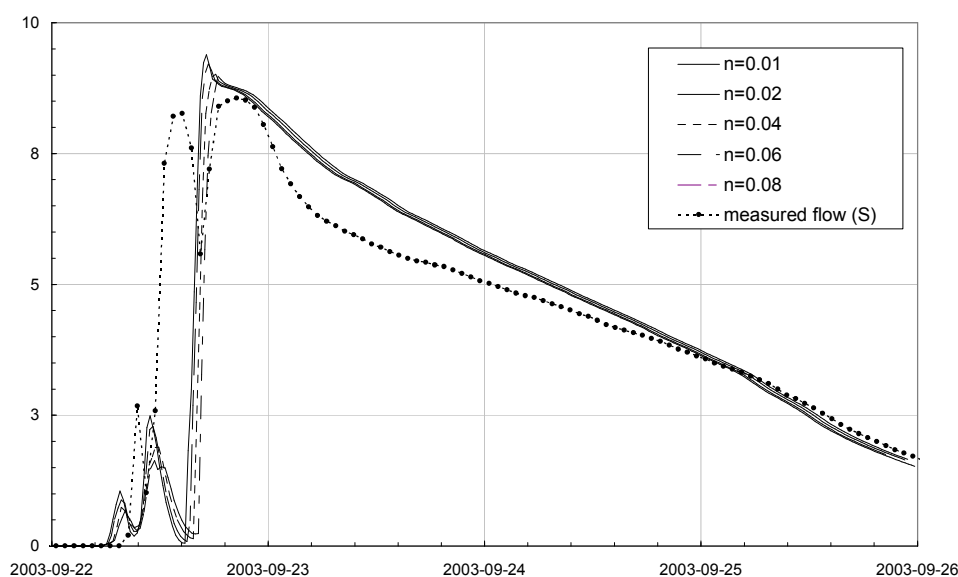


Figure 7-2: Variation of the Manning coefficient for the event of 2003-09-22 at site S

In the case of this flood, the fact that the first major peak could not be modelled does not seem to be influenced by the choice of the bed roughness. The analysis of hydrographs at other floods in this year showed an acceptable general coincidence with the measurements.

For the further simulation, a value of  $n=0.05$  was chosen, as it is also often recommended for “natural rivers” with light brush.

#### 7.3.2 Sensitivity of the transmission losses

Due to the absence of measurements for the hydraulic conductivity of the channel bed, the transmission losses had to be estimated. This was done on the basis of July 2004. In this month, the pool which was formed by the WWTP at Montbazin (d) (mean flow of about  $0.006 \text{ m}^3/\text{s}$ ) was approximated with a mean length of about 500m. The cross section in this part of the river has a steep, nearly rectangular trapezoidal shape with a width of 3 m. To balance the inputs of the WWTP, the transmission losses should equal the inflow of  $0.006 \text{ m}^3/\text{s}$  for the regarded section, otherwise, the pool would overflow. On the basis of the assumption that seepage losses are the

most important losses (normally one order of magnitude higher than evaporation), a hydraulic conductivity near  $5 \times 10^{-6} \text{ m}^3/(\text{m}^2\text{s})$  seemed to be appropriate.

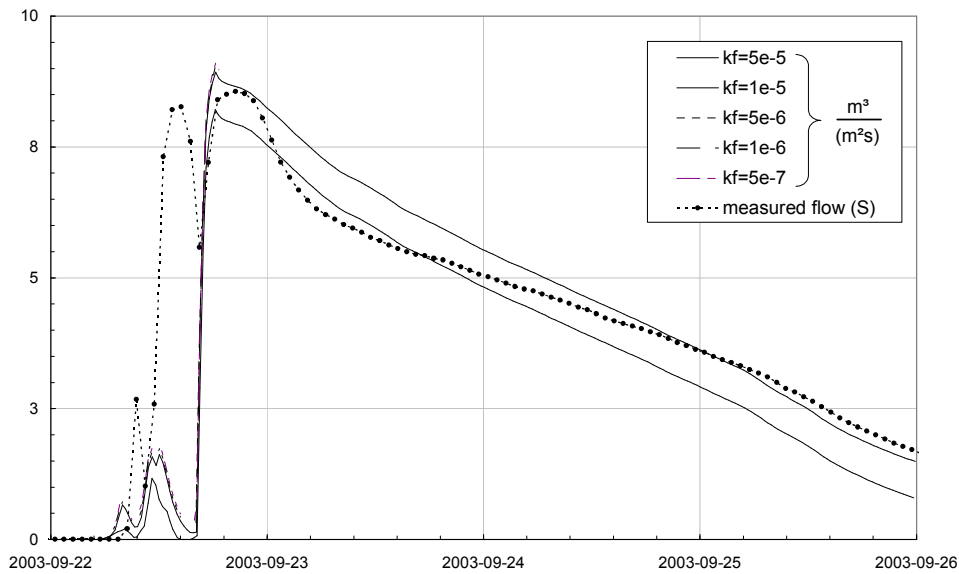


Figure 7-3: Calibration of hydraulic conductivity of the channel bed at site S for the flood of 2003-09-22

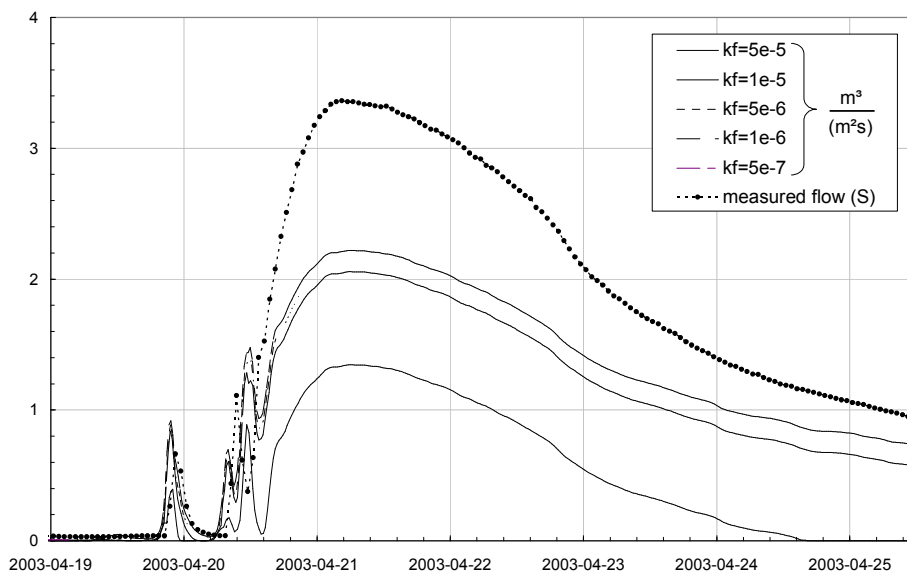


Figure 7-4: Calibration of hydraulic conductivity of the channel bed at site S in for the flood of 2003-04-19

Figure 7-3 and Figure 7-4 underline this hypothesis. Values above a hydraulic conductivity of  $1 \times 10^{-5}$  reduce significantly the flow rate in both floods, whereas the variation for lower values is much smaller. As it can be seen on the event from 2003-04-19, the instream seepage losses are not the cause of the underestimation of the flow, which was found in some floods. So the reason must be searched in the implementation of the delivery model or in unknown and unconsidered sources in the catchment, which have not been considered here.

### 7.3.3 Water quality properties

In the following the data shown in Table 5-2 ff. is visualised, extended by data of TSS and NO3-N.

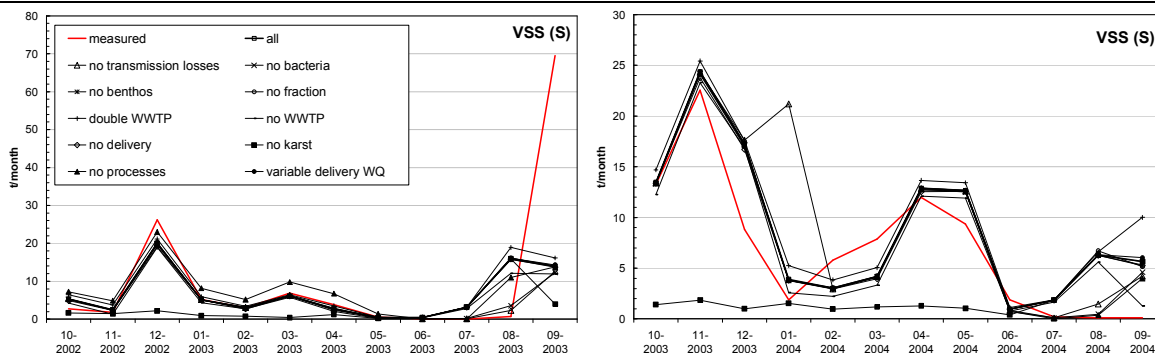


Figure 7-5: Absolute monthly loadings of VSS for the 2002-2004 at site S

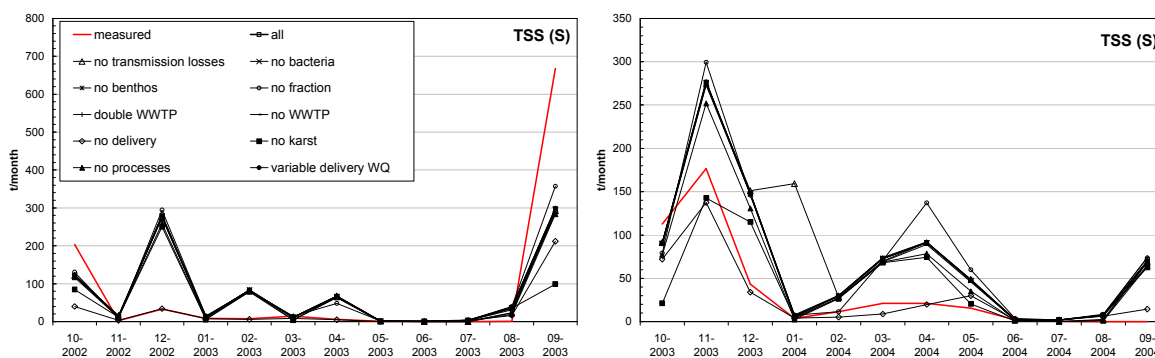


Figure 7-6: Absolute monthly loadings of TSS for the 2002-2004 at site S

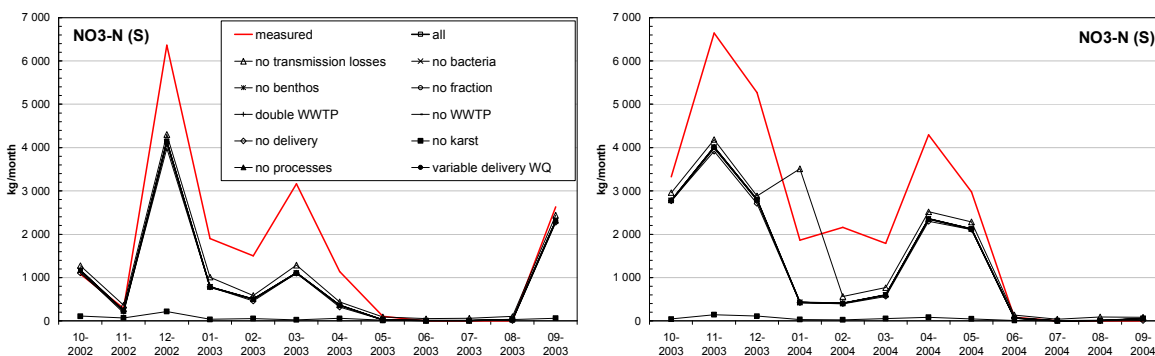


Figure 7-7: Absolute monthly loadings of NO3-N for the 2002-2004 at site S

### 7.4 NCL-plots for all scenarios

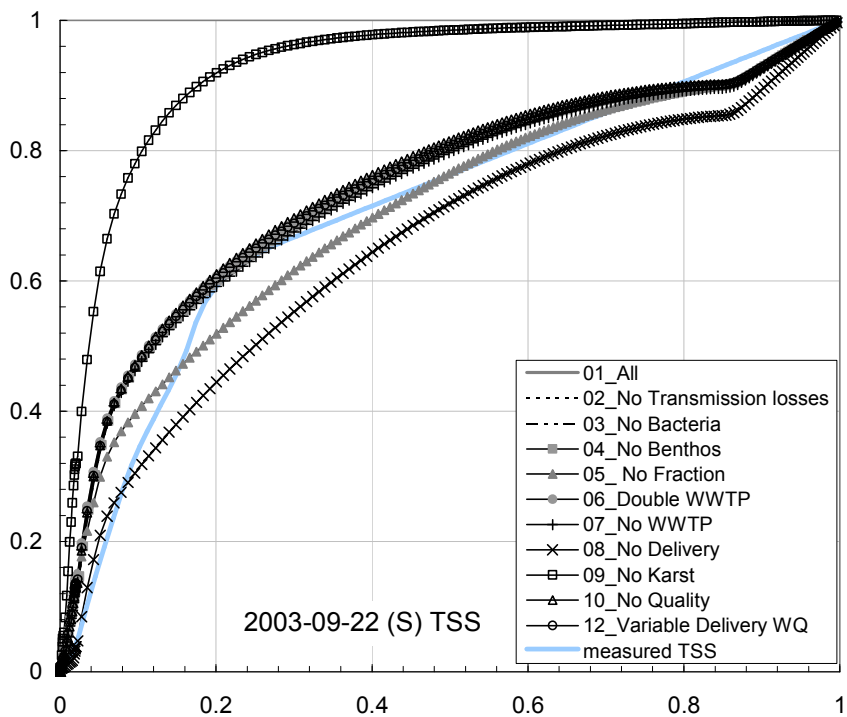
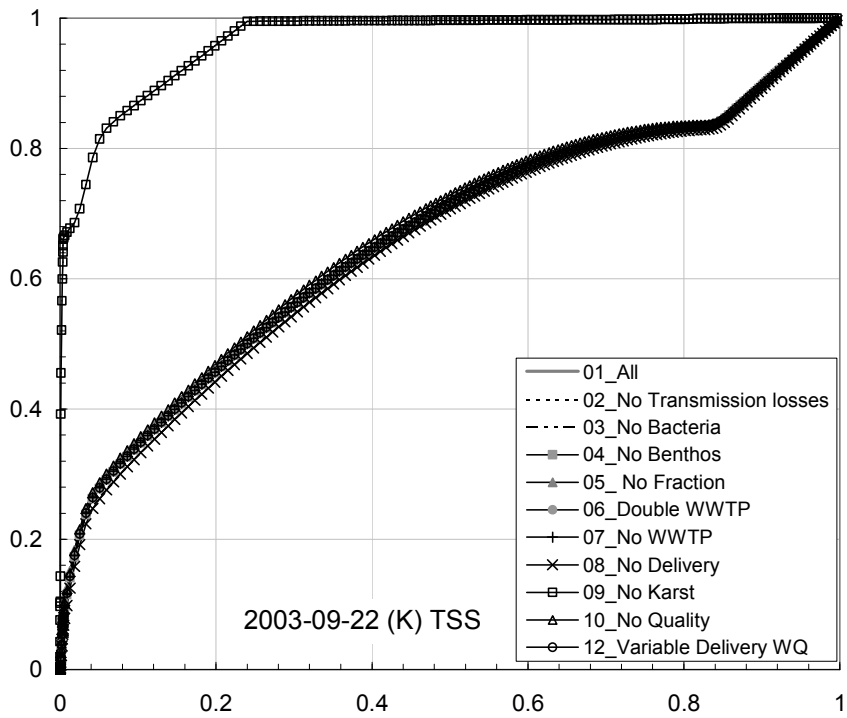


Figure 7-8: NCL- plots for measured TSS and all scenarios at sites K and S for 2003-09-22

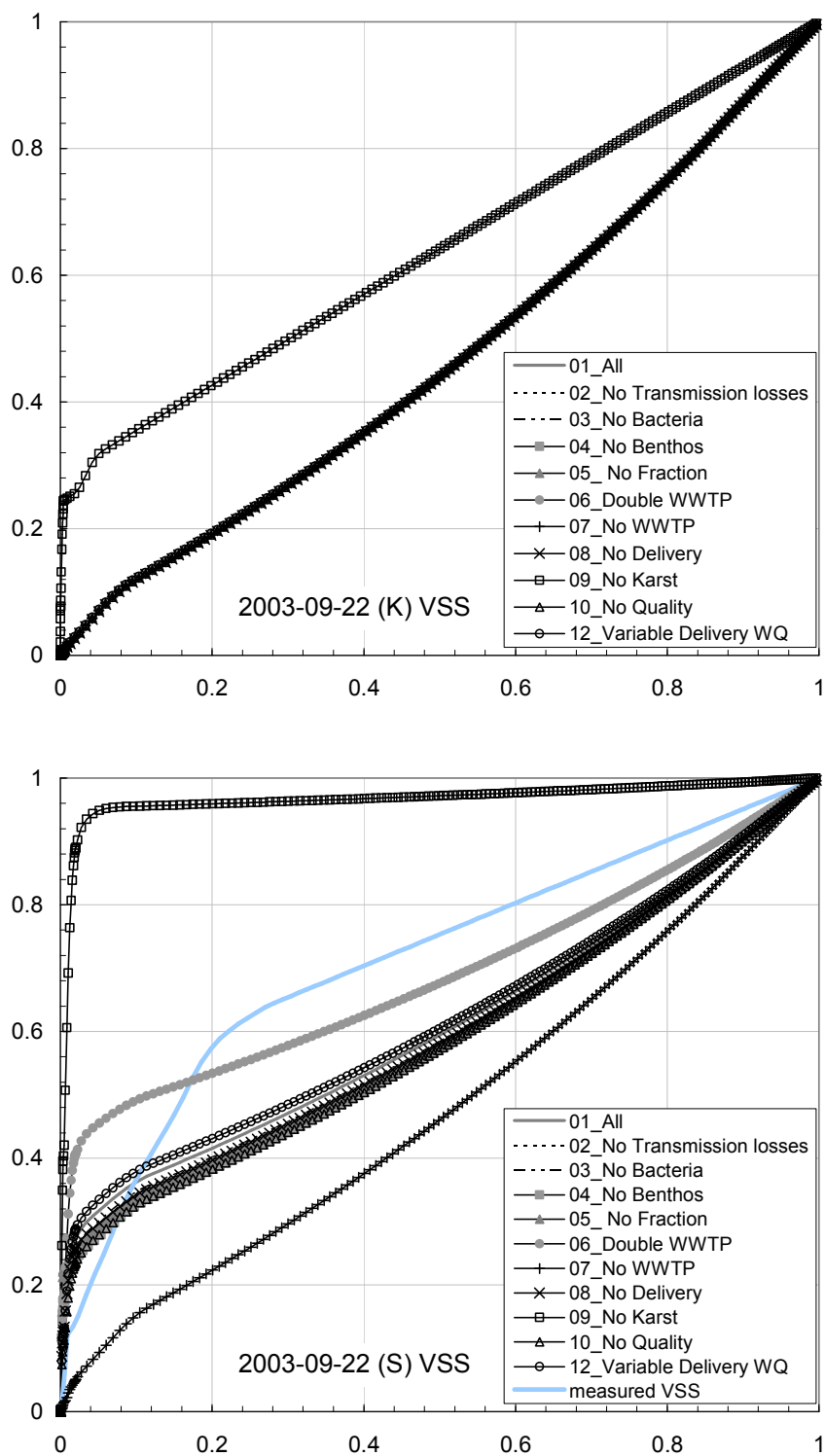


Figure 7-9: NCL- plots for measured VSS and all scenarios at sites K and S for 2003-09-22

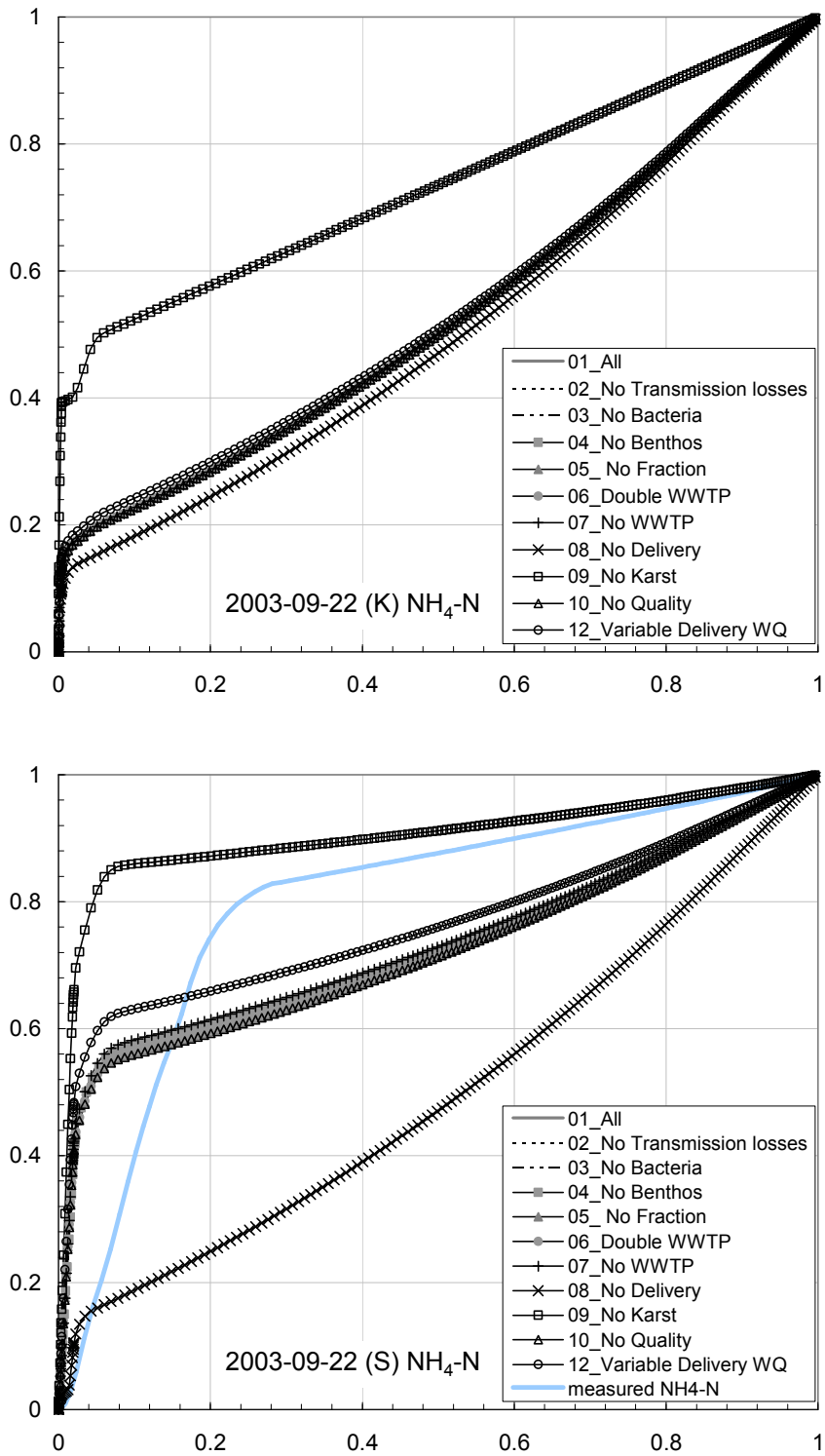


Figure 7-10: NCL- plots for measured NH<sub>4</sub>-N and all scenarios at sites K and S for 2003-09-22

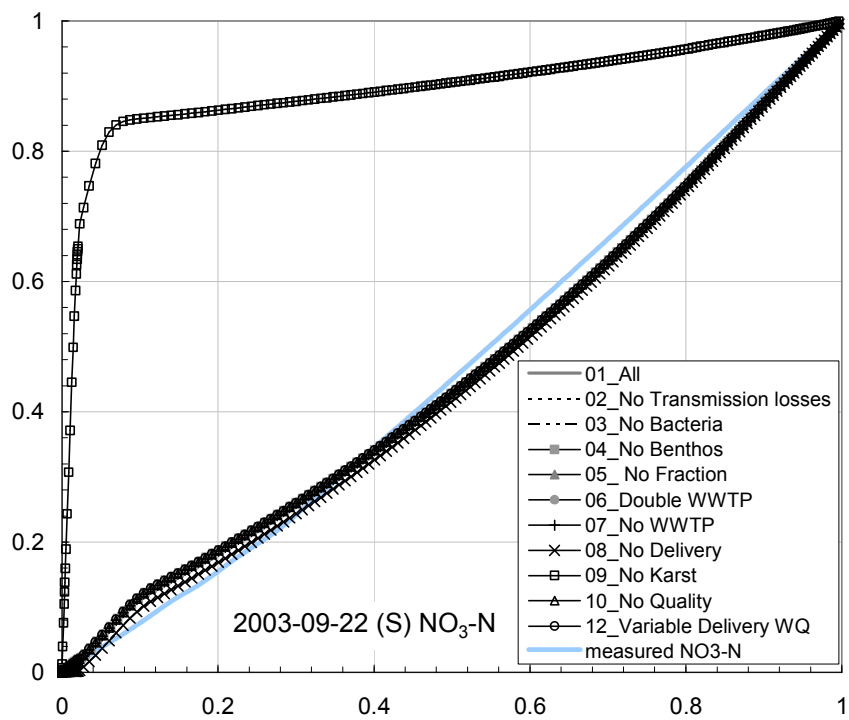
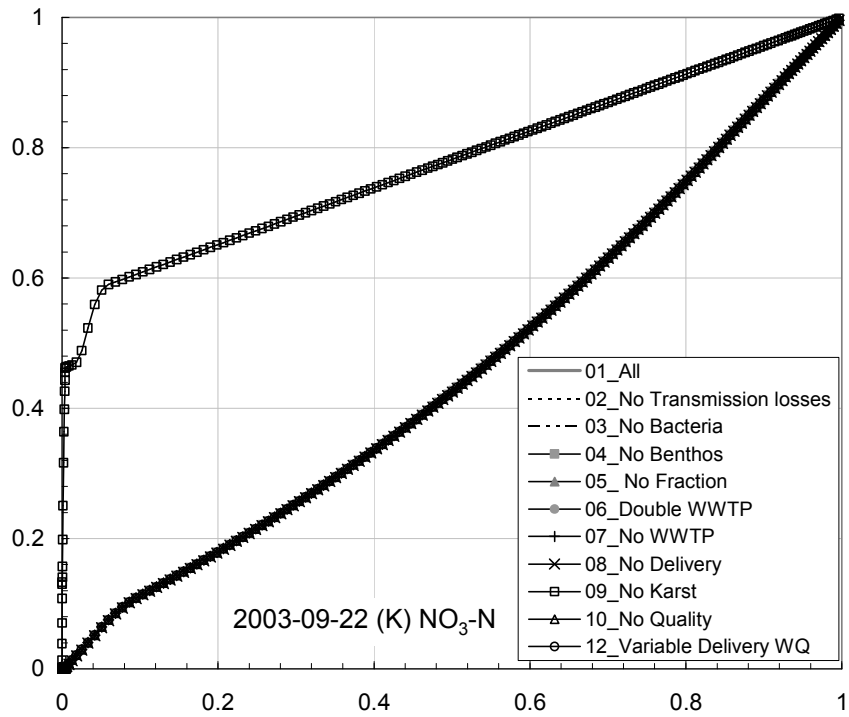


Figure 7-11: NCL- plots for measured NO<sub>3</sub>-N and all scenarios at sites K and S for 2003-09-22

## 7.5 Sensitivity of NCL-plots

Figure 7-12 shows examples for the sensitivity of NCL-plots for the flood of 2003-09-22. The event was analysed on the basis of two different periods: from 2003-09-20 until 2003-09-24 and from 2003-09-22 until 2003-09-26. The analysis was made on the basis of the same data and interpolation method.

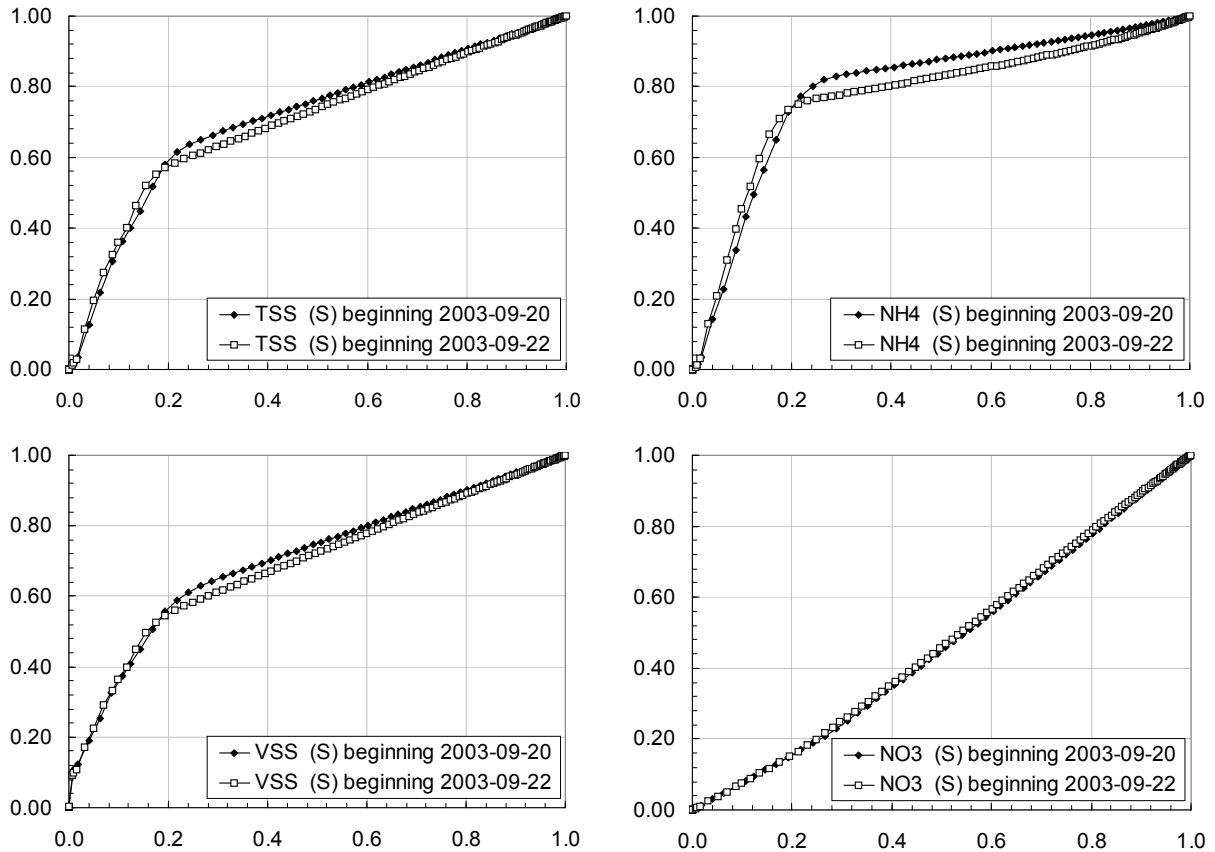


Figure 7-12: Sensitivity of NCL plots, comparison between two different periods of the of the same dataset at S

It can be seen that, even though there are some discrepancies, they seem to be small in this example. It can be concluded, that the essential part of the transport event is included in both of the regarded periods, event though the flow is still continuing.



## 7.6 Influences of low-flow variability of concentration on regression of datasets

In order to demonstrate the influence of rapid changes of concentrations in low flow, a test was made with artificial data. The aim of this test should be to show that even in an analysis of a nearly perfect simulation, there can be great deviations in terms of correlation coefficients.

In order to use a dense timeseries without greater gaps, a result of the model runs for PON concentration in the Vène was taken (data1). Starting from this, a second timeseries (data2) was created. This second timeseries shall represent a dataset with missing low-flow variation. The following rule was applied to obtain data2 from data1: if the water depth is lower than 0.05 m and the difference in concentration is higher than 10 mg/l from one step to another, the concentration was kept constant in data2. The timeseries data2 is therefore smoother and does not contain the low flow variation. This would be most likely also lacking in real measured data. Normally, measurements cannot be done with such a frequency, so that these short time variations cannot be covered in any detail. Even if measurements were done with very short time in between, the uncertainty of those -especially for particulate matter- in e.g. 5 cm flow would be extremely high in vertical as well as horizontal extent.

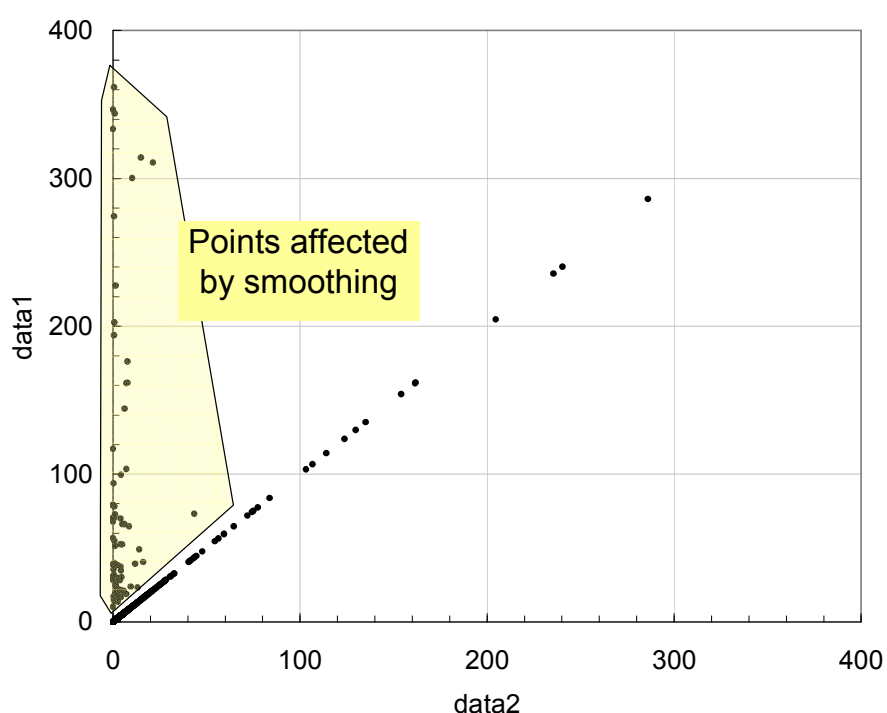


Figure 7-13: Demonstration of the influence of low flow variations on the regression of concentrations

Only 91 of 29111 points in time were replaced by this rule (points affected by smoothing in Figure 7-13), so the both datasets (data1 and data2) have more than 99.6% of their data in common. Nevertheless, those differences are important in the comparison of measurements and simulations. A calculation of the linear correlation coefficient yields only 0.25 for these two datasets, the Nash-Sutcliffe efficiency (Nash and Sutcliffe, 1970) even gives -17.6.

## 7.7 Testing and extension of the CASCADE Model

### 7.7.1 Time step

The input time step was changed to hourly values for the within-river part. Natural regimes in temporary rivers necessitate a rapid adaptation of the highly irregular flow conditions.

### 7.7.2 In-stream sediment formula

The suspended matter transport was replaced by a more physically based approach, using shear stress as the governing variable instead of velocity.

Erosion is now modelled using the formula of Partheniades (1962) and deposition is estimated with the formula of Krone (1962).

### 7.7.3 Transmission losses

As transmission losses gain importance in temporary waters, these were included in the model.

The routing calculation was based on balancing fluxes. With the need to account for transmission losses and mass retention the volume of water which is currently stored in the reach must be considered as a state variable as well. Only this will retain the mass balance.

This pool volume at a time  $n+1$  is derived from the addition of all fluxes participating to the reach inflow or outflow, so

$$\begin{aligned}\Delta V_{pool}^n &= V_{pool}^{n+1} - V_{pool}^n \\ &= (Q_{in}^n - Q_{out}^n - seep^n - evap^n) \Delta t\end{aligned}\quad \text{EQ. 7-7}$$

where

- $\Delta V_{pool}^n$ : change in pool volume at time  $n$  [ $L^3$ ]
- $V_{pool}^{n+1}$ : new pool volume at time  $n+1$  [ $L^3$ ]
- $Q_{in}, Q_{out}$ : Inflow to or outflow from reach [ $L^3T^{-1}$ ]
- seep, evap: seepage and evaporation [ $L^3T^{-1}$ ]
- $\Delta t$ : time step [T].

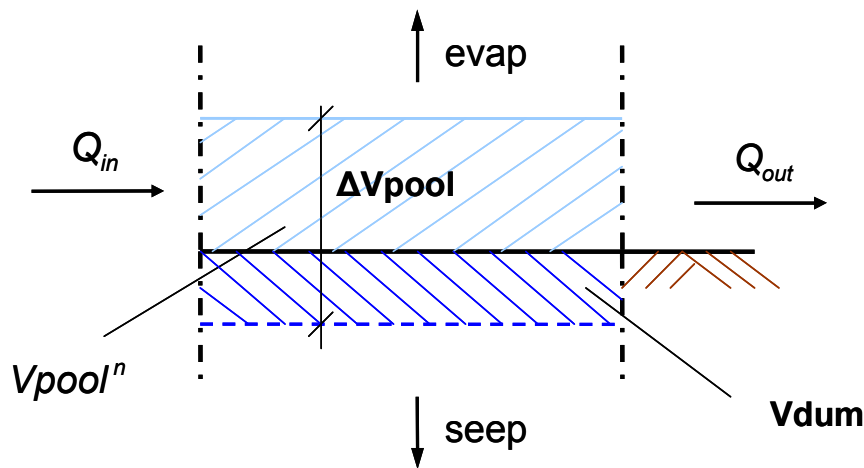


Figure 7-14: Interaction of pool volume, inflow and outflow

If the volume in the pool dries up from one time step to another the pool volume will likely become negative, on condition that transmission losses are considered.

In each time step this is tested in a two step approach:

- 1.) a temporary volume  $V_{dum}$  is calculated as sum of all fluxes and the old pool volume in the reach
- 2.) if  $V_{dum}$  is positive,  $V_{pool}$  will set to  $V_{dum}$ , if it is negative, the transmission fluxes will have to be adjusted.

$$\begin{aligned} \text{if } Q_{out} - seep - evap > Q_{in} \wedge \Delta V_{pool}^n < 0 \\ \Rightarrow V_{dum} < 0 \end{aligned} \quad \text{EQ. 7-8}$$

in which

$$V_{dum}: \quad \text{temporary value of the potential pool volume [L}^3\text{]}$$

In this case, the potential losses exceed the actual (and possible) losses.

The transmission losses are calculated on the basis of the stored water in the prior time step, the inflow and outflow as well as the seepage and evaporation (cp. EQ. 7-9)

$$\begin{aligned} tloss_{act} &= \frac{tloss_{pot} \cdot \Delta t + V_{dum}}{\Delta t} \\ seep_{act} &= m \cdot tloss_{act} \end{aligned} \quad \text{EQ. 7-9}$$

$$evap_{act} = (1-m) \cdot tloss_{act}$$

$$\text{in which: } m = \frac{seep_{pot}}{tloss_{pot}} \quad \text{EQ. 7-10}$$

To divide the total amount of lost water, the ratio of potential seepage to evaporation is calculated and multiplied with the actual transmission loss to obtain actual evaporation and seepage (cp. EQ. 7-10).

#### 7.7.4 Mass retention and first flush

In order to allow an accumulation of pollutants in standing water bodies within the reaches (here referred to as pools) the model had to be modified.

For modelling purposes, reach processes may be conceptualised as shown in Figure 3-2.

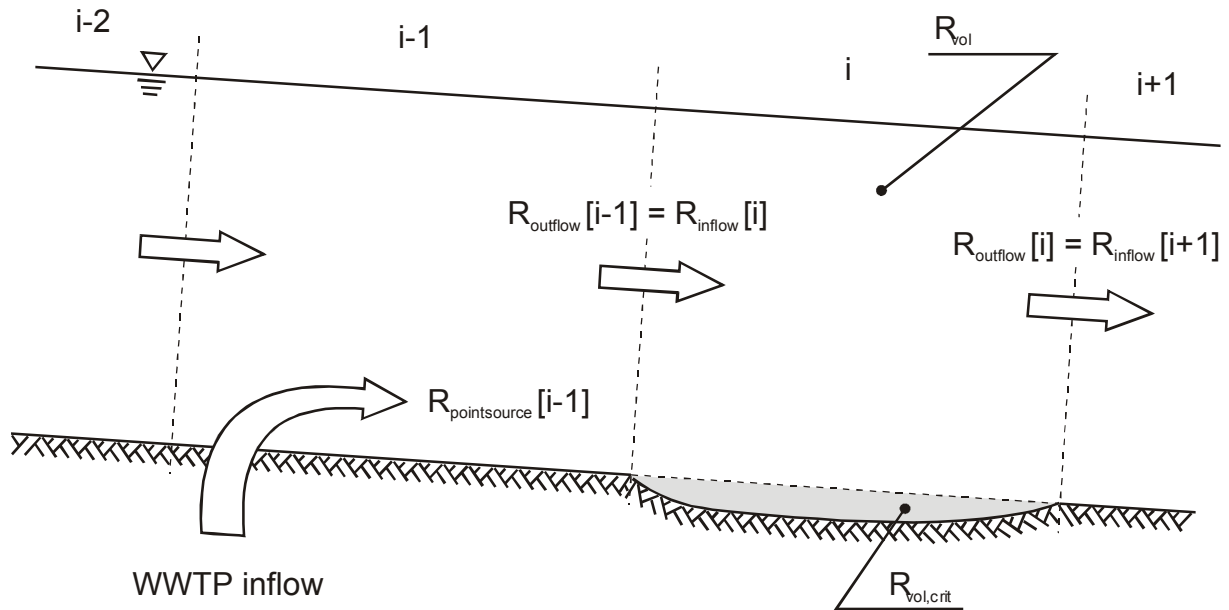


Figure 7-15: Effluent of the WWTP – situation in a typical model

A possible implementation of the annual dynamic and handling of the generation of the pools is shown in Figure 7-16. This is implemented in the CASCADE model.

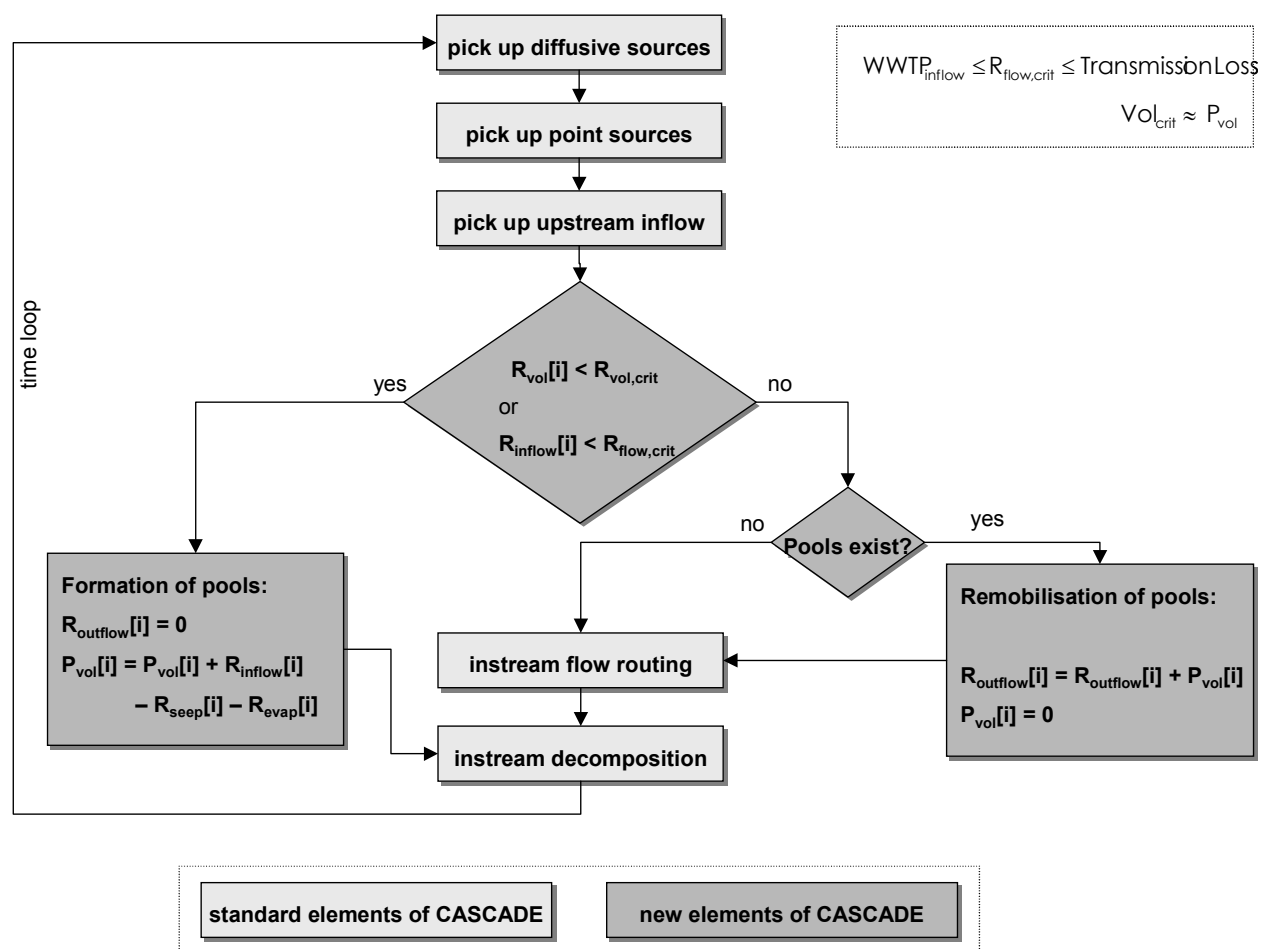


Figure 7-16: Flow chart for pool generation

In Figure 7-16 are

$R_{vol}$	Volume currently stored in the reach
$R_{outflow}[i-1]$	Outflow of the upstream reach
$R_{inflow}[i]$	inflow to the present reach
$R_{inflow}[i+1]$	inflow to the downstream reach
$R_{pointsource}[i-1]$	point sources draining into the upstream reach
$R_{vol,crit}$	critical volume of the reaches

Because reaches are normally considered to have a fixed slope between two points in common models (and approaches like the kinematic wave do not account for backwater or bi-directional flow), this approach would provide a mechanism for incorporating pools.

#### 7.7.5 Lack of mass conservation due to leading edge dip phenomena, test examples with the modified model

The model and its new pool algorithm was tested on a part of the Vène River (see above).

The integrated model contains only the main branch of the system and two point source inflows, cp. Figure 7-17.

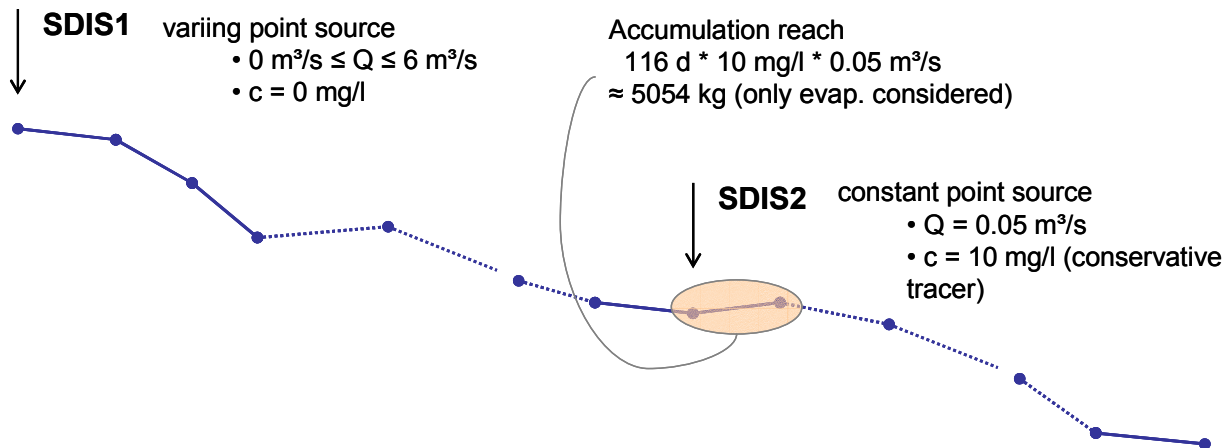


Figure 7-17: Network structure of the test cases

Point source #2 (SDIS2) represents a waste water treatment plant outlet, which was chosen to be constant both in flow and concentration over the time considered, i.e.  $0.05 \text{ m}^3/\text{s}$  ( $50 \text{ l/s}$ ) and  $10 \text{ mg/l}$  for a chosen inert soluble tracer to separate influences due to conversion of the substance.

If only evaporation is considered and if this is greater than the inflow in the following reach downstream SDIS2 no constituent will be lost during the accumulation period of 116 days and a possible accumulation of over 5000 kg may occur.

After this time in low flow condition (only point source #2 is feeding the system) the wet season starts, which means that the point source #1 (a karstic spring in this example, but it may be also any other upstream river) begins flowing.

There were three different floods with two differing intensities (in terms of time to the peak value) tested (see Figure 7-18) on two grids, the first with 34 reaches and reach length from 1000 to 1500m and the second with 160 reaches in total (reach length 200 to 300 m).

These 12 variants were all calculated within CASCADE without the pool approach, i.e. the situation before the implementation, and with the pool approach turned on.

For all 24 variants the time step was set to 5 minutes.

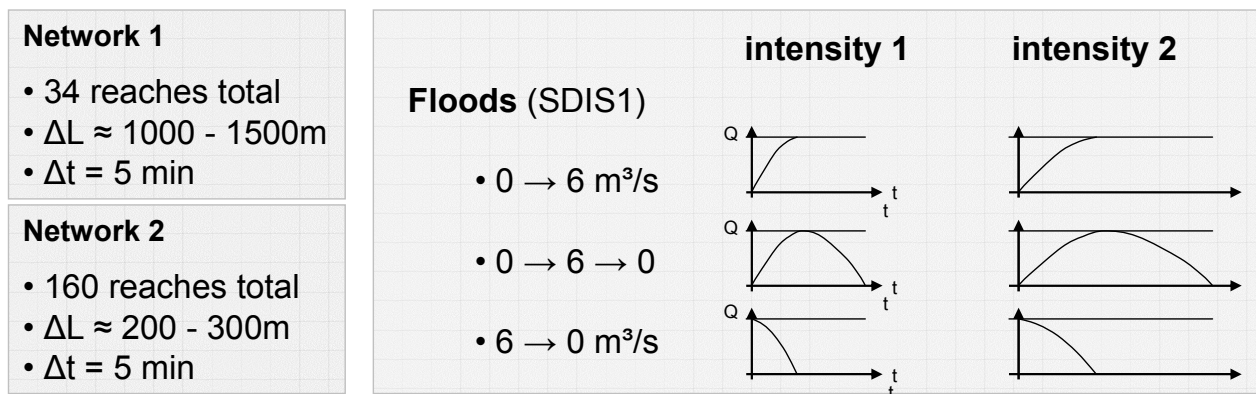


Figure 7-18: Characterization of networks and tested flood intensities

### Testing volume conservation in the application of the pool routine

To test the reliability of the implemented concept, fluxes were balanced at the accumulation reach downstream point source 2.

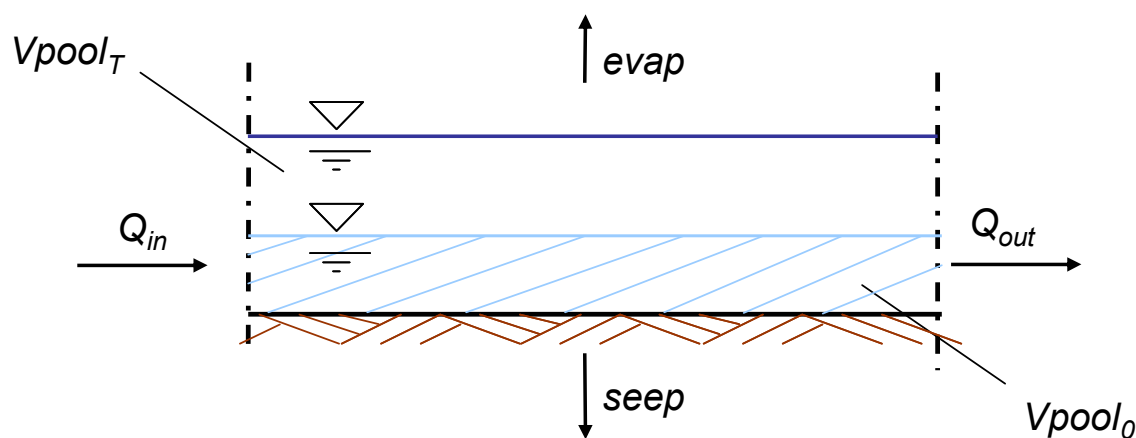


Figure 7-19: Scheme of fluxes at a reach segment

The overall computation included over 44000 time steps (more than 150 days), but only the 10000 containing the flood of SDIS1 were chosen for the sum in the mass balance.

There were two different balances, the first calculating the balance for water volume, the second balancing the mass of the transported constituent on the base of the load, see EQ. 7-11 EQ. 7-12.

$$V_{cons} [\%] = \frac{\int Q_{out} + (V_{pool_T} - V_{pool_0})}{\int Q_{in}} \cdot 100 \quad \text{EQ. 7-11}$$

$$M_{cons} [\%] = \frac{\int M_{out} + (mass_T - mass_0)}{\int M_{in}} \cdot 100 \quad \text{EQ. 7-12}$$

where

$V_{cons}, M_{cons}$ :	indicator for water volume or mass conservation resp. [%], 100 % means that all is conserved
$\int Q_{in}, \int Q_{out}$ :	sum of the inflow and outflow over all considered time steps [ $L^3T^{-1}$ ]
$\int M_{in}, \int M_{out}$ :	sum of the inflow and outflow load of the constituent [ $MT^{-1}$ ]
$V_{pool_0}, mass_0$ :	pool volume and mass stored at the beginning, [ $L^3$ ] and [M]
$V_{pool_T}, mass_T$ :	pool volume and mass stored after time T and T is equal to end of mass balance calculation, [ $L^3$ ] and [M]

The results of the mass balance calculation (see chapter 7.8) show that water is conserved in this example for all variants. The calculation for the routed constituent is still erroneous especially for the coarser grid with rapidly changing flows (intensity 1). The situation with net 2 and intensity 1 is slightly better.

The outcomes of the variants with the fine network seem to be reasonable. It was discovered that these calculation also did not lead to correct results (cp. Figure 7-20)

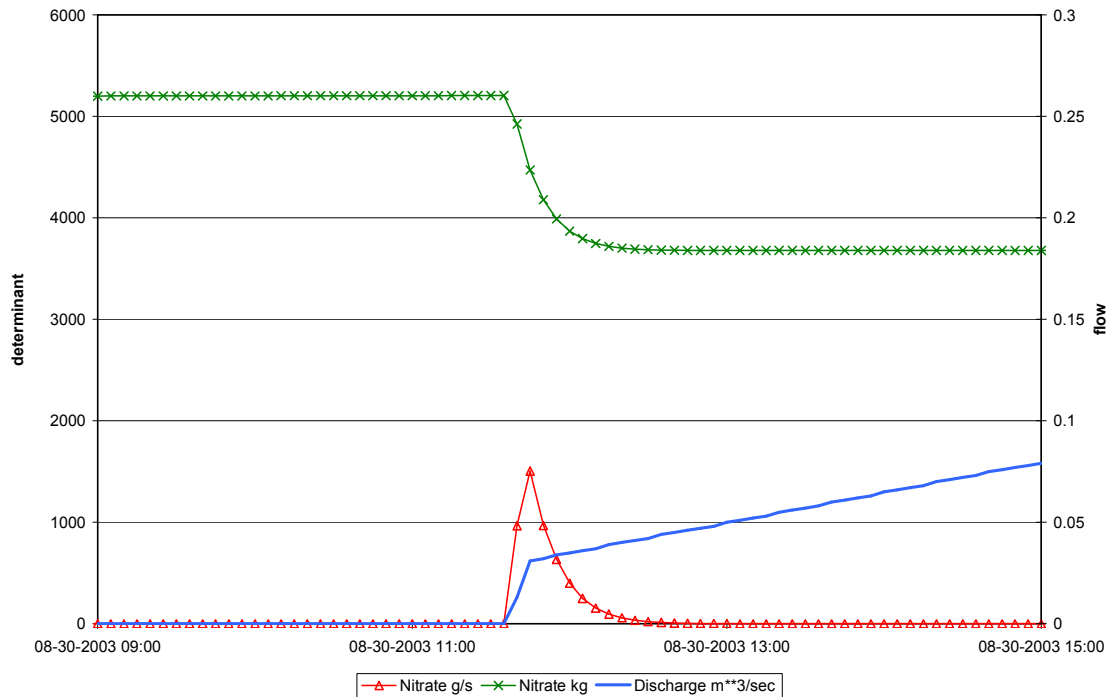


Figure 7-20: Resulting error in mass stored in an accumulation reach

Figure 7-20 shows the course of the mass stored in the reach, the discharge and the load of the constituent (i.e. the downstream release).

It can be seen that if the flow starts again after the period of accumulation, mass will be transported downstream again, but not all mass will be removed from storage.

The reason for the incomplete resuspension lies in the mode of discretisation in the routing of the finite differences approach and will be explained in the following.

If the pool volume is less than a threshold volume ( $\text{poolthresh} = \text{depth of depression} \times \text{width} \times \text{length}$ ) and the inflow volume is less or equal to the transmission losses, the outflow of the reach will be zero (see Figure 7-21).



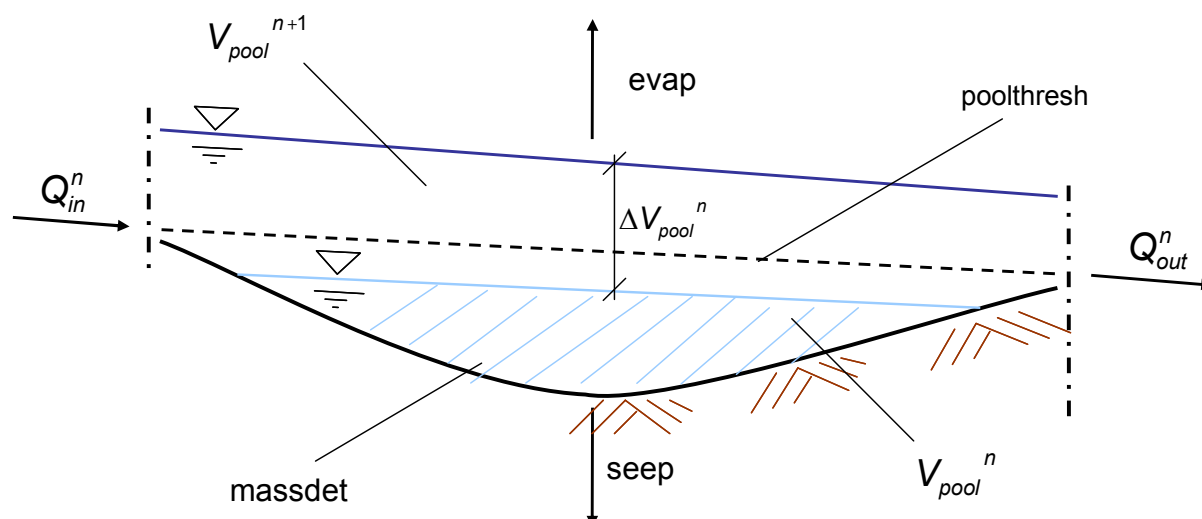


Figure 7-21: Situation in the pool at the transition phase from “no-flow” to “flow” condition

The pool is characterised by its volume ( $V_{pool}$ ) and its concentration ( $c_{pool}$ ) of the constituent.

$$\text{massdet}^{n+1} = (Q_{in}^n \cdot c_{in}^n - Q_{out}^n \cdot c_{out}^n) - c_{pool}^n \cdot \text{seep}^n \quad \text{EQ. 7-13}$$

$$c_{pool}^n = \frac{\text{massdet}^n}{V_{pool}^n} \quad \text{EQ. 7-14}$$

where

$\text{massdet}^{n+1}$ : mass stored in the reach at time n+1 [M]

$Q_{in}^n, Q_{out}^n$ : inflow and outflow load of constituent at time n [ $\text{MT}^{-1}$ ]

$c_{in}^n, c_{out}^n$ : inflow and outflow concentration of constituent at time n [ $\text{ML}^{-3}$ ]

$c_{pool}^n$ : concentration of the pool at time n [ $\text{ML}^{-3}$ ]

In the case of rising flows upstream (beginning of the flood at SDIS1) the pool volume will increase and exceed the critical pool threshold at some point. At this time in the transition from a non-flowing to flowing condition, the downstream concentration  $c_{out}^n$  will be equal to the pool concentration.

A problem occurs in this transition time step for the upstream node of the reach. On the left-hand side (upstream) the concentration will be equal to the inflow concentration but on the right-hand side (downstream) the concentration will be equal to the normally higher pool concentration.

For the example, the upstream inflow concentration was chosen as boundary condition. If advection and dispersion were considered, the distribution of the concentration of the conservative tracer would develop as in Figure 7-22.

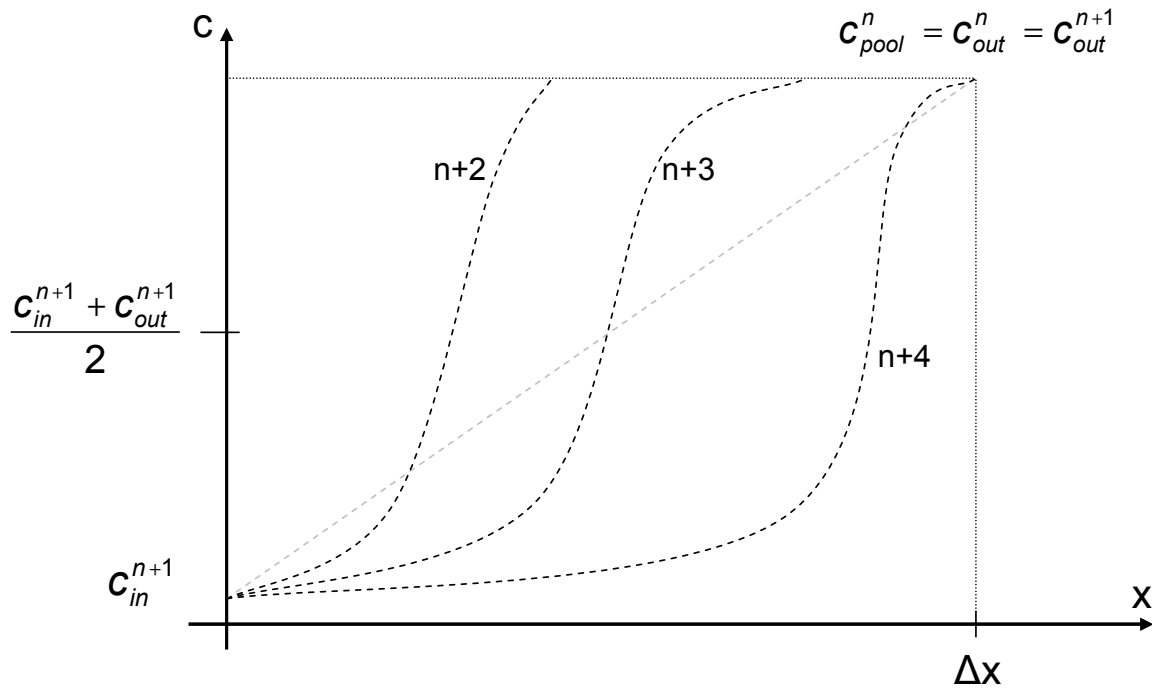


Figure 7-22: Development of concentration (conservative tracer) in a pool after flush of clear water

Because the derived system of algebraic equations which represents the discretised PDEs is solved only at the nodes, i.e. the reach length is the smallest unit, there must be some interpolation between the nodes.

CASCADE is based on a Variable Parameter Muskingum-Cunge method solved with an improved four-point interpolation scheme showed in Holden and Stevenson (1988) (see chapter 3.1).

Variable parameter means, that each time step an equation of the form (here without diffusive sources) of EQ. 7-15 is solved and the parameters for the equation are not fixed over the whole computation but are depending on the actual condition of the system and therefore are variable in time.

$$Q_4 = c_1 Q_1 + c_2 Q_2 + c_3 Q_3 \quad \text{or in other notation} \quad \text{EQ. 7-15}$$

$$Q_{n+1}^{n+1} = c_n^n Q_n^n + c_n^{n+1} Q_n^{n+1} + c_{n+1}^n Q_{n+1}^n$$

in which

- $Q_4, Q_{n+1}^{n+1}$ : Flow at downstream node at the new time step [ $L^3T^{-1}$ ]
- $Q_1, Q_n^n$ : Flow at upstream node at the old time step [ $L^3T^{-1}$ ]
- $Q_2, Q_n^{n+1}$ : Flow at the upstream node at the new time step [ $L^3T^{-1}$ ]
- $Q_3, Q_{n+1}^n$ : Flow at the downstream node at the old time step [ $L^3T^{-1}$ ]

The parameters could be as in Figure 7-23.

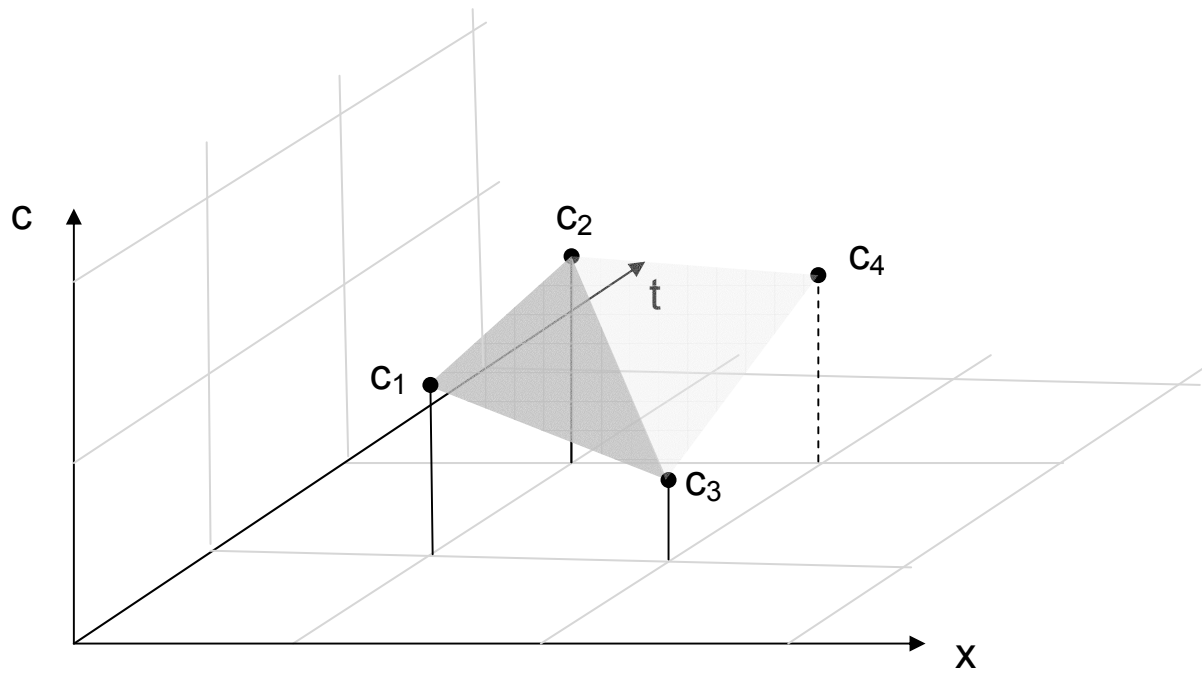


Figure 7-23: Parameter in the Variable Parameter Muskingum-Cunge method (VPMC)

It is now clear, that the new flow at point 4 is interpolated and weighted on the basis of the condition at the known time step and the boundary conditions (the slope and friction are among others used to calculate the parameters).

For simplicity it is assumed that the interpolating function is linear (which is not true because we have an interpolation in time and space with varying conditions) as shown in Figure 7-24.

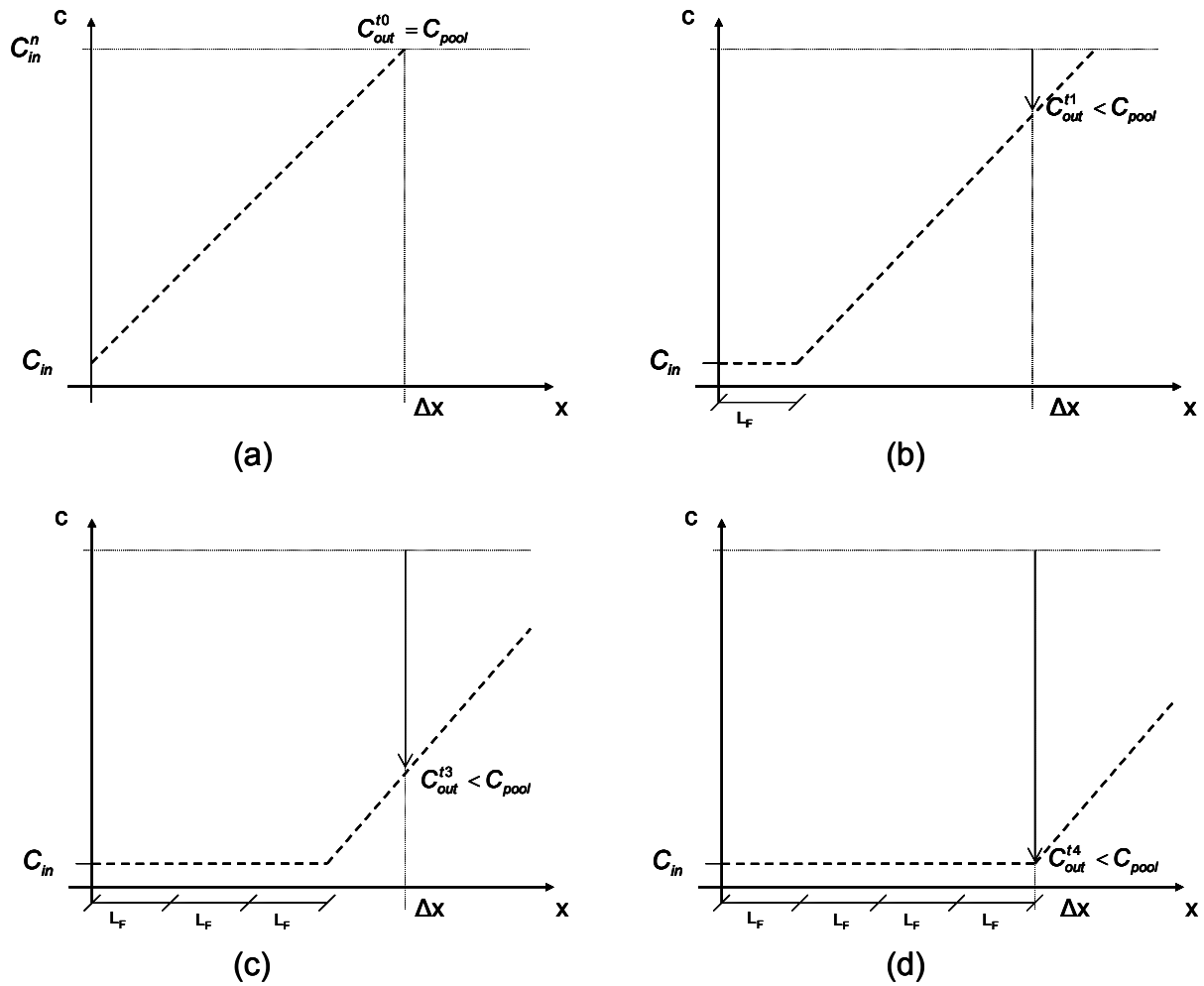


Figure 7-24: Development with a linear gradation of concentration as starting conditions

$$L_f = \Delta t \cdot \bar{v} \quad \text{EQ. 7-16}$$

$$\frac{R \text{ length}}{L_f} = k \quad \text{EQ. 7-17}$$

in which

$L_f$ : Travel Distance of a particle in  $\Delta t$  [L]  
 $\bar{v}$ : mean velocity [ $LT^{-1}$ ]

For the first time step when the flow starts (the transition time step) the situation is similar to the state (a).

If only advection will be considered this distribution is translated without changing its shape (b-c) and the outflow concentration will constantly decrease until it is equal to the inflow concentration at time (d).

If we compare the scheme from Figure 7-24 with the expected schematic in Figure 7-25, it is obvious, that approaches like this will underestimate the storage volume significantly.

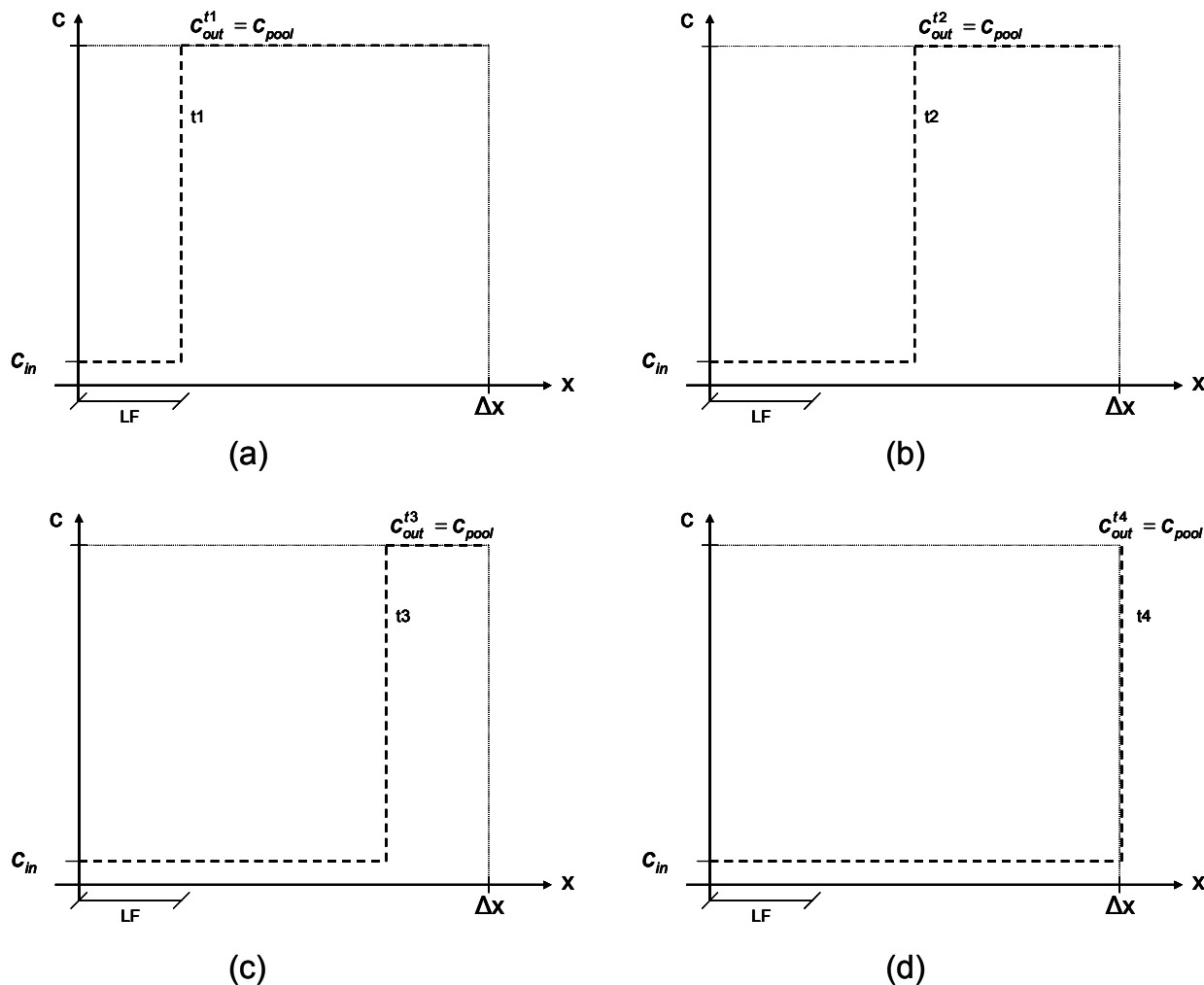


Figure 7-25: Expected development in an advection scheme without dispersion

The mass in the reach is the integral of the concentration over the control volume, thus

$$massdet = \int_{V_{pool}} c dV \quad \text{EQ. 7-18}$$

The problem is due to the mode how the amount of stored mass is handed over to the VPMC approach. If the concentrations are given as described above, the course of the concentration over time as shown in Figure 7-25 cannot reproduced easily. Due to these steep gradients in concentration, a great numerical diffusion is introduced.

### 7.7.6 Conclusions if the testing

A further use of the FDM discretisation in combination with the shown solution of the kinematic wave approach is not appropriate to simulate the interactive mass accumulation/mass release processes happening in temporary waters.

Although a good representation of the shape of the hydrograph (which is one strength of the method above) is of importance for the calibration and eventually short time management measures, mass balance must not be neglected in the context of temporary waters.

In the light of the above shown limitations in the mass balance –together with the fact, that the code is written in a traditional linear way which complicates a further development- other approaches seem to be more appropriate than the one applied in CASCADE.

This finally lead to the decision to only continue the effort to enhance the MOHID Water Modelling System and to the development of the new tempQsim – STREAM model. This model uses a finite volume approach that is mass conservative by construction and furthermore owes superior features in terms of GUI and an advanced programming structure.

## 7.8 Mass balance for pool accumulation in finite difference Muskingum-Cunge routing method

The tests were done at two different intensities (in terms of duration) for the flushing floods at SDIS1 with unchanged concentration levels at SDIS2 and similar shapes of the hydrographs. Each flood was tested in three differing intervals: from no-flow to the climax, from no-flow to climax again to no-flow and from climax to no-flow.

Table 7-1 and Table 7-2 show the results of the mass balance investigation described in chapter 7.7.5 for the coarser network 1 and the finer network 2 respectively.

For each network, the simulation was done either with consideration of a pool or without both for water volume and pollutant mass.

Table 7-1: Mass balance calculation for VAR1 with CASCADE

with pool								
NET1		SDIS1	SDIS2	total inflow volume m <sup>3</sup>	total outflow volume m <sup>3</sup>	pool storage start m <sup>3</sup>	pool storage end m <sup>3</sup>	volume conservation %
water volume	Flood1	0-6m <sup>3</sup> /s	0,05m <sup>3</sup> /s	8812429	8809982	0.00	2429.98	100.00
		0-6-0m <sup>3</sup> /s	10mg/l	598120	598505	0.00	0.00	100.06
		6-0m <sup>3</sup> /s		9275691	9278524	357.39	0.00	100.03
	Flood2	0-6m <sup>3</sup> /s		8887566	8884779	0.00	2787.89	100.00
		0-6-0m <sup>3</sup> /s		787021	787074	0.00	0.00	100.01
		6-0m <sup>3</sup> /s		9389455	9392295	357.39	0.00	100.03
		SDIS1	SDIS2	total inflow mass g	total outflow mass g	pool storage start g	pool storage end g	mass conservation%
pollutant mass	Flood1	0-6m <sup>3</sup> /s	0,05m <sup>3</sup> /s	1500000	10214144	4499850.00	-4701559.37	67.52
		0-6-0m <sup>3</sup> /s	10mg/l	1500000	9517946	4499850.00	699600.00	381.18
		6-0m <sup>3</sup> /s		1500000	789651	42446.28	752870.94	100.01
	Flood2	0-6m <sup>3</sup> /s		1500000	4130937	4499850.00	1878702.59	100.65
		0-6-0m <sup>3</sup> /s		1500000	3526936	4499850.00	2482778.13	100.66
		6-0m <sup>3</sup> /s		1500000	881848	42446.28	660674.17	100.01
without pool								
NET1		SDIS1	SDIS2	total inflow volume m <sup>3</sup>	total outflow volume m <sup>3</sup>	pool storage start m <sup>3</sup>	pool storage end m <sup>3</sup>	volume conservation %
water volume	Flood1	0-6m <sup>3</sup> /s	0,05m <sup>3</sup> /s	9148148	9145544	0.00	2604.62	100.00
		0-6-0m <sup>3</sup> /s	10mg/l	625065	625194	0.00	-137.42	100.00
		6-0m <sup>3</sup> /s		9626917	9629651	0.00	-2742.03	100.00
	Flood2	0-6m <sup>3</sup> /s		9278119	9275380	0.00	2739.70	100.00
		0-6-0m <sup>3</sup> /s		928112	928111	0.00	0.86	100.00
		6-0m <sup>3</sup> /s		9799993	9802732	0.00	-2738.84	100.00
		SDIS1	SDIS2	total inflow mass g	total outflow mass g	pool storage start g	pool storage end g	mass conservation %
pollutant mass	Flood1	0-6m <sup>3</sup> /s	0,05m <sup>3</sup> /s	1500000	1505524	0.00	-5388.33	100.01
		0-6-0m <sup>3</sup> /s	10mg/l	1500000	1503128	0.00	-2991.99	100.01
		6-0m <sup>3</sup> /s		1500000	1497604	0.00	2396.33	100.00
	Flood2	0-6m <sup>3</sup> /s		1500000	1502494	0.00	-2494.18	100.00
		0-6-0m <sup>3</sup> /s		1500000	1500012	0.00	-12.40	100.00
		6-0m <sup>3</sup> /s		1500000	1497518	0.00	2481.78	100.00

The test were done at two different intensities (in terms of duration) for the flushing floods at SDIS1 with unchanged concentration levels at SDIS2 and similar shapes of the hydrographs. Each flood was tested in three differing intervals: from no-flow to the climax, from no-flow to climax again to no-flow and from climax to no-flow.

Table 7-2: Mass balance calculation for VAR2 with CASCADE

with pool								
NET2		SDIS1	SDIS2	total inflow volume m <sup>3</sup>	total outflow volume m <sup>3</sup>	pool storage start m <sup>3</sup>	pool storage end m <sup>3</sup>	volume conservation %
water volume	Flood1	0-6m <sup>3</sup> /s	0,05m <sup>3</sup> /s	8058434	8058245	0.00	180.64	100.00
		0-6-0m <sup>3</sup> /s	10mg/l	535660	535675	0.00	0.00	100.00
		6-0m <sup>3</sup> /s		8482227	8482430	110.90	0.00	100.00
	Flood2	0-6m <sup>3</sup> /s		8068286	8068084	0.00	201.00	100.00
		0-6-0m <sup>3</sup> /s		581431	581434	0.00	0.00	100.00
		6-0m <sup>3</sup> /s		8518145	8518350	110.90	0.00	100.00
		SDIS1	SDIS2	total inflow mass g	total outflow mass g	pool storage start g	pool storage end g	mass conservation%
pollutant mass	Flood1	0-6m <sup>3</sup> /s	0,05m <sup>3</sup> /s	1500000	4431201	4499850.00	2288509.21	147.99
		0-6-0m <sup>3</sup> /s	10mg/l	1500000	3706075	4499850.00	3023544.94	148.65
		6-0m <sup>3</sup> /s		1500000	787590	46283.67	758772.52	100.01
	Flood2	0-6m <sup>3</sup> /s		1500000	2308347	4499850.00	3693227.15	100.12
		0-6-0m <sup>3</sup> /s		1500000	1658349	4499850.00	4343098.06	100.11
		6-0m <sup>3</sup> /s		1500000	819932	46291.36	726434.70	100.01
without pool								
NET2		SDIS1	SDIS2	total inflow volume m <sup>3</sup>	total outflow volume m <sup>3</sup>	pool storage start m <sup>3</sup>	pool storage end m <sup>3</sup>	volume conservation %
water volume	Flood1	0-6m <sup>3</sup> /s	0,05m <sup>3</sup> /s	9152668	9152523	0.00	146.25	100.00
		0-6-0m <sup>3</sup> /s	10mg/l	1174617	1174594	0.00	23.19	100.00
		6-0m <sup>3</sup> /s		10171951	10172073	0.00	-123.06	100.00
	Flood2	0-6m <sup>3</sup> /s		9283475	9283327	0.00	147.25	100.00
		0-6-0m <sup>3</sup> /s		928076	928076	0.00	0.04	100.00
		6-0m <sup>3</sup> /s		9794603	9794750	0.00	-147.21	100.00
		SDIS1	SDIS2	total inflow mass g	total outflow mass g	pool storage start g	pool storage end g	mass conservation %
pollutant mass	Flood1	0-6m <sup>3</sup> /s	0,05m <sup>3</sup> /s	1500000	1501244	0.00	-1507.92	99.98
		0-6-0m <sup>3</sup> /s	10mg/l	1500000	1500870	0.00	-1130.79	99.98
		6-0m <sup>3</sup> /s		1500000	1499626	0.00	377.13	100.00
	Flood2	0-6m <sup>3</sup> /s		1500000	1501086	0.00	-1086.05	100.00
		0-6-0m <sup>3</sup> /s		1500000	1500003	0.00	-2.96	100.00
		6-0m <sup>3</sup> /s		1500000	1498935	0.00	1065.09	100.00

In total there were made 24 runs for each of the two networks.



## 7.9 Important formulas for the benthos module in the tempQsim – STREAM model

### POM dynamic in stream

$$\begin{aligned} \frac{\partial \Phi^{PON}}{\partial t} = & \left[ (1 - f_{inorg}^{phy})(1 - f_{orgD}^{phy})(ex^{phy} + r^{phy}) + m^{phy} \right] \alpha_{N:C}^{phy} \Phi^{phy} \\ & - (\mu_{PON}^{bact} - m^{bact} \alpha_{N:C}^{bact}) \Phi^{bact} \\ & + \left[ (1 - f_{inorg}^{zoo})(1 - f_{orgD}^{zoo})(ex^{zoo}) + m^{phy} \right] \alpha_{N:C}^{zoo} \Phi^{zoo} + (\delta_N^{zoo} + \phi_N^{zoo}) \Phi^{zoo} \\ & - (1 - f_{org}) K_{doc}^{PON} \Phi^{PON} \end{aligned}$$

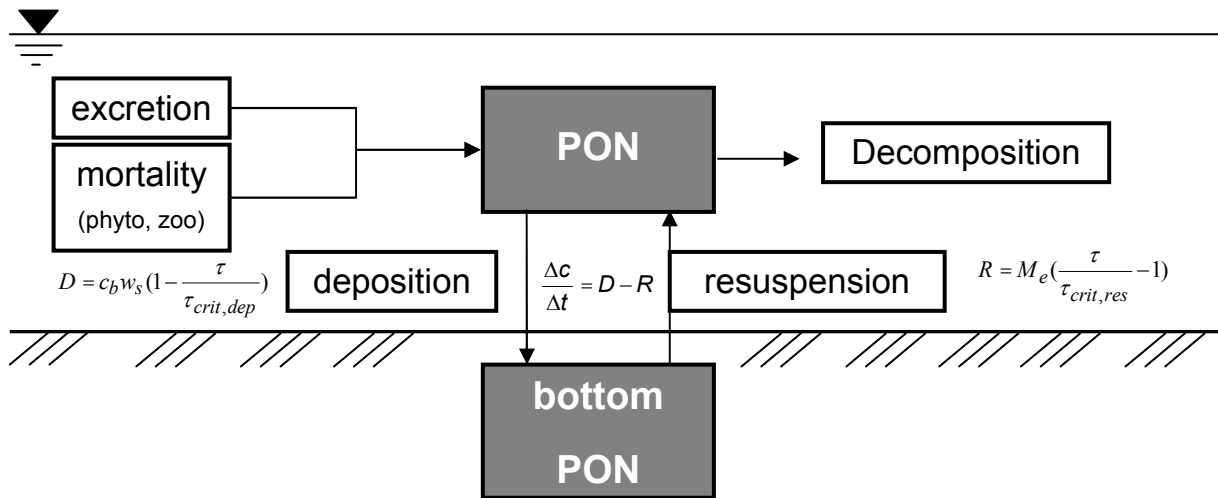


Figure 7-26: PON dynamics in the tempQsim - STREAM model

### DOM dynamic in stream

$$\begin{aligned} \frac{\partial \Phi^{PON}}{\partial t} = & (1 - f_{inorg}^{phy}) f_{orgD}^{phy} (ex^{phy} + r^{phy}) \alpha_{N:C}^{phy} \Phi^{phy} \\ & + (1 - f_{inorg}^{dia}) f_{orgD}^{dia} (ex^{dia} + r^{dia}) \alpha_{N:C}^{dia} \Phi^{dia} \\ & - \mu_{DONnr}^{bact} \Phi^{bact} \\ & + (1 - f_{inorg}^{cil}) f_{orgD}^{cil} ex^{cil} \Phi^{cil} \\ & + (1 - f_{inorg}^{zoo}) f_{orgD}^{zoo} ex^{zoo} \alpha_{N:C}^{zoo} \Phi^{zoo} \end{aligned}$$

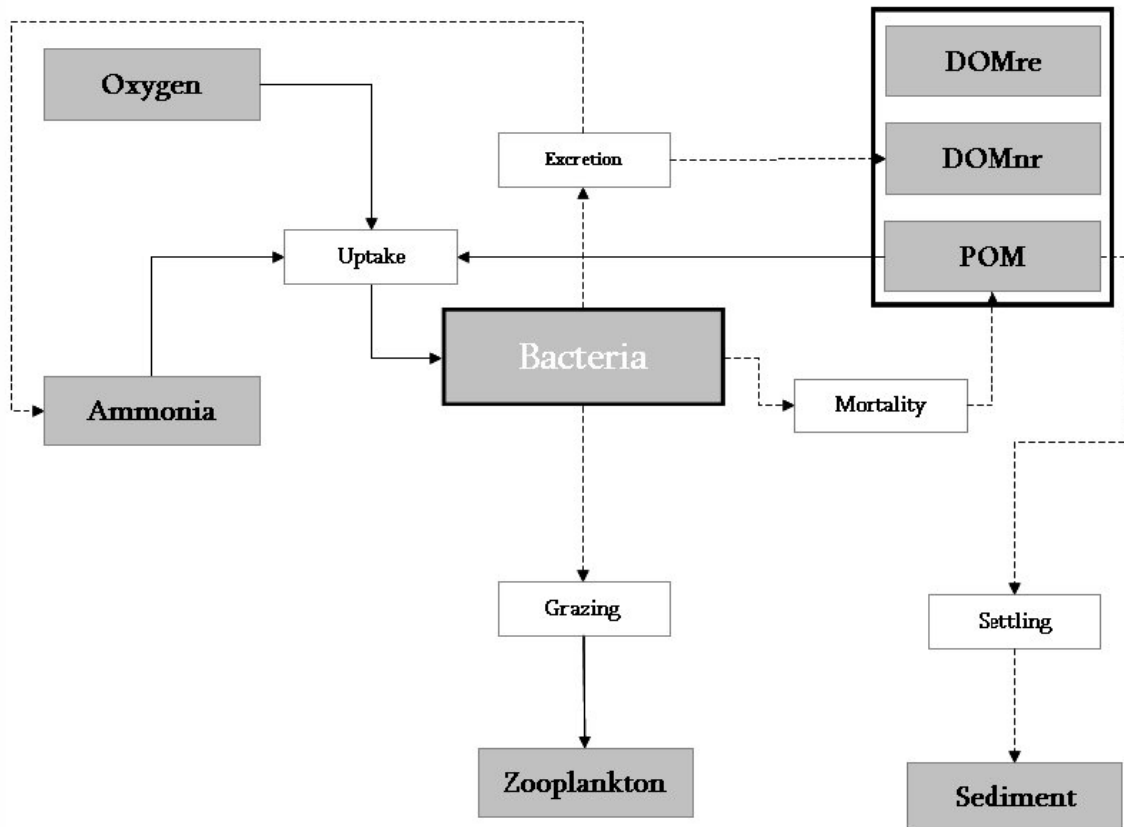
**Bacteria dynamic in stream**

Figure 7-27: Bacteria dynamics in the tempQsim - STREAM model

$$\frac{\partial \Phi^{bact}}{\partial t} = (\mu^{bact} - e^{bact} - m^{bact}) \Phi^{bact} - G^{bact}$$

in which

$\mu^{bact}$  : Total bacterial uptake

$e^{bact}$  : Excretion Rate

$m^{bact}$  : Natural Mortality Rate (non-predatory)

$G^{bact}$  : Grazing Rate

**POM dynamic in benthos**

$$\frac{\partial \Phi^{POM}}{\partial t} = \frac{\mu_{POM}^{bact} \cdot \Phi^{bact}}{\alpha_{N:C}^{bact}}$$

***DOMnr dynamic in benthos***

$$\frac{\partial \Phi^{DOM}}{\partial t} = \frac{\mu_{DOM}^{bact} \cdot \Phi^{bact}}{\alpha_{N:C}^{bact}}$$

***POMr dynamic in benthos***

$$\frac{\partial \Phi^{POMr}}{\partial t} = m^{bact} \Phi^{bact} \cdot \alpha_{N:C}^{bact}$$

$\alpha_{N:C}^{bact}$  : Bacteria Nitrogen/Carbon ratio

$m^{bact}$  : Natural mortality rate

$\Phi^{bact}$  : Bacteria concentration

## 7.10 Added and modified code in the tempQsim – STREAM model

In the following chapter, the most important enhancements and modifications of the tempQsim-STREAM model are collected.

### 7.10.1 ModuleBenthos

This module considers all biological conversion factors, which happen in the benthos. It interacts with the chosen water quality module for the aquatic phase. Exchanges can take place e.g. for particulates via erosion and deposition.

#### 7.10.1.1 Subroutine for the benthic bacteria computation

```

subroutine ComputeBenthicBact(Index, WaterVolume)

!Arguments-----
integer, intent(IN)                :: Index
real(8), dimension(:), pointer    :: WaterVolume

!Local-----
integer                :: PON
integer                :: BAC
integer                :: DONnr
integer                :: PONr
!
integer                :: O
real                   :: s1, s2, xa, xb, ya, yb
real                   :: Mortality                = null_real
real                   :: BacteriaPONUptake        = null_real
real                   :: BacteriaDONUptake        = null_real
real                   :: BacteriatotalUptake      = null_real

real                   :: BacteriatotalUptakeM    = null_real
real                   :: BacteriaPONUptakeM     = null_real
real                   :: BacteriaDONUptakeM     = null_real
!Temporary-----
real                   :: TBacteriaLimitationFactor = null_real
real                   :: BottomPONConc           = null_real
real                   :: BottomDONConc          = null_real

!Begin-----

PON = Me%PropIndex%PON
PONr = Me%PropIndex%PONr
BAC = Me%PropIndex%Bact
DONnr = Me%PropIndex%DONnr

!Concentration of bottom_PON in terms of the bottom reactor
! WaterVolume is the VolumeNew of the Node and the reactor Volume is taken as a percentage
! of this Volume
! *1000 is the conversion from kg/m3=g/l to mg/l

BottomPONConc = Me%ExternalVar%Mass(PON, index) &
/ (WaterVolume(index)*Me%Bact%BotReactorDepth)*1000.
BottomDONConc = Me%ExternalVar%Mass(DONnr, index) &
/ (WaterVolume(index))*1000.

!TBacteriaLimitationFactor : limitation by temperature
s1 = (1. / (Me%Bact%TOptBacteriaMin - Me%Bact%TBacteriaMin)) &
* log((Me%Bact%BK2 * (1.0 - Me%Bact%BK1)) &
/ (Me%Bact%BK1 * (1.0 - Me%Bact%BK2)))

s2 = (1. / (Me%Bact%TBacteriaMax - Me%Bact%TOptBacteriaMax)) &
* log((Me%Bact%BK3 * (1.0 - Me%Bact%BK4)) &
/ (Me%Bact%BK4 * (1.0 - Me%Bact%BK3)))

ya = exp(s1 * (Me%ExternalVar%Temperature(index) - Me%Bact%TBacteriaMin))
yb = exp(s2 * (Me%Bact%TBacteriaMax - Me%ExternalVar%Temperature(index)))

xa = (Me%Bact%BK1 * ya) / (1.0 + Me%Bact%BK1 * (ya - 1.0))
xb = (Me%Bact%BK4 * yb) / (1.0 + Me%Bact%BK4 * (yb - 1.0))

TBacteriaLimitationFactor = xa * xb

if ((BottomPONConc > Me%Bact%BacMinSub) .OR. &
(BottomDONConc > Me%Bact%BacminSub)) then

if (BottomPONConc > Me%Bact%BacMinSub) then
! Bacteria PON uptake (1/d)

```

```

BacteriaPONUptake = TBacteriaLimitationFactor &
                  * Me%Bact%BacMaxUptake &
                  * BottomPONConc &
                  / (Me%Bact%NSatConstBac &
                    + BottomPONConc)
! Bacteria PON uptake (kgC/d)
BacteriaPONUptakeM = BacteriaPONUptake &
                  * Me%ExternalVar%Mass(BAC, Index)

if (BacteriaPONUptakeM > Me%ExternalVar%Mass(PON, index)) then
  BacteriaPONUptakeM = Me%ExternalVar%Mass(PON, index)
endif
! Bacteria PON uptake (kgN/d)
BacteriaPONUptakeM = BacteriaPONUptakeM &
                  * Me%Bact%NC_Ratio

else
  BacteriaPONUptake = 0.0
  BacteriaPONUptakeM = 0.0
endif

if (BottomDONConc > Me%Bact%BacMinSub) then
! Bacteria DON uptake (1/d)
BacteriaDONUptake = TBacteriaLimitationFactor &
                  * Me%Bact%BacMaxUptake &
                  * BottomDONConc &
                  / (Me%Bact%NSatConstBac &
                    + BottomDONConc)
! Bacteria DON uptake (kgC/d)
BacteriaDONUptakeM = BacteriaDONUptake &
                  * Me%ExternalVar%Mass(BAC, Index)

if (BacteriaDONUptakeM > Me%ExternalVar%Mass(DONnr, index)) then
  BacteriaDONUptakeM = Me%ExternalVar%Mass(DONnr, index)
endif
! Bacteria PON uptake (kgN/d)
BacteriaDONUptakeM = BacteriaDONUptakeM &
                  * Me%Bact%NC_Ratio

else
  BacteriaDONUptake = 0.0
  BacteriaDONUptakeM = 0.0
endif
else
  BacteriaPONUptake = 0.0
  BacteriaPONUptakeM = 0.0
  BacteriaDONUptake = 0.0
  BacteriaDONUptakeM = 0.0
endif

!BacteriaTotalUptake, uptake in kgN/d
BacteriaTotalUptakeM = (BacteriaDONUptakeM &
                      + BacteriaPONUptakeM)

! Bacteria total uptake in kgC/d
BacteriatotalUptakeM= BacteriatotalUptakeM &
                    / Me%Bact%NC_Ratio

!Organic nitrogen from dead bacteria in kgC/d
Mortality = Me%ExternalVar%Mass(BAC, Index) &
          * Me%Bact%MortalityRate

Me%ExternalVar%Mass(BAC, Index) = Me%ExternalVar%Mass(BAC, Index) &
                                + (BacteriatotalUptakeM &
                                  -Mortality) &
                                * Me%DTDay

Me%ExternalVar%Mass(PONr, Index) = Me%ExternalVar%Mass(PONr, Index) &
                                + Mortality * Me%Bact%NC_Ratio &
                                * Me%DTDay

Me%ExternalVar%Mass(PON, Index) = Me%ExternalVar%Mass(PON, Index) &
                                - BacteriaPONUptakeM &
                                * Me%DTDay

Me%ExternalVar%Mass(DONnr, Index) = Me%ExternalVar%Mass(DONnr, Index) &
                                - BacteriaDONUptakeM &
                                * Me%DTDay

end subroutine ComputeBenthicBact

```

## 7.10.1.2 Parameters for bacteria computation in benthos

```

subroutine ReadBactParameters

!Local-----
integer                                :: iflag, STAT_CALL

!Begin-----

call GetData(Me%Bact%MortalityRate,      &
             Me%ObjEnterData, iflag,    &
             SearchType = FromFile,     &
             keyword    = 'BACT_MORTALITY', &
             Default    = 0.1,          &
             ClientModule = 'ModuleBenthos', &
             STAT      = STAT_CALL)
if(STAT_CALL .NE. SUCCESS_) stop 'ReadBactParameters - ModuleBenthos - ERR01'

call GetData(Me%Bact%NC_Ratio,          &
             Me%ObjEnterData, iflag,    &
             SearchType = FromFile,     &
             keyword    = 'BACT_NC_RATIO', &
             Default    = 0.18,         &
             ClientModule = 'ModuleBenthos', &
             STAT      = STAT_CALL)
if(STAT_CALL .NE. SUCCESS_) stop 'ReadBactParameters - ModuleBenthos - ERR10'

call GetData(Me%Bact%PC_Ratio,          &
             Me%ObjEnterData, iflag,    &
             SearchType = FromFile,     &
             keyword    = 'BACT_PC_RATIO', &
             Default    = 0.024,       &
             ClientModule = 'ModuleBenthos', &
             STAT      = STAT_CALL)
if(STAT_CALL .NE. SUCCESS_) stop 'ReadBactParameters - ModuleBenthos - ERR20'

call GetData(Me%Bact%BacMaxUptake,     &
             Me%ObjEnterData, iflag,    &
             SearchType = FromFile,     &
             keyword    = 'BMAXUPTA',   &
             Default    = 0.20,        &
             ClientModule = 'ModuleBenthos', &
             STAT      = STAT_CALL)
if(STAT_CALL .NE. SUCCESS_) stop 'ReadBactParameters - ModuleBenthos - ERR30'

call GetData(Me%Bact%NSatConstBac,     &
             Me%ObjEnterData, iflag,    &
             SearchType = FromFile,     &
             keyword    = 'BACNCONS',   &
             Default    = 0.08,        &
             ClientModule = 'ModuleBenthos', &
             STAT      = STAT_CALL)
if(STAT_CALL .NE. SUCCESS_) stop 'ReadBactParameters - ModuleBenthos - ERR40'

call GetData(Me%Bact%BotReactorDepth,  &
             Me%ObjEnterData, iflag,    &
             SearchType = FromFile,     &
             keyword    = 'BOTTOMRDEPTH', &
             Default    = 0.3,         &
             ClientModule = 'ModuleBenthos', &
             STAT      = STAT_CALL)
if(STAT_CALL .NE. SUCCESS_) stop 'ReadBactParameters - ModuleBenthos - ERR50'

call GetData(Me%Bact%BacMinSub,        &
             Me%ObjEnterData, iflag,    &
             SearchType = FromFile,     &
             keyword    = 'BACMINSUB',  &
             Default    = 0.01,        &
             ClientModule = 'ModuleBenthos', &
             STAT      = STAT_CALL)
if(STAT_CALL .NE. SUCCESS_) stop 'ReadBactParameters - ModuleBenthos - ERR60'

!TOptBacteriaMin, minimum temperature of the optimal interval for the Bacteria growth,
call GetData(Me%Bact%TOptBacteriaMin,  &
             Me%ObjEnterData, iflag,    &
             SearchType = FromFile,     &
             keyword    = 'TOPTBMIN',   &
             default    = 24.8,         &
             ClientModule = 'ModuleBenthos', &
             STAT      = STAT_CALL)
if (STAT_CALL .NE. SUCCESS_) stop 'ReadBactParameters - ModuleBenthos - ERR70'

!TOptBacteriaMax, maximum temperature of the optimal interval for the Bacteria growth,
call GetData(Me%Bact%TOptBacteriaMax,  &
             Me%ObjEnterData, iflag,    &
             SearchType = FromFile,     &
             keyword    = 'TOPTBMAX',   &

```

```

        default      = 25.1,                                &
        ClientModule = 'ModuleBenthos',                    &
        STAT         = STAT_CALL)
if (STAT_CALL .NE. SUCCESS_) stop 'ReadBactParameters - ModuleBenthos - ERR80'

!TBacteriaMin, minimum tolerable temperature of the interval for the Bacteria growth,
call GetData(Me%Bact%TBacteriaMin,
            Me%ObjEnterData, iflag,
            SearchType   = FromFile,
            keyword      = 'TBMIN',
            default      = 5.0,
            ClientModule = 'ModuleBenthos',
            STAT         = STAT_CALL)
if (STAT_CALL .NE. SUCCESS_) stop 'ReadBactParameters - ModuleBenthos - ERR90'

!TBacteriaMax, maximum tolerable temperature of the interval for the Bacteria growth,
call GetData(Me%Bact%TBacteriaMax,
            Me%ObjEnterData, iflag,
            SearchType   = FromFile,
            keyword      = 'TBMAX',
            default      = 35.0,
            ClientModule = 'ModuleBenthos',
            STAT         = STAT_CALL)
if (STAT_CALL .NE. SUCCESS_) stop 'ReadBactParameters - ModuleBenthos - ERR100'

!BK1, constant to control temperature response curve shape
call GetData(Me%Bact%BK1,
            Me%ObjEnterData, iflag,
            SearchType   = FromFile,
            keyword      = 'TBCONST1',
            default      = 0.05,
            ClientModule = 'ModuleBenthos',
            STAT         = STAT_CALL)
if (STAT_CALL .NE. SUCCESS_) stop 'ReadBactParameters - ModuleBenthos - ERR110'

!BK2, constant to control temperature response curve shape
call GetData(Me%Bact%BK2,
            Me%ObjEnterData, iflag,
            SearchType   = FromFile,
            keyword      = 'TBCONST2',
            default      = 0.98,
            ClientModule = 'ModuleBenthos',
            STAT         = STAT_CALL)
if (STAT_CALL .NE. SUCCESS_) stop 'ReadBactParameters - ModuleBenthos - ERR120'

!BK3, constant to control temperature response curve shape
call GetData(Me%Bact%BK3,
            Me%ObjEnterData, iflag,
            SearchType   = FromFile,
            keyword      = 'TBCONST3',
            default      = 0.98,
            ClientModule = 'ModuleBenthos',
            STAT         = STAT_CALL)
if (STAT_CALL .NE. SUCCESS_) stop 'ReadBactParameters - ModuleBenthos - ERR130'

!BK4, constant to control temperature response curve shape
call GetData(Me%Bact%BK4,
            Me%ObjEnterData, iflag,
            SearchType   = FromFile,
            keyword      = 'TBCONST4',
            default      = 0.02,
            ClientModule = 'ModuleBenthos',
            STAT         = STAT_CALL)
if (STAT_CALL .NE. SUCCESS_) stop 'ReadBactParameters - ModuleBenthos - ERR140'
end subroutine ReadBactParameters

```

### 7.10.2 *ModuleDrainageNetwork*

The drainage network module considers most of the hydraulic processes, including erosion and deposition, routing of water and of properties. It calls e.g. the modules responsible for water quality in the aquatic phase and in the benthos.

## 7.10.2.1 Calculate loads

```

subroutine CalculateLoad()

!Arguments-----
!Local-----
type (T_Property), pointer      :: Property
integer                       :: NodeID, i
type (T_Node), pointer        :: CurrNode
type (T_Reach), pointer       :: DownReach
real(8)                       :: Flow

nullify (Property)
Property => Me%FirstProperty

do while (associated (Property))

  if (Property%ComputeOptions%ComputeLoad) then

    do NodeID = 1, Me%TotalNodes

      if (Me%OpenpointsFlow(NodeID) == OpenPoint) then

        CurrNode => Me%Nodes (NodeID)

        Flow = 0.0

        !Adds Inflow due to channel flow
        do i = 1, CurrNode%DownStreamReaches
          DownReach => Me%Reaches (CurrNode%DownStreamReaches (i))
          Flow = Flow + dble(DownReach%FlowNew)
        enddo

        Property%Load(NodeID) = Property%Concentration(NodeID) * Flow

      endif

    enddo

  end if

  Property => Property%Next

enddo

end subroutine CalculateLoad

```

## 7.10.2.2 Calculate TSS

```

subroutine CalculateTSS(TSSProperty)

!Arguments-----
type (T_Property), pointer      :: TSSProperty

!Local-----
type (T_Property), pointer      :: Property
type (T_Property), pointer      :: PropertySedF !Cohesive Sediment Fine
type (T_Property), pointer      :: PropertySedM !Cohesive Sediment Medium
type (T_Property), pointer      :: PropertySedC !Cohesive Sediment Coarse
type (T_Property), pointer      :: PropertyVSS

integer                       :: NodeID
!-----

!Sum Porperties in TSS

if (Me%ComputeOptions%CalcFractionSediment) then
  call SearchProperty(PropertySedF, PropertyXIDNumber = COHSED_FINE_)
  call SearchProperty(PropertySedM, PropertyXIDNumber = COHSED_MEDIUM_)
  call SearchProperty(PropertySedC, PropertyXIDNumber = COHSED_COARSE_)
  call SearchProperty(PropertyVSS, PropertyXIDNumber = VSS_)
  do NodeID = 1, Me%TotalNodes
    !TSS in mgTS/l
    TSSProperty%Concentration(NodeID) = PropertySedF%Concentration(NodeID) &
    + PropertySedM%Concentration(NodeID) &
    + PropertySedC%Concentration(NodeID) &
    + PropertyVSS%Concentration(NodeID)

    TSSProperty%BottomConc(NodeID) = PropertySedF%BottomConc(NodeID) &
    + PropertySedM%BottomConc(NodeID) &
    + PropertySedC%BottomConc(NodeID) &
    + PropertyVSS%BottomConc(NodeID)
  enddo
else
  call SearchProperty(Property, PropertyXIDNumber = Cohesive_Sediment_)
  call SearchProperty(PropertyVSS, PropertyXIDNumber = VSS_)

```



```

do NodeID = 1, Me%TotalNodes
  !TSS in mgTS/l
  TSSProperty%Concentration(NodeID) = Property%Concentration(NodeID)      &
  + PropertyVSS%Concentration(NodeID)
  TSSProperty%BottomConc(NodeID) = Property%BottomConc(NodeID)          &
  + PropertyVSS%BottomConc(NodeID)
enddo
end if
!-----
end subroutine CalculateTSS

```

### 7.10.2.3 Calculate VSS

```

subroutine CalculateVSS(VSSProperty)
!Arguments-----
type (T_Property), pointer          :: VSSProperty
!External-----
integer                             :: STAT_CALL
!Local-----
type (T_Node ), pointer             :: CurrNode
type (T_Property), pointer          :: Property
integer                             :: NodeID
real                                 :: Ratio
!-----
!Sum Porperties in VSS
  nullify (CurrNode)
do NodeID = 1, Me%TotalNodes
  VSSProperty%Concentration(NodeID) = 0.0
  VSSProperty%BottomConc(NodeID) = 0.0
  Property => Me%FirstProperty
  do while (associated (Property))
    if (isVSS(Property%ID%IDNumber)) then
      call GetWQRatio(InterfaceID = Me%ObjInterface,      &
                    PropertyID = Property%ID%IDNumber,  &
                    Ratio = Ratio,                      &
                    STAT = STAT_CALL)
      !VSS in mgTS/l
      VSSProperty%Concentration(NodeID) = VSSProperty%Concentration(NodeID)      &
      + Ratio * Property%Concentration(NodeID)
      if (Property%ComputeOptions%BottomFluxes) then
        !VSS in kgTS/m2
        VSSProperty%BottomConc(NodeID) = VSSProperty%BottomConc(NodeID)      &
        + Ratio * Property%BottomConc(NodeID)
      endif
    endif
    Property => Property%Next
  end do
enddo
!-----
end subroutine CalculateVSS

```

### 7.10.3 ModuleGlobalData

This module reads, stores and manages global parameters for the computation. Most of them can be given in the steering file.

### 7.10.3.1 Function to define VSS

```

logical function isVSS(Property)
!Arguments-----
integer, intent (IN) :: Property

!-----

cd1 :   if ((Property == Phytoplankton_      ) .OR. (Property == Diatoms_          ) .OR.      &
           (Property == Zooplankton_       ) .OR. (Property == Ciliate_         ) .OR.      &
           (Property == Bacteria_         ) .OR. (Property == PON_             ) .OR.      &
           (Property == PONRefractory_    )) then

           isVSS = .TRUE.

       else

           isVSS = .FALSE.

       end if cd1

end function isVSS

```

### 7.10.4 Module WaterQuality

#### 7.10.4.1 Get NC-Ratios

```

subroutine GetNCRatio(WaterQualityID, Property, Ratio, STAT)

!Arguments-----
integer                :: WaterQualityID
real                  :: Ratio
integer               :: Property
integer, optional, intent (OUT) :: STAT

!External-----
integer                :: ready_

!Local-----
integer                :: STAT_
real                   :: AlphaNTS

!-----

STAT_ = UNKNOWN_

call Ready(WaterQualityID, ready_)

cd1 :   if ((ready_ .EQ. IDLE_ERR_      ) .OR.      &
           (ready_ .EQ. READ_LOCK_ERR_)) then
           !Ratio of gN in g dry substance according to Redfiel: 16mol*14gN/mol / 2749 gTS
           AlphaNTS = 16.*14./2749.
           Ratio = 1.0/AlphaNTS !for all non-living VSS as PON and PONr
           if (Property == Me%PropIndex%Phyto      ) Ratio = Me%AlfaPhytoNC /AlphaNTS
           if (Property == Me%PropIndex%Diatoms    ) Ratio = Me%OMAlfaNC /AlphaNTS
           if (Property == Me%PropIndex%Zoo       ) Ratio = Me%AlfaZooNC /AlphaNTS
           if (Property == Me%PropIndex%Ciliate   ) Ratio = Me%AlfaCilNC /AlphaNTS
           if (Property == Me%PropIndex%Bacteria   ) Ratio = Me%AlfaBacteriaNC/AlphaNTS

           STAT_ = SUCCESS_
       else
           STAT_ = ready_
       end if cd1

       if (present(STAT))      &
           STAT = STAT_

!-----

end subroutine GetNCRatio

```

## 7.11 Further enhancements of the delivery part in the Vène

### 7.11.1 Delivery Model

A delivery model was needed for the collection and concentration of the runoff derived from rainfall. During the time of the study, the catchment model MOHID Land was still under development.

As it was already fully operational and calibrated, the French model MERCEDES, developed by IRD was used in the beginning. The model was off-line coupled with the CASCADE model as well as with the tempQsim – STREAM model, i.e. output of MERCEDES was handed over to the instream models at predefined inflow points.

Due to the lack of longer time series it was later decided to construct a new delivery model, which also allowed some changes in the parameter settings. As this also allowed a joint calibration of delivery and instream part, the case of the flood of 2003-09-22 was regarded in more detail and the possibilities to solve the issue of the lacking first main peak with an adopted delivery model were investigated.

The model takes into account spatially variable rainfall from three sites (if available). For each of the 9 inflow points, the rainfall was interpolated by the Isohyeten method. Figure 7-28 shows results with varied runoff coefficients without the consideration of rainfall concentration.

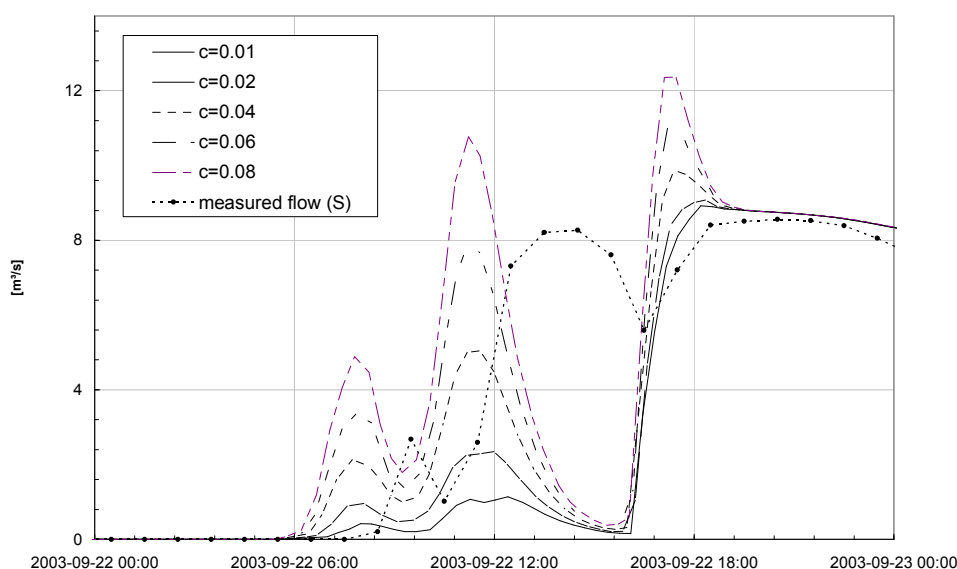


Figure 7-28: Variation of the runoff coefficient  $c$  in the delivery model without retention for 2003-09-22

Obviously, the computation without any delay in the transfer from rain over runoff to discharge shows a too fast reaction. To include a better representation of the flow concentration, a storage cascade approach with three linear storages according to the following formula was applied (Scholz, 1995):

$$q_t = 3\alpha \cdot q_{t-1} - 3\alpha^2 \cdot q_{t-2} + \alpha^3 q_{t-3} + (1 - \alpha)^3 \cdot I_t \quad \text{EQ. 7-19}$$

in which

$q_t$ :	runoff at time t [ $L^3M^0T^{-1}$ ]
$\alpha = \frac{2 \cdot k / \Delta t - 1}{2 \cdot k / \Delta t + 1}$ :	storage coefficient [-]
$q_{t-1}, q_{t-2}$ :	runoff at time t-1 and t-2 [ $L^3M^0T^{-1}$ ]
$I_t = (N_{eff-1} \cdot A_E) / \Delta t$ :	input of rainfall at time t-1 to t [ $L^3M^0T^{-1}$ ]
$N_{eff}$ :	effective rainfall [ $L^3M^0T^{-1}$ ]
$A_E$ :	area of effective rainfall [ $L^2$ ]
$k = 0.25 \cdot (t_f + t_a)$	storage constant [T], with $t_f=210$ min as longest flow time in the channel and $t_a=2$ min as longest overland flow time (Euler, 1978)
$\Delta t$ :	current time step, t-t <sub>1</sub> [ $L^0M^0T^1$ ]

A simulation with this approach is shown in Figure 7-29. The storage coefficient was calculated after Euler (1978).

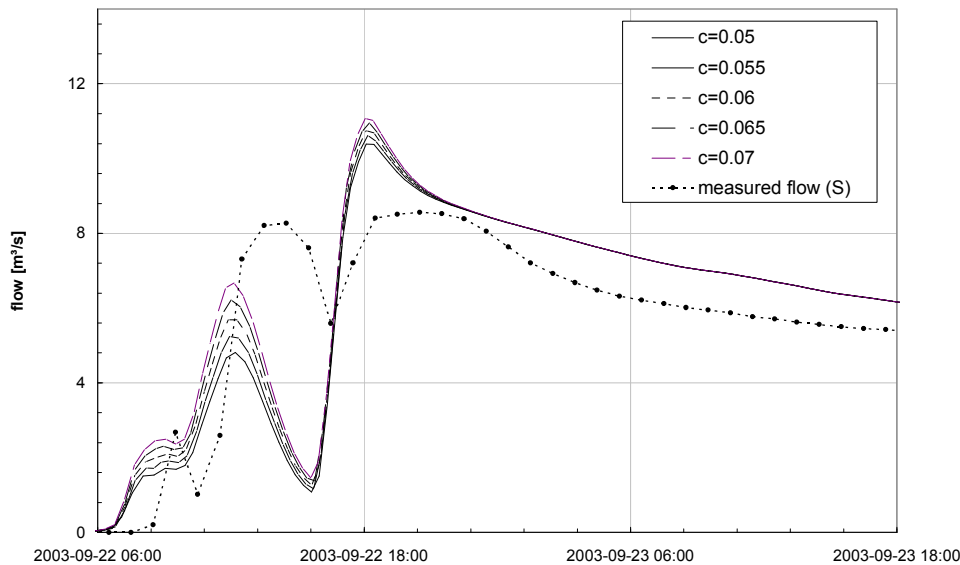


Figure 7-29: Variation of the runoff coefficient  $c$  in the delivery model with retention of a 3 linear storage cascade with storage constant = 53 min for 2003-09-22

The results of Figure 7-28 promised, that with a consideration of a flow concentration, the peaks of the delivery part would shift in the direction of the measurements and reduce the peak value.

It seems that, in order to reach the first maximum of the flood of 2003-09-22, the values for the runoff coefficient and the storage constant will exceed realistic value ranges. The test result in Figure 7-29 shows some progress for this flood and further improvements would definitely be possible through calibration. But the problems become obvious, when studying other floods –e.g. the one of 2003-04-19– with this parameter set (see Figure 7-30).

The variants in Figure 7-30 all enormously overestimate the flow at the onset of the rainfall event, so a further adoption of the delivery model in this direction was discarded.

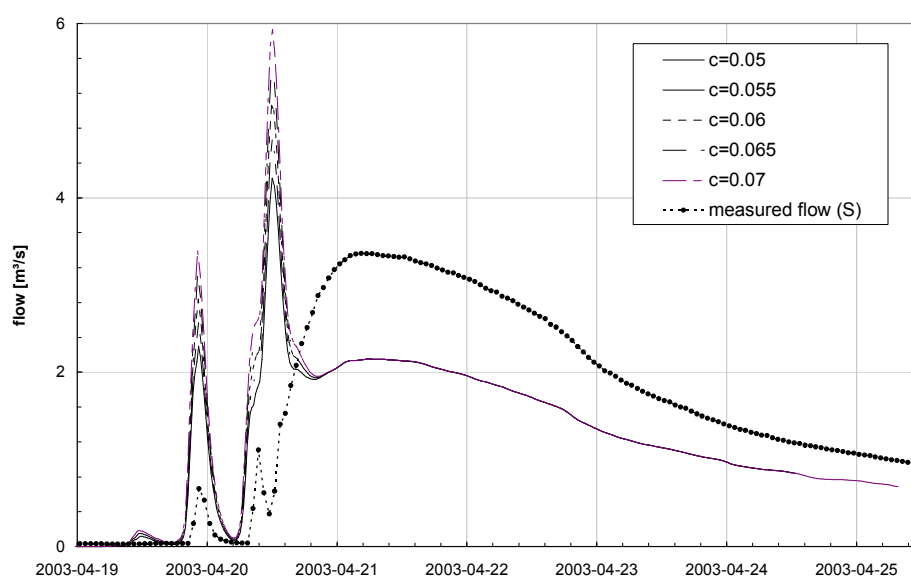


Figure 7-30: Variation of the runoff coefficient  $c$  in the delivery model with retention of a 3 linear storage cascade with storage constant = 53 min for 2003-04-19

The conclusion was made, that a better representation of the flood is not possible on the basis of the available data as well as with the used delivery models. A more sophisticated approach should be applied in this context in the future, taking into account a good representation of spatial rainfall distribution based on radar data as well as a sound simulation of the actual soil conditions at the onset of the flooding.

The scenarios of chapter 5.3 were computed with a version of this new delivery model with a consideration of the cascade retention, a storage constant of 50 min and a runoff coefficient of 0.015. Even if this set was not able to reproduce the biggest floods of the two studied years, it would be the best approximation possible.

### 7.11.2 Simulations with measured flow at S

In order to better verify the accumulation processes of the model and to exclude the influences of the delivery part of the catchment, the model was applied with an enhanced delivery flow. This delivery was derived from difference of the measurements at station S and at station K. The karst was eliminated from the flow at S including a transfer of one hour. The remaining flow is a good representation of the runoff which is added to the stream on the way from K to S. This was discharged as an additional source upstream of the WWTP at point d (Montbazin). It was created to represent the missing delivery inflow caused by the surrounding areas, which was not possible to reproduce in this flood (see above in chapter 7.3) The boundary conditions in terms of water quality concentrations for this new source were chosen the same as for the other delivery part inflows.

Figure 7-31 shows the results of the computation. The flow is reproduced correctly. Apart from recession of the karst it matches the measurements.

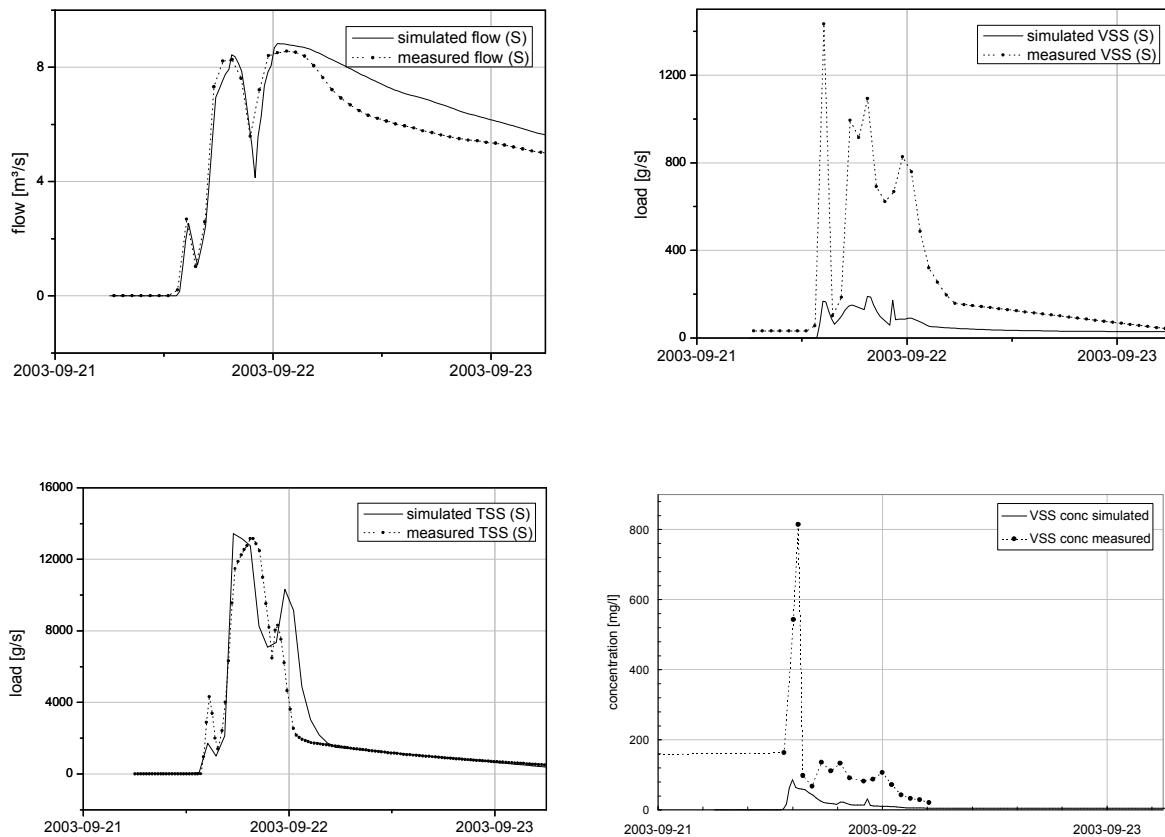


Figure 7-31: Simulation with input of measured flow from S upstream from d for 2003-09-22

The loads of TSS show good coincidence, but not the ones of VSS, where the concentrations as well as the loads are highly underestimated.

The comparison of the dynamic of the transport in Figure 7-31 shows, that with a better representation of the delivery part of the model, the results for at least TSS can be increased significantly.

However, the reasons for the increased VSS transport of the Vène must be further investigated. As pointed out earlier, the reason may be searched in the import of organic matter by the vegetation near the channel, by an overflow of the waste water treatment plants during these events or a combination of both.

### 7.11.3 Simulations with production function and variable delivery concentrations

It was found before (chapter 5.5) and also by other studies (e.g. Deletic et al., 1997), that a presetting of constant concentrations in the overland flow is inappropriate in many cases. It was shown here especially for volatile suspended solids.

Due to the fact that the overland flow and erosion were not modelled, the build-up on the surface was not approximated in terms of mass as in Deletic et al. (1997), but in terms of concentration.

A first attempt to account for this dynamic was done with the last scenario “variable delivery WQ”, which used an adjustment of the runoff concentration depending on the current overland flow intensity. Depending on the summed overland flow of all subbasins, the concentration of the delivery part was either in- or decreased, e.g. for PON in the range of 0.2 to 1.2 mg/l.

Because this adoption seemed to be a promising method for a further enhancement, additional tests were made on the basis of the two first flush floods in the Vène and results will be presented below for particulate organic nitrogen (PON) as a representation for the build-up of organic matter. In order to exclude the underestimation of the overland flow in the model, two different delivery models were created. They both included the enhanced flow representation shown in chapter 7.11.2. Further, they used two different approaches to account for varying overland runoff concentrations: (i) a production function in dependence of the cumulative rainfall of the last 3 days and (ii) with a direct dependence on the antecedent dry day period (ADD).

#### ***Adaptation with a production function***

With this approach, the concentration coming from the overland passage is rising during dry periods and falling during wet periods within a defined range.

$$\text{if } \sum_{t-72}^t R > 15 \wedge PON_{t-1} > 1$$

$$PON_t = PON_{t-1} - PON_{t-1} \cdot 0.5 \cdot \frac{\sum_{t-72}^t R}{(\sum_{t-72}^t R) + 60} \quad \text{EQ. 7-20}$$

$$\text{if } \sum_{t-72}^t R \leq 15 \wedge PON_{t-1} < 100$$

$$PON_t = PON_{t-1} + \frac{5}{PON_{t-1}} \quad \text{EQ. 7-21}$$

$$\text{else}$$

$$PON_t = PON_{t-1} \quad \text{EQ. 7-22}$$

in which

t:	current time [h]
R:	measured rainfall [mm]
$PON_{t-1}$ , $PON_t$ :	concentration of PON at time t-1 and t [mg/l]

As shown in EQ. 7-20, decrease of the concentration follows a Monod-kinetic, with 0.5 as maximum increment and 60mm rainfall as half saturation constant. This means that during a

storm with a total rainfall of 60mm over the last 3 days, the concentration is removed by  $\frac{1}{4}$  each hour. The increasing part follows a simpler approach.

### ***Adaptation depending on ADD***

In this approach the antecedent dry day period was calculated for each timestep. It was defined, that a dry day (without significant rainfall) will occur, if the daily rainfall does not exceed 20mm (EQ. 7-23).

$$\begin{aligned} & \text{if } \sum_{d-1}^d R < 20 \\ & \quad ADD = ADD + 1 \\ & \text{else} \\ & \quad ADD = 0 \end{aligned} \tag{EQ. 7-23}$$

$$PON_t = \frac{49}{35} ADD + 1 \tag{EQ. 7-24}$$

where

d:	current day [d]
t:	current time [h]
ADD:	antecedent dry days [d]

The concentration was then calculated by EQ. 7-24, which was determined by a linear interpolation of the assumed concentrations during the two first flush floods in 2003 and 2004. The concentration would therefore be 1 mg/l (for the event 2004-09-13) with no ADD and 50 mg/l for a ADD of 35 days, which is -following the definition of EQ. 7-23- the dry period before the event at 2003-09-22.

Because this adoption has a timestep of a day, it was later modified to consider dilution during the actual rainfall event.

$$\begin{aligned} & \text{if } \sum_{d-1}^d R < 20 \wedge R_t > 0 \\ & \quad PON_t = PON_{t-1} - \frac{R}{\max(R)} \cdot PON_{t-1} \\ & \text{else} \\ & \quad PON_t = \frac{49}{35} ADD + 1 \end{aligned} \tag{EQ. 7-25}$$

in which

$\max(R)$ :	maximum daily rainfall in the regarded period [mm]
-------------	--

The performance of this last approach is shown in Figure 7-32.



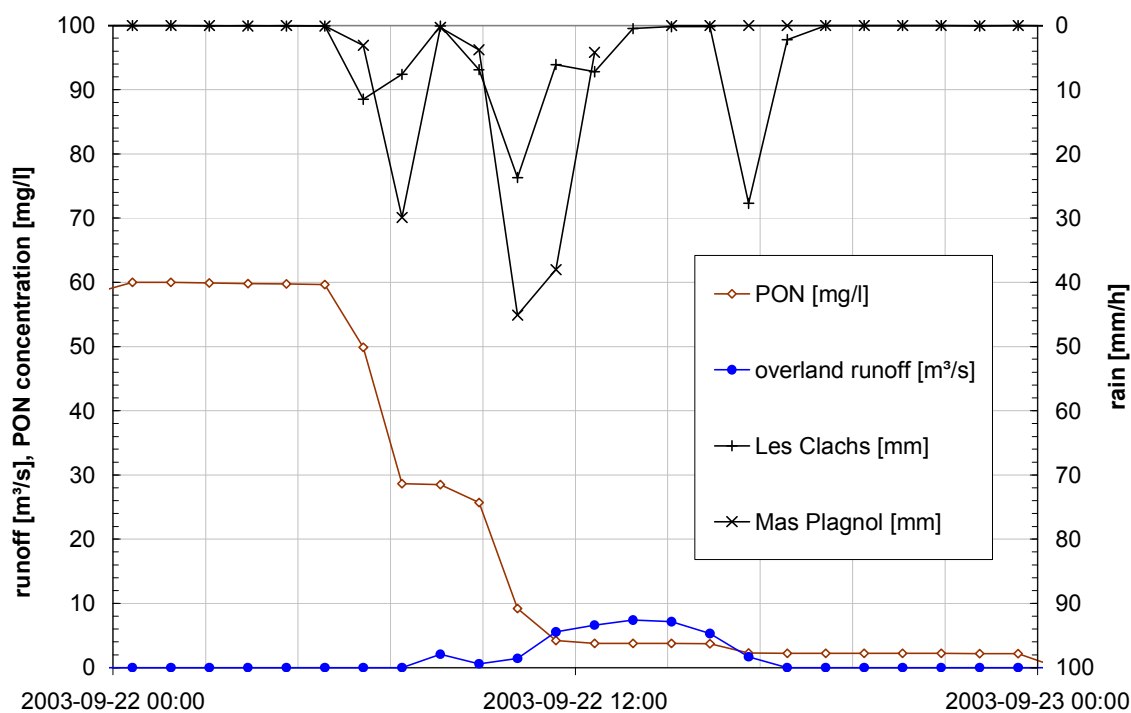


Figure 7-32: Variable runoff concentrations depending on antecedent dry day period and actual rainfall intensity for September 2003

Before the event, the anticipated concentration of 60 mg/l is reached, and is then later decreased continuously by the ongoing rainfall.

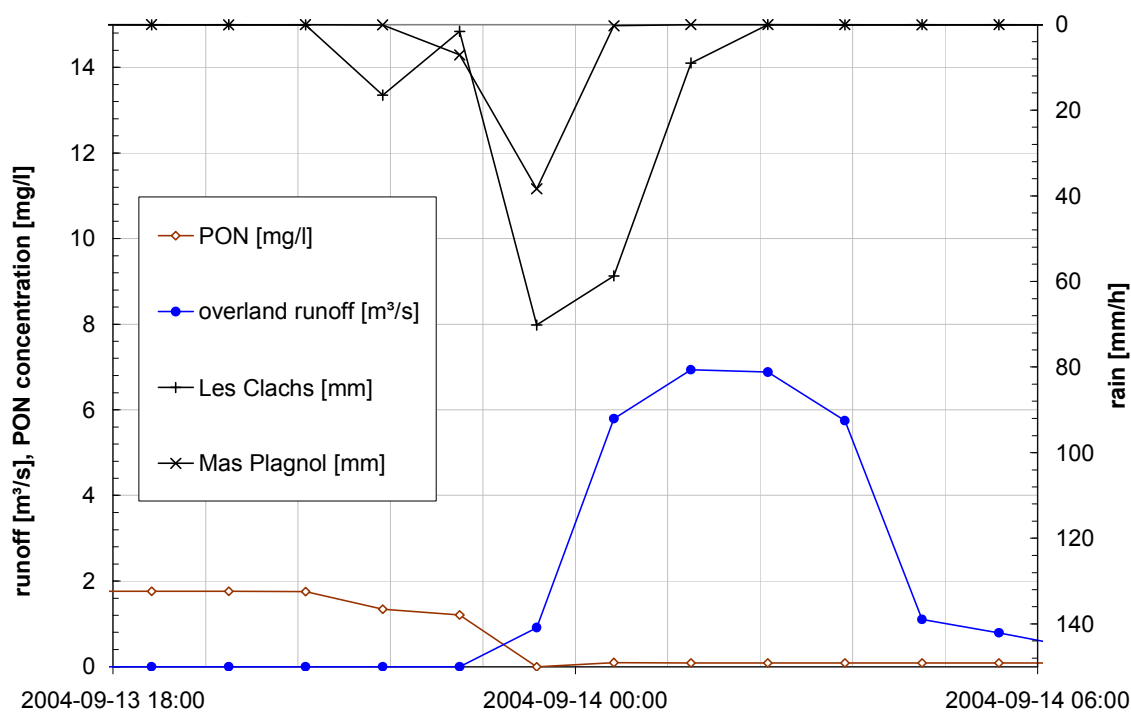


Figure 7-33: Variable runoff concentrations depending on antecedent dry day period and actual rainfall intensity for September 2004

## Results

The adoption of the overland flow concentration of PON aimed at the better representation of the changing system conditions and an advanced simulation of the concentration of volatile suspended solids. It was supposed, that there are other overland sources of VSS (e.g. the vegetation) and that the amount of stored mass was depending on the system dryness represented by the antecedent dry weather period. The concentration of the overland runoff was then assumed to be a function of the ADWP and in two of the variations to the actual rainfall.

In Figure 7-34 results for the event of September 2003 are compiled.

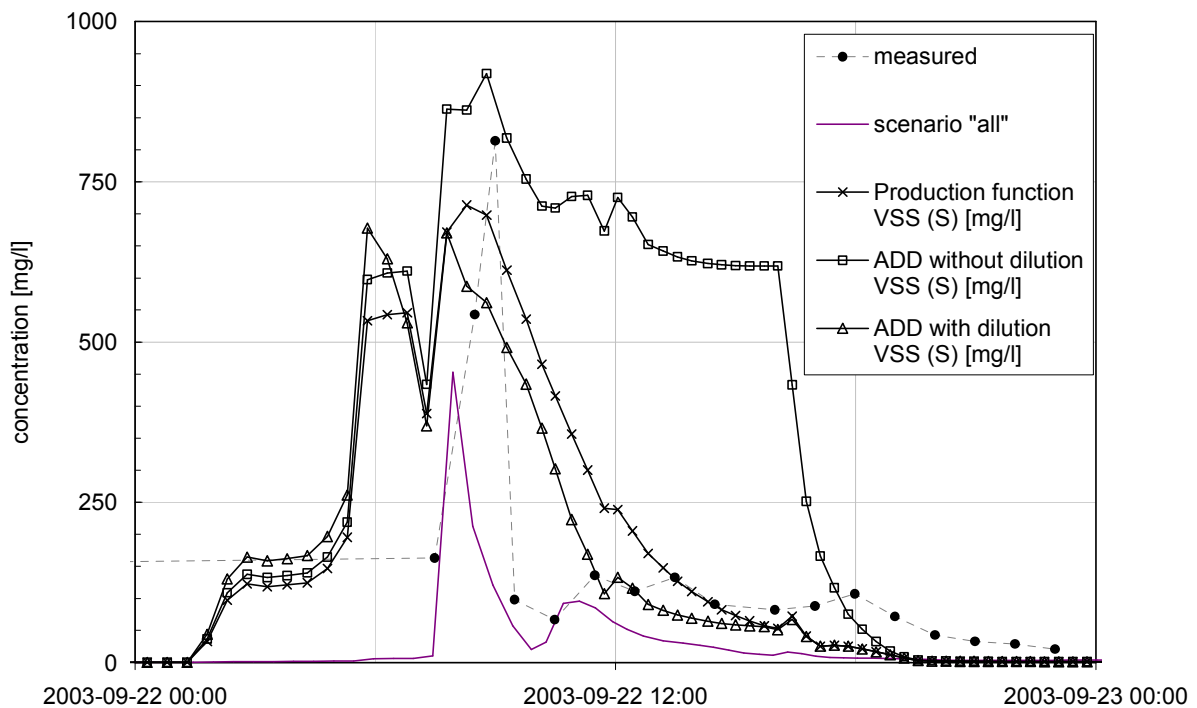


Figure 7-34: Results of the adoption of runoff concentrations for the event at 2003-09-22

Because the event had a ADD of 35 days after the definition of EQ. 7-23, every approach yields higher concentrations in comparison to the scenario “all”. The approach without dilution fails in the later stage of the flood, but the other two show better behaviour. Although none is capable to reproduce the sharp shape of the measured pollutograph the approach with the production function and “ADD with dilution” show an enhancement for this flood.

However, the simulation of September 2004 (Figure 7-35) does not seem to confirm this good impression.

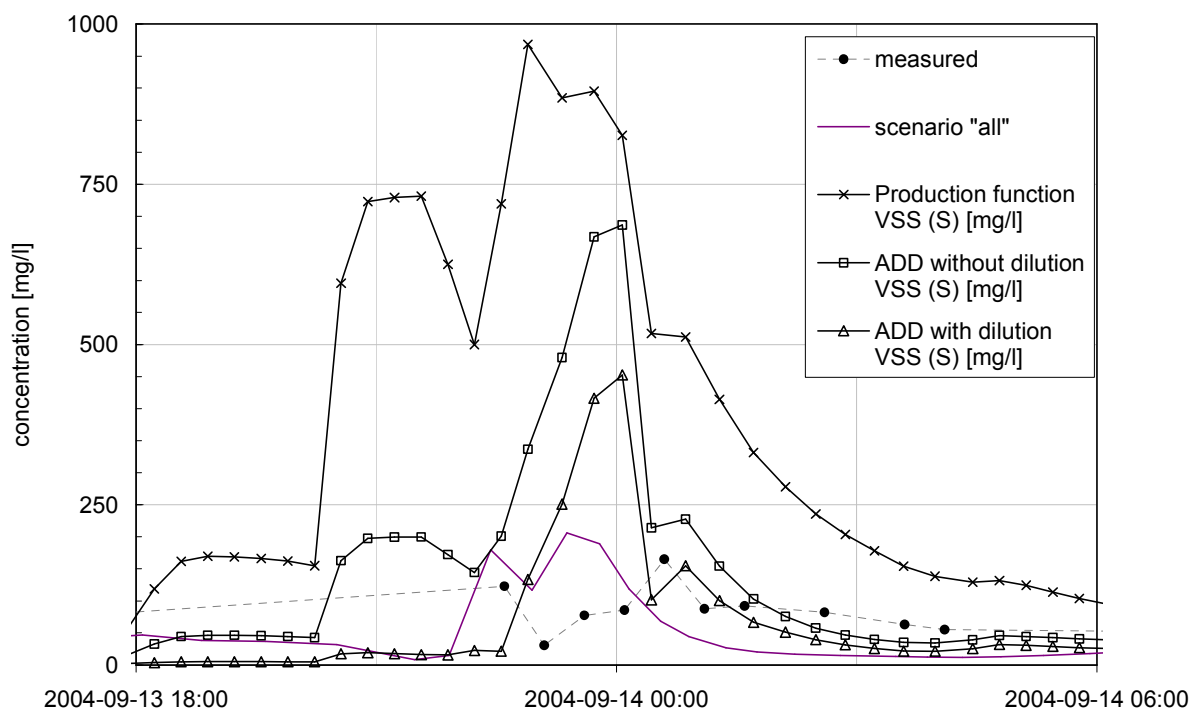


Figure 7-35: Results of the adoption of runoff concentrations for the event at 2004-09-13

The production function overestimates the concentration for the whole duration. Especially at the beginning, the approaches all fail to reproduce the first decline in concentration, in contrast they show all their peak values here, so the simulation could not be enhanced for the very beginning of the flush.

Because this all happens before the start of the actual runoff event, the concentrations are very sensitive to changes. In the simulation, the concentration of the overland runoff is already reduced to zero at 2004-09-14 23:30 due to the dilution of the rainwater (cp. Figure 7-33), so the overestimation is not directly caused by the delivery part. At that time, the overland runoff has just reached only 13% of its peak value for this event. In terms of the total event loadings, the deviation therefore happens in a less relevant part of the flood and is most likely a matter of overestimated releases of instream storages, but not of the delivery model itself.

For the more important part after midnight, especially the approach “ADD with dilution” shows good results when compared with the measurements.

Even though this procedure is vulnerable because it is not based on a proper verification by measurements, the results show nevertheless some good enhancements. The relatively rough approaches could probably be further defined, but keeping in mind the always limited knowledge of the regarded catchment and the constraints in transferability of measurements as well as their uncertainty, this would probably only increase the data needs.

## 7.12 Pictures of the Vène at different stages of the year

Following are some pictures taken in the year 2004 before and after the first flush events to illustrate the instream potential at two different sites. The first example in Figure 7-36 shows the situation directly downstream the WWTP inflow of Montbazin (point d, compare e.g. Figure 4-1).



Figure 7-36: Picture of the Vène at site d, directly downstream the WWTP outlet in July 2004 (left) and October 2004 (right)

The magenta circles were added at similar spots in every picture to ease orientation.

Figure 7-37 shows the situation at a downstream point (ca. 1 km) at the same day. This point still lies a bit upstream of the often mentioned site S, where many measurements were taken.



Figure 7-37: Picture of the Vène ca. one kilometre downstream site d, directly downstream the WWTP inflow at July 2004 (left) and October 2004 (right)

The accumulation here mainly takes place at the river bed, but also at the banks. The black colour indicates a strong oxygen deficit within the material. The accumulation spot (in the lower left picture bordered by the pointed yellow line) is not present any more in October.



## 8 References

---

- Abdulrazzak, M.J. and Sorman, A.U., 1994. Transmission Losses from Ephemeral Stream in Arid Region. *Journal of Irrigation and Drainage Engineering*, 120(3): 669-675.
- Ackers, P. and White, W.R., 1973. Sediment transport: new approach and analysis. *Journal of Hydraulic Division, ASCE*, 99(11): 2041-2060.
- Alexandrov, Y., Laronne, J.B. and Reid, I., 2003. Suspended sediment concentration and its variation with water discharge in a dryland ephemeral channel, northern Negev, Israel. *Journal of Arid Environments*, 53(1): 73-84.
- APHA, AWWA and WEF, 1992. *Standard Methods for the examination of water and wastewater*. American Public Health Association, Washington.
- ASCE Task Committee on Definition of Criteria for Evaluation of Watershed Models, Watershed Management Committee and Irrigation and Drainage Division, 1993. *Criteria for evaluation of watershed models*. *Journal of Irrigation and Drainage Engineering*, 199(3).
- Bagnold, R.A., 1966. *An approach to the sediment transport problem from general physics*, US Geological Survey Professional Paper 422-I, Washington.
- Baldwin, D.S., Mitchell, A.M., Rees, G.N., Watson, G.O. and Williams, J.L., 2006. Nitrogen processing by biofilms along a lowland river continuum. *River Research and Applications*, 22(3): 319-326.
- Baldwin, D.S., Rees, G.N., Mitchell, A.M. and Watson, G., 2005. Spatial and temporal variability of nitrogen dynamics in an upland stream before and after a drought. *Marine and Freshwater Research*, 56(4): 457-464.
- Balloffet, A. and Scheffler, M.L., 1982. Numerical-Analysis of the Teton-Dam Failure Flood. *Journal of Hydraulic Research*, 20(4): 317-328.
- Barkau, R.L., 1993. *UNET: One-Dimensional Unsteady Flow through a Full Network of Open Channels: User's Manual*. U.S. Army Corps of Engineers, Hydrologic Engineering Center, Davis, California.
- Bayly, I.A.E. and Williams, W.D., 1973. *Inland waters and their ecology*. Longman Australia Pty Limited, Camberwell, 316 pp.
- Bedient, P.B., Harned, D.A. and Characklis, W.G., 1978. Stormwater Analysis and Prediction in Houston. *Journal of the Environmental Engineering Division-ASCE*, 104(6): 1087-1100.
- Belmonte, A.M.C. and Beltran, F.S., 2001. Flood events in Mediterranean ephemeral streams (ramblas) in Valencia region, Spain. *CATENA*, 45: 229-249.
- Bertrand-Krajewski, J.L., Chebbo, G. and Saget, A., 1998. Distribution of pollutant mass vs volume in stormwater discharges and the first flush phenomenon. *Water Resources*, 32(8): 2341-2356.

- 
- Bollrich, G., Preißler, G., Martin, H. and Elze, R., 1989. Technische Hydromechanik. Bd. 2: Spezielle Probleme. Verl. für Bauwesen, Berlin (u.a.).
- Boorman, D.B., 2003. LOIS in-stream water quality modelling. Part 1. Catchments and methods. *Science of the Total Environment*, 314: 379-395.
- Borah, D.K. and Bera, M., 2003. Watershed-scale hydrologic and nonpoint-source pollution models: Review of mathematical bases. *Transactions of the ASAE*, 46(6): 1553-1566.
- Braunschweig, F., Leitao, P., Fernandes, L., Pina, P. and Neves, R., 2004. The object oriented design of the integrated Water Modelling System MOHID. In: C.T. Miller, M.W. Farthing, W.G. Gray and G.F. Pinder (Editors), 15th International Conference on Computational Methods in Water Resources (CMWR XV). ELSEVIER, Chapel Hill, NC, USA.
- Bull, L.J. and Kirkby, M.J., 2002. Dryland River Characteristics and Concepts. In: M.J. Kirkby and L.J. Bull (Editors), *Dryland Rivers - Hydrology and Geomorphology of Semi-Arid Channels*. Wiley & Sons Ltd., West Sussex, England, pp. 3-15.
- Bunn, S.E., Thoms, M.C., Hamilton, S.K. and Capon, S.J., 2006. Flow variability in dryland rivers: boom, bust and the bits in between. *River Research and Applications*, 22(2): 179-186.
- Carreira, J.A., Vinegla, B. and Lajtha, K., 2006. Secondary CaCO<sub>3</sub> and precipitation of P-Ca compounds control the retention of soil P in arid ecosystems. *Journal of Arid Environments*, 64(3): 460-473.
- Chanson, H., 1999. *The hydraulics of open channel flow - An Introduction*. University of Queensland, London.
- Chapelle, A., 1995. A Preliminary Model of Nutrient Cycling in Sediments of a Mediterranean Lagoon. *Ecological Modelling*, 80(2-3): 131-147.
- Cheng, N.-S., 1997. Simplified Settling Velocity Formula for Sediment Particle. *Journal of Hydraulic Engineering*, 123(2): 149-152.
- Colby, B.R., 1964. Discharge of sands and mean-velocity relationships in sand-bed streams. U. S. Geological Survey Professional Paper 462-A.
- Cooper, D.M., House, W.A., May, L. and Gannon, B., 2002a. The phosphorus budget of the Thames catchment, Oxfordshire, UK: 1. Mass balance. *Science of the Total Environment*, 282: 233-251.
- Cooper, D.M., House, W.A., Reynolds, B., Hughes, S., May, L. and Gannon, B., 2002b. The phosphorus budget of the Thames catchment, Oxfordshire: 2. Modelling. *Science of the Total Environment*, 282: 435-457.
- Cooper, D.M. and Naden, P.S., 1998. Approaches to delivery modelling in LOIS. *Science of the Total Environment*, 210(1-6): 483-498.
- Cunge, J.A., 1969. On the subject of flood propagation method (Muskingum method). *Journal of Hydraulic Research*, 7(2): 205- 230.
-

- Davies, B.R., Thoms, M.C., Walker, K.F., O'Keefe, J.H. and Gore, J.A., 1994. Dryland rivers, their ecology, conservation and management. In: P. Calow and G.E. Petts (Editors), *The Rivers Handbook Vol. 2*. Blackwell Scientific Publications, Oxford.
- Decyk, V.K., Norton, C.D. and Szymanski, B.K., 1997. Expressing Object-Oriented Concepts in Fortran90. *ACM Fortran Forum*, Vol. 16.
- Deletic, A., 1998. The first flush load of urban surface runoff. *Water Research*, 32(8): 2462-2470.
- Deletic, A., Maksimovic, C. and Ivetic, M., 1997. Modelling of storm wash-off of suspended solids from impervious surfaces. *Journal of Hydraulic Research*, 35(1): 99-118.
- Deng, Z.Q., de Lima, J. and Singh, V.P., 2005. Fractional kinetic model for first flush of stormwater pollutants. *Journal of Environmental Engineering-ASCE*, 131(2): 232-241.
- Donigian, A.S., Beyerlein, D.C., Davis, H.H. and Crawford, N.H., 1977. *Agricultural Runoff Management (ARM) Model Version II: Refinement and Testing*. EPA 600/3-77-098, Environmental Research Laboratory, Athens, GA.
- Donigian, A.S. and Crawford, N.H., 1976a. Modeling Nonpoint Pollution From the Land Surface. EPA 600/3-76-083, Environmental Research Laboratory, Athens, GA.
- Donigian, A.S. and Crawford, N.H., 1976b. Modelling Pesticides and Nutrients on Agricultural Lands. EPA 600/2-7-76-043, Environmental Research Laboratory, Athens, GA.
- Donohue, I., Styles, D., Coxon, C. and Irvine, K., 2005. Importance of spatial and temporal patterns for assessment of risk of diffuse nutrient emissions to surface waters. *Journal of Hydrology*, 304(1-4): 183-192.
- Einstein, H.A., 1950. The bed-load function for sediment transportation in open channel flows, Technical Bulletin No. 1026, U.S. Department of Agriculture, Soil Conservation Service, Washington, D.C.
- Engelund, F. and Hansen, E., 1967. A monograph on sediment transport in alluvial streams, Teknisk Forlag, Copenhagen, Denmark.
- Epa, 1993. Manual for combined sewer overflow control, EPA, Cincinnati, USA.
- Epa, 1998. Better assessment science integrating point and nonpoint sources: BASINS Version 2.0. EPA-823.B98.006, USEPA, Washington D.C.
- Euler, G., 1978. Regenabflußellen aus Siedlungsgebieten und deren Verlauf im Vorfluter, Regenwetterabflüsse. Haus der Technik e.V. und Lehrstuhl und Institut für Siedlungswasserwirtschaft der TH Aachen, Aachen.
- Froebrich, J. et al., 2006. Critical issues in the water quality dynamics of temporary waters - Evaluation and recommendations from the tempQsim project, University of Hannover, Hannover.
- Gallart, F., Latron, J. and Soler, M., 2003. Preliminary application of EUROSEM for hydrological and erosion modelling in small catchments with badlands in the Pyrenees, Conference on Soil erosion and sediment redistribution in river catchments: measurement, modelling and management in the 21st century, Cranfield University at Silsoe, UK.



- 
- Gallart, F., Llorens, P., Latron, J. and Regues, D., 2002. Hydrological processes and their seasonal controls in a small Mediterranean mountain catchment in the Pyrenees. *Hydrology and Earth System Sciences*, 6(3): 527-537.
- Geiger, W.F., 1984. Characteristics of combined sewer runoff, Proc. 3rd International Conference on Urban Storm drainage, Göteborg, Sweden, pp. 851-860.
- Geiger, W.F., 1987. Flushing effects in combined sewer systems, Proc. 4th International Conference on Urban Storm Drainage, Lausanne, Lausanne, Switzerland, pp. 40-46.
- Gelbrecht, J., Lengsfeld, H., Pothig, R. and Opitz, D., 2005. Temporal and spatial variation of phosphorus input, retention and loss in a small catchment of NE Germany. *Journal of Hydrology*, 304(1-4): 151-165.
- Gibbs, R.J., Matthews, M.D. and Link, D.A., 1971. Relationship between Sphere Size and Settling Velocity. *Journal of Sedimentary Petrology*, 41(1): 7-18.
- Graf, W.L., 1988. *Fluvial Processes in Dryland Rivers*. Springer Series in Physical Environment, Vol 3. Springer.
- Grillot, C., 2006. Fonctionnement hydrologique et dynamique des nutriments d'une rivière intermittente méditerranéenne en étiage et en crues. Analyse spatiale et temporelle., Université Montpellier II, Montpellier, France.
- Gujer, W., Henze, M., Mino, T. and Loosdrecht, M.v., 1999a. Activated Sludge Model No. 3. *Water Science and Technology*, 39(1): 183-193.
- Gujer, W., Henze, M., Mino, T. and Loosdrecht, M.v., 1999b. Activated Sludge Model No. 3, IAWQ Task Group on Mathematical Modelling for Design and Operation of Biological Wastewater Treatment.
- Gupta, K. and Saul, A.J., 1996. Specific relationships for the first flush load in combined sewer flows. *Water Research*, 30(5): 1244-1252.
- Hai Cohen, J.B.L., 2005. High rates of sediment transport by flashfloods in the Southern Judean Desert, Israel. *Hydrological Processes*, 19(8): 1687-1702.
- Holden, A.P. and Stephenson, D., 1988. Improved 4-Point Solution of the Kinematic Equations. *Journal of Hydraulic Research*, 26(4): 413-423.
- House, W.A., 2003. Geochemical cycling of phosphorus in rivers. *Applied Geochemistry*, 18(5): 739-748.
- Hummel, P., Kittle, J. and Gray, M., 2001. WDMUtil, Version 2.0, A tool for managing watershed modeling time-series data - user's manual. AQUA TERRA consultants, Georgia, USA.
- Humphries, P. and Baldwin, D.S., 2003. Drought and aquatic ecosystems: an introduction. *Freshwater Biology*, 48(7): 1141-1146.
- Hydrocomp, 1976. *Hydrocomp Simulation Programming: Operations Manual*, 2nd ed., Hydrocomp, Inc., Palo Alto, CA.
-

- Hydrocomp, 1977. Hydrocomp Water Quality Operations Manual, Hydrocomp, Inc., Palo Alto, CA.
- Jordan, P.R., 1977. Streamflow Transmission Losses in Western Kansas. *Journal of the Hydraulics Division, ASCE*, 77(8): 905-919.
- Julien, P.Y., 1995. *Erosion and Sedimentation*. Cambridge University Press, 304 pp.
- Karim, F., 1998. Bed material discharge prediction for nonuniform bed sediments. *Journal of Hydraulic Engineering, ASCE*, 124(6): 597-604.
- Kittle, J.L., Lumb, A.M., Hummel, P.R., Duda, P.B. and Gray, M.H., 1998. A Tool for the Generation and Analysis of Model Simulation Scenarios for Watersheds (GenScn). Report 98-4134, Aqua Terra Consultants for U.S. Geological Survey.
- Kneis, D., Knoesche, R. and Bronstert, A., 2006. Analysis and simulation of nutrient retention and management for a lowland river-lake system. *Hydrol. Earth Syst. Sci.*, 10: 575-588.
- Krebs, P., Holzer, P., Huisman, J.L. and Rauch, W., 1999. First flush of dissolved compounds. *Water Science and Technology*, 39(9): 55-62.
- Kretschmer, S., Höke, S. and Burghardt, W., 2006. Evaluation and Improvement of Water Quality Models for Application to Temporary Waters in Southern European Catchments, University Duisburg - Essen, Department of Soil Technology, Essen, Germany.
- Krone, R.B., 1962. Flume Studies of the Transport of Sediment in Estuarial Shoaling Processes, Final Report prepared for Army Engineer District, San Francisco.
- La Jeunesse, I., Deslous-Paoli, J.M., Ximenes, M.C., Cheylan, J.P., Mende, C., Borrero, C. and Scheyer, L., 2002. Changes in point and non-point sources phosphorus loads in the Thau catchment over 25 years (Mediterranean Sea - France). *Hydrobiologia*, 475(1): 403-411.
- Lane, E.W. and Hansen, D.S., 1949. Low temperature increases in sediment transportation in Colorado River. *Civil Engineering, ASCE*, 19(9).
- Lane, L.J., 1982. Distributed model for small semiarid watersheds. *Journal of the Hydraulics Division, ASCE*, 82(10): 1114-1131.
- Larsen, T., Broch, K. and Andersen, M.R., 1998. First flush effects in an urban catchment area in Aalborg. *Water Science and Technology*, 37(1): 251-257.
- Lee, H., Lau, S.L., Kayhanian, M. and Stenstrom, M.K., 2004. Seasonal first flush phenomenon of urban stormwater discharges. *Water Research*, 38(19): 4153-4163.
- Lee, J.H. and Bang, K.W., 2000. Characterization of urban stormwater runoff. *Water Research*, 34(6): 1773-1780.
- Lee, J.H., Yu, M.J., Bang, K.W. and Choe, J.S., 2003. Evaluation of the methods for first flush analysis in urban watersheds. *Water Science and Technology*, 48(10): 167-176.
- Leeks, G.J.L. and Jarvie, H.P., 1998. Introduction to the Land-Ocean Interaction Study (LOIS): Rationale and international context. *Science of the Total Environment*, 210(1-6): 5-20.

- 
- Li, Y., Lau, S.-L., Kayhanian, M. and Stenstrom, M.K., 2005. Particle Size Distribution in Highway Runoff. *Journal of Environmental Engineering*, 131(9): 1267-1276.
- Lighthill, M.J. and Whitham, G.B., 1955a. On Kinematic Waves .1. Flood Movement in Long Rivers. *Proceedings of the Royal Society of London Series a-Mathematical and Physical Sciences*, 229(1178): 281-316.
- Lighthill, M.J. and Whitham, G.B., 1955b. On Kinematic Waves .2. a Theory of Traffic Flow on Long Crowded Roads. *Proceedings of the Royal Society of London Series a-Mathematical and Physical Sciences*, 229(1178): 317-345.
- Malcherek, A., 2001. Hydromechanik der Fließgewässer. Habilitation Thesis, Universität Hannover, Hannover, 382 pp.
- Matthews, W.J., 1988. North American streams as systems for ecological study. *Journal of the North American Benthological Society*, 7(4): 387-409.
- McCarthy, G.T., 1938. The unit hydrograph and flood routing, Conf. North Atlantic Div. U.S. Corps of Engineers (unpublished), New London, Conn.
- McMahon, T.A., 1979. Hydrological characteristics of arid zones, Hydrology of areas of low precipitation. International Association of Hydrological Sciences Publication 128. IAHS Press, Wallingford, England, pp. 105-123.
- McMahon, T.A., Finlayson, B.L. and Srikanthan, R., 1987. Runoff variability: a global perspective. In: S.I. Solomon, M. Beran and W. Hogg (Editors), The influence of climate change and climate variability on the hydrologic regime and water resources. International Association of Hydrological Sciences Publication 168. IAHS Press, Wallingford, England, pp. 3-12.
- Metcalf and Eddy, 1916. American sewerage practice, Disposal of sewage. McGraw-Hill, New York.
- Michaelis, L. and Menten, M.L., 1913. Die Kinetik der Invertinwirkung. *Biochemische Zeitschrift*, 49: 333-369.
- Miranda, R., Braunschweig, F., Leitao, P., Martins, F. and Santos, A., 2000. MOHID2000 - a coastal integrated object oriented model. In: W.R. Blain and C.A. BREBBIA (Editors), Hydraulic Engineering Software VIII. Wessex Institute of Technology, Southampton, pp. 480.
- Nash, J.E. and Sutcliffe, J.V., 1970. River flow forecasting through conceptual models part I — A discussion of principles. *Journal of Hydrology*, 10(3): 282-290.
- NCSA and Technologies, S.D., 2005. HDF Reference Manual. HDF Version 4.2 Release.
- Neitsch, S.L., Arnold, J.G., Kiniry, J.R., Williams, J.R. and King, K.W., 2002. Soil and water assessment tool - theoretical documentation, version 2000. College Station, Texas Water Resources Institute.
- Neves, R., 1985. Etude Experimentale et Modelisation des Circulations Transitoire et Residuelle dans l'Estuaire du Sado. Ph. D. Thesis Thesis, University de Liege, Liege.
-

- Obermann, M., Froebrich, J., Perrin, J.-L. and Tournoud, M.-G., 2006. Impact of significant floods on the annual load distribution in an agricultural catchment in the Mediterranean. *Journal of Hydrology*, In Press, Corrected Proof (doi:10.1016/j.jhydrol.2006.09.029).
- Odd, N.V.M. and Owen, M.W., 1972. 2-layer model of mud transport in thames estuary, *Proceedings of the Institution of Civil Engineers*, pp. 714--.
- Onishi, Y. and Wise, S.E., 1979. Mathematical Model, SERATRA, for Sediment-Contaminant Transport in Rivers and its Application to Pesticide Transport in Four Mile and Wolf Creeks in Iowa, Battelle, Pacific Northwest Laboratories, Richland, WA.
- Parks, S.J. and Baker, L.A., 1997. Sources and Transport of Organic Carbon in an Arizona River-Reservoir System. *Water Resources*, 31(7): 1751-1759.
- Partheniades, E., 1962. A study of erosion and deposition of cohesive soils in salt water. Ph. D. in Civil Engineering Thesis, Univ. of California, Berkeley, 182 pp.
- Perrin, J.L., 2006. Personal communication concerning estimations of the runoff coefficient of the event 2003-09-22.
- Pickup, G., 1991. Event Frequency and Landscape Stability on the Floodplain Systems of Arid Central Australia. *Quaternary Science Reviews*, 10(5): 463-473.
- Plant, L.J. and House, W.A., 2002. Precipitation of calcite in the presence of inorganic phosphate. *Colloids and Surfaces A: Physicochemical and Engineering Aspects*, 203(1-3): 143-153.
- Plus, M., Jeunesse, I.L., Bouraoui, F., Zaldivar, J.-M., Chapelle, A. and Lazure, P., 2006. Modelling water discharges and nitrogen inputs into a Mediterranean lagoon: Impact on the primary production. *Ecological Modelling*, Special Issue on Southern European Coastal Lagoons - Selected Papers from the Conference on Southern European Coastal Lagoons: The Influence of River Basin--Coastal Zone Interactions, Ferrara, Italy, 10 - 12 November 2003, 193(1-2): 69-89.
- Raudkivi, A.J., 1982. *Grundlagen des Sedimenttransports*. Springer, Berlin (u.a.), 255 pp.
- Redfield, A.C., 1934. On the proportions of organic derivatives in seawater and their relation to the composition of plankton. In: R.J. Daniel (Editor), *James Johnson Memorial Volume*. University Press of Liverpool, Liverpool, England, pp. 177-192.
- Saget, A., Chebbo, G. and Bertrand-Krajewski, J.L., 1996. The first flush in sewer systems. *Water Science Technology*, 33(9): 101-108.
- Saget, A., Chebbo, G. and Bertrand-Krajewski, J., 1995. The first flush in sewer system, *International Conference on Sewer Solids-Characteristics, Movement, Effects and Control*, Dundee, U.K., pp. 58-65.
- Saint-Venant, B., 1871. Théorie du mouvement non permanent des eaux avec une application aux crues des rivières et à l'introduction des marées dans leur lit. *Comptes rendus de l'Académie des Sciences*, 73: 147-154 et 237-240.
- Sansalone, J.J. and Buchberger, S.G., 1997. Partitioning and first flush of metals in urban roadway storm water. *Journal of Environmental Engineering-Asce*, 123(2): 134-143.

- 
- Sansalone, J.J. and Cristina, C.M., 2004. First flush concepts for suspended and dissolved solids in small impervious watersheds. *Journal of Environmental Engineering-Asce*, 130(11): 1301-1314.
- Scholz, K., 1995. *Stochastische Simulation urbanhydrologischer Prozesse*. Universität Hannover, Hannover, 258 pp.
- Shields, A., 1936. Anwendung der Ähnlichkeitsmechanik und der Turbulenzforschung auf die Geschiebebewegung. *Mitteilungen der Preußischen Versuchsanstalt für Wasser-, Erd- und Schiffbau Berlin*, Heft 26.
- Singh, V.P., 2001. Kinematic wave modelling in water resources: a historical perspective. *Hydrological Processes*, 15(4): 671-706.
- Stenstrom, M.K. and Kayhanian, M., 2005. First Flush Phenomenon Characterization. CTSW-RT-05-73-02.6, California Department of Transportation, Sacramento, CA.
- Stokes, G., 1851. On the effect of internal friction of fluids on the motion of pendulums. *Transactions of the Cambridge Philosophical Society*, No. 9, Part II.
- Strelkoff, T., 1970. Numerical Solution of Saint-Venant Equations. *Journal of the Hydraulics Division*, 96(1): 223-252.
- Tang, X.N., Knight, D.W. and Samuels, P.G., 1999. Volume conservation in variable parameter Muskingum-Cunge method. *Journal of Hydraulic Engineering-Asce*, 125(6): 610-620.
- Tofaletti, F.B., 1969. Definitive computations of Sand Discharge in Rivers. *Journal of the Hydraulics Division*, 95(HY1): 225-246.
- Tournoud, M.G., Perrin, J.L., Gimbert, F. and Picot, B., 2005. Spatial evolution of nitrogen and phosphorus loads along a small Mediterranean river: implication of bed sediments. *Hydrological Processes*, 19(18): 3581-3592.
- Tournoud, M.G., Rodier, C., Joseph, C., Casteill, L., Moine, S. and Pacalin, M., 1997. Suivi des apports du bassin versant de l'étang de Thau et des échanges avec la mer par les canaux de Sète, Rapport final, Contrat pour l'étang de Thau, Université Montpellier I & II, Montpellier, France.
- Trancoso, A.R., Saraiva, S., Fernandes, L., Pina, P., Leitao, P. and Neves, R., 2005. Modelling macroalgae using a 3D hydrodynamic-ecological model in a shallow, temperate estuary. *Ecological Modelling*, 187(2-3): 232-246.
- Tsai, C.W., 2003. Applicability of kinematic, noninertia, and quasi-steady dynamic wave models to unsteady flow routing. *Journal of Hydraulic Engineering-ASCE*, 129(8): 613-627.
- UNEP, 1997. *World Atlas of Desertification*. United Nations / Environment Programme, London, 182 pp.
- Uys, M.C. and O'Keeffe, J.H., 1997. Simple Words and Fuzzy Zones: Early Directions for Temporary River Research in South Africa. *Environmental Management*, 21(4): 517-531.
- van der Lee, G.E.M., Venterink, H.O. and Asselman, N.E.M., 2004. Nutrient retention in floodplains of the Rhine distributaries in The Netherlands. *River Research and Applications*, 20(3): 315-325.
-

- van Rijn, L.C., 1993. Principles of sediment transport in rivers, estuaries and coastal seas. Aqua Publications, Amsterdam, The Netherlands.
- Venohr, M., Donohue, I., Fogelberg, S., Arheimer, B., Irvine, K. and Behrendt, H., 2005. Nitrogen retention in a river system and the effects of river morphology and lakes. *Water Science and Technology*, 51(3-4): 19-29.
- Vorreiter, L. and Hickey, C., 1994. Incidence of the first flush phenomenon in catchments of the Sydney region. *National Conf. Publication - Institution of Engineers*, 3: 359-364.
- Wall, D.J. and Englot, M.E., 1985. Correlation of Annual Peak Flows for Pennsylvania Streams. *Water Resources Bulletin*, 21(3): 459-464.
- Walters, M.O., 1990. Transmission Losses in Arid Region. *Journal of Hydraulic Engineering-Asce*, 116(1): 129-138.
- Welter, J.R., Fisher, S.G. and Grimm, N.B., 2005. Nitrogen Transport and Retention in an Arid Land Watershed: Influence of Storm Characteristics on Terrestrial-aquatic Linkages. *Biogeochemistry*, 76(3): 421 - 440.
- Whitehead, P., Young, P. and Hornberger, G., 1979. Systems-Model of Stream Flow and Water-Quality in the Bedford-Ouse River .1. Stream Flow Modeling. *Water Research*, 13(12): 1155-1169.
- Wool, T., Ambrose, R. and Martin, J., 1993. The Water Quality Analysis and Simulation Program, WASP5. U.S. Environmental Protection Agency, Environmental Research Laboratory, Athens, Georgia.
- Wu, W.M., Wang, S.S.Y. and Jia, Y.F., 2000. Nonuniform sediment transport in alluvial rivers. *Journal of Hydraulic Research*, 38(6): 427-434.
- Yang, C.H. and Simões, F.J.M., 2000. Generalized stream tube model for alluvial river simulation version 2.1, user's manual. U.S. Department of the Interior, Sedimentation and River Hydraulics Group, Denver, Colorado, USA.
- Yen, B.C. and Tsai, C.W.S., 2001. On noninertia wave versus diffusion wave in flood routing. *Journal of Hydrology*, 244(1-2): 97-104.
- Zhang, R. and Xia, J., 1995. Sedimentation Research in China: Systematic Selections. China Water and Power Press, Beijing.
- Zielke, W., 1999. Numerische Modelle von Flüssen, Seen und Küstengewässern. Deutscher Verband für Wasserwirtschaft und Kulturbau e.V., (DVWK), Bonn, 440 pp.